Ecosystem controls on carbon export efficiency from the naturally iron-fertilised phytoplankton bloom over the Kerguelen Plateau

by

Emmanuel C. Laurenceau-Cornec
M.Sc. Biological Oceanography, M.Sc. Earth Sciences

Under the supervision of **Pr. T.W. Trull, Pr. P.W. Boyd and Dr. M. Mongin**

Submitted in partial fulfilment of the requirements
for the degree of Doctor of Philosophy

University of Tasmania
Institute for Marine and Antarctic Studies (IMAS)
Antarctic Climate and Ecosystem Cooperative Research Centre (ACE CRC)
Commonwealth Scientific and Industrial Research Organisation,
Marine and Atmospheric Research (CSIRO)

November 2015

Ecosystem controls on carbon export efficiency from the naturally iron-fertilised phytoplankton bloom over the Kerguelen Plateau

by

Emmanuel C. Laurenceau-Cornec

Abstract

In the ocean, the perpetual 'snowfall' of biogenic marine particles exports organic carbon from the well-lit surface layer to the deep sediments, promoting its sequestration. The efficiency of this 'biological carbon pump' (BCP), presents strong spatio-temporal variations that are not yet fully explained. Changes in surface plankton communities and trophic interactions appear important because they lead to modifications of sinking particle characteristics (e.g. composition, structure, sinking velocity). These controls are explored here via the characterization of sinking particles originating from varying planktonic community structures and evaluation of their ability to export carbon. During the second KErguelen Ocean and Plateau compared Study (KEOPS2) conducted in Oct.-Nov. 2011, six sites were sampled over and downstream of the Kerguelen Plateau (Southern Ocean), where a mosaic of phytoplankton blooms of changing communities forms in response to natural iron fertilisation. Sinking particles were collected with free-drifting sediment traps at four mesopelagic depths to examine their form and composition, including optical characterization using polyacrylamide gel filled traps. Concurrently, aggregates were formed in roller tanks from surface water phytoplankton assemblages, to explore the intricate influences of particle size, structure and composition on the sinking velocity. At each site, carbon export efficiencies were calculated as the ratio of carbon flux to net primary productivity (e-ratio).

High productivity was associated with the lowest carbon export efficiency (e-ratio $\sim$0.02) while maximum export efficiency (e-ratio $\sim$0.2) was found at low-productivity sites. Two explanations were identified. Firstly, at high-biomass sites, strong zooplankton grazing generated large fecal pellets sustaining high carbon fluxes at 100-200 m (180 mg C m^{-2} d^{-1}). This export pathway represented a 'dead end' due to rapid attenuation of the fecal pellet flux at 200-400 m, releasing most of the carbon (48$\pm$21 % carbon flux decrease). Secondly, based on the roller tank results, the morphology of dominant diatom species appeared to be an important control on aggregate sinking velocities, possibly via species-specific coagulation efficiency affecting particle structure and density. At high-biomass sites, dominant small spine-forming species formed loose slow-sinking aggregates ($\sim$10 m d^{-1}), whereas chain-forming diatoms without spines, at low-productivity sites, produced compact fast-sinking aggregates ($\sim$250 m d^{-1}). The similarity of aggregate morphology and structure from roller tank and gel traps (2-D fractal number = 1.8 and 1.9 respectively), increased confidence in applying these results to in situ conditions. A generic 3-D physical-biogeochemical (BGC) model was modified to investigate conceptually the influence of planktonic community variations on carbon export efficiency through their control on detritus composition and sinking velocity. This was achieved by introducing in the model a variable detritus sinking velocity based on phytoplankton and zooplankton detrital fractions (using experimental results). Changes from a constant (100 m d^{-1}) to a variable sinking velocity induced a significant increase of the annual integrated carbon flux at 100 m (45$\pm$23 %) highlighting the importance of sinking velocity parameterisation in BGC models. Simulations indicate that export efficiency could depend upon subtle trophic interactions between phyto- and zooplankton communities influencing the relative rates of productivity and associated carbon flux and determining the conditions of biomass retention or export. The insights and tools developed here improve our understanding of how a climate-mediated shift of surface plankton communities can alter the efficiency of the BCP.

I dedicate this thesis to my beloved parents Dominique and Christian who always unconditionally supported me. You have been my faithful lighthouse showing me the path every time that I was lost.

Declaration and statements

Declaration of originality

This thesis contains no material which has been accepted for a degree or diploma by the University or any other institution, except by way of background information and duly acknowledged in the thesis, and to the best of my knowledge and belief no material previously published or written by another person except where due acknowledgement is made in the text of the thesis, nor does the thesis contain any material that infringes copyright.

Authority of access and statement regarding published work contained in the thesis

The publishers of the papers comprising Chapters 2 and 3 hold the copyright for that content, and access to the material should be sought from the respective journals. The remaining non published content of the thesis may be made available for loan and limited copying and communication in accordance with the Copyright Act 1968.

Signed:

Emmanuel C. Laurenceau-Cornec
PhD candidate
Date: 30/05/2015

Statement of co-authorship

The following people and institutions contributed to the publication of work undertaken as part of this thesis:

(1) Emmanuel C. Laurenceau-Cornec (candidate) — Institute for Marine and Antarctic Studies (IMAS), Antarctic Climate and Ecosystem Cooperative Research Centre (ACE CRC), University of Tasmania, Commonwealth Scientific and Industrial Research Organisation (CSIRO), Hobart (TAS), Australia.
(2) Thomas W. Trull — Commonwealth Scientific and Industrial Research Organisation (CSIRO), Antarctic Climate and Ecosystem Cooperative Research Centre (ACE CRC), University of Tasmania, Hobart (TAS), Australia.
(3) Diana M. Davies — Antarctic Climate and Ecosystem Cooperative Research Centre (ACE CRC),

University of Tasmania, Hobart TAS 7000, Australia.
(4) Stephen G. Bray — Antarctic Climate and Ecosystem Cooperative Research Centre (ACE CRC), University of Tasmania, Hobart TAS 7000, Australia.
(5) Jacqui Doran — UWA Oceans Institute, The University of Western Australia (M470), 35 Stirling Highway, Crawley WA 6009, Australia.
(6) Frédéric Planchon — Laboratoire des Sciences de l'Environnement Marin (LEMAR), Université de Brest, CNRS, IRD, UMR6539, IUEM, Technopôle Brest Iroise, Place Nicolas Copernic, 29280 Plouzané, France.
(7) François Carlotti — Mediterranean Institute of Oceanography (MIO), Aix-Marseille Université, CNRS-IRD, 13288 Marseille, CEDEX 09, France.
(8) Marie-Paule Jouandet — Mediterranean Institute of Oceanography (MIO), Aix-Marseille Université, CNRS-IRD, 13288 Marseille, CEDEX 09, France.
(9) Anne-Julie Cavagna — Vrije Universiteit Brussel, Analytical, Environmental and Geo-Chemistry and Earth System Sciences, Brussels, Belgium.
(10) Anya M. Waite — UWA Oceans Institute, The University of Western Australia (M470), 35 Stirling Highway, Crawley WA 6009, Australia; Alfred Wegener Institute Helmholz Centre for Polar and Marine Research, Building E-2155, Am Handelshafen 12, 27570 Bremerhaven, Germany.
(11) Stéphane Blain — Sorbonne Universités, UPMC Univ. Paris 06, UMR 7621, Laboratoire d'Océanographie Microbienne, Observatoire Océanologique, 66650 Banyuls/mer, France.
(12) Christina L. De La Rocha — CNRS, UMR 6539, Institut Universitaire Européen de la Mer, Université de Bretagne Occidentale, Technopôle Brest-Iroise, Rue Dumont d'Urville, Plouzané 29280, France.
(13) D. Ballas — Vrije Universiteit Brussel, Analytical, Environmental and Geo-Chemistry and Earth System Sciences, Brussels, Belgium.
(14) Andrew R. Bowie — Institute for Marine and Antarctic Studies (IMAS), Antarctic Climate and Ecosystem Cooperative Research Centre (ACE CRC), University of Tasmania, Hobart TAS 7000, Australia.
(15) Pier van der Merwe — Antarctic Climate and Ecosystem Cooperative Research Centre (ACE CRC), University of Tasmania, Hobart TAS 7000, Australia.
(16) Frank Dehairs — Vrije Universiteit Brussel, Analytical, Environmental and Geo-Chemistry and Earth System Sciences, Brussels, Belgium.

Author's contributions

PAPER 1 (Chapter 2): *The relative importance of phytoplankton aggregates and zooplankton fecal pellets to carbon export: insights from free-drifting sediment trap deployments in naturally iron-fertilised waters near the Kerguelen Plateau.*
E.C. Laurenceau-Cornec (first author): field work, laboratory work, data processing, manuscript writing.
T.W. Trull (author 2): field work, laboratory work, data processing, manuscript writing.
D.M. Davies (author 3): field work, laboratory work, data processing, manuscript writing.
S.G. Bray (author 4): material preparation.
J. Doran (author 5): data processing.
F. Planchon (author 6): field work, data processing.
F. Carlotti (author 7): field work, data processing.
M.-P. Jouandet (author 8): field work, data processing.
A.-J. Cavagna (author 9): field work, data processing.
A.M. Waite (author 10): design data processing.
S. Blain (author 11): general design, field work, data processing, manuscript writing.

PAPER 2 (Chapter 3): *Phytoplankton morphology controls on marine snow sinking velocity*

E.C. Laurenceau-Cornec (first author): experiment design, field work, laboratory work, data processing, manuscript writing.
T.W. Trull (author 2): experiment design, field work, laboratory work, manuscript writing.
D.M. Davies (author 3): field work, laboratory work, data processing, manuscript writing.
C.L. De La Rocha (author 4): general design, material preparation, manuscript writing.
S. Blain (author 5): general design, field work, data processing, manuscript writing.

PAPER 3 (Appendix): *Carbon export in the naturally iron-fertilized Kerguelen area of the Southern Ocean based on the* ^{234}Th *approach*
F. Planchon (first author): experiment design, field work, laboratory work, data processing, manuscript writing
D. Ballas (author 2): laboratory work, data processing.
A.-J. Cavagna (author 3): field work, data processing.
A.R. Bowie (author 4): field work, data processing, manuscript writing.
D.M. Davies (author 5): field work, data processing.
T.W. Trull (author 6): field work, data processing, manuscript writing.
E.C. Laurenceau-Cornec (author 7): field work, data processing, manuscript writing.
P. van der Merwe (author 8): field work, data processing, manuscript writing.
F. Dehairs (author 9): field work, data processing, manuscript writing.

We the undersigned agree with the above stated 'proportion of work undertaken' for each of the above published (or submitted) peer-reviewed manuscripts contributing to this thesis:

Signed:

Pr. Philip W. Boyd
Supervisor
Institute for Marine and Antarctic Studies (IMAS)
University of Tasmania

Date: 27/05/2015

Signed:

Pr. Craig Johnson
Head of centre
Institute for Marine and Antarctic Studies (IMAS)
University of Tasmania

Date: 29/05/2015

Acknowledgments

Tom, if someone asked me to describe you in 10 words, I would probably say: clever, fun, wise, fair, busy, available, honest, challenging, caring, and charismatic. Clever: because I don't remember a single moment over these years when I did not tell to myself "this guy is a pure genius"; fun: because deploying free–drifting sediment traps off the Kerguelen Islands listening a hell of a good loud blues on the back deck of the RV *Marion Dufresne* is pretty cool stuff; wise: because you don't say what people want to hear, you say what you think, and your advices often worth gold; fair: because when you're right, you're right, when you're wrong, you're wrong; busy: well, this one is not a quality it's a matter of fact, great minds come with great responsibilities; available: because you always found my emails lost in the hundreds that you receive every day and took the time to answer; honest: because whenever my work was shit or good, you always told me exactly how it was: no sugar–coated truth!; challenging: because you never told me the work is done unless you thought nothing more can be done; caring: because when we left the Kerguelen Islands without putting a foot onshore, you saw me so sad that you started to describe me the island as if I was actually there; charismatic: not because of all the previous, because of how you play frisbee! I think everybody who had the chance to meet you would say something pretty much similar. Be sure of one thing: what I learnt with you during these years will be gospel truth for all my career.

Mathieu, I think I could have titled my last chapter: *Manu's adventures in Modellingland*! For a field experimentalist, modelling is scary at first, but very quickly it becomes fascinating and with endless possibilities. I want to thank you for your patience each time that I said "But it doesn't make any sense in the real world!". You made me understand that a model doesn't necessarily have to make sense, it just have to learn you something that couldn't be learnt from observations alone. Thank you for all the unplanned but expected meetings at Rektango where we always had discussions about everything else than work!

Phil, first of all I swear I don't live at Preachers! It was just pure randomness that you saw me there every time that you came (which was pretty often by the way...). Thank you again for accepting to supervise me during my last year of candidature. Thank you for sharing your amazing experiences in fishing, beer tasting, and of course, Science! Given your knowledge of the literature, I now suspect that you are an immortal Highlander who was already doing research when the Dinosaurs were still around... and at some point I would not been surprised to hear you saying "Ummm, Manu you should read this paper from Boyd et al., 1687 b.c., we did some modelling work that might be useful for your research". Don't worry, your secret is safe with me!

I want to thank Christina De La Rocha who first believed in me and transmitted me the virus of marine aggregates. Christina, without you nothing would have been possible, I'm so thankful for that! Also, thanks to Frederic Le Moigne who one day told me about the Sarmiento and Gruber's book *Ocean Biogeochemical Dynamics*: "This, my friend, is a bible!". Well, I can confirm now: "Yes, my friend, you were right!" Many thanks to Diana Davies, whose incredible knowledge and kindness made at least half of my PhD an easy task where it could have been a nightmare! Thank you so much Di, you are a star! Thanks to Simon Wotherspoon, or 'Spoon' as everybody call him here, for having always ensured that I was on the right track! Thanks

to Heidi Auman, Denbeigh Armstrong and Amy Conley who have been really helpful in solving every paperwork issue that I encountered. Thanks to the two IT gurus Kevin and Antony who saw me very close to commit suicide when I thought that I lost 2 years of data! Many many thanks to Wenneke ten Hout, who is "not bossy, but has skills... leadership skills!" To understand how resourceful Wen is, just search for 'Wenneke' on Google Australia and you will understand.

Thanks to Morgane Gallinari who helped me in all my lab work in France. Thanks to Ruth Eriksen and Kerrie Swadling for sharing their expertise in microscopy. Thanks to Anya Waite who brought her invaluable experience in imaging of particles embedded in polyacrylamide gel. Thanks to Jacqui Doran for her amazing work in processing the images. Thank to all the people that I met during the KEOPS2 cruise, or here at the institute and who became good friends and respected colleagues. Thanks to Leanne Armand the 'Diatom Goddess'. Thanks to Francesco d'Ovidio for his invaluable insights into the evolution of the Kerguelen bloom and for his now famous "ma jé né comprrrends pas!". Thanks to Pier van der Merwe for having convinced me, after just one session on the North South track (Mt Wellington, Hobart) that bike riding is definitely not for me. Thanks to his adorable wife and talented researcher Delphine. Thanks to Klaus Meiners for the fly fishing lesson (and the leaking waders...). Thanks to Fred Planchon for the invaluable lessons on fusball, darts, DJ...and ^{234}Th method! Thanks to my best mate onboard the RV *Marion Dufresne*, Andy Bowie who first taught me how to say "How ya goin' mayyyte?" before I arrived in Australia. Thanks to Marie–Paule, Anne–Ju, Fabien P., Marine, Fanny, Laure, Cédric, Marie–Lise, Ivia, Bruno, Marine, Elodie, Audrey, Joan, Mustapha, Gégé, Peter, Ester, Urania, and all the others who participated in making the KEOPS2 cruise an amazing time. Thanks to Stéphane Blain and Bernard Quéguiner for the two slabs of 'Dodo lé La' offered during the Malgache party, and for the complete success of KEOPS2.

Thanks to Romain and Mélanie for having been so fun during their time here. We miss you so much guys and especially every time that we hear "tuuuuu tu tututuuuuu tu, tututu, pompompom pompompom pompompom"... Thanks to all my mates from the Astrolabe, and especially mon pote Stan! Thanks to my dear housemates (when I'm actually at home...) Adrienne, Joe, Melle and Brendan. Je tiens à remercier tous mes potes en France du monde de l'Océano, de la Géologie, de l'enseignement ou d'ailleurs qui m'ont soutenu dans ma reconversion. Merci surtout bande de jeunes blanc–becs pour les blagues récurrentes sur mon âge! Malwenn, te revoir chaque année était une véritable bouffée d'oxygène, je t'adore! Fabien, merci de m'avoir mis en garde sur à quel point on peut en baver en fin de thèse, c'était très instructif de te voir tenir un cycle 10 heures labo - 2 heures dodo pendant plusieurs semaines! Ty Tom, c'était un plaisir de t'héberger pendant ton séjour ici! Merci pour les extraordinaires photos et timelapse. Je le répète, t'es un artiste un vrai! Merci à Skippy pour la conduite musclée durant notre East Coast trip (Ty tom ne se joindra probablement pas à ces remerciements...). Merci aux membres de l'organisation secrète KTD: Pô, Foun, Pocabonasse, Ejac and Gwen (désolé tu es le seul à ne pas avoir signé tes emails par son nom KTD et impossible de m'en souvenir...). Vous me manquez tellement les copains! Merci à tous mes collègues de l'Education Nationale pour avoir continué à partager leurs aventures sur Facebook et m'avoir conforté dans l'idée que j'ai fait le bon choix! Merci à mon jojo et mon gregoun pour avoir toujours été mon jojo et mon gregoun!

Alright, the time has come to thank you my dear friends, my companions, my mates from here and everywhere in the World. You have been (and you will stay) a second family for me. I enjoyed all the parties, pub sessions (followed by variably intense hangovers), Christmas week–ends, hiking trips, fishing trips, diving trips, running races, dinners, climbing trips, swimming–pool sessions, breakfasts, tea breaks, coffee breaks, wood fires, barbies, and all the laughs that we had and will have together. Thanks to Sally (New Zealand; yes you are in first position but it could be just because you threatened me when I was writing this...), Mana my dear Imoto (Japan), Lucho (Chile), Andreas my climbing, diving and drinking buddy (Austria), Mauro (Costa Rica), Tania and Nick (Peru and Zimbabwe), Ramos (Mexico), Lara (Spain), Mono

(Chile), Dani (Chile), Molly (China), Roland the bastard who never came back (UK), Amelia my much preferred diving instructor and buddy (Australia), Nicoletta and Andres (Germany and Portugal), Rob the Matlab guru (Australia), Sandra (Chile), Jimmy the cook (Australia), Jimmy the barman (Australia), Ben the aussie–french cook (Tassie), Margaux (France), Nina (France), Mez and Tom (Australia), Narissa (New Zealand), Anna (Denmark), Martin (France), Martin (Australia), Indi (Australia), Veronique (Québec), Pablo and Pamela (Chile), Elena (Italy), Louise (Australia), Juan Diego (Chile), Pearse (Australia), Sarah-Jane (Australia), Sara (Spain), Sara (France), Eric and Ceci (Canada and Argentina), Lavy (Malaysia), Lev my dive buddy forever (Hungary), Elias (Greece), Cedric and Marcelina (New Caledonia and Poland), Pearse (Australia), Linda Malinda (Malaysia), Elsa and Felipe (France and Chile), Clara (France), Kathy (Germany), Merel (Australia), German (Columbia), Sébastien (Switzerland), Zya (Iran), Nico and Anthony (France), Kate (France,US), Tom and Christine (Australia and Canada), Cesar (Ecuador), Sjoerd and Malou (Netherlands), Waldo and Carla (Spain and Brasil), Anicee and my dear fellow Santa (Belgium), Alvaro my very first diving student and Sara (Spain), Thibone (France), Arthur (France), Ana (Brasil), Simon my DiveMaster companion (Australia), Mario (Chile), Ivan and Fernanda (Chile), Marnie (Australia), Manuel and Camilla (Chile), Eva and Javier (France and Chile), Camilla (Italy), Alice (Italy), Elroy (Malaysia, Australia), Makrina (Australia,Greece), my sweet Jaimie (Australia), Alyce (Australia), Andrea (Australia), Karine and Malcolm (France and Australia), Beltran and Martha (Spain), Anna (UK), Felix (Germany), Mathieu and Clémence (France), Geoff (Canada), Gigi (Chile), Laurent bouvard (France), GK the baker (Malaysia), Leo (Italy), Rowena (Australia), Delphie (Australia), Xavier and Marie (France). I want to thank all the Tasmanians and more generally Australian people for being such amazing and nice humans!

In the VIP room: Julie, my much preferred Belgium (assuming that there are several of these elsewhere...). Yes, we make fun at Belgiums all the time but it's only because we love you so much guys! Axel my best french–almost–aussie mate. I heard Axel saying 'barrel, overhead, take–off, offshore, fish, gun, swell, point, right, left', etc. (whatever!) at every single lunch during 3 years! Merci mon pote, pour les nombreuses pauses cafés où l'on cherchait le moyen le plus inventif d'éradiquer les mouettes! Claudio, my MFPP chilean compadre you became a true friend over these years, mi casa será siempre tu casa! And the last but not the least (I know if I didn't have reserved you this place of honour I would have been in trouble...), ma Crecre mother of Pilichaw premier le siamois roi des pusses et des prussiens, my favorite crazy, adorable, female counterpart! I'm still seriously thinking of writing a book about you, but I might need many other years of study before starting, so expect me to stay around for quite a bit!

My final thanks go to my precious family that I love more than anything: Mon parrain Christian et ma marraine (choisie!) Jannik, ma cousine/soeur Virginie et son mari Amaury, leurs enfants Côme, Calixte et ma Faustine adorée, mon frérot Jean–Charles, sa Diane et mes délicieuses nièces Marie et Camille, mes indispensables et extraordinaires parents Dominique et Christian à qui je dois absolument tout. Ma dernière pensée va à mes grand–parents adorés Louis et Yvette qui me manquent...

Contents

List of Figures

List of Tables

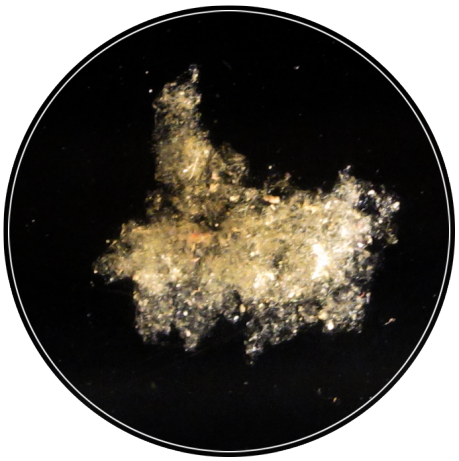

"You know nothing, Marine Snow."

Chapter 1

Introduction

1.1 The Biological Carbon Pump: components and processes

The oceanic biological carbon pump (BCP) includes all the biologically-driven processes that deplete the upper ocean total CO_2 relative to its concentration in the deep ocean, thereby creating a concentration gradient (Volk and Hoffert, 1985). This gradient is maintained by a perpetual fall of biogenic particles that transport carbon from the surface ocean to its interior. In the well-lit surface layer, atmospheric CO_2 dissolves into the upper ocean by air-sea gas exchange and is fixed by phytoplankton photosynthetic activity into organic molecules required for cell growth (Fig. 1.1). At a stage of their life cycle, phytoplankton cells sink in the water column either because they are then unable to afford the energetic cost needed to maintain their buoyancy (Waite et al., 1992), or as a physiological strategy to maximise their survival (Acuña et al., 2010; Gross and Zeuthen, 1948; Smayda and Boleyn, 1965). Differential settling (i.e. large cells typically sink faster than small cells), Brownian motion and fluid shear are the main physical processes that bring phytoplankton cells into contact in the ocean (Burd and Jackson, 2009). If their probability to stick together upon collision (i.e. their stickiness) and biomass are high enough (Jackson, 1990), they can attach and form large fast–sinking and organic-rich aggregates able to scavenge various suspended particles during their descent (i.e. other cells, fecal material, zooplankton carcasses and feeding structures, bacterias, micro-organisms and their tests, exopolymer particles, bubbles, minerals...) (Alldredge, 2001). Phytoplankton cells can also be aggregated biologically. Higher in the food web, zooplankton graze on phytoplankton to produce their own organic matter and egest organic-rich and tightly packed fecal pellets, prone to sink at very high velocity (up to 200 m d^{-1}; Turner, 2015). Zooplankton fecal pellets and

large phytodetrital aggregates (> 0.5 mm in diameter) composed of miscellaneous debris called 'marine snow', started to be the focus of extensive research efforts in the 1970's and 1980's. They were soon identified as major vectors of the BCP because of their ability to transport high quantities of particulate organic carbon (POC) at high sinking velocity to the deep ocean (Alldredge, 1979; Alldredge and Silver, 1988; Bishop et al., 1977; Fowler and Knauer, 1986; Shanks and Trent, 1980; Suess, 1980).

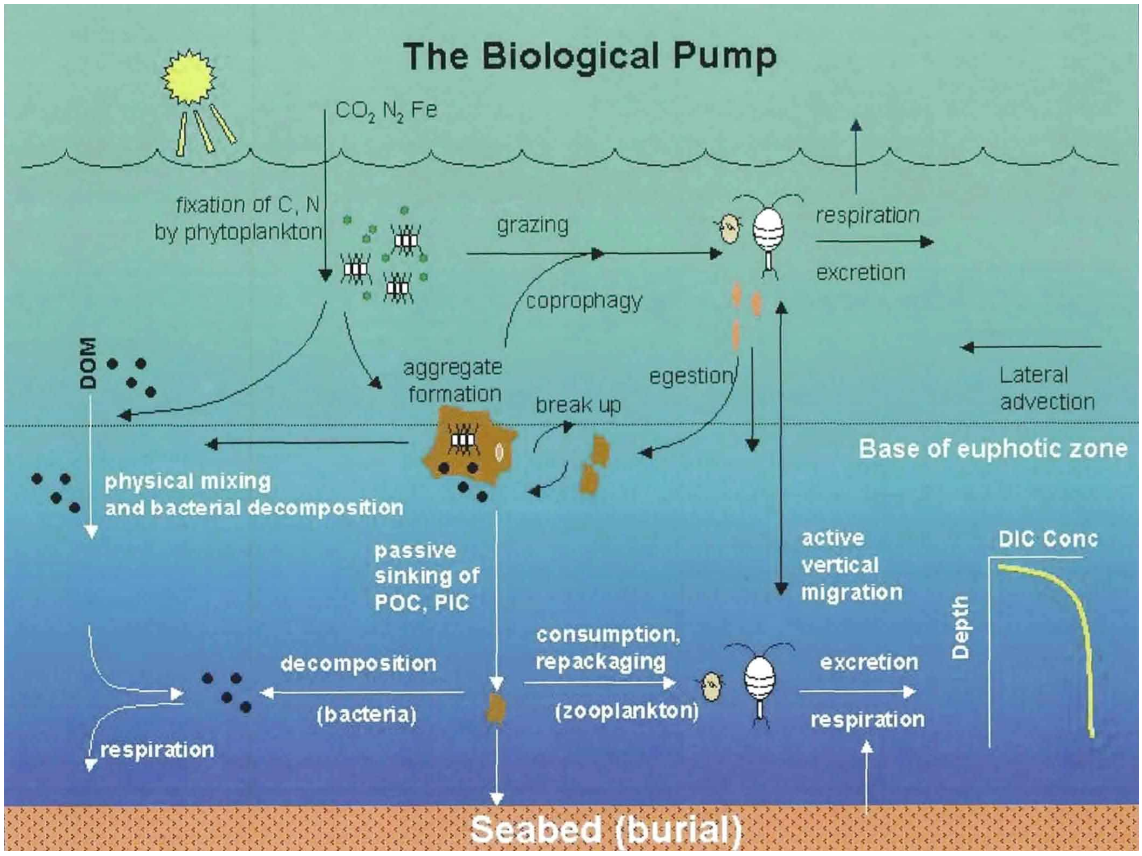

Figure 1.1: Representation of the components of the biological carbon pump and the processes contributing to the formation of a dissolved inorganic carbon (DIC) concentration gradient between the surface and deep ocean (from Ducklow et al., 2001). Atmospheric carbon dioxide (CO_2) dissolves into the surface ocean by air-sea gas exchange. Phytoplankton cells fix this DIC by photosynthetic activity and with other nutrients (e.g. N_2 and Fe) incorporate it into organic molecules. The organic matter produced is partitioned between particulate and dissolved organic matter pools (POM and DOM). Particulate matter (POC: particulate organic carbon; PIC: particulate inorganic carbon) can then be aggregated physically, or biologically through zooplankton grazing, and sink passively in the form of large aggregates of miscellaneous detritus and fecal pellets. Pronounced attenuation of the sinking flux occurs below the euphotic zone due to aggregate break-up, bacterial decomposition and consumption by actively migrating zooplankton, promoting the return of organic matter to the dissolved pool. Excretion and respiration by heterotrophic organisms induce losses at several steps and promote the return of carbon to its inorganic form and subsequent ventilation by physical mixing.

At several steps of the BCP, a part of the POC can go to the dissolved organic carbon pool (DOC). POC consumption by heterotrophic organisms (e.g. zooplankton) promotes losses by respiration, excretion and 'messy (or sloppy) feeding' (Corner et al., 1972; Møller, 2005). As

a result, the flux of carbon carried by sinking particles that leaves the base of the euphotic zone, referred to hereafter as 'export flux', represents often a very small fraction of the total carbon initially fixed by phytoplankton. The ratio between export and production is often less than 5 to 15% (Buesseler, 1998; Giering et al., 2014; Henson et al., 2011). It is however during their downward journey through the mesopelagic layer (or 'Twilight Zone', between the base of the euphotic zone and 1000 m) that phyto- and zoo–detritus exported out of the surface ocean, will encounter most of their physical and biological transformations leading to a large attenuation of the flux (Buesseler and Boyd, 2009; Buesseler et al., 2007; Martin et al., 1987). Particle break-up will potentially occur (Burd and Jackson, 2009), facilitating their bacterial decomposition. Zooplankton actively migrating in the water column will accompany the sinking flux and keep modifying it by either grazing on phytodetritus, or degrading fecal pellets through coprophagy (ingestion), coprorhexy (fragmentation) and coprochaly (loosening), occasioning additional losses by respiration and promoting bacterial remineralisation, but also sustaining the flux at depth by egesting new fecal pellets (Giering et al., 2014; Iversen and Poulsen, 2007). Progressive bacterial remineralisation of the DOC to its inorganic form (DIC) in the water column, maintains the carbon concentration gradient between the surface and deep ocean. Lateral advection and vertical mixing promote the return of DIC to the surface and its subsequent ventilation. The average time for the DIC to return back to the surface, known as the 'remineralisation length scale' (RLS) depends on the depths over which carbon was remineralised. Below 1000 m in the deep ocean, the time for the DIC to return back to the surface by physical processes is on a scale of centuries to millennia, with strong geographic variations (Passow and Carlson, 2012; Primeau, 2006).

The flux of particulate carbon transferred through the mesopelagic layer which reaches the deep ocean (below 1000 meters) hereafter called the 'sequestration flux', is generally less than 10% of the POC exported out of the surface ocean (François et al., 2002; Henson et al., 2012; Honjo et al., 1982). The consumption by benthic communities induces additional losses and the flux of carbon actually buried in deep-sea sediments represents only 0.01% of the carbon initially produced in the surface layer (Honjo, 1996; Jahnke, 1996; Martin et al., 1987; Suess, 1980). The term 'sequestration' generally describes the removal of inorganic or organic carbon from the global cycle for a period $\geq$ 100 years (Legendre et al., 2015). The BCP appears quite inefficient at sequestering carbon because of all the losses occurring during the transfer from its fixation

to its sequestration. The relative contributions of the BCP in the total oceanic carbon pump (the physically–mediated 'solubility pump' + the BCP) (Volk and Hoffert, 1985) still suffer large uncertainties (Gruber and Sarmiento, 2002; Reid et al., 2009), but two thirds of the total uptake of CO_2 by the global ocean (total uptake estimated at 2.6±0.5 Gt C yr^{-1} for the period 2004-2013; Le Quéré et al., 2014) could be operated by the BCP (Passow and Carlson, 2012). An alteration of the biologically-mediated BCP, feared as a consequence of the global climate change (mostly via increased stratification and ocean acidification; Bopp et al., 2013; see Turner 2015 for a review) would have largely unknown and potentially serious consequences. Thus, it appears crucial to clearly identify the controls on the efficiency of the BCP, in order to better predict the potential consequences of its alteration. It is particularly important to investigate these controls in the Southern Ocean which plays a major role in mitigating atmospheric CO_2 (e.g. in 2008, it contributed over 40% of the anthropogenic CO_2 inventory in the global ocean; Khatiwala et al., 2009).

1.2 Controls on the efficiency of the BCP

The efficiency of the BCP, i.e. the fraction of the carbon fixed in the euphotic zone that is effectively sequestered, presents large spatio–temporal variations (mostly at regional and seasonal scales) (Buesseler, 1998; De La Rocha and Passow, 2007; Henson et al., 2015; Honjo et al., 2008; Neuer et al., 2002). The difficulty of explaining these variations is that controls can operate at each step of the processes involved and because of their dependence to the multiple possible interactions between the different trophic levels involved (Boyd and Trull, 2007; De La Rocha and Passow, 2007). Disentangling the physical from the biological influences and weighting their relative importance also appear to be big challenges. After more than 30 years of research, many gaps remain in our knowledge of the BCP.

The importance of large phytoplankton aggregates and zooplankton fecal pellets in the export of organic carbon have long been known, but the conditions in which one or the other carry the largest fraction of the carbon flux remain unclear. Studies report fluxes dominated by either large phytodetrital aggregates (Alldredge and Gotschalk, 1989; Burd and Jackson, 2009; De La Rocha and Passow, 2007; Jackson, 1990; Turner, 2002) or fecal pellets (Bishop et al., 1977; Cavagna et al., 2013; Ebersbach and Trull, 2008; Fowler and Knauer, 1986; Pilskaln and Honjo, 1987;

Wassmann et al., 2000). There is a great interest in understanding the factors which promote a direct export by phytoplankton aggregates, because it could be the most efficient mode of the biological carbon pump since it minimises the losses otherwise associated with the consumption by higher trophic levels (Buesseler and Boyd, 2009). Ecosystem structure, reflected by planktonic community composition appears to elect the dominant carbon export mode (Ebersbach and Trull, 2008; Ebersbach et al., 2011; Wassmann, 1998; Wiedmann et al., 2014). During the growing season, phyto- and zooplankton biomass variations related to their trophic interactions depend on several factors including plankton assemblages and their respective initial biomass levels, physiological rates and resistance to grazing (Miller and Wheeler, 2012). The particle sinking flux generated by these interactions, acquires its initial characteristics in term of volume and size spectra (Fowler and Knauer, 1986; McCave, 1984; Michaels and Silver, 1988; Silver and Gowing, 1991). Most of the questions related to the efficiency of the BCP lies in the observation that the biomass accumulation itself does not determine the 'strength' of the BCP (i.e. the magnitude of the concentration gradient it creates; Volk and Hoffert, 1985). It is suggested by many studies reporting inconsistencies between the primary production in the surface layer and its associated carbon export flux (Buesseler, 1998; Ebersbach et al., 2011; Lam and Bishop, 2007). It is possibly due to the variety of particles produced (i.e. single cells, marine snow, fecal pellets) having different abilities to transport carbon to the deep ocean. Within a same category of particles a wide range of export efficiency can also be observed. This is true for the large marine snow aggregates which display great variations of their size, structure and composition (Alldredge, 1979; Alldredge and Gotschalk, 1988; Alldredge and Silver, 1988; Asper, 1986; Shanks and Trent, 1980). The relative efficiency of each particle category at exporting carbon appears to depend on their physical and biological properties. The three 'pillars' of a particle efficiency at exporting carbon are its carbon content, its sinking velocity and its sensitivity to degradation. Therefore, the best candidate to the most efficient carbon export is a carbon–rich, fast–sinking, and degradation–resistant particle. Far from this simplistic view, observations show a large range of combinations of these three properties amongst natural particles (Turner, 2015 and references therein).

The sinking velocity started to receive attention in the 1970's (e.g. Kajihara, 1971; Fowler and Small, 1972). Based on theoretical laws, particle size was first investigated as the main control of the sinking velocity, but discrepancies highlighted a higher complexity (Diercks and

Asper, 1997; Engel and Schartau, 1999; Iversen and Ploug, 2010). Today, controls on the sinking velocity of large marine aggregates are still unclear. The main reasons are the large variety of the components that these particles scavenge during their fall and the various ways that they are assembled, defining different sinking properties for almost every single particle. Especially, the excess density of each particle composing the aggregate (defined as the density difference between the particle and the surrounding water) can strongly vary. The role of phytoplankton community structure in setting the efficiency of carbon export has been suggested since the 1990's, but most of the studies explained these controls through phytoplankton cell size (Boyd and Newton, 1995; Boyd et al., 1999) and ballasting of the cells with biominerals (Armstrong et al., 2001; Klaas and Archer, 2002). It is unclear, however how different phytoplankton assemblages affect the sinking velocity of their aggregates.

Variability in planktonic community structure is observed at a wide range of spatio–temporal scales. Based on the potential links between plankton community structure, flux characteristics and particle sinking properties, it seems possible that the variations of plankton communities could play a large role in spatio–temporal variations of the efficiency of the BCP. By focusing on the ecosystem controls on carbon export efficiency in the Southern Ocean, this thesis addressed three of the main gaps in our understanding of the BCP:

i. How does ecosystem trophic structure determine the dominant carbon export mode (via phytodetrital aggregates or zooplankton fecal pellets) and which one is the most efficient vector for carbon export?

ii. What is the role played by planktonic community structure in the control of marine snow sinking velocities?

iii. How do spatio–temporal variations in planktonic community structure affect carbon export efficiency?

Different approaches and methods were used to answer these questions. Experiments, field sampling and modelling studies were combined to explore the links between ecosystem structure and carbon export efficiency. The Kerguelen region (Southern Ocean) was chosen for its context of natural iron–fertilisation which frames a variety of ecosystem structures and associated carbon export efficiencies (Armand et al., 2008; Blain et al., 2008a). The last section of this

'Introduction' chapter presents the study area and describes briefly the approaches and methods used.

1.3 Study area and methodology

1.3.1 The Kerguelen region: a natural laboratory

The Kerguelen Plateau is the largest volcanic plateau in the Southern Ocean, lying approximately from 45 to 62°S Latitude and 63 to 84°E Longitude (Fig. 1.2). This large volcanic formation induces an 'island mass effect' (Doty and Oguri, 1956) and promotes one of the largest seasonal phytoplankton biomass accumulations (or 'bloom') in the Southern Ocean. Hart (1942) was the first to mention that a release of iron might be responsible for the observed increase of biomass in the vicinity of islands in the Southern Ocean. However, Martin (1990) provided the first evidence and formulated the so-called 'iron hypothesis' which postulates that iron is a limiting micronutrient able to fuel the primary productivity in the High Nutrient–Low Chlorophyll (HNLC) waters of the Southern Ocean. This hypothesis has been confirmed by numerous purposeful mesoscale iron–enrichment and natural iron–fertilisation experiments conducted in the Southern Ocean (Blain et al., 2007; Boyd et al., 2000; Coale et al., 2004; Pollard et al., 2009; Smetacek, 2001; Smetacek et al., 2012). The KErguelen Ocean and Plateau compared study (KEOPS) was the first major investigation of the effect of iron fertilisation on carbon sequestration in a natural context (Blain et al., 2008a). KEOPS, conducted in January-February 2005 investigated the bloom to explore the role of natural iron supply on biologically–driven carbon sequestration over the Kerguelen Plateau.

Two distinct regions of the bloom can be distinguished (Fig. 1.3): a long plume extending eastward of the Kerguelen Islands and impacted by complex mesoscale structures due to the close proximity of the polar and subantarctic fronts (PF and SAF), and a bloom over the plateau between the Kerguelen and Heard Islands (Blain et al., 2008b). The KEOPS study revealed a bloom dominated by diatom assemblages which varied in space and time over the course of the survey (less than one month in duration). At the on–plateau bloom reference station, the phytoplankton community was first dominated by the small *Chaetoceros Hyalochaete* spp. and later by a remnant *Eucampia antarctica* assemblage (Armand et al., 2008). In contrast, the HNLC reference station (i.e. low iron waters) was dominated by *Fragilariopsis pseudonana* and

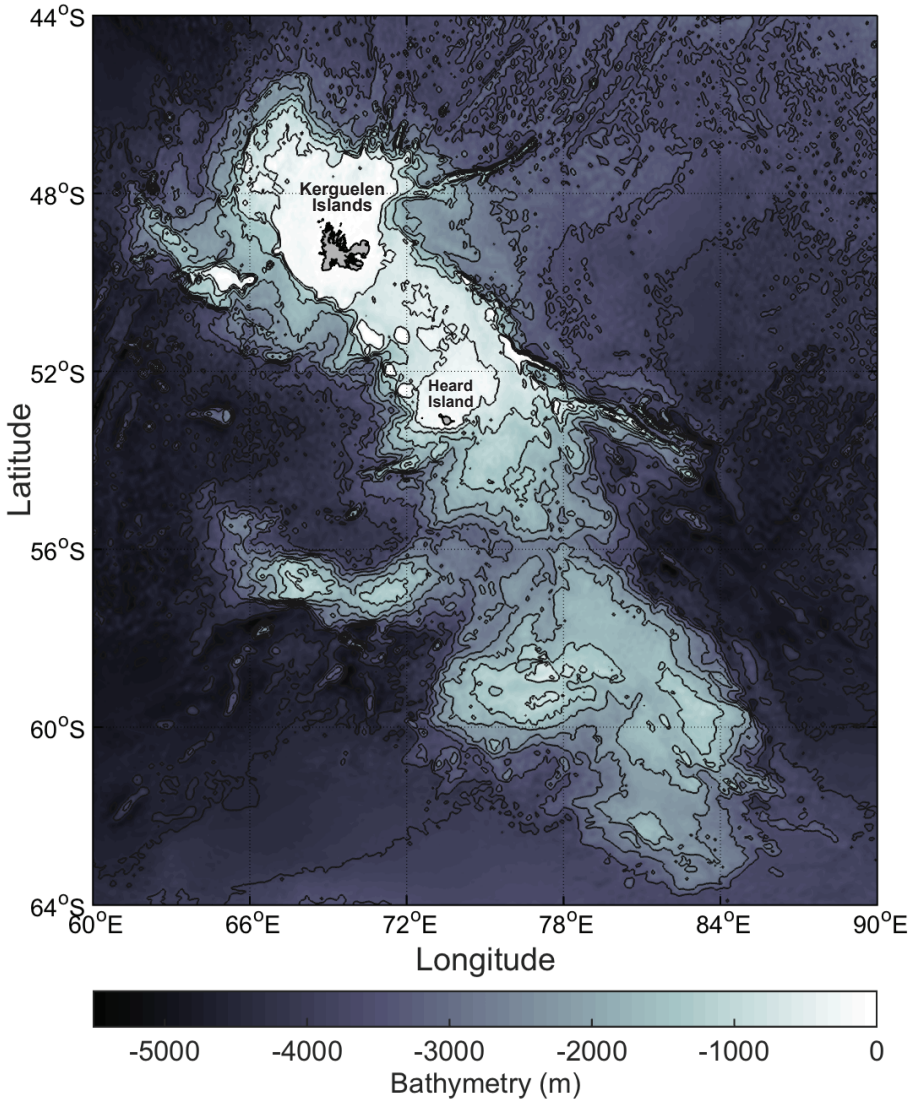

Figure 1.2: Bathymetric map of the Kerguelen Plateau showing the location of Kerguelen and Heard Islands. Data from the NOAA 1 Arc-Minute Global Relief Model ETOPO1 (Amante and Eakins, 2009).

Fragilariopsis kerguelensis throughout the survey. The study of sinking particles collected over the plateau and at its periphery revealed an important role played by zooplankton in the export of carbon in late summer (Ebersbach and Trull, 2008).

The questions tackled by this thesis (see previous section) were addressed using data from the second KErguelen Ocean and Plateau compared study (KEOPS2). KEOPS2 was conducted onboard the RV *Marion Dufresne*, over and downstream of the Kerguelen Plateau to re–investigate the bloom earlier in the season, during its initiation (October–November 2011). The main objectives of KEOPS2 were to explore further the modes of iron supply and their effects on ecosystem structure and subsequent carbon export efficiency.

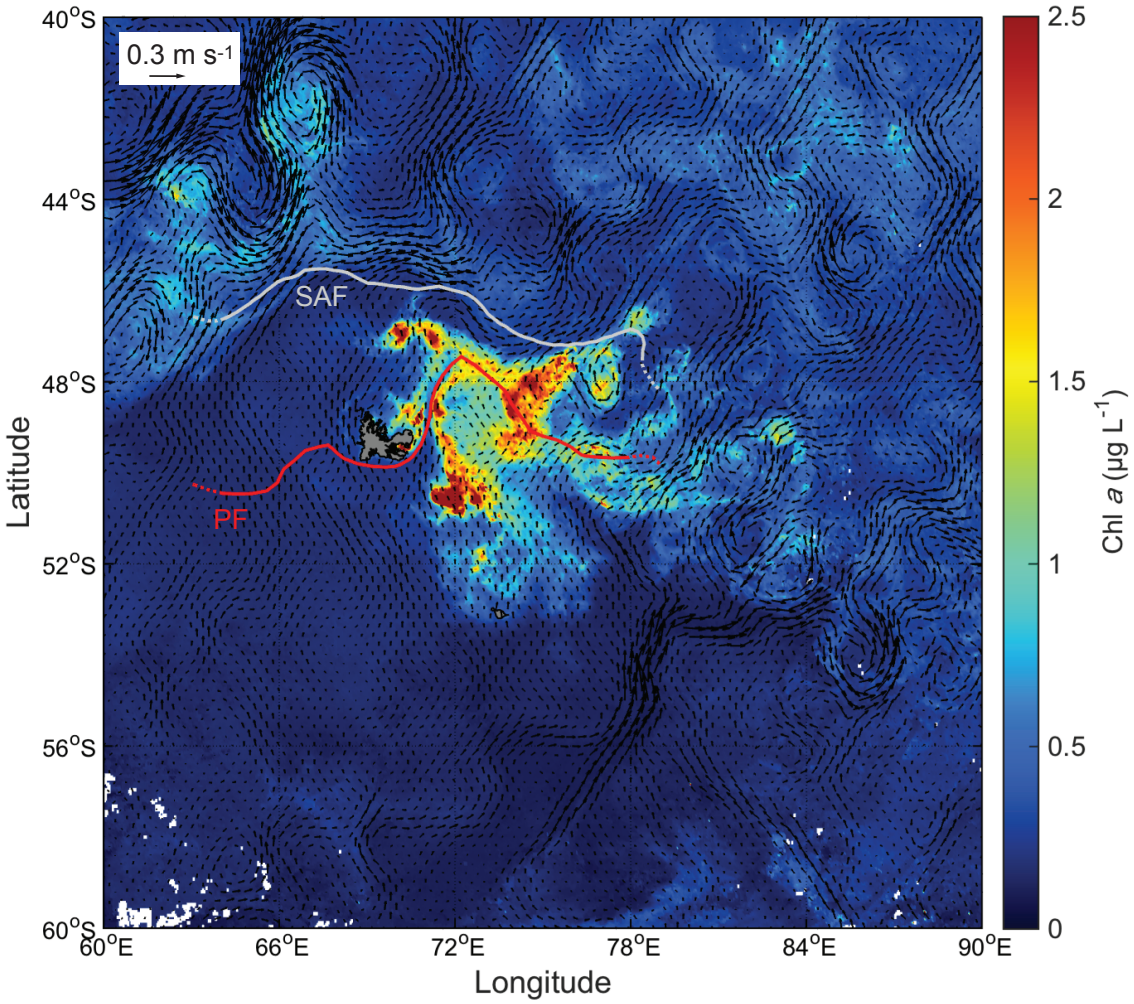

Figure 1.3: Map of the average surface chlorophyll *a* concentration (Chl. *a*) in the Kerguelen region in November 2011 [data from MODIS-Aqua satellite (CLS-CNES)]. Surface geostrophic velocities (arrows) derived from sea surface height are represented for the same period [data from the Integrated Marine Observing System (IMOS)]. The location of the main Southern Ocean fronts limited to the vicinity of the Kerguelen Islands (from 63 °E to 79 °E) is also indicated based on Park et al. (2014). SAF: Sub–Antarctic front (grey line); PF: Polar front (red line). The map illustrates the interactions between Chl. *a* concentrations and the complex physical context induced by the presence of the two oceanic fronts.

1.3.2 Approaches, material and methods

The modes and efficiency of carbon export at the early stage of the Kerguelen bloom were explored by collecting natural sinking particles at sites presenting various biomass levels and contrasting planktonic community structures. Free-drifting standard sediment traps (PPS3/3) and polyacrylamide gel–filled sediment traps were deployed at several depths below the mixed layer (between 100 and 400 m depth) in HNLC waters and at sites under variable iron-fertilisation influences. PPS3/3 traps (Technicap, La Turbie, France) consist of a cylinder with an internal conical funnel, which collects the sinking flux in individual cups over a pre–determined duration and according to a pre–programmed sequence. Once in a cup, all particles collected can break–

up, collide and aggregate, thus this type of trap is used to measure the bulk chemical composition of the flux but cannot inform on the categories of particle constitutive of the flux. To isolate the sinking particles and preserve their initial structure by a slow deceleration, cups filled with a highly viscous medium (polyacrylamide gel) were placed at the base of cylindrical sediment traps (Ebersbach and Trull, 2008; Lundsgaard, 1995). These were deployed at the same sites and depths as the PPS3/3 traps to relate biogeochemical composition of the sinking flux to its characteristics in term of particle type, number and size. This work is presented in Chapter 2.

Controls on the sinking velocity of large phytodetrital aggregates ('marine snow') forming the main numerical fraction of the flux collected in traps, were investigated by an experimental approach. At similar sites to the trap deployments, phytoplankton assemblages were sampled from Niskin bottles mounted on a CTD rosette deployed in the euphotic zone, and incubated in cylindrical tanks placed on a rotating table. By always keeping the particles in suspension, this 'roller tank' technique developed by Shanks and Edmondson (1989) simulates the continuous fall of particles in the water column and allow their aggregation by differential settling as it would occur in the water column (i.e. the large fast-sinking particles scavenge the smaller suspended or slow-sinking particles). An extensive set of morphological, chemical and biological properties were measured on the aggregates formed and explored as potential controls on the sinking velocity. Particular focus was made on relating particle sinking velocity determinant of carbon export efficiency and variation of phytoplankton mixtures composing the aggregates. This experimental study is shown in Chapter 3.

The relationship identified between the proportion of different phytoplankton morphological types composing the aggregates and their sinking velocity, was introduced in a generic 3–D coupled physical-biogeochemical model. The model was used to explore further the influence of plankton community variations on carbon export efficiency. The physical module was the Sparse Hydrodynamic Ocean Code or 'SHOC' part of the Ecosystem Modelling Suite (EMS) developed at the Commonwealth Scientific and Industrial Research Organisation, division of Marine and Atmospheric Research (CSIRO CMAR, Hobart, Australia). Because of the complexity of the physical context around the Kerguelen Islands, mainly due to the proximity of the polar and subantarctic fronts, the physics was resolved at the Southern Ocean Time Series (SOTS) located South of Tasmania (between the sub–tropical and sub–antarctic fronts near 140°E, 47°S) where an extensive dataset is provided by the Integrated Marine Observing System (IMOS). The

biogeochemical module of the model is a classical Nutrient Phytoplankton Zooplankton Detritus (NNPPZZDD) model where physiological rates are scaled on temperature. Phytoplankton growth depends on dissolved nutrients and light availability, and small and large zooplankton graze respectively on small and large phytoplankton. The relative contributions of small and large phytoplankton and zooplankton to the flux directed toward the detritus are used to compute a variable detritus sinking velocity. The carbon flux is then calculated below the euphotic zone. Seasonal and inter–annual variability in planktonic community structure induced by the physical forcing from SHOC, were related to the changes of carbon flux and thus assessed in term of carbon export efficiency. This is presented in Chapter 4.

Conclusions from these field, experimental and model observations are then summarised in Chapter 5, to provide an overall perspective on future research needs.

References

Acuña, J. L., López-Alvarez, M., Nogueira, E., and González-Taboada, F.: Diatom flotation at the onset of the spring phytoplankton bloom: an *in situ* experiment, Marine Ecology Progress Series, 400, 115–125, doi:10.3354/meps08405, 2010.

Alldredge, A. L.: The chemical composition of macroscopic aggregates in two neretic seas, Limnology and Oceanography, 24, 855–866, doi:10.2307/2835325, 1979.

Alldredge, A. L.: Particle Aggregation Dynamics, Encyclopedia of Ocean Sciences, 4, 2090–2097, 2001.

Alldredge, A. L. and Gotschalk, C.: In Situ Settling Behavior of Marine Snow, Limnology and Oceanography, 33, 339–351, doi:10.2307/2837008, 1988.

Alldredge, A. L. and Gotschalk, C. C.: Direct observations of the mass flocculation of diatom blooms: characteristics, settling velocities and formation of diatom aggregates, Deep Sea Research Part A. Oceanographic Research Papers, 36, 159–171, doi:10.1016/0198-0149(89)90131-3, 1989.

Alldredge, A. L. and Silver, M. W.: Characteristics, dynamics and significance of marine snow, Progress in Oceanography, 20, 41–82, doi:10.1016/0079-6611(88)90053-5, 1988.

Amante, C. and Eakins, B.: ETOPO1 1 Arc-Minute Global Relief Model: Procedures, Data Sources and Analysis. NOAA Technical Memorandum NESDIS NGDC-24, National Geophysical Data Center, NOAA, 2009.

Armand, L. K., Cornet-Barthaux, V., Mosseri, J., and Queguiner, B.: Late summer diatom biomass and community structure on and around the naturally iron-fertilised Kerguelen Plateau in the Southern Ocean, Deep Sea Research Part II: Topical Studies in Oceanography, 55, 653–676, doi:10.1016/j.dsr2.2007.12.031, 2008.

Armstrong, R. A., Lee, C., Hedges, J. I., Honjo, S., and Wakeham, S. G.: A new, mechanistic model for organic carbon fluxes in the ocean based on the quantitative association of POC with ballast minerals, Deep-Sea Research Part II: Topical Studies in Oceanography, 49, 219–236, doi:10.1016/S0967-0645(01)00101-1, 2001.

Asper, V.: Accelerated settling of particular matter by marine snow aggregates, Ph.D. thesis, Woods Hole Oceanographic Institution and Massachusetts Institute of Technology, Massachusetts, 1986.

Bishop, J. K. B., Edmond, J. M., Ketten, D. R., Bacon, M. P., and Silker, W. B.: The chemistry, biology, and vertical flux of particulate matter from the upper 400 m of the equatorial Atlantic Ocean, Deep Sea Research, 24, 511–548, doi:10.1016/0146-6291(77)90526-4, 1977.

Blain, S., Quéguiner, B., Armand, L., Belviso, S., Bombled, B., Bopp, L., Bowie, A., Brunet, C., Brussaard, C., Carlotti, F., Christaki, U., Corbière, A., Durand, I., Ebersbach, F., Fuda,

J. L., Garcia, N., Gerringa, L., Griffiths, B., Guigue, C., Guillerm, C., Jacquet, S., Jeandel, C., Laan, P., Lefèvre, D., Lo Monaco, C., Malits, A., Mosseri, J., Obernosterer, I., Park, Y. H., Picheral, M., Pondaven, P., Remenyi, T., Sandroni, V., Sarthou, G., Savoye, N., Scouarnec, L., Souhaut, M., Thuiller, D., Timmermans, K., Trull, T., Uitz, J., van Beek, P., Veldhuis, M., Vincent, D., Viollier, E., Vong, L., and Wagener, T.: Effect of natural iron fertilization on carbon sequestration in the Southern Ocean, Nature, 446, 1070–1074, doi:10.1038/nature05700, 2007.

Blain, S., Queguiner, B., and Trull, T.: The natural iron fertilization experiment KEOPS (KErguelen Ocean and Plateau compared Study): An overview, Deep-Sea Research Part Ii-Topical Studies in Oceanography, 55, 559–565, doi:10.1016/j.dsr2.2008.01.002, 2008a.

Blain, S., Sarthou, G., and Laan, P.: Distribution of dissolved iron during the natural iron-fertilization experiment KEOPS (Kerguelen Plateau, Southern Ocean), Deep-Sea Research Part Ii-Topical Studies in Oceanography, 55, 594–605, doi:10.1016/j.dsr2.2007.12.028, 2008b.

Bopp, L., Resplandy, L., Orr, J. C., Doney, S. C., Dunne, J. P., Gehlen, M., Halloran, P., Heinze, C., Ilyina, T., Séférian, R., Tjiputra, J., and Vichi, M.: Multiple stressors of ocean ecosystems in the 21st century: projections with CMIP5 models, Biogeosciences, 10, 6225–6245, doi:10.5194/bg-10-6225-2013, 2013.

Boyd, P. and Newton, P.: Evidence of the potential influence of planktonic community structure on the interannual variability of particulate organic carbon flux, Deep Sea Research Part I: Oceanographic Research Papers, 42, 619–639, doi:10.1016/0967-0637(95)00017-Z, 1995.

Boyd, P. and Trull, T.: Understanding the export of biogenic particles in oceanic waters: Is there consensus?, Progress In Oceanography, 72, 276–312, doi:10.1016/j.pocean.2006.10.007, 2007.

Boyd, P. W., Sherry, N. D., Berges, J. A., Bishop, J. K. B., Calvert, S. E., Charette, M. A., Giovannoni, S. J., Goldblatt, R., Harrison, P. J., Moran, S. B., Roy, S., Soon, M., Strom, S., Thibault, D., Vergin, K. L., Whitney, F. A., and Wong, C. S.: Transformations of biogenic particulates from the pelagic to the deep ocean realm, Deep Sea Research Part II: Topical Studies in Oceanography, 46, 2761–2792, doi:10.1016/S0967-0645(99)00083-1, 1999.

Boyd, P. W., Watson, A. J., Law, C. S., Abraham, E. R., Trull, T., Murdoch, R., Bakker, D. C. E., Bowie, A. R., Buesseler, K. O., and Chang, H.: A mesoscale phytoplankton bloom in the polar Southern Ocean stimulated by iron fertilization, Nature, 407, 695–702, doi:10.1038/35037500, 2000.

Buesseler, K. O.: The decoupling of production and particulate export in the surface ocean, Global Biogeochemical Cycles, 12, 297–310, doi:10.1029/97GB03366, 1998.

Buesseler, K. O. and Boyd, P. W.: Shedding light on processes that control particle export and flux attenuation in the twilight zone of the open ocean, Limnology and Oceanography, 54, 1210–1232, doi:10.4319/lo.2009.54.4.1210, 2009.

Buesseler, K. O., Lamborg, C. H., Boyd, P. W., Lam, P. J., Trull, T. W., Bidigare, R. R., Bishop, J. K. B., Casciotti, K. L., Dehairs, F., Elskens, M., Honda, M., Karl, D. M., Siegel, D. A., Silver, M. W., Steinberg, D. K., Valdes, J., Van Mooy, B., and Wilson, S.: Revisiting Carbon Flux Through the Ocean's Twilight Zone, Science, 316, 567–570, doi:10.1126/science.1137959, 2007.

Burd, A. B. and Jackson, G. A.: Particle Aggregation, Annual Review of Marine Science, 1, 65–90, doi:10.1146/annurev.marine.010908.163904, 2009.

Cavagna, A.-J., Dehairs, F., Bouillon, S., Woule-Ebongué, V., Planchon, F., Delille, B., and Bouloubassi, I.: Water column distribution and carbon isotopic signal of cholesterol, brassicasterol and particulate organic carbon in the Atlantic sector of the Southern Ocean, Biogeosciences, 10, 2787–2801, doi:10.5194/bg-10-2787-2013, 2013.

Coale, K. H., Johnson, K. S., Chavez, F. P., Buesseler, K. O., Barber, R. T., Brzezinski, M. A., Cochlan, W. P., Millero, F. J., Falkowski, P. G., Bauer, J. E., Wanninkhof, R. H., Kudela, R. M., Altabet, M. A., Hales, B. E., Takahashi, T., Landry, M. R., Bidigare, R. R., Wang, X., Chase, Z., Strutton, P. G., Friederich, G. E., Gorbunov, M. Y., Lance, V. P., Hilting, A. K., Hiscock, M. R., Demarest, M., Hiscock, W. T., Sullivan, K. F., Tanner, S. J., Gordon, R. M., Hunter, C. N., Elrod, V. A., Fitzwater, S. E., Jones, J. L., Tozzi, S., Koblizek, M., Roberts, A. E., Herndon, J., Brewster, J., Ladizinsky, N., Smith, G., Cooper, D., Timothy, D., Brown, S. L., Selph, K. E., Sheridan, C. C., Twining, B. S., and Johnson, Z. I.: Southern Ocean Iron Enrichment Experiment: Carbon Cycling in High- and Low-Si Waters, Science, 304, 408–414, doi:10.1126/science.1089778, 2004.

Corner, E. D. S., Head, R. N., and Kilvington, C. C.: On the nutrition and metabolism of zooplankton. VIII. the grazing of *Biddulphia* cells by *Calanus helgolandicus*, Journal of the Marine Biological Association of the United Kingdom, 52, 847–861, doi:10.1017/S0025315400040595, 1972.

De La Rocha, C. L. and Passow, U.: Factors influencing the sinking of POC and the efficiency of the biological carbon pump, Deep Sea Research Part II: Topical Studies in Oceanography, 54, 639–658, doi:10.1016/j.dsr2.2007.01.004, 2007.

Diercks, A.-R. and Asper, V. L.: In situ settling speeds of marine snow aggregates below the mixed layer: Black Sea and Gulf of Mexico, Deep Sea Research Part I: Oceanographic Research Papers, 44, 385–398, doi:10.1016/S0967-0637(96)00104-5, 1997.

Doty, M. S. and Oguri, M.: The Island Mass Effect, Journal du Conseil, 22, 33–37, doi:10.1093/icesjms/22.1.33, 1956.

Ducklow, H., Steinberg, D., and Buesseler, K.: Upper ocean carbon export and the biological pump, Oceanography, 14, 50–58, doi:10.5670/oceanog.2001.06, 2001.

Ebersbach, F. and Trull, T. W.: Sinking particle properties from polyacrylamide gels during the KErguelen Ocean and Plateau compared Study (KEOPS): Zooplankton control of carbon export in an area of persistent natural iron inputs in the Southern Ocean, Limnology and Oceanography, 53, 212–224, doi:10.2307/40006162, 2008.

Ebersbach, F., Trull, T. W., Davies, D. M., and Bray, S. G.: Controls on mesopelagic particle fluxes in the Sub-Antarctic and Polar Frontal Zones in the Southern Ocean south of Australia in summer—Perspectives from free-drifting sediment traps, Deep Sea Research Part II: Topical Studies in Oceanography, 58, 2260 – 2276, doi:10.1016/j.dsr2.2011.05.025, 2011.

Engel, A. and Schartau, M.: Influence of transparent exopolymer particles (TEP) on sinking velocity of Nitzschia closterium aggregates, Marine Ecology Progress Series, 182, 69–76, doi:10.3354/meps182069, 1999.

Fowler, S. W. and Knauer, G. A.: Role of large particles in the transport of elements and organic compounds through the oceanic water column, Progress in Oceanography, 16, 147–194, doi:10.1016/0079-6611(86)90032-7, 1986.

Fowler, S. W. and Small, L. F.: Sinking rates of euphausiid fecal pellets, Limnology and Oceanography, 17, 293–296, doi:10.1016/0079-6611(86)90032-7, 1972.

François, R., S., H., P., K., and S., M.: Factors controlling the flux of organic carbon to the bathypelagic zone of the ocean, Global Biogeochemical Cycles, 16, doi:10.1029/2001gb001722, 2002.

Giering, S. L. C., Sanders, R., Lampitt, R. S., Anderson, T. R., Tamburini, C., Boutrif, M., Zubkov, M. V., Marsay, C. M., Henson, S. A., Saw, K., Cook, K., and Mayor, D. J.: Reconciliation of the carbon budget in the ocean's twilight zone, Nature, 507, 480–483, doi:10.1038/nature13123, 2014.

Gross, F. and Zeuthen, E.: The Buoyancy of Plankton Diatoms: A Problem of Cell Physiology, Proceedings of the Royal Society of London. Series B, Biological Sciences, 135, 382–389, doi:10.2307/82472, 1948.

Gruber, N. and Sarmiento, J. L.: Large-scale biogeochemical-physical interactions in elemental cycles, in: The sea, edited by Robinson, A. R., McCarthy, J. J., and Rothschild, B. J., vol. 12, chap. 9, pp. 337–399, John Wiley & Sons, 2002.

Hart, T.: Phytoplankton periodicity in Antarctic surface water, Discovery Reports, 21, 261–356, 1942.

Henson, S. A., Sanders, R., Madsen, E., Morris, P. J., Le Moigne, F., and Quartly, G. D.: A reduced estimate of the strength of the ocean's biological carbon pump, Geophysical Research Letters, 38, doi:10.1029/2011gl046735, 2011.

Henson, S. A., Sanders, R., and Madsen, E.: Global patterns in efficiency of particulate organic carbon export and transfer to the deep ocean, Global Biogeochemical Cycles, 26, GB1028, doi:10.1029/2011GB004099, 2012.

Henson, S. A., Yool, A., and Sanders, R.: Variability in efficiency of particulate organic carbon export: A model study, Global Biogeochemical Cycles, 29, 33–45, doi:10.1002/2014GB004965, 2015.

Honjo, S.: Fluxes of particles to the interior of the open oceans, in: Particle flux in the Ocean, edited by Ittekkot, V., Schafer, P., Honjo, S., and Depetris, P., pp. 91–154, Wiley, 1996.

Honjo, S., Manganini, S. J., and Cole, J. J.: Sedimentation of biogenic matter in the deep ocean, Deep Sea Research Part A. Oceanographic Research Papers, 29, 609–625, doi:10.1016/0198-0149(82)90079-6, 1982.

Honjo, S., Manganini, S. J., Krishfield, R. A., and Francois, R.: Particulate organic carbon fluxes to the ocean interior and factors controlling the biological pump: A synthesis of global sediment trap programs since 1983, Progress in Oceanography, 76, 217–285, doi:10.1016/j.pocean.2007.11.003, 2008.

Iversen, M. H. and Ploug, H.: Ballast minerals and the sinking carbon flux in the ocean: carbon-specific respiration rates and sinking velocity of marine snow aggregates, Biogeosciences, 7, 2613–2624, doi:10.5194/bg-7-2613-2010, 2010.

Iversen, M. H. and Poulsen, L. K.: Coprorhexy, coprophagy, and coprochaly in the copepods *Calanus helgolandicus*, *Pseudocalanus elongatus*, and *Oithona similis*, Marine Ecology Progress Series, 350, 79–89, doi:10.3354/meps07095, 2007.

Jackson, G. A.: A model of the formation of marine algal flocs by physical coagulation processes, Deep-Sea Research Part I: Oceanographic Research Papers, 37, 1197–1211, doi:10.1016/0198-0149(90)90038-W, 1990.

Jahnke, R. A.: The global ocean flux of particulate organic carbon: Areal distribution and magnitude, Global Biogeochemical Cycles, 10, 71–88, 1996.

Kajihara, M.: Settling velocity and porosity of large suspended particle, Journal of the Oceanographical Society of Japan, 27, 158–162, doi:10.1007/BF02109135, 1971.

Khatiwala, S., Primeau, F., and Hall, T.: Reconstruction of the history of anthropogenic CO2 concentrations in the ocean, Nature, 462, 346–349, doi:10.1038/nature08526, 2009.

Klaas, C. and Archer, D. E.: Association of sinking organic matter with various types of mineral ballast in the deep sea: Implications for the rain ratio, Global Biogeochemical Cycles, 16, 1116, doi:10.1029/2001GB001765, 2002.

Lam, P. J. and Bishop, J. K. B.: High biomass, low export regimes in the Southern Ocean, Deep Sea Research Part II: Topical Studies in Oceanography, 54, 601–638, doi:10.1016/j.dsr2.2007.01.013, 2007.

Le Quéré, C., Moriarty, R., Andrew, R. M., Peters, G. P., Ciais, P., Friedlingstein, P., Jones, S. D., Sitch, S., Tans, P., Arneth, A., Boden, T. A., Bopp, L., Bozec, Y., Canadell, J. G., Chevallier, F., Cosca, C. E., Harris, I., Hoppema, M., Houghton, R. A., House, J. I., Jain, A., Johannessen, T., Kato, E., Keeling, R. F., Kitidis, V., Klein Goldewijk, K., Koven, C., Landa, C. S., Landschützer, P., Lenton, A., Lima, I. D., Marland, G., Mathis, J. T., Metzl, N., Nojiri, Y., Olsen, A., Ono, T., Peters, W., Pfeil, B., Poulter, B., Raupach, M. R., Regnier, P., Rödenbeck, C., Saito, S., Salisbury, J. E., Schuster, U., Schwinger, J., Séférian, R., Segschneider, J., Steinhoff, T., Stocker, B. D., Sutton, A. J., Takahashi, T., Tilbrook, B., van der Werf, G. R., Viovy, N., Wang, Y.-P., Wanninkhof, R., Wiltshire, A., and Zeng, N.: Global carbon budget 2014, Earth System Science Data Discussions, 7, 521–610, doi:10.5194/essdd-7-521-2014, 2014.

Legendre, L., Rivkin, R. B., Weinbauer, M. G., Guidi, L., and Uitz, J.: The microbial carbon pump concept: Potential biogeochemical significance in the globally changing ocean, Progress in Oceanography, pp. –, doi:10.1016/j.pocean.2015.01.008, 2015.

Lundsgaard, C.: Use of a high viscosity medium in studies of aggregates, in: Sediment trap studies in the Nordic countries. 3. Proceeding of the Symposium on Seasonal Dynamics of Planktonic Ecosystems and Sedimentation in Coastal Nordic Waters. Finnish Environment Agency, edited by Floderus, S., Heisakanen, A. S., Oleson, M., and Wassmann, P., pp. 141–152, Numi Print, Oy, Germany, 1995.

Martin, J. H.: Glacial-interglacial CO_2 change: The iron hypothesis, Paleoceanography, 5, 1–13, doi:10.1029/PA005i001p00001, 1990.

Martin, J. H., Knauer, G. A., Karl, D. M., and Broenkow, W. W.: VERTEX: carbon cycling in the northeast Pacific, Deep Sea Research Part A. Oceanographic Research Papers, 34, 267–285, doi:10.1016/0198-0149(87)90086-0, 1987.

McCave, I. N.: Size spectra and aggregation of suspended particles in the deep ocean, Deep Sea Research Part A. Oceanographic Research Papers, 31, 329–352, doi:10.1016/0198-0149(84)90088-8, 1984.

Michaels, A. F. and Silver, M. W.: Primary production, sinking fluxes and the microbial food web, Deep Sea Research Part A. Oceanographic Research Papers, 35, 473–490, doi:10.1016/0198-0149(88)90126-4, 1988.

Miller, C. and Wheeler, P.: Biological oceanography, Wiley-Blackwell, second edn., 2012.

Møller, E. F.: Sloppy feeding in marine copepods: prey-size-dependent production of dissolved organic carbon, Journal of Plankton Research, 27, 27–35, doi:10.1093/plankt/fbh147, 2005.

Neuer, S., Davenport, R., Freudenthal, T., Wefer, G., Llinás, O., Rueda, M.-J., Steinberg, D. K., and Karl, D. M.: Differences in the biological carbon pump at three subtropical ocean sites, Geophysical Research Letters, 29, 32–1–32–4, doi:10.1029/2002GL015393, 2002.

Park, Y.-H., Durand, I., Kestenare, E., Rougier, G., Zhou, M., d'Ovidio, F., Cotté, C., and Lee, J.-H.: Polar Front around the Kerguelen Islands: An up-to-date determination and associated circulation of surface/subsurface waters, Journal of Geophysical Research: Oceans, 119, 6575–6592, doi:10.1002/2014JC010061, 2014.

Passow, U. and Carlson, C.: The biological pump in a high CO_2 world, Marine Ecology Progress Series, 470, 249–271, doi:10.3354/meps09985, 2012.

Pilskaln, C. H. and Honjo, S.: The fecal pellet fraction of biogeochemical particle fluxes to the deep sea, Global Biogeochemical Cycles, 1, 31–48, doi:10.1029/GB001i001p00031, 1987.

Pollard, R. T., Salter, I., Sanders, R. J., Lucas, M. I., Moore, C. M., Mills, R. A., Statham, P. J., Allen, J. T., Baker, A. R., Bakker, D. C. E., Charette, M. A., Fielding, S., Fones, G. R., French, M., Hickman, A. E., Holland, R. J., Hughes, J. A., Jickells, T. D., Lampitt, R. S., Morris, P. J., Nedelec, F. H., Nielsdottir, M., Planquette, H., Popova, E. E., Poulton, A. J., Read, J. F., Seeyave, S., Smith, T., Stinchcombe, M., Taylor, S., Thomalla, S., Venables, H. J., Williamson, R., and Zubkov, M. V.: Southern Ocean deep-water carbon export enhanced by natural iron fertilization, Nature, 457, 577–580, doi:10.1038/nature07716, 2009.

Primeau, F.: On the variability of the exponent in the power law depth dependence of {POC} flux estimated from sediment traps, Deep Sea Research Part I: Oceanographic Research Papers, 53, 1335 – 1343, doi:10.1016/j.dsr.2006.06.003, 2006.

Reid, P. C., Fischer, A. C., Lewis-Brown, E., Meredith, M. P., Sparrow, M., Andersson, A. J., Antia, A., Bates, N. R., Bathmann, U., Beaugrand, G., Brix, H., Dye, S., Edwards, M., Furevik, T., Gangstø, R., Hátún, H., Hopcroft, R. R., Kendall, M., Kasten, S., Keeling, R., Quéré, C. L., Mackenzie, F. T., Malin, G., Mauritzen, C., Ólafsson, J., Paull, C., Rignot, E., Shimada, K., Vogt, M., Wallace, C., Wang, Z., and Washington, R.: Impacts of the Oceans on Climate Change, in: Advances in Marine Biology, edited by Sims, D. W., vol. 56 of *Advances in Marine Biology*, chap. 1, pp. 1–150, Academic Press, 2009.

Shanks, A. L. and Edmondson, E. W.: Laboratory-made artificial marine snow: a biological model of the real thing, Marine Biology, 101, 463–470, doi:10.1007/BF00541648, 1989.

Shanks, A. L. and Trent, J. D.: Marine snow: sinking rates and potential role in vertical flux, Deep Sea Research Part A. Oceanographic Research Papers, 27, 137–143, doi:10.1016/0198-0149(80)90092-8, 1980.

Silver, M. W. and Gowing, M. M.: The"Particle" Flux: Origins and biological components, Progress in Oceanography, 26, 75–113, doi:10.1016/0079-6611(91)90007-9, 1991.

Smayda, T. J. and Boleyn, B. J.: Experimental Observations on the Flotation of Marine Diatoms. I. Thalassiosira CF. Nana, Thalassiosira rotula and Nitzschia seriata, Limnology and Oceanography, 10, 499–509, 1965.

Smetacek, V.: EisenEx: International team conducts iron experiment in Southern Ocean, U.S. JGOFS Newsletter, 11, 11–14, 2001.

Smetacek, V., Klaas, C., Strass, V. H., Assmy, P., Montresor, M., Cisewski, B., Savoye, N., Webb, A., d'Ovidio, F., Arrieta, J. M., Bathmann, U., Bellerby, R., Berg, G. M., Croot, P., Gonzalez, S., Henjes, J., Herndl, G. J., Hoffmann, L. J., Leach, H., Losch, M., Mills, M. M., Neill, C., Peeken, I., Rottgers, R., Sachs, O., Sauter, E., Schmidt, M. M., Schwarz, J., Terbruggen, A., and Wolf-Gladrow, D.: Deep carbon export from a Southern Ocean iron-fertilized diatom bloom, Nature, 487, 313–319, doi:10.1038/nature11229, 2012.

Suess, E.: Particulate organic carbon flux in the oceans—surface productivity and oxygen utilization, Nature, 288, 260–263, doi:10.1038/288260a0, 1980.

Turner, J. T.: Zooplankton fecal pellets, marine snow and sinking phytoplankton blooms, Aquatic Microbial Ecology, 27, 57–102, doi:10.3354/ame027057, 2002.

Turner, J. T.: Zooplankton fecal pellets, marine snow, phytodetritus and the ocean's biological pump, Progress in Oceanography, 130, 205 – 248, doi:10.1016/j.pocean.2014.08.005, 2015.

Volk, T. and Hoffert, M. I.: Ocean carbon pumps: Analysis of relative strengths and efficiencies in ocean-driven atmospheric CO_2 changes, in: The Carbon Cycle and Atmospheric CO_2: Natural Variations Archean to Present, vol. 32, pp. 99–110, AGU, Washington, DC, 1985.

Waite, A. M., Thompson, P. A., and Harrison, P. J.: Does energy control the sinking rates of marine diatoms?, Limnology and Oceanography, 37, 468–477, doi:10.2307/2837978, 1992.

Wassmann, P.: Retention versus export food chains: processes controlling sinking loss from marine pelagic systems, Hydrobiologia, 363, 29–57, doi:10.1023/A:1003113403096, 1998.

Wassmann, P., Ypma, J. E., and Tselepides, A.: Vertical flux of faecal pellets and microplankton on the shelf of the oligotrophic Cretan Sea (NE Mediterranean Sea), Progress in Oceanography, 46, 241–258, doi:10.1016/S0079-6611(00)00021-5, 2000.

Wiedmann, I., Reigstad, M., Sundfjord, A., and Basedow, S.: Potential drivers of sinking particle's size spectra and vertical flux of particulate organic carbon (POC): Turbulence, phytoplankton, and zooplankton, Journal of Geophysical Research: Oceans, 119, 6900–6917, doi:10.1002/2013JC009754, 2014.

Chapter 2

The relative importance of phytoplankton aggregates and zooplankton fecal pellets to carbon export: insights from free–drifting sediment trap deployments in naturally iron–fertilised waters near the Kerguelen Plateau

This chapter was published as an article under the same title in Biogeosciences, 2015, volume 12(4), pages 1007–1027, doi:10.5194/bg-12-1007-2015.

Emmanuel C. Laurenceau–Cornec[1,2], Thomas W. Trull[2,3], Diana M. Davies[2], Stephen G. Bray[2], Jacqui Doran[4], Frédéric Planchon[5], François Carlotti[6], Marie–Paule Jouandet[6], Anne–Julie Cavagna[7], Anya M. Waite[4,8], and Stéphane Blain[9]

[1]CSIRO–UTAS Quantitative Marine Sciences PhD Program, Institute for Marine and Antarctic Studies, University of Tasmania, Private Bag 129, Hobart TAS 7001, Australia

[2]Antarctic Climate and Ecosystems Cooperative Research Centre, University of Tasmania, Private Bag 80, Hobart TAS 7001, Australia

[3]Commonwealth Scientific and Industrial Research Organisation, Marine and Atmospheric Research, Castray Esplanade, Hobart TAS 7000, Australia

[4]UWA Oceans Institute, The University of Western Australia (M470), 35 Stirling Highway, Crawley WA 6009, Australia

[5]Laboratoire des Sciences de l'Environnement Marin (LEMAR), Université de Brest, CNRS, IRD, UMR6539, IUEM, Technopôle Brest Iroise, Place Nicolas Copernic, 29280 Plouzané, France

[6]Mediterranean Institute of Oceanography (MIO), Aix–Marseille Université, CNRS–IRD, 13288 Marseille, CEDEX 09, France

[7]Vrije Universiteit Brussel, Analytical and Environmental Geochemistry Dept., Brussels, Belgium

[8]Alfred Wegener Institute Helmholz Centre for Polar and Marine Research, Building E-2155, Am Handelshafen 12, 27570 Bremerhaven, Germany

[9]Sorbonne Universités, UPMC Univ. Paris 06, CNRS, UMR 7621, Laboratoire d'Océanographie Microbienne, Observatoire Océanologique, 66650 Banyuls/mer, France

Abstract

The first KErguelen Ocean and Plateau compared Study (KEOPS1) conducted in the naturally iron–fertilised Kerguelen bloom, demonstrated that fecal material was the main pathway for exporting carbon to the deep ocean during summer (January–February 2005) suggesting a limited role of direct export via phytodetrital aggregates. The KEOPS2 project reinvestigated this issue during the spring bloom initiation (October–November 2011) when zooplankton communities may exert limited grazing pressure, and further explored the link between carbon flux, export efficiency and dominant sinking particles depending upon surface plankton community structure. Sinking particles were collected in polyacrylamide gel–filled and standard free–drifting sediment traps (PPS3/3) deployed at six stations between 100 and 400 m, to examine flux composition, particle origin and their size distributions. Results revealed an important contribution of phytodetrital aggregates (49 ± 10 and 45 ± 22 % of the total number and volume of particles respectively, all stations and depths averaged). This high contribution dropped when converted to carbon content (30 ± 16 % of total carbon, all stations and depths averaged) with cylindrical fecal pellets then representing the dominant fraction (56 ± 19 %).

At 100 and 200 m depth, iron- and biomass–enriched sites exhibited the highest carbon fluxes (maxima of 180 and 84 ± 27 mg C m^{-2} d^{-1}, based on gel and PPS3/3 trap collection respectively) especially where large fecal pellets dominated over phytodetrital aggregates. Below these depths, carbon fluxes decreased (48 ± 21 % decrease on average between 200 and 400 m), and mixed aggregates composed of phytodetritus and fecal matter dominated, suggesting an important role played by physical aggregation in deep carbon export.

Export efficiencies determined from gels, PPS3/3 traps and ^{234}Th disequilibria (200 m carbon flux/net primary productivity) were negatively correlated to net primary productivity with observed decreases from ~ 0.2 at low–iron sites to ~ 0.02 at high–iron sites. Varying phytoplankton communities and grazing pressure appear to explain this negative relationship. Our work emphasises the need to consider detailed plankton communities to accurately identify the controls on carbon export efficiency, which appear to include small spatio–temporal variations in ecosystem structure.

2.1 Introduction

Physical and biological processes occurring in the surface ocean generate a vast diversity of particles. These particles represent potential vehicles to export organic carbon to the deep ocean, where a small fraction can eventually be sequestered in the sediments. This process, known as the 'biological carbon pump' (BCP) influences the level of atmospheric carbon dioxide and thus the global climate system (Lam et al., 2011; Volk and Hoffert, 1985)

Primary production in the euphotic layer builds a stock of phytoplankton cells. If their concentration and stickiness are high enough (Jackson, 1990), these cells can collide, attach and form large phytodetrital aggregates (Burd and Jackson, 2009; McCave, 1984), with those reaching sizes greater than 0.5 mm known as 'marine snow' (Alldredge and Silver, 1988). Alternatively, phytoplankton cells can be tightly packed into dense fecal pellets through zooplankton grazing (Silver and Gowing, 1991). Because of their large size and high density respectively,

phytodetrital aggregates and fecal pellets are major constituents of the downward flux, and several studies have found either fecal pellets (Bishop et al., 1977; Cavagna et al., 2013; Ebersbach and Trull, 2008; Fowler and Knauer, 1986; Pilskaln and Honjo, 1987; Wassmann et al., 2000) or large organic aggregates (Alldredge and Gotschalk, 1989; Burd and Jackson, 2009; De La Rocha and Passow, 2007; Jackson, 1990; Turner, 2002) to be the dominant vectors of carbon to depth.

Because grazing causes losses of organic carbon by respiration (Alldredge et al., 1995; Michaels and Silver, 1988), direct export via the sinking of phytodetrital aggregates represents the most efficient operating mode of the BCP. However, the ecosystem structure and environmental conditions under which primary production can be exported directly via phytodetrital aggregates are still unclear, and their determination would considerably improve the predictions of the efficiency of the BCP in varying conditions. The volume fraction of phytodetrital aggregates vs. fecal pellets in the total flux and their volume–to–carbon–content ratio select the dominant carbon export mode; these relative contributions depend on numerous parameters, including primary productivity, biomass, interactions between primary producers and heterotrophic communities (Michaels and Silver, 1988), physical fragmentation, microbial decomposition, coprophagy and the velocity at which particles settle (Turner, 2002).

The Southern Ocean contains the largest high–nutrient, low–chlorophyll (HNLC) area of the world ocean and is an essential player in global biogeochemistry (Sigman and Boyle, 2000). In these waters, abundant macronutrients (silicic acid, nitrate and phosphate) can fuel primary production given available light and sufficient iron, a limiting micronutrient (de Baar et al., 1995; Martin, 1990). The Kerguelen Plateau offers the opportunity to study the functioning of the BCP in a naturally iron–fertilised region (Blain et al., 2007). The first KErguelen Ocean and Plateau compared Study (KEOPS1) demonstrated that most of the sinking flux collected in polyacrylamide gel sediment traps was derived from copepod fecal detritus (intact or degrading pellets and fecal material reaggregated with phytodetritus, hereafter called 'fecal aggregates'), and reported limited evidence for phytodetrital aggregates formed by direct flocculation of phytoplankton cells (Ebersbach and Trull, 2008). Number and volume fluxes were dominated by aggregates but represented a small fraction of the total carbon flux, owing to their low volume–to–carbon–content ratio. Several natural and artificial iron–fertilisation experiments conducted at the same time of the year but in different locations in the Southern Ocean (e.g. SAZ–Sense study and SOFeX) displayed similar export modes relying mainly on fecal matter (Bowie et al.,

2011; Coale et al., 2004; Ebersbach et al., 2011; Lam and Bishop, 2007). In contrast, other artificial and natural iron experiments (SOIREE, CROZEX and EiFeX) have demonstrated a direct export via the sinking of phytodetrital aggregates or single phytoplankton cells (Boyd et al., 2000; Pollard et al., 2007; Salter et al., 2007; Smetacek et al., 2012; Waite and Nodder, 2001).

These variations among studies may reflect the time–varying aspects of export. In his review of Southern Ocean ecosystem contribution to carbon export, Quéguiner (2013) suggests that from the onset of a bloom to its decline and subsequent export event, phytoplankton and to a lesser extent zooplankton communities, is subject to several rapid successions. The complexity of the processes is also reflected by the past 30 years of empirical and modelling studies attempting to relate deep carbon export variations to surface productivity (Eppley and Peterson, 1979; Guidi et al., 2009; Suess, 1980; Wassmann, 1990). In general, the ratio between export and production in the surface ocean is low (< 5–$10\,\%$; Buesseler, 1998), but decoupling associated with high–export events (e.g. high–latitude blooms) or even negative relationships, has been noted (Buesseler, 1998; Ebersbach et al., 2011; Lam and Bishop, 2007; Maiti et al., 2013). This highlights the complexity of food web structure and its multiple controls on carbon export (Michaels and Silver, 1988; Wassmann, 1998).

In the present study we test the hypothesis that direct export via phytodetrital aggregates occurs during the early stage of the Kerguelen naturally iron–fertilised bloom, when zooplankton communities present in the water column are not fully developed. We further explore the relative export abilities of each carbon export mode (i.e. phytodetrital aggregates vs. fecal pellets) by looking at their variation with depth and over time and their links to spatio–temporal variations in plankton communities.

We collected sinking particles in free–drifting polyacrylamide gel and standard sediment traps. Gel traps allowed for the collection of intact natural particles as they sank in the water column (Ebersbach and Trull, 2008; Jannasch et al., 1980; McDonnell and Buesseler, 2010), and thus gave a direct 'picture' of the sinking flux at the depth of trap deployment. Image analysis of particles embedded in gels provided particle statistics (e.g. number and volume fraction of each category of particle), and conversion from area to volume and from volume to carbon content, using empirical relationships, allowed for estimation of the carbon flux and the relative importance of each category of particle. In parallel, standard sediment traps serving as a reference permitted direct quantitative estimates based on bulk chemical analyses of the

material collected and from ^{234}Th depletion method (Planchon et al., 2015). Then, to test our main hypothesis, the relative contribution of each category of particles was linked to the amount of carbon effectively exported in order to determine which one led the carbon export.

2.2 Material and methods

2.2.1 The KEOPS2 study

The second KErguelen Ocean and Plateau compared Study (KEOPS2) was conducted onboard the RV *Marion Dufresne* over and downstream of the Kerguelen Plateau, from 8 October to 30 November 2011. Sinking particle flux and composition were assessed by the use of free–drifting sediment traps deployed at six stations, inside and outside the naturally iron–fertilised area, in waters with varying biomass and surface chlorophyll *a* (Chl *a*) levels (Figs. 2.1 and 2.2). For more information on the complex spatio–temporal evolution of the phytoplankton bloom over the full 2011–2012 annual cycle, we refer the reader to an animation of NASA MODIS Aqua chlorophyll images, provided as a supplementary material in Trull et al. (2014). Combination of sediment trap collection with volume–to–carbon conversion factors allowed to determine preferential modes of carbon export (Ebersbach and Trull, 2008; Ebersbach et al., 2011).

2.2.2 Water column properties and biomass at each station

In addition to trap–derived measurements, POC concentrations were estimated in the water column using a WET Labs C–Star (6000 m) transmissometer (660 nm wavelength and 25 cm path length) linked to a conductivity–temperature–depth (CTD) system (Sea–Bird SBE–911+CTD). Xmiss transmissometer data (%) were converted to POC concentrations ($\mu mol\,L^{-1}$) following a calibration based on in situ POC measurements from Niskin bottles. A Seapoint Chelsea Aquatracka III (6000 m) chlorophyll fluorometer linked to the CTD was used to determine fluorescence profiles. Fluorescence was converted to chlorophyll *a* (Chl *a*; $\mu g\,L^{-1}$) by comparison with total Chl *a* in situ measurements from Niskin bottles (Lasbleiz et al., 2014).

Figure 2.2 shows water column properties and biomass at each site. The HNLC reference station R–2 located outside the fertilised area was characterised by a relatively deep mixed layer (96 m), low net primary productivity (NPP) (euphotic zone 1 % PAR–integrated

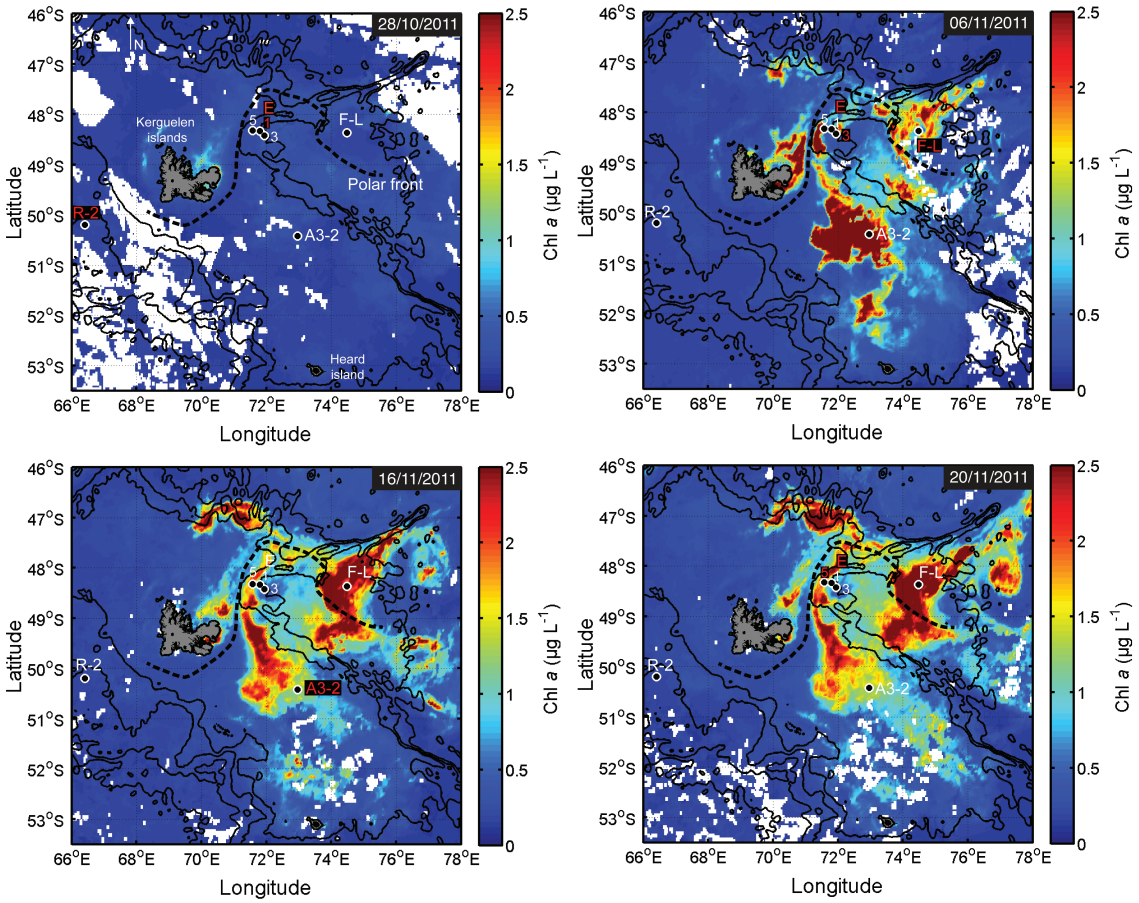

Figure 2.1: MODIS–Aqua satellite (CLS–CNES) images of surface chlorophyll *a* concentration (Chl *a*) at different bloom stages from 28 October to 20 November 2011. Images show free–drifting sediment trap deployment locations in contrasting biomass levels. On each map, red labels represent the station(s) sampled at the date of the map ±3 days.

NPP = 135±6 mg C m^{-2} d^{-1}; Cavagna et al., 2014), low surface chlorophyll (chlorophyll *a* mixed layer average = 0.6 µg Chl *a* L^{-1}), and biomass (mixed–layer–integrated POC = 4.7 g C m^{-2}). Stations E–1, E–3 and E–5 were located in an eddy–like, bathymetrically trapped recirculation feature in deep waters east of the Kerguelen Islands (stationary meander of the polar front) with a mixed layer depth varying from 33 (E–3) to 70 m (E–1). These stations had moderate NPP (523 ± 55, 686 ± 97 and 943 ± 113 mg C m^{-2} d^{-1} respectively), Chl *a* (0.8, 0.7 and 1.1 µg Chl *a* L^{-1} respectively), and biomass (5.3, 3 and 4.8 g C m^{-2} respectively). They were used as a time series assuming a pseudo–Lagrangian evolution (d'Ovidio et al., 2014). F–L was the only station located north of the polar front and exhibited the shallowest mixed layer (31 m). A3–2 was the second visit to the on–plateau bloom reference station of KEOPS1 and had the deepest mixed layer (149 m). F–L and A3–2 displayed the highest NPP (3.4 ± 0.1 and 1.9 ± 0.2 g C m^{-2} d^{-1} respectively), chlorophyll *a* (3 and 1.8 µg Chl *a* L^{-1} respectively) and

biomass (6.2 and 20.4 g C m^{-2}).

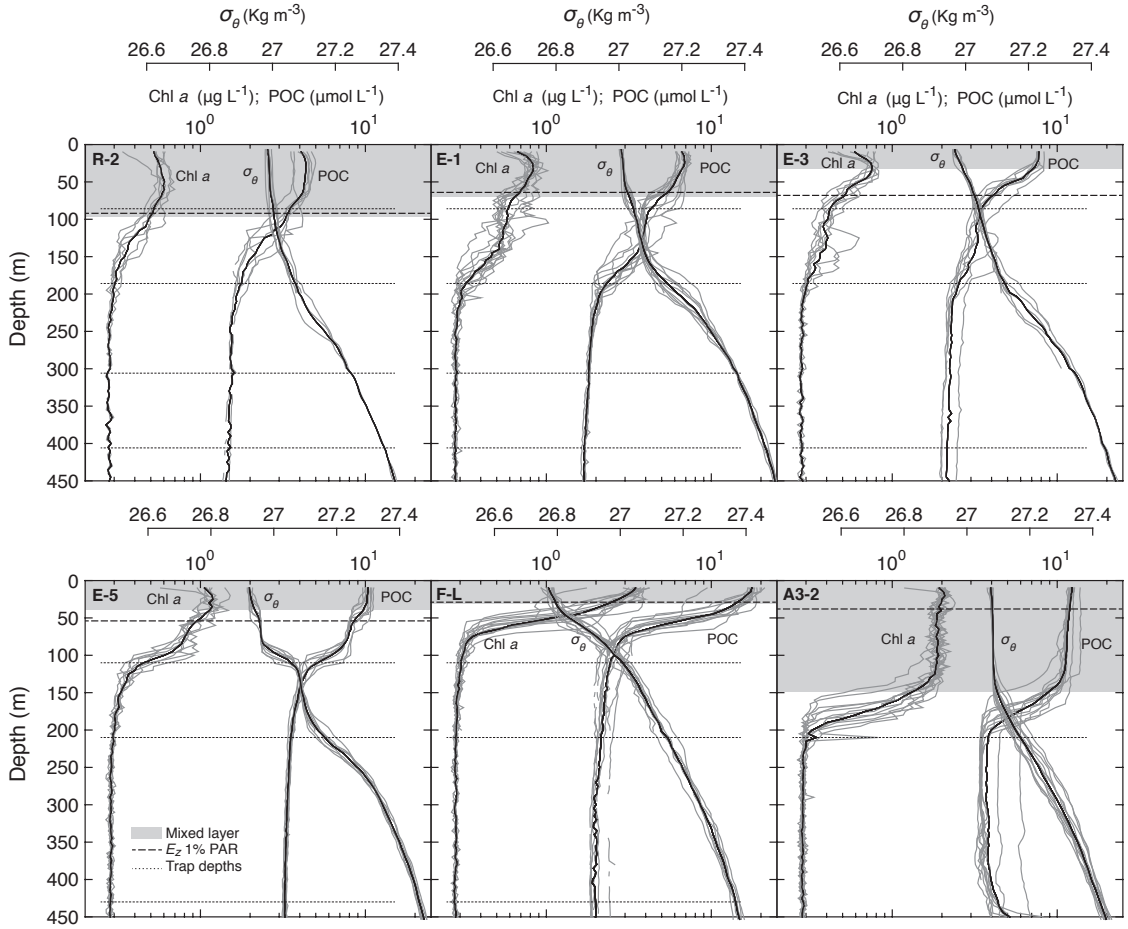

Figure 2.2: Water column properties and biomass at each site. Chl *a*: chlorophyll *a* (µg L^{-1}); σ_θ: potential density anomaly (kg m^{-3}); POC: particulate organic carbon (µmol L^{-1}). Grey lines indicate CTD profiles and black lines represent their average values. E_Z 1 % PAR: base of the euphotic zone assumed at 1 % of the photosynthetic available radiation (PAR).

2.2.3 Sediment trap preparation, deployments and recovery

Two different types of trap were deployed during KEOPS2. Bulk fluxes of particulate organic carbon (POC), total particulate nitrogen (TPN), biogenic silica (BSi), particulate inorganic carbon (PIC), particulate iron (PFe; data shown in Bowie et al., 2014), and thorium 234 (^{234}Th) were estimated using PPS3/3 traps (Technicap, La Turbie, France). A PPS3/3 trap consists of a single cylindrical trap with an internal conical funnel at its base with a collection area of 0.125 m^2 that transfers samples into a carousel of 12 cups. During KEOPS2, these traps were deployed for a maximum period of 6 days. Cups were filled with brine with a salinity of $\sim$ 52 psu, made by freezing filtered (0.2 µm pore size) surface seawater. Some cups were also amended with

mercuric chloride ($1\,g\,L^{-1}$) as a biocide (as detailed in Table 2.4). No poison was added to the cups used for trace metal studies (Bowie et al., 2014).

Table 2.1: Deployment schedules for free–drifting sediment trap arrays.

Area	Site ID	Array	Trap depths (m)	± SD (m)	Event	Time (UTC)*	Latitude	Longitude	Duration (days)	Drift (km)	Tilt ± SD (°)
HNLC reference	R–2	Gel traps	110, 210, 330, 430	0.8	Deploy	26 Oct 2011, 15:33	50°21.58′ S	66°42.93′ E	0.92	3.8	–
					Recover	27 Oct 2011, 13:33	50°20.10′ S	66°40.69′ E			
		P trap	210	–	Deploy	18 Oct 2011, 00:56	50°42.57′ S	66°41.47′ E	–	–	–
					Lost	–	–	–			
Off-plateau meander (time series)	E–1	Gel traps	110, 210, 330, 430	1	Deploy	28 Oct 2011, 23:00	48°28.72′ S	72°12.68′ E	1.25	2.9	–
					Recover	30 Oct 2011, 05:00	48°27.48′ S	72°11.27′ E			
		P trap	210	0. 6	Deploy	29 Oct 2011, 10:35	48°29.66′ S	72°14.28′ E	5.32	35	2.5 ± 0.7
					Recover	3 Nov 2011, 18:14	48°38.44′ S	71°48.99′ E			
	E–3	Gel traps	110, 210, 430	0.9	Deploy	3 Nov 2011, 14:30	48°41.92′ S	71°57.89′ E	1.02	4	–
					Recover	4 Nov 2011, 15:00	48°43.90′ S	71°56.66′ E			
		P trap	210	0.7	Deploy	5 Nov 2011, 07:52	48°42.06′ S	71°56.96′ E	5.11	43	0.3 ± 1
					Recover	10 Nov 2011, 10:37	48°40.77′ S	72°32.08′ E			
	E–5	Gel traps	110, 210, 430	0.9	Deploy	18 Nov 2011, 13:50	48°25.07′ S	71°59.84′ E	1.06	10.1	–
					Recover	19 Nov 2011, 15:17	48°30.25′ S	71°57.42′ E			
		P trap	210	2.4	Deploy	18 Nov 2011, 14:42	48°25.03′ S	71°58.11′ E	1.55	15.1	4 ± 1.7
					Recover	20 Nov 2011, 03:54	48°33.16′ S	71°56.86′ E			
North polar front	F–L	Gel traps	110, 210, 430	0.9	Deploy	6 Nov 2011, 14:30	48°31.64′ S	74°39.53′ E	0.92	14.2	–
					Recover	7 Nov 2011, 12:37	48°36.60′ S	74°48.40′ E			
On-plateau reference	A3–2	P trap (+gel)	210 (210)	1	Deploy	15 Nov 2011, 21:28	50°37.80′ S	72°4.81′ E	1.85	10.4	1 ± 0.9
					Recover	17 Nov 2011, 17:46	50°42.52′ S	72°9.67′ E			

* Times and locations are at the start of the deck operation.

To examine sinking flux characteristics (particle type, number and size), intact particles were also collected in cylindrical polyacrylamide gel–filled sediment traps with a collection area of $0.011\,m^2$. These deployments lasted less than 2 days so as not to overload the gels (Table 2.1). Polyacrylamide gels were prepared following the method developed by Lundsgaard (1995), modified as described in Ebersbach and Trull (2008).

Due to different required deployment durations (shorter for gel traps to avoid overloading; see above) each category of trap was deployed on separate arrays, except at A3–2 (combined deployment, Table 2.1). All separated deployments of gel and PPS3/3 traps overlapped in time and location (except at station E–3, where they were successive) to optimise the collection of similar particle fields. The arrays had broadly the same design consisting of a surface float sustaining a mooring line where the traps were fixed at different depths. PPS3/3 traps were fixed at 210 m, and one to four gel traps, depending on the station, were fixed at 110, 210, 330 and 430 m. Wave–induced motions were dampened by an elastic link to keep the traps at a constant depth (Trull et al., 2008). Pressure sensors mounted on the deepest gel trap and PPS3/3 trap on most of the arrays confirmed very small vertical motions during the deployments, with depth standard deviations ranging from 0.6 m at E–1 to 2.4 m at E–5 (Table 2.1). The average trap drift speed of $8.5 \pm 5\,cm\,s^{-1}$ was in the range of horizontal velocities determined by drogued drifter trajectories (Zhou et al., 2014). Inclinometers recorded small tilts of the mooring lines (from $0.3 \pm 1°$ at E–3 to a maximum of $4 \pm 1.7°$ at E–5) guaranteeing minimum perturbation of

particle collection due to hydrodynamic conditions. No particular difficulties were encountered during trap recoveries, ensuring unperturbed gel structure. The seawater overlying the gels was removed directly after recovery to prevent particles collected in the trap cylinder during the recovery from entering the gels. Unfortunately, the PPS3/3 trap array deployed at R–2 was lost.

2.2.4 Chemical analysis

Protocols used for particulate organic carbon (POC), total particulate nitrogen (TPN), particulate inorganic carbon (PIC), and biogenic silica (BSi) analyses are described in Trull et al. (2008). ^{234}Th flux analysis is detailed in Planchon et al. (2015).

2.2.5 Image analysis

Within a few hours after recovery, each gel was photographed onboard against a laser–etched glass grid of 36 cells (each 14 mm × 12.5 mm) at a magnification of ×6.5 using a light field transmitted illumination and a Zeiss Stemi 2000–CS stereomicroscope coupled to a Leica DFC–280 1.5 MP digital camera and Leica Firecam software on an Apple iMac G4 computer. Observations at higher magnification (from × 10 to × 50) confirmed particle identifications when needed.

Pictures of incomplete grid cells, with unequally distributed particles (i.e. containing at least a quarter of their area without particles) or large zooplankton, were removed from the analysis to avoid bias. Ten grid cells per gel (total of 180 pictures) were selected randomly. The average sum of the surface analysed per gel was $15.7 \pm 0.7\,\mathrm{cm}^2$, corresponding to $14.3 \pm 0.7\,\%$ of the trap collection area.

Particles collected in gels (Fig. 2.3) were phytodetrital aggregates (PA), cylindrical fecal pellets (CFP), oval fecal pellets, fecal aggregates (FA), and diatoms in the form of chains (e.g. the pennate *Fragilariopsis* spp.) or single cells (e.g. the centric *Thalassiosira* spp.). A few mesozooplankton specimens were collected (less than 10 per gel), and were mostly represented by copepods (adult and copepodite stages) and appendicularians. Foraminifera and radiolarians were also occasionally observed. Phytodetrital aggregates were loose and green, while fecal aggregates contained dense, brown material. Most cylindrical fecal pellets had sharp edges and relatively constant diameters, but some were tapered along their length and had blurred edges composed of unpacked fecal material or attached phytodetritus (Fig. 2.3B).

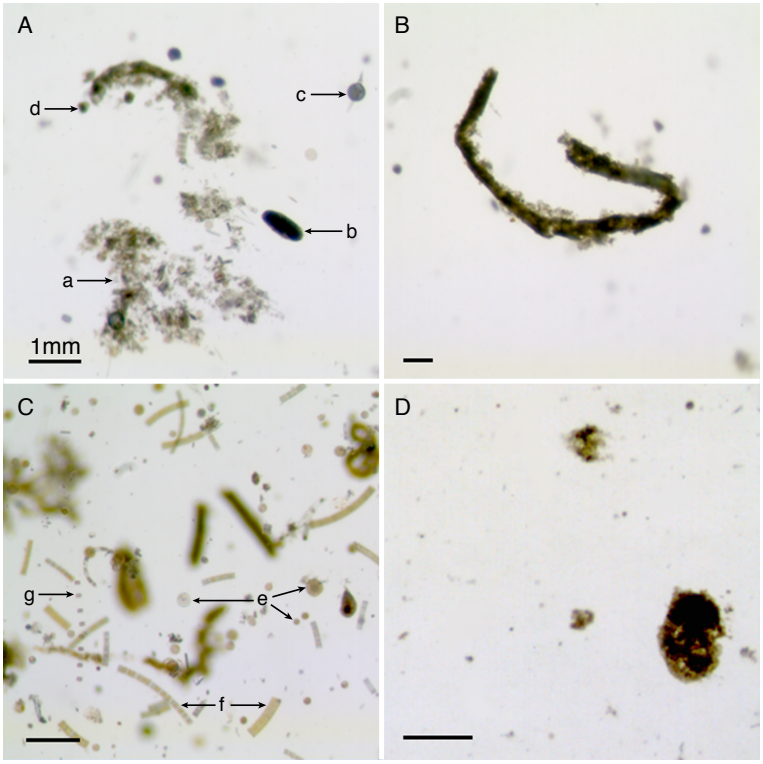

Figure 2.3: High–resolution pictures of particles embedded in polyacrylamide gels showing the main categories of particles collected. **(A)** Phytodetrital aggregate (a), oval fecal pellet (b), radiolarian (c), foraminifera (d); **(B)** large cylindrical fecal pellet; **(C)** small and large centric diatom single cells (e), chains of pennate diatoms of the genera *Fragilariopsis* spp. (f), chain of small centric diatom cells (g); **(D)** fecal aggregate. Note the difference in compactness and optical density between phytodetrital and fecal aggregates.

A preliminary image analysis was conducted to select the best analysis method in terms of particle identification. Particles were classified into three main categories based on their significant contribution to the flux: phytodetrital aggregates, cylindrical fecal pellets and fecal aggregates. A fourth category, oval fecal pellets, was rare (less than one pellet per image in total), and its contribution to the flux was assumed negligible. Pictures were converted to binary images, with threshold levels adjusted manually on each picture to ensure a minimum alteration of particle areas. The average alteration of particle area estimated on a subsample was an increase of $21.6 \pm 7\,\%$ ($n = 169$) for particles with irregular shapes (e.g. aggregates sensu lato including phytodetrital and fecal aggregates), and an increase of $11.6 \pm 7\,\%$ ($n = 44$) for cylindrical fecal pellets. Cylindrical fecal pellet and aggregate areas were systematically corrected for this overestimation.

Pictures were analysed with the US National Institutes of Health's free software ImageJ. Typical shapes of each category of particle were determined manually on a subsample of particles. MATLAB routines using specific sets of shape descriptors were then applied to all images to

identify and separate each category of particle. Because fecal and phytodetrital aggregates had similar complex shapes, automated routines could not separate these particles efficiently. All fecal material was thus isolated manually from all other particles based on the assumption that fecal matter is brown and denser than biologically unprocessed phytoplankton (Ebersbach et al., 2011). From the resulting set of pictures, fecal aggregates were easily separated from cylindrical fecal pellets due to their very contrasted shapes. Tests on the efficiency of our automated selection, conducted on a large sample, showed that 93.4 % ($n = 397$) of cylindrical fecal pellets and 67.2 % ($n = 171$) of fecal aggregates were correctly identified by the set of shape descriptors chosen.

Table 2.2: Particle characteristics and bins for phytodetrital aggregates, cylindrical fecal pellets and fecal aggregates.

Characteristics name					Unit			Definition		
Projected area					cm^2			Pixel area of the particle image		
Volume					cm^3			Volume calculated from area		
Equivalent spherical diameter (ESD)					cm			Diameter of a sphere with the same image area		
Perimeter					cm			Sum of pixel lengths at particle edge		
Length					cm			Major axis of ellipse fit to particle		
Numerical flux					$m^{-2}\,d^{-1}$			Number flux of sinking particles		
Volume flux					$cm^3\,m^{-2}\,d^{-1}$			Volume flux of sinking particles		
Carbon flux					$mg\,C\,m^{-2}\,d^{-1}$			Organic carbon flux in sinking particles		
Number flux spectrum					$cm^{-1}\,m^{-2}\,d^{-1}$			Number flux per unit ESD size interval		
Volume flux spectrum					$cm^3\,m^{-2}\,d^{-1}\,cm^{-1}$			Volume flux per unit ESD size interval		
Number, volume and carbon flux fractional contributions					none			Number, volume and carbon flux of particle types as a fraction of total		
Bins (cm)	1	2	3	4	5	6	7	8	9	10
Lower limits (ESD)	0.0071	0.0102	0.0145	0.0207	0.0296	0.0422	0.0603	0.0860	0.1228	0.1752
Upper limits (ESD)	0.0102	0.0145	0.0207	0.0296	0.0422	0.0603	0.0860	0.1228	0.1752	–
Centre (ESD)	0.0087	0.0124	0.0176	0.0252	0.0359	0.0513	0.0732	0.1044	0.1490	–

All particle characteristics investigated in this study and their units are reported in Table 2.2. An area cut–off applied at 0.004 mm^2 (0.07 mm equivalent spherical diameter) removed all 'fake particles' deriving from small gel imperfections and glass–grid or microscope lens cleanliness. This cut–off removed 38 % of the total number of particles (mostly spurious particles and small single cells) but represented a loss of only 5.2 % of the total area of particles in the images, introducing a negligible bias.

Aggregate area was converted to equivalent spherical diameter (ESD) assuming spherical shape, and the volume was calculated from the ESD. Because cylindrical fecal pellets were not always straight, their volume could not be accurately measured directly from their length and was calculated from their perimeter and area (independent of pellet curvature) assuming a cylinder. The radius r of the cylinder section was determined by finding the minimum root of the polynomial

$$4r^2 - Pr + A = 0, \tag{2.1}$$

where P is the perimeter and A is the projected area of the pellet. The length L was calculated from the projected area and radius using the formula

$$L = A/2r. \tag{2.2}$$

The volume was then calculated from the radius and length.

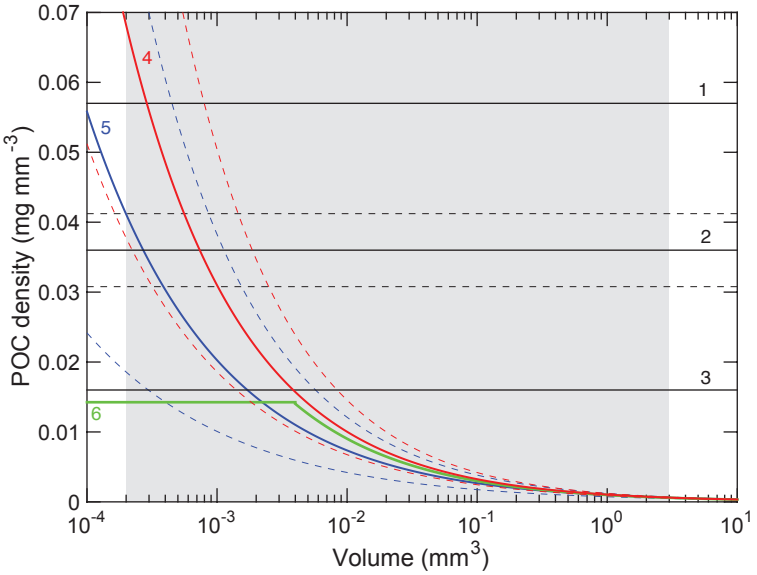

Figure 2.4: Empirical relationships of particulate organic carbon (POC) density as a function of volume for different categories of sinking particles. 1, 2 and 3: copepod fecal pellets, average of euphausiids and copepod fecal pellets and euphausiids fecal pellets respectively (González and Smetacek, 1994); 4 (red line): fecal marine snow (Alldredge, 1998); 5 (blue line): diatom marine snow (Alldredge, 1998); 6 (green line): small and large aggregates (sensu lato) respectively (Ebersbach and Trull, 2008). Standard errors on the fitting parameters are indicated in dashed lines for the relationships 2 (black), 4 (red) and 5 (blue) used in this study. The grey area represents the size range of particles processed in this study. Note the constant carbon mass per unit volume in fecal pellets based on solid geometry (linear relationship) and its decrease with increasing volume scaled on fractal geometry (power relationship) in the case of aggregates.

The conversion from volume to carbon content was done by using different ratios and relationships depending on the particle considered. Figure 2.4 shows the relationship between carbon content and particle volume for different algorithms from the literature and those selected in this study. Based on values published by González and Smetacek (1994), the volume of cylindrical fecal pellets was converted to their organic carbon content using a ratio of $0.036\,\mathrm{mg\,C\,mm^{-3}}$ (Fig. 2.4, line 2) as an average value for copepod (Fig. 2.4, line 1) and euphausiid fecal pellets (Fig. 2.4, line 3). For fecal aggregates, we used the power relationship between POC content and aggregate volume V, $\mathrm{POC\,(\mu g)} = 1.05V(\mathrm{mm^3})^{0.51}$, based on the fractal decrease in carbon content with size and determined empirically by Alldredge (1998) for fecal marine snow (Fig. 2.4, line 4).

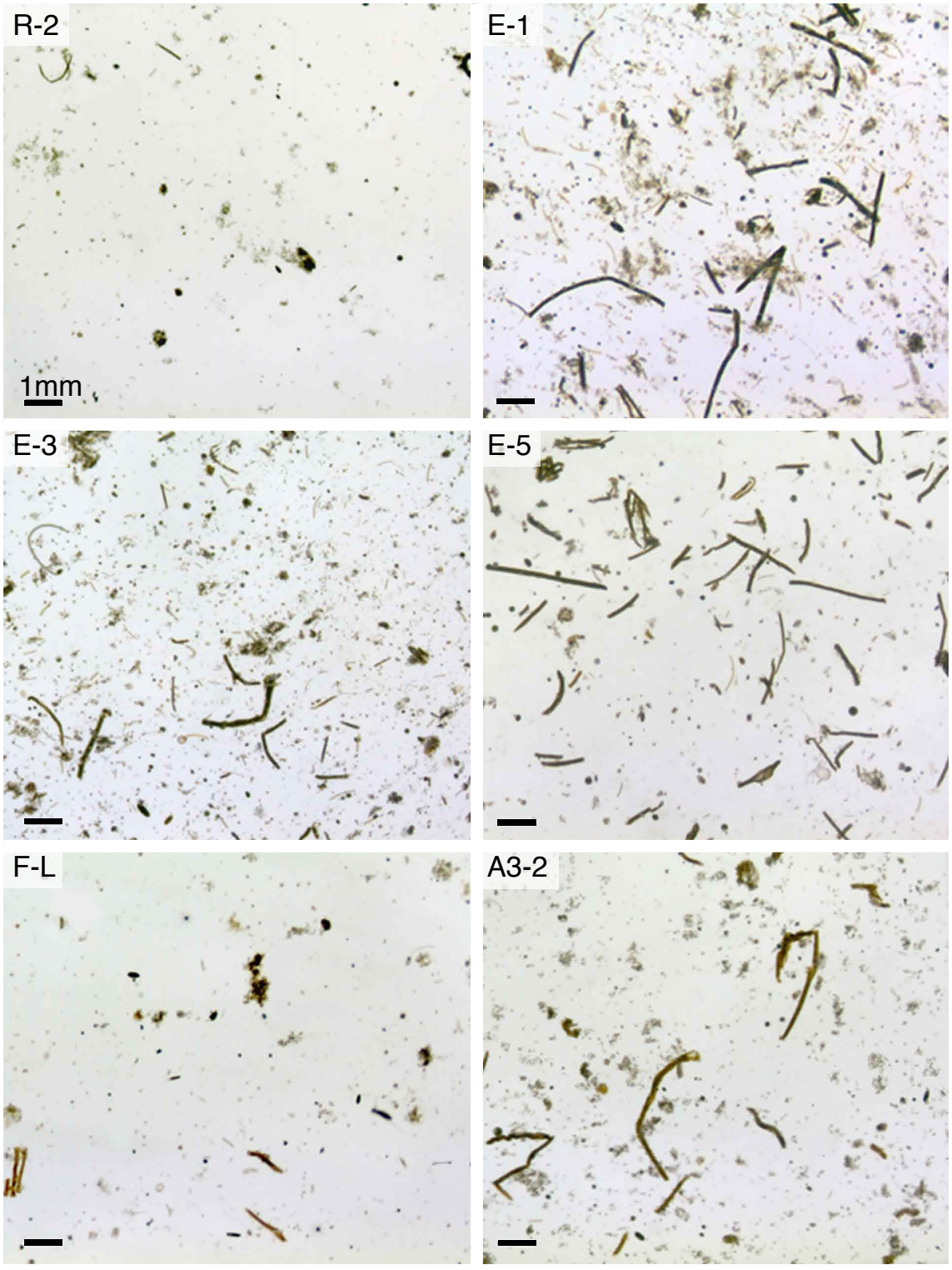

Figure 2.5: Images of sinking particles embedded in polyacrylamide gels, collected at each site at 210 m. Comparison of images suggests differences in terms of particles abundance and nature at each site.

The volume of phytodetrital aggregates was converted to carbon content using also a power relationship determined by Alldredge (1998) for diatom marine snow, $\mathrm{POC\,(\mu g)} = 0.97V(\mathrm{mm}^3)^{0.56}$ (Fig. 2.4, line 5) assuming aggregates composed of phytoplankton not biologically processed. In contrast to Ebersbach and Trull (2008; Fig. 2.4, line 6), very small particles (large single cells and aggregates composed of few cells) were included in the category of phytodetrital aggregates and their volume–to–carbon conversion was done using the same relationship (Fig. 2.4, line 5).

Particle number and volume fluxes are presented in the section 2.3 as a function of size spectra. All particles were binned in 10 size classes spaced logarithmically to give the best representation of the whole size range (Jackson et al., 1997, 2005). To avoid bias, bins containing five or fewer particles were not included in the flux spectrum analyses, as recommended by Jackson et al. (2005).

2.3 Results

2.3.1 Particles collected in polyacrylamide gel–filled sediment traps

Particle number, projected area and volume fluxes

Despite variations in deployment duration among sites exceeding 80 % (between 0.9 and 5.3 days, Table 2.1), an observation of raw images (Fig. 2.5) gives a broad preliminary indication on flux differences in terms of particle abundance (e.g. low fluxes at R–2 and F–L, and higher at E stations and A3–2). The lowest particle numbers, projected particle area and volume fluxes were collected at R–2 and F–L (Table 2.3 and Fig. 2.6) with particle volume fluxes of 2.5 ± 1 and $3 \pm 0.7\,\mathrm{cm^3\,m^{-2}\,d^{-1}}$ respectively (all depths averaged). In contrast, high fluxes were collected at E stations with an average volume flux of $7.5 \pm 3\,\mathrm{cm^3\,m^{-2}\,d^{-1}}$ (all E stations and depths averaged). Station A3–2 also presented a relatively high flux of $6.1\,\mathrm{cm^3\,m^{-2}\,d^{-1}}$.

Phytodetrital aggregates dominated in number at most stations and depths (49 ± 10 % of the total number of particles for all stations and depths averaged). Particles not selected automatically as phytodetrital aggregates, cylindrical fecal pellets or fecal aggregates ('others' in Table 2.3) represented the second–largest numerical fraction (38 ± 8 %) but less than 9 % of the total projected particle area, and thus were assumed negligible in volume fluxes. Phytodetrital

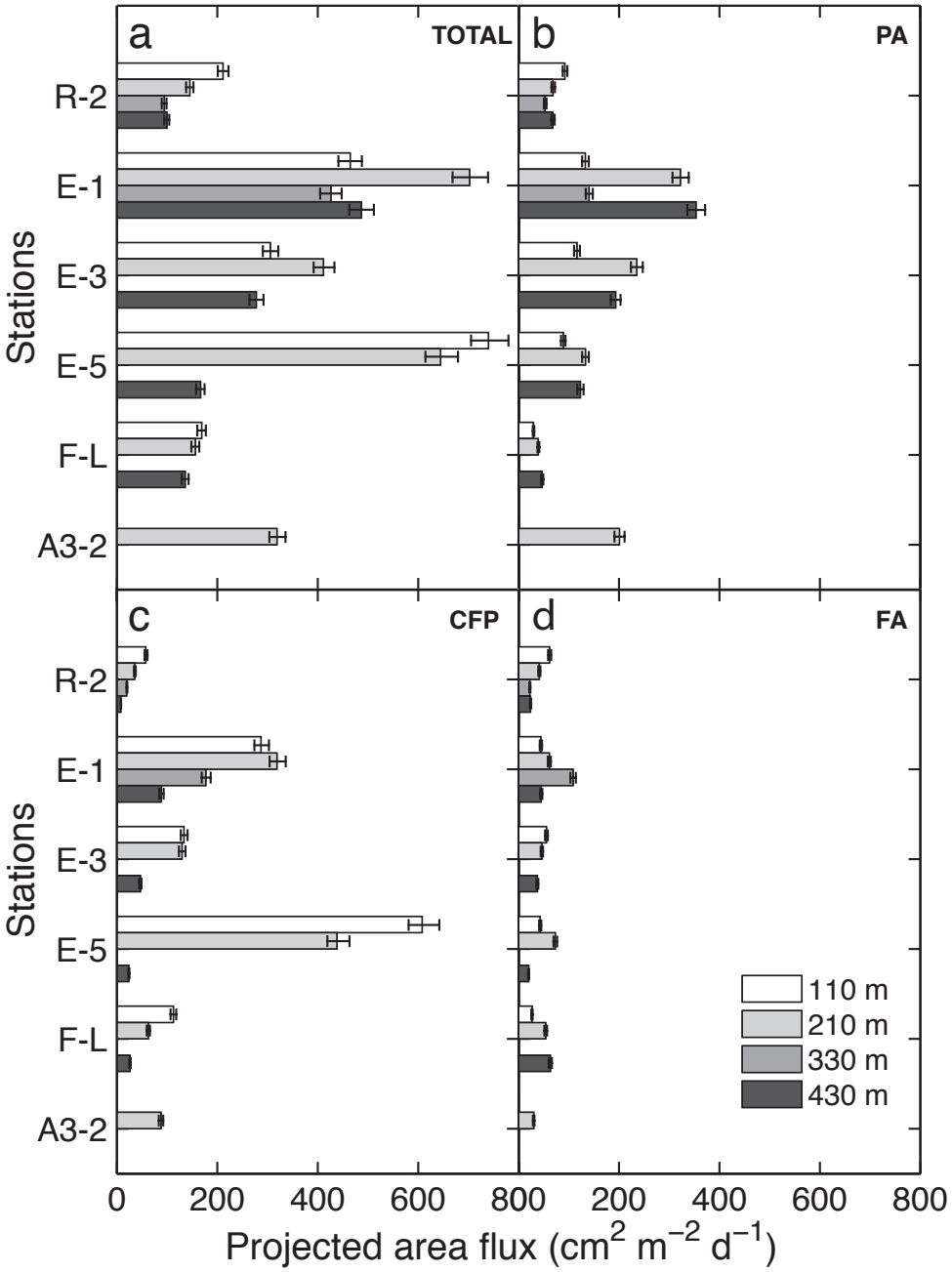

Figure 2.6: Projected area of particles estimated from image analysis at each site and depth and expressed as fluxes ($cm^2\,m^{-2}\,d^{-1}$). **(a)** All particles (TOTAL), **(b)** phytodetrital aggregates (PA), **(c)** cylindrical fecal pellets (CFP) and **(d)** fecal aggregates (FA). 5% error bars are indicated. The figure suggests a sinking flux dominated by cylindrical fecal pellets at the surface, except at R–2, where phytodetrital aggregates represented the most important fraction. The attenuation of the cylindrical fecal pellet flux with depth observable at all stations was combined with an increase in the flux of phytodetrital and fecal aggregates at almost all stations. At 430 m, phytodetrital aggregates were then the most dominant particles.

Table 2.3: Total numerical, volume and particulate organic carbon (POC) fluxes and fractional contributions of each category of particle. Maximum and minimum fluxes are indicated in bold. PA: phytodetrital aggregates; CFP: cylindrical fecal pellets; FA: fecal aggregates; O: others.

Site ID	Depth (m)	Numerical flux ($\#10^4\,m^{-2}\,d^{-1}$)	Fractional contributions				Volume flux ($cm^3\,m^{-2}\,d^{-1}$)	Fractional contributions			POC flux ($mg\,C\,m^{-2}\,d^{-1}$)	Fractional contributions		
			PA	CFP	FA	O		PA	CFP	FA		PA	CFP	FA
R–2	110	97	0.45	0.04	0.07	0.44	4	0.43	0.14	0.43	43	0.3	0.48	0.22
	210	84	0.46	0.03	0.05	0.46	2.8	0.39	0.14	0.47	30	0.34	0.46	0.2
	330	72	0.49	0.02	0.04	0.45	1.7	0.52	0.15	0.33	20	0.39	0.43	0.18
	430	91	0.49	0.01	0.04	0.46	**1.6**	0.61	0.04	0.35	**16**	0.63	0.13	0.24
E–1	110	178	0.52	0.16	0.04	0.28	5.2	0.34	0.45	0.21	112	0.18	0.76	0.06
	210	208	0.6	0.07	0.03	0.3	**13**	0.56	0.27	0.17	176	0.24	0.71	0.05
	330	142	0.51	0.07	0.06	0.36	8	0.3	0.25	0.45	108	0.19	0.67	0.14
	430	184	0.65	0.02	0.02	0.31	12.3	0.78	0.1	0.12	96	0.47	0.46	0.07
E–3	110	131	0.47	0.12	0.05	0.36	4.8	0.4	0.24	0.36	67	0.25	0.63	0.12
	210	216	0.58	0.05	0.03	0.34	6.6	0.61	0.19	0.2	85	0.4	0.52	0.08
	430	92	0.61	0.02	0.04	0.33	7.6	0.73	0.1	0.17	56	0.43	0.47	0.1
E–5	110	**225**	0.34	0.33	0.04	0.29	6.1	0.15	0.72	0.13	**180**	0.08	0.88	0.04
	210	194	0.4	0.19	0.06	0.35	7.9	0.28	0.51	0.21	177	0.11	0.82	0.07
	430	93	0.49	0.02	0.04	0.45	3.5	0.8	0.08	0.12	30	0.55	0.34	0.11
F–L	110	85	0.31	0.12	0.05	0.52	2.1	0.16	0.48	0.36	45	0.11	0.8	0.09
	210	87	0.32	0.07	0.07	0.54	3.5	0.15	0.19	0.66	38	0.16	0.64	0.2
	430	**56**	0.46	0.04	0.09	0.41	3.3	0.23	0.09	0.68	26	0.26	0.41	0.33
A3–2	210	123	0.65	0.04	0.03	0.28	6.1	0.7	0.16	0.14	66	0.41	0.52	0.07

aggregates also dominated the volume fluxes ($45.3 \pm 22\,\%$, all stations and depths averaged) with a maximum of 70 % at A3–2. However, volumes of cylindrical fecal pellets collected at E–5 ($44 \pm 33\,\%$, all depths averaged) and volumes of fecal aggregates collected at F–L ($57 \pm 18\,\%$, all depths averaged) represented the highest fractions at these stations.

Projected area fluxes at all stations and depths (Fig. 2.6) showed a clear attenuation of the total flux between 210 and 430 m (loss of $38 \pm 21\,\%$ on average) with a maximum attenuation of 74 % at E–5 (Fig. 2.6a). A decrease in the flux of cylindrical fecal pellets with depth was combined with an increase in the flux of aggregates (mainly phytodetrital) except at R–2, where a general flux attenuation was observed (all particle categories), and only a small increase in phytodetrital aggregates at 430 m.

Fluxes at E stations at 110 and 210 m decreased with time between E–1 and E–3, followed by a strong increase in cylindrical fecal pellet flux at E–5 (Fig. 2.6c).

Number and volume flux spectra

Smallest particles were the most numerous at every site and depth (Fig. 2.7). Particle numbers decreased by more than 3 orders of magnitude for a 1 order of magnitude increase in size (0.008–0.07 cm) leading to slopes values around −3, and therefore in the range expected for particle size distribution (PSD) in natural waters (−2 to −5; Buonassissi and Dierssen, 2010; Guidi et al., 2009). Phytodetrital aggregates, representing the largest fraction of total particles,

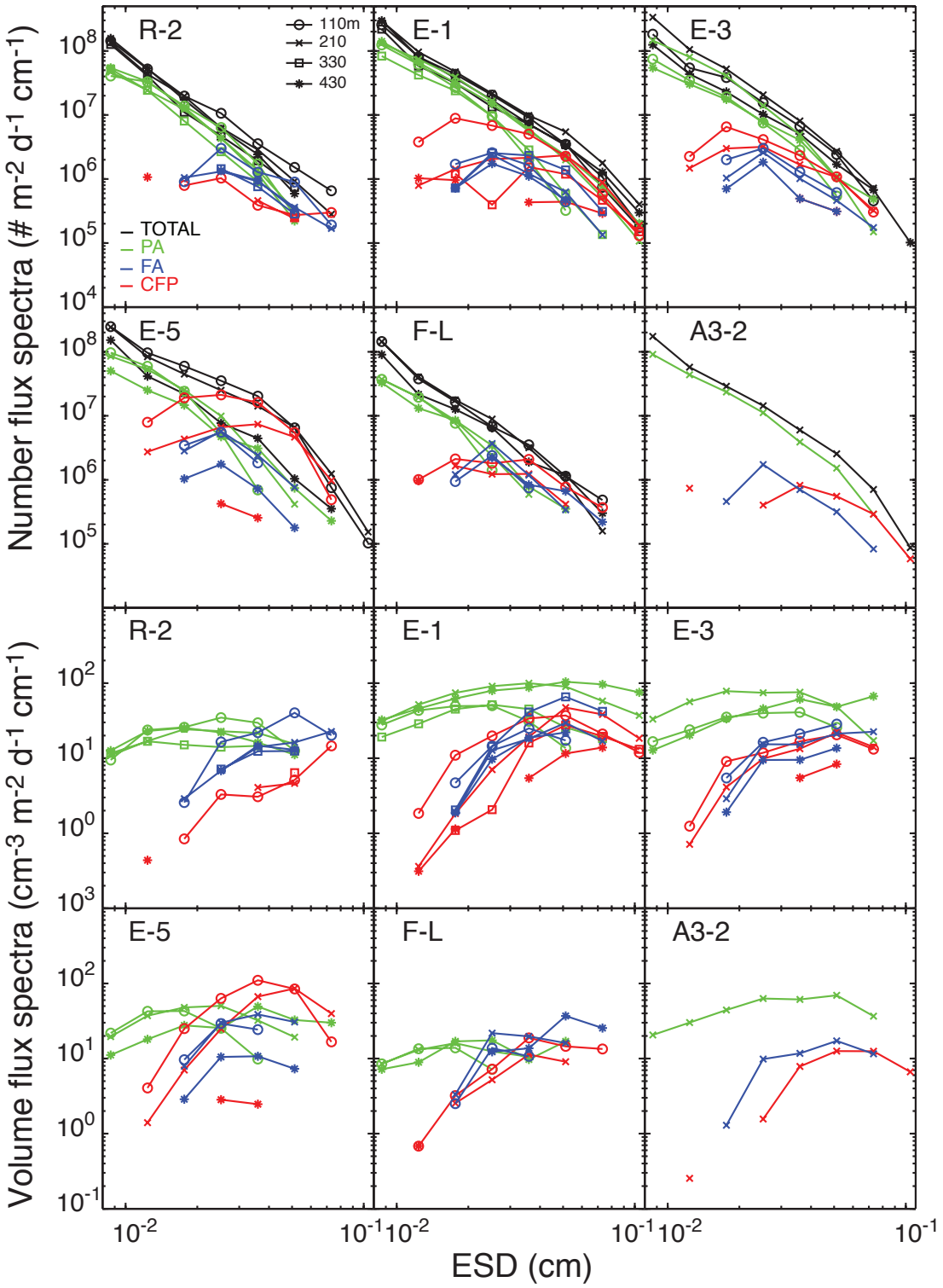

Figure 2.7: Total number and volume fluxes of particles binned in 10 size classes. Bins with less than five particles were removed (see Table 2.2 and text for explanations). Results are shown for each category of particles at all depths and sites. TOTAL: all particles; PA: phytodetrital aggregates; FA: fecal aggregates; CFP: cylindrical fecal pellets. Smallest particles represented by phytodetrital aggregates were the most numerous at every site and depth. Middle–sized phytodetrital aggregates and fecal particles (pellets and aggregates) contributed the most to the volume flux due to the overall rarity of very large particles relative to all particles.

broadly followed the same spectra. Most cylindrical fecal pellets and fecal aggregates were middle–sized (ESD of 0.015–0.1 cm) with maximum abundances in the range 0.015–0.03 cm. E–5 presented the highest abundance of large fecal pellets (0.025 to 0.035 cm) with values exceeding 2×10^7 and 7×10^6 # $m^{-2}\,d^{-1}\,cm^{-1}$ at 110 and 210 m respectively.

At all sites, most of the volume flux of phytodetrital aggregates was carried by middle–sized particles (ESD of 0.01–0.03 cm) due to the small contribution of large aggregates to the total number. Middle–sized and large cylindrical fecal pellets and fecal aggregates (ESD of 0.03–0.07 cm) carried most of the volume flux, but again the largest particles did not bring the highest contribution due to their rarity relative to smaller particles (except at R–2, where the largest cylindrical fecal pellets and fecal aggregates contributed significantly to the volume flux).

The most notable change in the number flux spectra with depth was observed for middle–sized cylindrical fecal pellets at E stations, for which a decrease in number was generally combined with an increase in size. E–1 presents the best illustration, with most of the cylindrical fecal pellets with a size around 0.01 cm at 110 m increasing to 0.06 cm at 210 m.

POC flux from image analysis

The lowest carbon fluxes were estimated at R–2 and F–L (Table 2.3) with values of 27 ± 12 and 36 ± 10 mg C $m^{-2}\,d^{-1}$ respectively (all depths averaged). The highest carbon fluxes were observed at E stations (107 ± 33 mg C $m^{-2}\,d^{-1}$, all E stations and depths averaged) with a maximum value of 180 mg C $m^{-2}\,d^{-1}$ at E–5, 110 m. A3–2 presented a moderate carbon flux of 66 mg C $m^{-2}\,d^{-1}$ at 210 m.

Cylindrical fecal pellets carried most of the carbon flux at all stations and depths, with an average fractional contribution of 56 ± 19 % (Table 2.3). This was particularly true at E stations, where fecal pellets drove on average 63 ± 17 % of the carbon flux (maximum of 88 % at E–5, 110 m), and at F–L (62 ± 20 %, all depths averaged). However, at several stations, a transition was observed at 430 m, where phytodetrital aggregates brought a larger fractional contribution with 63, 47 and 55 % at R–2, E–1 and E–5 respectively. Fecal aggregates generally carried a small fraction of the carbon flux, with an average of 13 ± 8 % (all stations and depths), but their contribution tended to increase with depth (e.g. 24 and 33 % at 430 m at R–2 and F–L respectively).

Table 2.4: Particle fluxes at 210 m depth from free-drifting deployments of the 12-cup-carousel cylindrical PPS3/3 trap. The trap collection area was 0.125 m^2. Particles were washed through a 350 µm Nitex screen to remove zooplankton and were collected on a 1 mm silver filter. Mean values and their standard deviations are indicated in bold.

Cup ID #	Opening time (UTC)[a] [duration (h)]	Poison in cup	Mass flux	POC flux	TPN flux	BSi flux	PIC flux	^{234}Th flux	POC : TPN	POC : BSi	POC : PIC	POC : ^{234}Th	POC : mass
			($g\,m^{-2}\,d^{-1}$)	($mg\,C\,m^{-2}\,d^{-1}$)	($mmol\,m^{-2}d^{-1}$)			($dpm\,m^{-2}\,d^{-1}$)	($mol\,mol^{-1}$)			($\mu mol\,dpm^{-1}$)	($g\,g^{-1}$)
E–1													
1	29 Oct 11, 13:00 [12]	none	–	–	–	–	–	–	–	–	–	–	–
2	30 Oct 11, 01:00 [12]	none	–	–	–	–	–	–	–	–	–	–	–
3	30 Oct 11, 13:00 [12]	$HgCl_2$	2.55	120.10	1.46	34	0.01	722	6.84	0.29	1016	13.8	0.05
4	31 Oct 11, 01:00 [12]	$HgCl_2$	2.34	103.17	1.22	32	0.00	675	7.04	0.27	8809	12.7	0.04
5	31 Oct 11, 13:00 [12]	none	–	–	–	–	–	–	–	–	–	–	–
6	1 Nov 11, 01:00 [12]	none	–	–	–	–	–	–	–	–	–	–	–
7	1 Nov 11, 13:00 [12]	none	1.14	64.73	0.71	11	0.83	869	7.56	0.51	6.53	6.2	0.06
8	2 Nov 11, 01:00 [12]	none	1.06	43.24	0.60	11	0.58	826	5.99	0.34	6.21	4.4	0.04
9	2 Nov 11, 13:00 [12]	none	–	–	–	–	–	–	–	–	–	–	–
10	3 Nov 11, 01:00 [12]	none	1.72	90.44	1.10	17	0.67	1311	6.87	0.44	11.30	5.7	0.05
11	3 Nov 11, 01:00 [Blk]	none	–	–	–	–	–	–	–	–	–	–	–
12	3 Nov 11, 01:00 [Blk]	none	–	0	0.00	–	0.00	–	3.86	–	11.60	–	–
		mean[b]	**1.76**	**84.31**	**1.02**	**21.03**	**0.52**	**881**	**6.90**	**0.33**	**13.49**	**8.6**	**0.05**
		SD[c]	**0.61**	**27.38**	**0.32**	**10.41**	**0.31**	**226**	**0.57**	**0.10**	**NA**	**3.9**	**0.01**
E–3													
1	5 Nov 11, 07:00 [1]	none	–	–	–	–	–	–	–	–	–	–	–
2	5 Nov 11, 08:00 [8]	none	–	–	–	–	–	–	–	–	–	–	–
3	5 Nov 11, 09:00 [1]	$HgCl_2$	1.34	40.95	0.38	10	0.39	997	8.89	0.33	8.69	3.4	–
4	5 Nov 11, 17:00 [8]	$HgCl_2$	0.99	45.64	0.55	11	0.60	1073	6.89	0.36	6.38	3.5	0.05
5	6 Nov 11, 01:00 [12]	none	–	–	–	–	–	–	–	–	–	–	–
6	6 Nov 11, 13:00 [12]	none	–	–	–	–	–	–	–	–	–	–	–
7	7 Nov 11, 01:00 [12]	none	1.11	35.07	0.45	9	1.11	947	6.43	0.31	2.62	3.1	0.03
8	7 Nov 11, 13:00 [12]	none	0.97	28.10	0.38	8	1.01	813	6.14	0.28	2.31	2.9	0.03
9	8 Nov 11, 01:00 [12]	none	–	–	–	–	–	–	–	–	–	–	–
10	8 Nov 11, 13:00 [12]	none	–	–	–	–	–	–	–	–	–	–	–
11	9 Nov 11, 01:00 [12]	$HgCl_2$	1.21	64.13	0.71	11	0.71	1240	7.47	0.49	7.53	4.3	0.05
12	9 Nov 11, 13:00 [12]	$HgCl_2$	2.17	116.50	1.48	22	1.19	1565	6.55	0.44	8.14	6.2	0.05
		mean	**1.35**	**58.49**	**0.72**	**12.35**	**0.94**	**1129**	**6.74**	**0.39**	**5.19**	**4.02**	**0.04**
		SD	**0.46**	**18.50**	**0.21**	**2.48**	**0.20**	**177**	**1.01**	**0.08**	**2.80**	**1.24**	**0.01**
E–5													
1	18 Nov 11, 13:00 [3]	none	–	–	–	–	–	–	–	–	–	–	–
2	18 Nov 11, 16:00 [3]	none	–	–	–	–	–	–	–	–	–	–	–
3	18 Nov 11, 19:00 [3]	$HgCl_2$	–	–	–	–	–	–	–	–	–	–	–
4	18 Nov 11, 22:00 [3]	$HgCl_2$	1.6	40.83	0.4	32	0.8	1688	7.79	0.11	4.39	2.0	0.03
5	19 Nov 11, 01:00 [3]	none	–	–	–	–	–	–	–	–	–	–	–
6	19 Nov 11, 04:00 [3]	none	–	–	–	–	–	–	–	–	–	–	–
7	19 Nov 11, 07:00 [3]	none	–	–	–	–	–	–	–	–	–	–	–
8	19 Nov 11, 10:00 [3]	none	0.42	16.81	0.2	6	0.4	378	6.83	0.25	3.34	3.8	0.04
9	19 Nov 11, 13:00 [3]	none	–	–	–	–	–	–	–	–	–	–	–
10	19 Nov 11, 16:00 [3]	none	–	–	–	–	–	–	–	–	–	–	–
11	19 Nov 11, 19:00 [3]	$HgCl_2$	0.29	14.41	0.2	5	0.2	800	7.41	0.22	6.37	1.4	0.05
12	19 Nov 11, 19:00 [n.r.]	–	–	–	–	–	–	–	–	–	–	–	–
		mean	**0.78**	**24.02**	**0.27**	**14.25**	**0.46**	**955**	**7.46**	**0.14**	**4.32**	**2.42**	**0.03**
		SD	**0.60**	**12.01**	**0.12**	**12.41**	**0.24**	**546**	**0.48**	**0.08**	**1.54**	**1**	**0.01**
A3–2													
1	15 Nov 11, 22:00 [3]	none	–	–	–	–	–	–	–	–	–	–	–
2	16 Nov 11, 01:00 [3]	none	–	–	–	–	–	–	–	–	–	–	–
3	16 Nov 11, 04:00 [3]	$HgCl_2$	–	–	–	–	–	–	–	–	–	–	–
4	16 Nov 11, 07:00 [3]	$HgCl_2$	0.42	19.34	0.22	6	0.19	498	7.19	0.29	8.32	3.2	0.05
5	16 Nov 11, 10:00 [3]	none	–	–	–	–	–	–	–	–	–	–	–
6	16 Nov 11, 13:00 [3]	none	–	–	–	–	–	–	–	–	–	–	–
7	16 Nov 11, 16:00 [3]	none	–	–	–	–	–	–	–	–	–	–	–
8	16 Nov 11, 19:00 [3]	none	0.42	22.94	0.30	6	0.27	535	6.36	0.34	7.19	3.6	0.05
9	16 Nov 11, 22:00 [3]	none	–	–	–	–	–	–	–	–	–	–	–
10	16 Nov 11, 01:00 [3]	none	–	–	–	–	–	–	–	–	–	–	–
11	17 Nov 11, 04:00 [3]	$HgCl_2$	–	–	–	–	–	–	–	–	–	–	–
12	17 Nov 11, 07:00 [3]	$HgCl_2$	0.42	38.19	0.55	10	0.28	486	5.79	0.31	11.51	6.5	0.09
		mean	**0.42**	**26.78**	**0.36**	**7.17**	**0.25**	**506**	**6.24**	**0.31**	**9.11**	**4.45**	**0.06**
		SD	**0.00**	**8.17**	**0.14**	**2.24**	**0.04**	**21**	**0.71**	**0.02**	**2.24**	**1.48**	**0.02**

[a] Local time was UTC + 5 h.
[b] For all stations, mean values are the total collection divided by the total time over the entire deployment.
[c] For all stations, flux standard deviations are weighted by cup duration times. Component ratio standard deviations are unweighted.
n.r.: not rotated.
NA: Not available
Blk: Blank

2.3.2 Biogeochemical fluxes collected in PPS3/3 traps

Bulk fluxes from PPS3/3 traps are reported in Table 2.4. The highest mass, POC, ^{234}Th and TPN fluxes were collected at E stations. POC fluxes decreased over time from 84 ± 27 at E–1, to 58 ± 18 at E–3, to 24 ± 12 at E–5 $\mathrm{mg\,C\,m^{-2}\,d^{-1}}$. A3–2 presented a POC flux of $27\,\mathrm{mg\,C\,m^{-2}\,d^{-1}}$. An average ^{234}Th activity of $988 \pm 127\,\mathrm{dpm\,m^{-2}\,d^{-1}}$ was recorded at E stations, with a maximum of $1129 \pm 177\,\mathrm{dpm\,m^{-2}\,d^{-1}}$ at E–3. ^{234}Th fluxes are detailed in Planchon et al. (2014). Over all sites, BSi fluxes were very high (7 ± 2 to $21 \pm 10\,\mathrm{mmol\ BSi\ m^{-2}\,d^{-1}}$), suggesting the large contribution of diatoms to the phytoplankton community. Conversely, very low particulate inorganic carbon (PIC) fluxes (1–4 orders of magnitude lower than POC fluxes) suggested the limited role of calcium carbonate ($CaCO_3$) in biogenic mineral fluxes. POC : TPN ratios were close to the canonical Redfield ratio of 6.6 for phytoplankton at all stations except E–5 (7.5) which also displayed the lowest POC : BSi ratio (0.1). At E stations, POC : ^{234}Th and POC : mass ratios decreased over time (POC : ^{234}Th ratios from 8 at E–1 to $2.1\,\mathrm{\mu mol\,dpm^{-1}}$ at E–5; POC : mass ratio from 0.05 at E–1 to $0.03\,\mathrm{g\,g^{-1}}$ at E–5) suggesting an attenuation of export fluxes combined with a degradation of sinking particles. A3–2 displayed POC : ^{234}Th and POC : mass ratios of $4.4\,\mathrm{\mu mol\,dpm^{-1}}$ and $0.06\,\mathrm{g\,g^{-1}}$ respectively. In general, no consistent differences in fluxes could be resolved between poisoned and unpoisoned cups.

2.3.3 POC flux comparisons and export efficiencies

POC fluxes determined from gel images (using particle volume–to–carbon–content conversion factors) were in the same range of values as those determined from particle collection in PPS3/3, with maximum differences at a same station never exceeding 1 order of magnitude (Tables 2.3 and 2.4). POC fluxes from PPS3/3 were systematically lower than those derived from image analysis (on average 57 ± 22 % less).

E–ratios, calculated as the ratio of POC fluxes from gel image analysis to 1 % PAR–integrated net primary productivity (Cavagna et al., 2014; Table 2.5) indicated a high export efficiency at R–2 and E–1 (0.2 ± 0.08 and 0.23 ± 0.07 respectively, all depths averaged), intermediate at E–3 and E–5 (0.1 ± 0.02 and 0.13 ± 0.09 respectively, all depths averaged), and very low at F–L (0.01 ± 0.0, similar value at all depths) and A3–2 (0.03). E–ratios derived from POC fluxes estimated from PPS3/3 traps showed lower values but followed the same trend: E–1 > E–3 > E–

Table 2.5: Export efficiency at each site estimated from several methods. Maximum and minimum export efficiencies are indicated in bold.

Site	Depth	E–ratios		ThE_C	$\%\sum POC_{ML}$ export 1 d	
ID	(m)	Gels	PPS3/3		Gels	PPS3/3
R–2	100 ± 10	0.32	–	**0.34**	0.92	–
	200 ± 10	0.22	–	0.16	0.64	–
	330	0.15	–	–	0.43	–
	430	0.12	–	–	0.34	–
E–1	100 ± 10	0.21	–	0.27	2.12	–
	200 ± 10	**0.34**	**0.16** ± 0.05	0.18	3.34	1.59 ± 0.52
	330	0.21	–	–	2.05	–
	430	0.18	–	–	1.82	–
E–3	100 ± 10	0.10	–	0.21	2.22	–
	200 ± 10	0.12	0.08 ± 0.03	0.14	2.82	1.92 ± 0.64
	430	0.08	–	–	1.86	–
E–5	100 ± 10	0.19	–	0.11	3.76	–
	200 ± 10	0.19	0.03 ± 0.02	0.1	3.69	0.50 ± 0.25
	430	0.03	–	–	0.63	–
F–L	100 ± 10	**0.01**	–	**0.01**	0.73	–
	200 ± 10	0.01	–	0.01	0.62	–
	430	0.01	–	–	0.42	–
A3–2	100 ± 10	–	–	0.05	–	–
	200 ± 10	0.03	**0.01** ± 0.004	0.02	0.32	0.13 ± 0.04

E-ratio: POC flux (gels, PPS3/3) / NPP (E_Z integration 1 % PAR; data from Cavagna et al., 2014).
ThE_C: POC flux (^{234}Th; data from Planchon et al., 2015) / NPP.
$\%\sum POC_{ML}$ export 1 d: percentage of mixed-layer-integrated POC exported in 1 day.

5 > A3–2. Export efficiencies derived from ^{234}Th disequilibria, ThE_C (Planchon et al., 2015), are shown in Table 2.5 for comparison, and are discussed in the next section.

According to calculations based on gel trap POC flux and transmissometer POC concentration estimates (Fig. 2.2), E stations exported the largest percentage of their mixed–layer–integrated POC (ΣPOC_{ML}) per day (2.4 ± 1 %, all E stations and depths averaged) with the maximum observed at E–5 (2.7 ± 1.8 %, all depths averaged) and values of 2.3 ± 0.7 and 2.3 ± 0.5 % at E–1 and E–3 respectively (all depths averaged). R–2 and F–L exported respectively 0.58 ± 0.2 and 0.59 ± 0.15 % of their ΣPOC_{ML} per day (all depths averaged), and A3–2 exported 0.32 % of its ΣPOC_{ML} per day (210 m). A similar trend was obtained using POC fluxes from PPS3/3 traps (E stations > A3–2).

2.4 Discussion

2.4.1 Comparison of POC flux estimations

Two different approaches were used to estimate POC fluxes. PPS3/3 trap collection providing a direct determination of the flux served as a reference method. POC fluxes estimated from

image analysis of particles embedded in polyacrylamide gels were in the same range as those derived from PPS3/3 but were systematically higher (see section 2.3). This difference is most likely due to the uncertainty in the volume–to–carbon conversion factors (Fig. 2.4) used to estimate POC fluxes from particle image analysis. A comparison with the direct estimation of bulk fluxes collected in PPS3/3 suggests that our volume–to–carbon–content conversion factors tended to slightly overestimate the carbon carried by sinking particles (Tables 2.3 and 2.4) especially at E–5, where it was up to 7–fold higher. At this station the large contribution of cylindrical fecal pellets to the volume flux (Table 2.3; 72 % at 110 m and 51 % at 210 m) suggests that the volume–to–carbon conversion factor used for these particles may be responsible for the mismatch observed. The value of $0.036\,\mathrm{mg\,C\,mm^{-3}}$ used as an average for copepod and euphausiid fecal pellets may not reflect the actual carbon contained in the cylindrical fecal pellets collected. Feeding behaviours (e.g. herbivorous or coprophagous) specific to each zooplankton group will produce fecal pellets with variable carbon content due to variable fraction of undigested food, compaction or vulnerability to physical or biological degradation (Urban-Rich et al., 1998). Constant carbon to volume ratios are thus unable to reflect the myriad of fecal pellet compositions linked to ecosystem structure variations. Values of carbon content in cylindrical fecal pellets found in the literature range over approximately 1 order of magnitude between 0.01 and $0.1\,\mathrm{mg\,C\,mm^{-3}}$ (Carroll et al., 1998; González and Smetacek, 1994; González et al., 1994, 2000), leading to potential strong variations in carbon flux estimations if large volumes of fecal pellets are involved, as was the case at E–5. Mesozooplankton communities collected in Bongo nets from 250 m to the surface (day and night haulings, except at R–2 and F–L, where only day haulings were conducted), and analysed with a ZooScan integrated system (Carlotti et al., 2015), generally revealed a large dominance of the size fraction 500–1000 µm with values from 54 to 79 % (considering only the stations where the traps were deployed). Microscopic identifications confirmed a community largely dominated by copepods (Carlotti et al., 2015). However, most of the fecal pellets collected in gel traps at E–5 were large fragments (Fig. 2.5) with a peritrophic membrane interrupted at their extremities suggesting more probably an origin from euphausiids rather than copepods, which produce smaller fecal pellets with a continuous peritrophic membrane terminated by a pellicle (Gauld, 1957; Martens, 1978; Yoon et al., 2001). Differences in euphausiid and copepod fecal pellet sinking velocities due to size variations, ballast content or compaction (Fowler and Small, 1972; Small et al., 1979), as well as contrasted sensitivities to

degradation or zooplankton vertical migration behaviours (Wallace et al., 2013), could explain the mismatch between the zooplankton community identified from net haulings and the fecal pellets collected in gel traps. A reduced collection efficiency of euphausiids compared to copepods could also be responsible for this mismatch, knowing that specific nets like the Multiple Opening and Closing Nets and Environment Sensing System (MOCNESS; Wiebe et al., 1976) are needed to efficiently capture both mesozooplankton and euphausiids in the layer 0–250 m (e.g. Espinasse et al., 2012). Most studies show that zooplankton net avoidance is complex and variable; it depends on environmental conditions (e.g. light regime), net characteristics, and various zooplankton characteristics, including size, shape, species, sex and developmental stage (Brinton, 1967; Fleminger and Clutter, 1965; Wiebe et al., 1982).

Assuming a dominance of euphausiid fecal pellets at E–5, the use of the reference value of $0.016\,\mathrm{mg\,C\,mm^{-3}}$ improves the match between POC fluxes estimated from PPS3/3 and gel traps (ratios $\mathrm{POC_{gels}}\,/\,\mathrm{POC_{PPS3/3}} = 4$) although it cannot fully explain the discrepancy, presumably due to other factors (e.g. particle field heterogeneity or small differences in sediment trap collection efficiencies).

2.4.2 Evolution of the flux at depth

POC fluxes presented in Fig. 2.8 were estimated through two different approaches: gel trap image analysis (at 110, 210, 330 and 430 m) and total ^{234}Th activity measured at 11–14 depths at all stations (Planchon et al., 2015) and calculated at 100, 150 and 200 m. Fluxes estimated from PPS3/3 trap collection at only one depth (210 m) are not presented here. Figure 2.8 shows the evolution of POC fluxes with depth and its comparison with the empirical flux attenuation known as the 'Martin curve' (Martin et al., 1987), estimating the flux at depth from values at 100 m ranging from 20 to $500\,\mathrm{mg\,C\,m^{-2}\,d^{-1}}$. Agreements between POC flux determination methods and this empirical relationship were the best for R–2 and F–L, showing a continuous attenuation of the flux with depth, but always at a lower rate than predicted by the Martin curve.

For all other stations POC fluxes above 210 m presented complex patterns suggesting distinct POC export episodes to be more likely than a continuous downward flux. Between 210 and 430 m the attenuation of POC fluxes estimated from the gel traps tends to be more consistent with the Martin curve, except for E–5, which displayed a strong decrease (as already noted in the

section 2.3). A fecal pellet loss at depth was particularly strong at E–5, due to the large role played by these particles at this site, but was observed at all stations (Fig. 2.6).

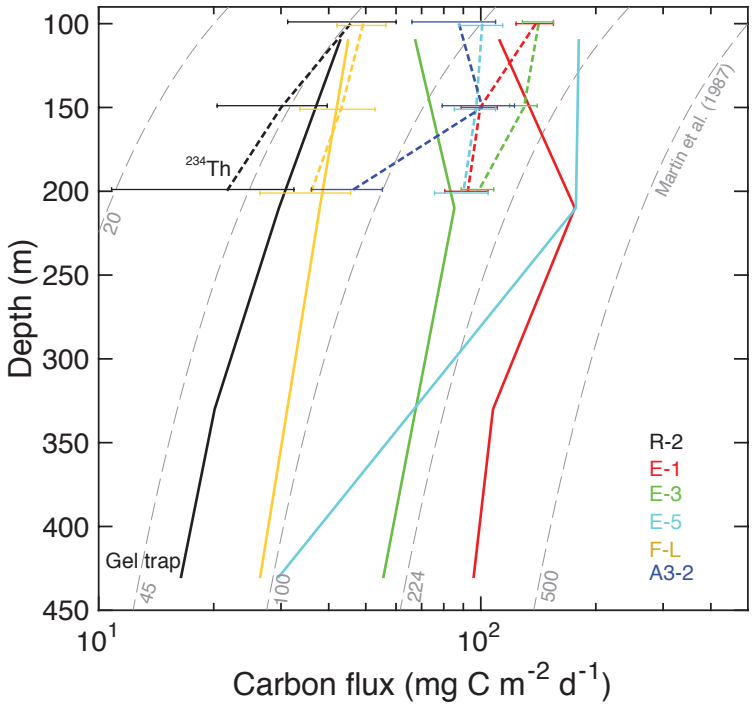

Figure 2.8: Variation in the carbon flux with depth estimated from gel trap and ^{234}Th methods. The empirical attenuation of the flux with depth (Martin curve) is represented by grey dashed lines for initial values of the carbon flux at 100 m from 20 to 500 mg C m^{-2} d^{-1}. Error bars are indicated for the ^{234}Th data. Results show overall poor agreements between observed fluxes and the Martin curve, suggesting the complexity of the processes affecting the carbon flux with depth.

Our data revealed two major trends of particle flux evolution with depth: (i) the fecal pellet flux decreased, and (ii) phytodetrital and fecal aggregate fluxes remained constant or even increased. Establishing a link between these two processes is tempting. It suggests the importance of physical reaggregation in sustaining the carbon flux at depth from fecal pellets that have undergone bacterial degradation or zooplankton coprorhexy (Iversen and Poulsen, 2007; Lampitt et al., 1990; Suzuki et al., 2003). A recent study from Giering et al. (2014) suggests that half of fast–sinking particles in the twilight zone of the eastern Atlantic Ocean (between 50 and 1000 m) are fragmented and ingested by zooplankton, and that more than 30 % may be released as suspended and slowly sinking organic matter. Even if the gel trap technique does not offer enough information on aggregation processes and particle sources to permit any clear conclusion, the hypothesis of a reaggregation of unpacked fecal pellets into 'secondary' phytodetrital aggregates still deserves careful consideration.

Since the rate of physical aggregation is largely controlled by particle concentration (Jack-

son, 1990), a reaggregation at depth implies that sufficient material has been released by fecal pellet disaggregation. If single cells represented most of the material released during fecal pellet disaggregation, their concentration should have increased with depth in the case of no secondary aggregation, or remained constant as a balance between aggregate formation and loss by sinking (notion of critical concentration; (Jackson, 1990; Jackson et al., 2005). The number flux spectra (Fig. 2.7) suggest that the smallest particles had a constant concentration until 210 m at almost every site. Station E–3 shows an increase in the number of small particles between 110 and 210 m and then a decrease at 430 m, which could indicate reaggregation processes occurring at depth. This decrease at 430 m is also observable at E–5 and F–L. However, data evaluation in this way implies a steady–state assumption which considers that traps measured the occurrence of a unique sinking event; the flux collected at depth being a direct temporal evolution of the same shallower flux. This appears unlikely considering the episodic nature of export and its dependence on highly dynamical ecosystem interactions responsible for high flux variability at short spatio–temporal scales as evidenced by the PPS3/3 individual cup variations (Table 2.4). In addition, if assuming phytodetrital aggregates at E–3, sinking at an average velocity of $150\,\mathrm{m\,d^{-1}}$ (based on results from Laurenceau–Cornec et al., 2015a, Chapter 3), a particle field would need approximately 1.5 days to sink from 210 to 430 m, neglecting any advection. Considering this calculation and the short trap deployment at E–3 (1.02 days), a non–steady–state assumption appears more reasonable, and the increase in phytodetrital and fecal aggregates observed at depth could reflect an earlier production event.

2.4.3 Temporal POC flux variations during KEOPS2 and comparison with KEOPS1

From E–1 to E–5, the POC flux varied with the depth and estimation method. Collection of POC flux in PPS3/3 trap at 210 m revealed a monotonic decrease in the flux with time (Table 2.4). Temporal evolution of the flux between E–1, E–3 and E–5, at 100 ± 10 and 200 ± 10 m, using gel trap and ^{234}Th methods (Planchon et al., 2015), shows a almost constant flux (undistinguishable differences within the uncertainties). At 430 m, gel traps measured flux evolutions comparable to those identified in the PPS3/3 at 210 m, i.e. a continuous decrease in the flux with time. With the results from 110 and 210 m at E–5 excluded (likely linked to an episodic flux of euphausiid

fecal pellets at these depths; see text above), the gel traps also show a decrease in the total flux over time, consistent with PPS3/3 trap method. The unusual increase at E–5, against the steady background of the other E stations, highlights the importance of zooplankton in modifying the particle flux.

At the KEOPS1 (January–February 2005) bloom reference station A3, POC flux values estimated at 200 m from gel trap image analysis and PPS3/3 traps were 62 and 13–20 mg C m^{-2} d^{-1} respectively (Ebersbach and Trull, 2008), i.e. in the same range as during KEOPS2 at the same station and using the same methods (gels: 66 mg C m^{-2} d^{-1}; PPS3/3: 27 mg C m^{-2} d^{-1}). During KEOPS1, the ^{234}Th–based method assuming a non–steady–state system (NSS) yielded 200 m POC fluxes of 294 mg C m^{-2} d^{-1} at A3 (flux averaged over 21 days) and 124 mg C m^{-2} d^{-1} at the KEOPS1 HNLC reference station C11 (flux averaged over 10 days; Savoye et al., 2008). These values are well above the KEOPS2 values of 46 and 22 mg C m^{-2} d^{-1} determined at 200 m at A3–2 and R–2 respectively using the same method (average over 28 days, except for R–2 assumed in steady state; Planchon et al., 2015). The ^{234}Th–based method assuming NSS integrated the POC flux over a period longer than 20 days, contrasting with the 1 day to 1 week period provided by gel and PPS3/3 trap estimations.

Seasonal trends are more reliable if calculated over a longer period, and the ^{234}Th–based method then gives the best insight into the temporal evolution of the POC flux from the onset of the bloom to its decline. ^{234}Th results suggest that the POC flux was approximately 5- to 6–fold higher at the decline of the bloom (January–February) than during its onset (October–November), agreeing with the common view that most of the export flux occurs in late bloom stage (Wassmann, 1998). During KEOPS1, at A3 and C11, the NPP integrated within the euphotic zone was 1030±43 and 224±30 mg C m^{-2} d^{-1} respectively (based on ^{13}C incorporation; Mosseri et al., 2008; Lefévre et al., 2008). In comparison, values of 1903 ± 186 and 135 ± 6 mg C m^{-2} d^{-1} were determined at A3–2 and R–2 during KEOPS2 (euphotic zone, E_Z 1 % PAR–integrated NPP based on ^{13}C incorporation; Cavagna et al., 2014). Carbon export efficiencies estimated at 200 m, based on ^{234}Th–derived POC export flux (reported as ThE_C), were 30 % at A3 and 49 % at C11 during KEOPS1 (calculations using data from Savoye et al., 2008; Mosseri et al., 2008). In contrast, ThE_C values of 2 % (NSS model) and 16 % (SS model) were calculated at 200 m at A3–2 and R–2 respectively during KEOPS2 (Planchon et al., 2015). These results show that (i) primary productivity at the on–plateau site was approximately 2–fold higher in

spring than during summer and (ii) carbon export fluxes were approximately 5–fold lower during early than late bloom stage, leading to (iii) carbon export efficiencies up to 10–fold lower during the early bloom stage (spring) than during late bloom stage (summer).

2.4.4 Toward an explanation of the negative relationship between primary productivity and carbon export efficiency

We examined two different export efficiency indicators (Table 2.5): (i) e–ratios calculated as the ratio between POC fluxes estimated from gel images or PPS3/3 traps, and net primary productivity integrated over the euphotic zone (E_Z 1 % PAR; Cavagna et al., 2014), and (ii) ThE_C calculated as the ratio between POC flux estimated from ^{234}Th method and net primary productivity. KEOPS2 results suggest a negative relationship between primary productivity and carbon export efficiency, the most productive sites being those where carbon is exported the least efficiently. Figure 2.9a shows the relationship between primary productivity and export efficiency (with POC fluxes estimated at 200 ± 10 m from gels, PPS3/3 traps and ^{234}Th water column disequilibria) for KEOPS2 sites. For comparison purposes, KEOPS1 data are also indicated (Savoye et al., 2008). The empirical relationship proposed recently by Maiti et al. (2013), based on surface tethered cylindrical sediment traps and ^{234}Th data from up to 130 stations in the Southern Ocean, is also reported. While this negative relationship has now been observed in several field studies in the Southern Ocean (Jacquet et al., 2011; Morris et al., 2007; Savoye et al., 2008), and elsewhere (e.g. González et al., 2009), the reasons for its existence remain unclear. Maiti et al. (2013) mentioned differences in trophic structure, grazing intensity, recycling efficiency, high bacterial activity, or increase in DOC export as possible explanations for high–productivity, low–export–efficiency regimes. Phytoplankton physiological state has also been suggested as a possible control of carbon export mode and efficiency (González et al., 2009), although this could not be verified here due to a generally good phytoplankton physiological state confirmed via microscopy over the course of the KEOPS2 study (M. Lasbleiz and K. Leblanc, personal communication, 2014). In addition, due to their degradation–resistant and heavily silicified valves (Hargraves and French, 1983; Kuwata and Takahashi, 1990), the abundance of diatom resting spores in the sinking flux, as observed during KEOPS1 (Armand et al., 2008), could also be a major factor to consider when evaluating carbon export efficiency as suggested

by Salter et al. (2012) and Rynearson et al. (2013).

It was beyond the scope of this study to explore each of these potential controls of carbon export efficiency. However, in the light of KEOPS1 and KEOPS2 results, phytoplankton and zooplankton community structure and their trophic relationships through grazing, seem to have played an important role in carbon export mode and efficiency via controls on sinking particle composition.

Table 2.6 presents a summary of site characteristics based on net primary productivity, surface plankton communities determined from Niskin bottle sampling and net haulings (most abundant species and biomass), carbon export features at 200 ± 10 m (mode and efficiency), and iron fertilisation status (e.g. HNLC or iron–fertilised). Due to their importance in export fluxes demonstrated by high BSi fluxes (see section 2.3), only diatoms were examined in the phytoplankton community. Data are presented for all stations, but only stations R–2 and A3–2 will be discussed in detail here because of their reference status (i.e. HNLC and on–plateau bloom).

Table 2.6: Summary of site characteristics based on their primary productivity, plankton communities, iron–fertilisation and carbon export efficiency.

Site ID	E_Z–MLD (m)	NPP	Diatom community[a] (see text for %)	Mesozoo. community (%)[b] [Total mesozoo. biomass ($mm^3\,m^{-3}$)]	Export mode	E–ratio	Fe source – biomass/export
R–2	92–96	Lowest	*Fragilariopsis* spp. *Thalassionema nitzschioides* Centrics (< 25 µm)	*Ctenocalanus citer* (16) + cop. (19) *Oithona frigida* (12) *Paraeuchaeta* sp. C1–C3 (11) *Rhincalanus gigas* C1–C3 (10) [90]	PA, FA	Highest	HNLC – low biomass, high export efficiency
E–1	64–70	Moderate	*Thalassionema nitzschioides* *Fragilariopsis* spp. Centrics (< 25 µm)	Euphausiid eggs (16) *Ctenocalanus citer* (5) + cop. (11) Calanidae C1–C3 (6) [55]	CFP, PA	High	Fe-fertilised, mesoscale recirculation feature – moderate biomass moderate export efficiency
E–3	68–33	Moderate	*Thalassionema nitzschioides* *Fragilariopsis* spp.	*Ctenocalanus citer* (27) + cop. (34) *Oithona frigida* (4) [350]	CFP, PA	Moderate	
E–5	54–39	Moderate	*Thalassionema nitzschioides* *Chaetoceros Hyalochaete* spp. Centrics (< 25 µm)	*Ctenocalanus citer* (18) + cop. (18) Calanidae C1–C3 (15) + cop. (2) *Metridia lucens* cop. (6) [203]	CFP	Low	
F–L	29–31	Highest	*Thalassiosira* spp. (< 25 µm) *Chaetoceros Hyalochaete* spp.	Euphausiid eggs (26) *Ctenocalanus citer* (11) + cop. (12) *Triconia* sp. (6) [290]	CFP, FA	Lowest	Fe-fertilised, north polar front mixed zone – high biomass low export efficiency
A3–2	38–149	High	*Chaetoceros Hyalochaete* spp.	Euphausiid eggs (19) *Paraeuchaeta* sp. C1–C3 (12) Appendicularians (12) *Oithona similis* (8) *Ctenocalanus citer* (7) + cop. (8) [310]	PA	Low	Fe-fertilised, on-plateau bloom site – high biomass, low export efficiency

E_Z: depth of the base of the euphotic zone assumed at 1 % of the photosynthetic available radiation (PAR).
MLD: mixed layer depth calculated using the density difference criterion of $0.02\,\sigma_\theta$ [potential density at MLD = potential density at 10 m + $0.02\,kg\,m^{-3}$ (Park et al., 1998)].
NPP: euphotic–zone- (1 % PAR) integrated net primary productivity (Cavagna et al., 2014).
PA: phytodetrital aggregates.
CFP: cylindrical fecal pellets.
FA: fecal aggregates.
[a] Most abundant diatom genera or species presented in decreasing order of abundance. Data from M. Lasbleiz (personal communication, 2014) from Niskin bottle samples. Sampling depths: R–2: 116 m; E–1: 80 m; E–3: 137 m; E–5: 110 m; F–L: 52 m; A3–2: 151 m. See text for fractions of total live diatom cell counts (%).
[b] Mesozooplankton community and fraction of the total mesozooplankton biomass, presented by decreasing order of abundance. Data from Carlotti et al. (2015), from day net haulings only (250 m to the surface). Cop.: copepodite stage; C1–C3: development stages 1–3.

At the HNLC reference station R–2, characterised by the lowest net primary productivity (Cavagna et al., 2014), the diatom community was dominated by the heavily silicified *Fragilariopsis* spp. (34.6 %: fraction of total live diatom cell counts; see Table 2.6 for sampling depths;

M. Lasbleiz, personal communication, 2014) and *Thalassionema nitzschioides* (25.6 %) as well as by a limited mesozooplankton biomass represented mainly by middle–sized copepods (Carlotti et al., 2015). The export was mostly mediated through physical aggregation as suggested by the dominance of phytoplankton and fecal aggregates. The highest e–ratio estimated during KEOPS2 was observed at R–2. In contrast, the iron–fertilised on–plateau bloom station A3–2 displayed a high net primary productivity (Cavagna et al., 2014), and a diatom community largely dominated by the lightly silicified *Chaetoceros* subgenus *Hyalochaete* (87 %). The mesozooplankton biomass was up to 3–fold higher at A3–2 than at R–2. Small- and middle–sized copepods dominated, along with euphausiid eggs and appendicularians (Carlotti et al., 2015). Particles exported were mostly phytodetrital aggregates. One of the lowest e–ratios was recorded at A3–2. At E stations, used as a time series, the net primary productivity was moderate (Cavagna et al., 2014), and a shift from a high e–ratio at E–1 to a low e–ratio at E–5 was associated with plankton community shifts. This is indicated, for instance, by the remarkable increase in *Chaetoceros* subgenus *Hyalochaete* biomass from 10 and 2.3 % at E–1 and E–3 respectively to 22.5 % at E–5.

At stations R–2 and A3–2, although presenting very contrasted export efficiencies, physical aggregation seemed to dominate over biological aggregation, as suggested by the rarity of fecal pellets. If explained from this perspective, the inverse relationship between net primary productivity and export efficiency somewhat needs to be linked to the different nature of the aggregates produced at each station and their ability to export carbon to depth (e.g. slow- or fast–sinking). In parallel with the present study, roller tank experiments have been conducted to explore the influence of different phytoplankton communities on the sinking velocity of large phytodetrital aggregates and their aggregation processes (Laurenceau-Cornec et al., 2015a) (Chapter 3). These experiments consisted of the physical aggregation of natural assemblages sampled with Niskin bottles at high and low biomass sites during KEOPS2. Results suggest that the proportions of different phytoplankton types forming the phytodetrital aggregates could influence their sinking velocity (and potentially their efficiency at exporting carbon) via a control on their structure and excess density. A strong relationship ($r^2 = 0.98$) was found between the proportion of small spine–forming diatom cells included in marine snow aggregates (e.g. *Chaetoceros* subgenus *Hyalochaete*) and their sinking velocity, suggesting an important role for phytoplankton morphology with regard to export efficiency. However, no evidence has been found that natural

phytoplankton communities present at each site, as determined from Niskin bottle sampling (Table 2.6), reflect the composition of their aggregates, something required to approximate their sinking velocity from roller tank experiment results. Experimental and field studies noted that the proportions of diatoms in aggregates are not necessarily the same as their proportions in the surrounding water (Crocker and Passow, 1995; Riebesell et al., 1991; Waite and Nodder, 2001). Without direct estimation of the sinking velocity of natural aggregates formed in the water column at each station, no conclusion is possible and further investigations will be needed.

The potential control of export efficiency through zooplankton grazing is another hypothesis that we explored here. In the case of high grazing pressure, carbon export is driven mostly via fecal pellets, but these, even if sinking fast, potentially experience coprophagy or coprorhexy (Iversen and Poulsen, 2007; Lampitt et al., 1990; Suzuki et al., 2003), and disaggregation processes facilitating bacterial remineralisation (Giering et al., 2014). In Fig. 2.9b, mesozooplankton biomass data from KEOPS2 (250 m to surface Bongo net haulings; Carlotti et al., 2015) is shown as a simple index of zooplankton abundance against export efficiency. Considering all POC flux estimation methods, a correlation has been found ($n = 15$, $r^2 = 0.72$, $p < 0.0005$) suggesting that zooplankton may exert an important control on export efficiency. In this perspective, however, E–3 presented an unexpectedly high export efficiency considering its high zooplankton biomass, suggesting that factors predominantly affecting carbon export efficiency can vary locally and over time.

In the low–productivity systems (e.g. R–2) a direct export can be efficient if processed via fast–sinking aggregates composed of heavy–silicified diatoms that are also assumed to be grazing–resistant. In contrast, in the sites of high productivity (e.g. A3–2 and F–L) the export flux can be strongly attenuated if a large fraction of the organic carbon flows towards paths promoting its retention in the surface layer (i.e. grazing, microbial remineralisation and biomass accumulation). At A3, Christaki et al. (2014) proposed a carbon budget integrated over the mixed layer showing the carbon flows through microbial and higher trophic levels for early and late bloom stages. This budget indicates that, during KEOPS2, 2400 $\mathrm{mg\,C\,m^{-2}\,d^{-1}}$ was still available for phytoplankton biomass accumulation and/or export after subtracting the different loss terms, such as bacterial, microplankton and mesozooplankton respiration, as well as viral lysis of bacterial cells, from the gross community production (GCP). Using our carbon flux value at 200 m and phytodetrital aggregate contributions to this export, the relative fractions of the

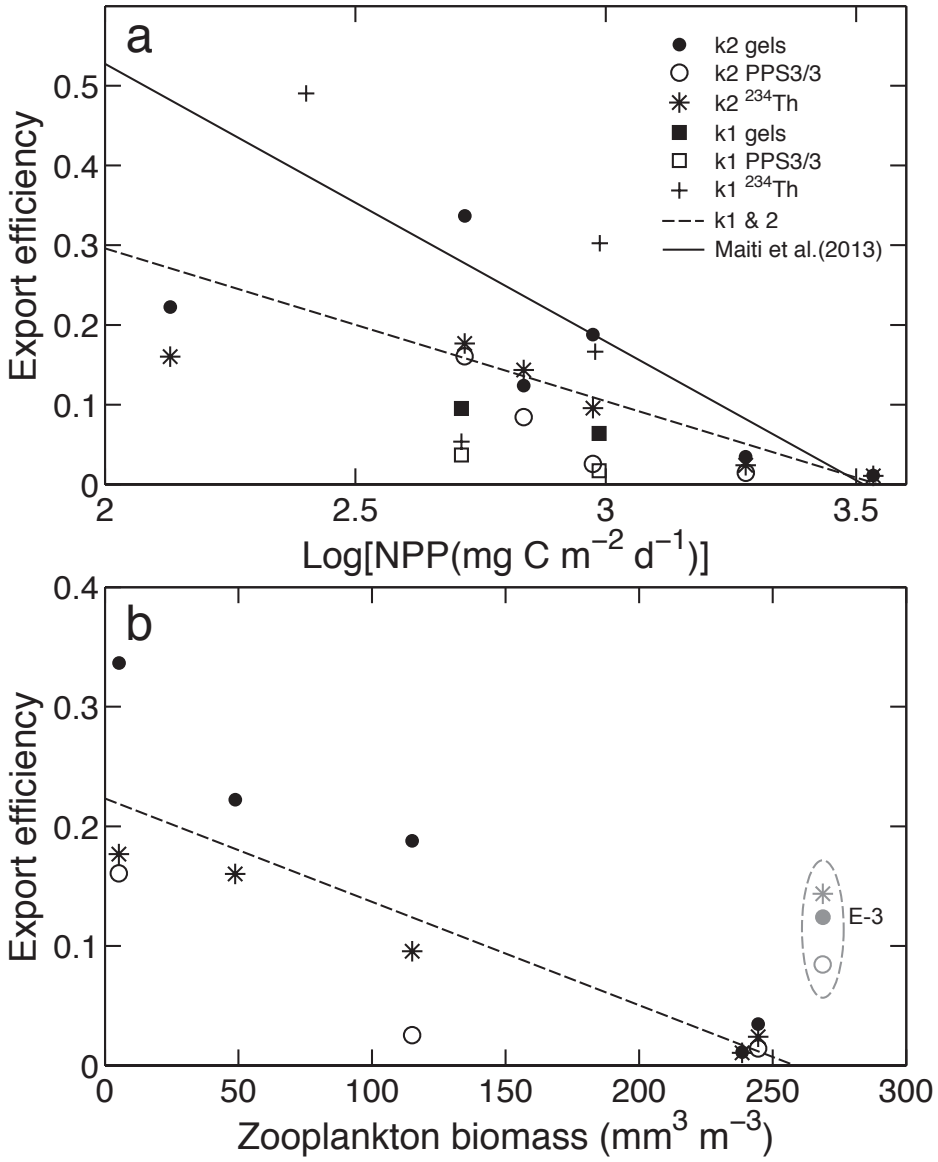

Figure 2.9: Relationships between net primary productivity **(a)**, zooplankton biomass **(b)** and export efficiency calculated using particulate organic carbon fluxes estimated at 200 ± 10 m from PPS3/3 traps, gel traps and ^{234}Th methods for the KEOPS2 (k2) and KEOPS1 (k1, **(a)** only) studies. **(a)** The black line represents the empirical relationship from Maiti et al. (2013) estimated in the Southern Ocean ($y = -0.35x + 1.22$; $r^2 = 0.97$), and the dashed line represents the regression line for all KEOPS data ($y = -0.19x + 0.68$; $n = 24$, $r^2 = 0.33$, $p < 0.005$). **(b)** The dashed line represents the regression line for KEOPS2 data ($y = -0.00086x + 0.2232$; $n = 15$, $r^2 = 0.72$, $p < 0.0005$). E–3 was assumed an outlier and was excluded from the best fit calculation (see text for possible explanation). Panel **(a)** suggests that the most productive sites are the less efficient to export carbon. Panel **(b)** suggests that zooplankton biomass could influence the efficiency of carbon export by bypassing direct export via phytodetrital aggregates.

available carbon actually used for biomass accumulation and/or export can be estimated here. At A3–2, the carbon flux at 200 m was 66 mg C m^{-2} d^{-1} (gel trap results) with 41 % contributed by phytodetrital aggregates (Table 2.3). This leads to 27 mg C m^{-2} d^{-1} exported (1.1 % of the remaining available carbon) and 2373 mg C m^{-2} d^{-1} used for biomass accumulation (98.9 %). The same calculations can be made for the late–bloom situation using the values of 384 mg C m^{-2} d^{-1} for the carbon still available for biomass accumulation and/or export (Christaki et al., 2014), the KEOPS1 200 m POC flux at A3 (62 mg C m^{-2} d^{-1}; Ebersbach and Trull, 2008), and a 36 % aggregate contribution (including both phytodetrital and mixed aggregates; Ebersbach and Trull, 2008). Results lead to 22 mg C m^{-2} d^{-1} exported (5.7 %) and 362 mg C m^{-2} d^{-1} used for biomass accumulation (94.3 %). These estimations show that the fraction of the carbon available that is exported is subject to large variations during the season (increased by a factor of ~ 5), while the fraction allocated to biomass accumulation varied comparatively much less (decreased by a factor of ~ 1.05). This suggests that A3 progressed over the whole season from a retention- to an export–dominated food web system (Wassmann, 1998), possibly related to successions of plankton communities prone to large variations in their export ability, as suggested in this study.

This general picture can be compared with the conceptual scheme of the development of planktonic communities in the Southern Ocean recently proposed by Quéguiner (2013). Direct export can occur efficiently when the phytoplankton community is dominated by the large heavily silicified species (e.g. *Fragilariopsis* spp.) which are highly grazing–resistant and form fast–sinking aggregates. This type of slow–growing species develops through the whole season and forms a 'persistent' background encountered at almost all sites. In bloom conditions (during the growth season), smaller fast–growing, lightly silicified species are added to the community, leading to an increased primary productivity. Because these small species are possibly less efficient at exporting carbon (e.g. rapidly grazed and/or sinking slowly), the increase in primary productivity is not accompanied by an increase in carbon export — though 2- to 5–fold higher in sites under Fe–fertilisation influence than in the HNLC site — required to obtain a high export efficiency.

2.5 Conclusions

Our study conducted in early spring, during bloom initiation, demonstrated the following points:

i. Phytodetrital aggregates represented the main numerical and volume fractions of the flux, especially at depth, and could have played a major role in sustaining export fluxes where fecal pellet flux attenuation occurred. This contrasts with summertime (KEOPS1) when fecal material largely dominated the flux, while phytodetrital aggregates brought only a minor contribution to the flux (Ebersbach and Trull, 2008). However, when converted to carbon content, and where their degradation was limited, cylindrical fecal pellets still represented the dominant fraction of the flux.

ii. Primary productivity was negatively correlated to export efficiency, the sites of highest productivity being the least efficient to export carbon. This supports the emergent vision of high–productivity, low–export regimes already noted in the Southern Ocean (Lam and Bishop, 2007). The decrease in productivity from bloom initiation (KEOPS2) to its decline (KEOPS1) related to a shift from autotroph- to heterotroph–dominated regimes (i.e. production exported via phytodetrital vs. fecal material), could explain why major export tends to occur at the end of the season essentially via the sinking of fecal matter.

iii. Plankton community structure influenced by productivity regimes could have controlled export efficiency via variations in phytoplankton species and zooplankton grazing pressure (Table 2.6).

Acknowledgments

This work received support through funding from the Australian Commonwealth Cooperative Research Centres Program to the ACE CRC, as well as through the Australian National Network in Marine Science via UTAS IMAS. We thank the personnel of RV *Marion Dufresne*, Institut Paul Emile Victor, Institut National des Sciences de l'Univers, and the KEOPS2 voyage leader Bernard Queguiner and KEOPS2 science team for assistance at sea. Peter Jansen (IMOS), Danny McLaughlan (CSIRO) and David Cherry (CSIRO) contributed to preparation of the free–drifting sediment trap arrays. MODIS (NASA) satellite ocean–colour images courtesy of Francesco d'Ovidio (Univ. Paris). The altimeter and colour/temperature products for the Kerguelen area were produced by Ssalto/Duacs and CLS with support from CNES. We thank the two anonymous referees for their comments, which helped improve the manuscript.

References

Alldredge, A. L.: The carbon, nitrogen and mass content of marine snow as a function of aggregate size, Deep Sea Research Part I: Oceanographic Research Papers, 45, 529 – 541, doi:10.1016/S0967-0637(97)00048-4, 1998.

Alldredge, A. L. and Gotschalk, C. C.: Direct observations of the mass flocculation of diatom blooms: characteristics, settling velocities and formation of diatom aggregates, Deep Sea Research Part A. Oceanographic Research Papers, 36, 159–171, doi:10.1016/0198-0149(89)90131-3, 1989.

Alldredge, A. L. and Silver, M. W.: Characteristics, dynamics and significance of marine snow, Progress in Oceanography, 20, 41–82, doi:10.1016/0079-6611(88)90053-5, 1988.

Alldredge, A. L., Gotschalk, C., Passow, U., and Riebesell, U.: Mass aggregation of diatom blooms: insights from a mesocosm study, Deep-Sea Research Part II: Topical Studies in Oceanography, 42, 9–27, doi:10.1016/0967-0645(95)00002-8, 1995.

Armand, L. K., Crosta, X., Quéguiner, B., Mosseri, J., and Garcia, N.: Diatoms preserved in surface sediments of the northeastern Kerguelen Plateau, Deep Sea Research Part II: Topical Studies in Oceanography, 55, 677–692, doi:10.1016/j.dsr2.2007.12.032, 2008.

Bishop, J. K. B., Edmond, J. M., Ketten, D. R., Bacon, M. P., and Silker, W. B.: The chemistry, biology, and vertical flux of particulate matter from the upper 400 m of the equatorial Atlantic Ocean, Deep Sea Research, 24, 511–548, doi:10.1016/0146-6291(77)90526-4, 1977.

Blain, S., Quéguiner, B., Armand, L., Belviso, S., Bombled, B., Bopp, L., Bowie, A., Brunet, C., Brussaard, C., Carlotti, F., Christaki, U., Corbière, A., Durand, I., Ebersbach, F., Fuda, J. L., Garcia, N., Gerringa, L., Griffiths, B., Guigue, C., Guillerm, C., Jacquet, S., Jeandel, C., Laan, P., Lefèvre, D., Lo Monaco, C., Malits, A., Mosseri, J., Obernosterer, I., Park, Y. H., Picheral, M., Pondaven, P., Remenyi, T., Sandroni, V., Sarthou, G., Savoye, N., Scouarnec, L., Souhaut, M., Thuiller, D., Timmermans, K., Trull, T., Uitz, J., van Beek, P., Veldhuis, M., Vincent, D., Viollier, E., Vong, L., and Wagener, T.: Effect of natural iron fertilization on carbon sequestration in the Southern Ocean, Nature, 446, 1070–1074, doi:10.1038/nature05700, 2007.

Bowie, A. R., Trull, T. W., and Dehairs, F.: Estimating the sensitivity of the subantarctic zone to environmental change: The SAZ-Sense project, Deep Sea Research Part II: Topical Studies in Oceanography, 58, 2051–2058, doi:10.1016/j.dsr2.2011.05.034, 2011.

Bowie, A. R., van der Merwe, P., Quéroué, F., Trull, T., Fourquez, M., Planchon, F., Sarthou, G., Chever, F., Townsend, A. T., Obernosterer, I., Sallée, J.-B., and Blain, S.: Iron budgets for three distinct biogeochemical sites around the Kerguelen archipelago (Southern Ocean) during the natural fertilisation experiment KEOPS-2, Biogeosciences Discussions, 11, 17 861–17 923, doi:10.5194/bgd-11-17861-2014, 2014.

Boyd, P. W., Watson, A. J., Law, C. S., Abraham, E. R., Trull, T., Murdoch, R., Bakker, D. C. E., Bowie, A. R., Buesseler, K. O., and Chang, H.: A mesoscale phytoplankton bloom in the polar Southern Ocean stimulated by iron fertilization, Nature, 407, 695–702, doi:10.1038/35037500, 2000.

Brinton, E.: Vertical migration and avoidance capability of euphausiids in the California Current, Limnology and Oceanography, 12, 451–483, doi:10.4319/lo.1967.12.3.0451, 1967.

Buesseler, K. O.: The decoupling of production and particulate export in the surface ocean, Global Biogeochemical Cycles, 12, 297–310, doi:10.1029/97GB03366, 1998.

Buonassissi, C. and Dierssen, H.: A regional comparison of particle size distributions and the power law approximation in oceanic and estuarine surface waters, Journal of Geophysical Research, 115, C10 028, doi:10.1029/2010JC006256, 2010.

Burd, A. B. and Jackson, G. A.: Particle Aggregation, Annual Review of Marine Science, 1, 65–90, doi:10.1146/annurev.marine.010908.163904, 2009.

Carlotti, F., Jouandet, M.-P., Nowaczyk, A., Harmelin-Vivien, M., Lefèvre, D., Guillou, G., Zhu, Y., and Zhou, M.: Mesozooplankton structure and functioning during the onset of the Kerguelen phytoplankton bloom during the Keops2 survey, Biogeosciences Discussions, 12, 2381–2427, doi:10.5194/bgd-12-2381-2015, 2015.

Carroll, M. L., Miquel, J.-C., and Fowler, S. W.: Seasonal patterns and depth-specific trends of zooplankton fecal pellet fluxes in the Northwestern Mediterranean Sea, Deep Sea Research Part I: Oceanographic Research Papers, 45, 1303–1318, doi:10.1016/S0967-0637(98)00013-2, 1998.

Cavagna, A.-J., Dehairs, F., Bouillon, S., Woule-Ebongué, V., Planchon, F., Delille, B., and Bouloubassi, I.: Water column distribution and carbon isotopic signal of cholesterol, brassicasterol and particulate organic carbon in the Atlantic sector of the Southern Ocean, Biogeosciences, 10, 2787–2801, doi:10.5194/bg-10-2787-2013, 2013.

Cavagna, A. J., Fripiat, F., Elskens, M., Dehairs, F., Mangion, P., Chirurgien, L., Closset, I., Lasbleiz, M., Flores-Leiva, L., Cardinal, D., Leblanc, K., Fernandez, C., Lefèvre, D., Oriol, L., Blain, S., and Quéguiner, B.: Biological productivity regime and associated N cycling in the vicinity of Kerguelen Island area, Southern Ocean, Biogeosciences Discussions, 11, 18 073–18 104, doi:10.5194/bgd-11-18073-2014, 2014.

Christaki, U., Lefèvre, D., Georges, C., Colombet, J., Catala, P., Courties, C., Sime-Ngando, T., Blain, S., and Obernosterer, I.: Microbial food web dynamics during spring phytoplankton blooms in the naturally iron-fertilized Kerguelen area (Southern Ocean), Biogeosciences, 11, 6739–6753, doi:10.5194/bg-11-6739-2014, 2014.

Coale, K. H., Johnson, K. S., Chavez, F. P., Buesseler, K. O., Barber, R. T., Brzezinski, M. A., Cochlan, W. P., Millero, F. J., Falkowski, P. G., Bauer, J. E., Wanninkhof, R. H., Kudela, R. M., Altabet, M. A., Hales, B. E., Takahashi, T., Landry, M. R., Bidigare, R. R., Wang, X., Chase, Z., Strutton, P. G., Friederich, G. E., Gorbunov, M. Y., Lance, V. P., Hilting, A. K., Hiscock, M. R., Demarest, M., Hiscock, W. T., Sullivan, K. F., Tanner, S. J., Gordon, R. M., Hunter, C. N., Elrod, V. A., Fitzwater, S. E., Jones, J. L., Tozzi, S., Koblizek, M., Roberts, A. E., Herndon, J., Brewster, J., Ladizinsky, N., Smith, G., Cooper, D., Timothy, D., Brown, S. L., Selph, K. E., Sheridan, C. C., Twining, B. S., and Johnson, Z. I.: Southern Ocean Iron Enrichment Experiment: Carbon Cycling in High- and Low-Si Waters, Science, 304, 408–414, doi:10.1126/science.1089778, 2004.

Crocker, K. M. and Passow, U.: Differential aggregation of diatoms, Marine Ecology Progress Series, 117, 249–257, doi:10.3354/meps117249, 1995.

de Baar, H. J. W., de Jong, J. T. M., Bakker, D. C. E., Loscher, B. M., Veth, C., Bathmann, U., and Smetacek, V.: Importance of iron for plankton blooms and carbon dioxide drawdown in the Southern Ocean, Nature, 373, 412–415, doi:10.1038/373412a0, 1995.

De La Rocha, C. L. and Passow, U.: Factors influencing the sinking of POC and the efficiency of the biological carbon pump, Deep Sea Research Part II: Topical Studies in Oceanography, 54, 639–658, doi:10.1016/j.dsr2.2007.01.004, 2007.

Ebersbach, F. and Trull, T. W.: Sinking particle properties from polyacrylamide gels during the KErguelen Ocean and Plateau compared Study (KEOPS): Zooplankton control of carbon export in an area of persistent natural iron inputs in the Southern Ocean, Limnology and Oceanography, 53, 212–224, doi:10.2307/40006162, 2008.

Ebersbach, F., Trull, T. W., Davies, D. M., and Bray, S. G.: Controls on mesopelagic particle fluxes in the Sub-Antarctic and Polar Frontal Zones in the Southern Ocean south of Australia in summer—Perspectives from free-drifting sediment traps, Deep Sea Research Part II: Topical Studies in Oceanography, 58, 2260 – 2276, doi:10.1016/j.dsr2.2011.05.025, 2011.

Eppley, R. W. and Peterson, B. J.: Particulate organic matter flux and planktonic new production in the deep ocean, Nature, 282, 677–680, doi:10.1038/282677a0, 1979.

Espinasse, B., Zhou, M., Zhu, Y., Hazen, E. L., Friedlaender, A. S., Nowacek, D. P., Chu, D., and Carlotti, F.: Austral fall-winter transition of mesozooplankton assemblages and krill aggregations in an embayment west of the Antarctic Peninsula, Marine Ecology Progress Series, 452, 63–80, doi:10.3354/meps09626, 2012.

Fleminger, A. and Clutter, R. I.: Avoidance of towed nets by zooplankton, Limnology and Oceanography, 10, 96–104, doi:10.4319/lo.1965.10.1.0096, 1965.

Fowler, S. W. and Knauer, G. A.: Role of large particles in the transport of elements and organic compounds through the oceanic water column, Progress in Oceanography, 16, 147–194, doi:10.1016/0079-6611(86)90032-7, 1986.

Fowler, S. W. and Small, L. F.: Sinking rates of euphausiid fecal pellets, Limnology and Oceanography, 17, 293–296, doi:10.1016/0079-6611(86)90032-7, 1972.

Gauld, D. T.: A Peritrophic Membrane in Calanoid Copepods, Nature, 179, 325–326, doi:10.1038/179325a0, 1957.

Giering, S. L. C., Sanders, R., Lampitt, R. S., Anderson, T. R., Tamburini, C., Boutrif, M., Zubkov, M. V., Marsay, C. M., Henson, S. A., Saw, K., Cook, K., and Mayor, D. J.: Reconciliation of the carbon budget in the ocean's twilight zone, Nature, 507, 480–483, doi:10.1038/nature13123, 2014.

González, H. E. and Smetacek, V.: The possible role of the cyclopoid copepod Oithona in retarding vertical flux of zooplankton faecal material, Marine Ecology Progress Series, 113, 233–246, doi:10.3354/meps113233, 1994.

González, H. E., González, S. R., and Brummer, G. J. A.: Short-term sedimentation pattern of zooplankton, faeces and microplankton at a permanent station in the Bjornafjorden (Norway) during April-May 1992, Marine ecology Progress series, 105, 31–45, doi:10.3354/meps105031, 1994.

González, H. E., Ortiz, V. C., and Sobarzo, M.: The role of faecal material in the particulate organic carbon flux in the northern Humboldt Current, Chile (23 °S), before and during the 1997–1998 El Niño, Journal of Plankton Research, 22, 499–529, doi:10.1093/plankt/22.3.499, 2000.

González, H. E., Daneri, G., Iriarte, J. L., Yannicelli, B., Menschel, E., Barría, C., Pantoja, S., and Lizárraga, L.: Carbon fluxes within the epipelagic zone of the Humboldt Current System off Chile: The significance of euphausiids and diatoms as key functional groups for the biological pump, Progress in Oceanography, 83, 217–227, doi:10.1016/j.pocean.2009.07.036, 2009.

Guidi, L., Stemmann, L., Jackson, G. A., Ibanez, F., Claustre, H., Legendre, L., Picheral, M., and Gorsky, G.: Effects of phytoplankton community on production, size and export of large aggregates: A world-ocean analysis, Limnology and Oceanography, 54, 1951–1963, doi:10.4319/lo.2009.54.6.1951, 2009.

Hargraves, P. E. and French, F. W.: Diatom resting spores: Significance and strategies, in: Survival Strategies of the Algae, edited by Fryxell, G., pp. 49–68, Cambridge University Press, New York, 1983.

Iversen, M. H. and Poulsen, L. K.: Coprorhexy, coprophagy, and coprochaly in the copepods *Calanus helgolandicus*, *Pseudocalanus elongatus*, and *Oithona similis*, Marine Ecology Progress Series, 350, 79–89, doi:10.3354/meps07095, 2007.

Jackson, G. A.: A model of the formation of marine algal flocs by physical coagulation processes, Deep-Sea Research Part I: Oceanographic Research Papers, 37, 1197–1211, doi:10.1016/0198-0149(90)90038-W, 1990.

Jackson, G. A., Maffione, R., Costello, D. K., Alldredge, A. L., Logan, B. E., and Dam, H. G.: Particle size spectra between 1 μm and 1 cm at Monterey Bay determined using multiple instruments, Deep Sea Research Part I: Oceanographic Research Papers, 44, 1739–1767, doi:10.1016/S0967-0637(97)00029-0, 1997.

Jackson, G. A., Waite, A. M., and Boyd, P. W.: Role of algal aggregation in vertical carbon export during SOIREE and in other low biomass environments, Geophysical Research Letters, 32, L13 607, doi:10.1029/2005GL023180, 2005.

Jacquet, S. H. M., Lam, P. J., Trull, T., and Dehairs, F.: Carbon export production in the subantarctic zone and polar front zone south of Tasmania, Deep Sea Research Part II: Topical Studies in Oceanography, 58, 2277–2292, doi:10.1016/j.dsr2.2011.05.035, 2011.

Jannasch, H. W., Zafiriou, O. C., and Farrington, J. W.: A sequencing sediment trap for time-series studies of fragile particles, Limnology and Oceanography, 25, 939–3590, doi:10.4319/lo.1980.25.5.0939, 1980.

Kuwata, A. and Takahashi, M.: Life-form population responses of a marine planktonic diatom, *Chaetoceros pseudocurvisetus*, to oligotrophication in regionally upwelled water, Marine Biology, 107, 503–512, doi:10.1007/BF01313435, 1990.

Lam, P. J. and Bishop, J. K. B.: High biomass, low export regimes in the Southern Ocean, Deep Sea Research Part II: Topical Studies in Oceanography, 54, 601–638, doi:10.1016/j.dsr2.2007.01.013, 2007.

Lam, P. J., Doney, S. C., and Bishop, J. K. B.: The dynamic ocean biological pump: Insights from a global compilation of particulate organic carbon, $CaCO_3$, and opal concentration profiles from the mesopelagic, Global Biogeochemical Cycles, 25, GB3009, doi: 10.1029/2010GB003868, 2011.

Lampitt, R. S., Noji, T., and Bodungen, B.: What happens to zooplankton faecal pellets? Implications for material flux, Marine Biology, 104, 15–23, doi:10.1007/BF01313152, 1990.

Lasbleiz, M., Leblanc, K., Blain, S., Ras, J., Cornet-Barthaux, V., Hélias Nunige, S., and Quéguiner, B.: Pigments, elemental composition (C, N, P, and Si), and stoichiometry of particulate matter in the naturally iron fertilized region of Kerguelen in the Southern Ocean, Biogeosciences, 11, 5931–5955, doi:10.5194/bg-11-5931-2014, 2014.

Laurenceau-Cornec, E. C., Trull, T. W., Davies, D. M., De La Rocha, C. L., and Blain, S.: Phytoplankton morphology controls on marine snow sinking velocity, Marine Ecology Progress Series, 520, 35–56, doi:10.3354/meps11116, 2015a.

Lefévre, D., Guigue, C., and Obernosterer, I.: The metabolic balance at two contrasting sites in the Southern Ocean: The iron-fertilized Kerguelen area and HNLC waters, Deep Sea Research Part II: Topical Studies in Oceanography, 55, 766–776, doi:10.1016/j.dsr2.2007.12.006, 2008.

Lundsgaard, C.: Use of a high viscosity medium in studies of aggregates, in: Sediment trap studies in the Nordic countries. 3. Proceeding of the Symposium on Seasonal Dynamics of Planktonic Ecosystems and Sedimentation in Coastal Nordic Waters. Finnish Environment Agency, edited by Floderus, S., Heisakanen, A. S., Oleson, M., and Wassmann, P., pp. 141–152, Numi Print, Oy, Germany, 1995.

Maiti, K., Charette, M. A., Buesseler, K. O., and Kahru, M.: An inverse relationship between production and export efficiency in the Southern Ocean, Geophysical Research Letters, 40, 1557–1561, doi:10.1002/grl.50219, 2013.

Martens, P.: Faecal pellets, in: Fiches d'identification du zooplancton, edited by Fraser, J., vol. 162, p. 4, Conseil International pour l'Exploration de la Mer, 1978.

Martin, J. H.: Glacial-interglacial CO_2 change: The iron hypothesis, Paleoceanography, 5, 1–13, doi:10.1029/PA005i001p00001, 1990.

Martin, J. H., Knauer, G. A., Karl, D. M., and Broenkow, W. W.: VERTEX: carbon cycling in the northeast Pacific, Deep Sea Research Part A. Oceanographic Research Papers, 34, 267–285, doi:10.1016/0198-0149(87)90086-0, 1987.

McCave, I. N.: Size spectra and aggregation of suspended particles in the deep ocean, Deep Sea Research Part A. Oceanographic Research Papers, 31, 329–352, doi:10.1016/0198-0149(84)90088-8, 1984.

McDonnell, A. M. P. and Buesseler, K. O.: Variability in the average sinking velocity of marine particles, Limnology and Oceanography, 55, 2085–2096, doi:10.4319/lo.2010.55.5.2085, 2010.

Michaels, A. F. and Silver, M. W.: Primary production, sinking fluxes and the microbial food web, Deep Sea Research Part A. Oceanographic Research Papers, 35, 473–490, doi:10.1016/0198-0149(88)90126-4, 1988.

Morris, P. J., Sanders, R., Turnewitsch, R., and Thomalla, S.: ^{234}Th-derived particulate organic carbon export from an island-induced phytoplankton bloom in the Southern Ocean, Deep Sea Research Part II: Topical Studies in Oceanography, 54, 2208–2232, doi:10.1016/j.dsr2.2007.06.002, 2007.

Mosseri, J., Quéguiner, B., Armand, L., and Cornet-Barthaux, V.: Impact of iron on silicon utilization by diatoms in the Southern Ocean: A case study of Si/N cycle decoupling in a naturally iron-enriched area, Deep Sea Research Part II: Topical Studies in Oceanography, 55, 801–819, doi:10.1016/j.dsr2.2007.12.003, 2008.

Park, Y. H., Charriaud, E., Pino, D. R., and Jeandel, C.: Seasonal and interannual variability of the mixed layer properties and steric height at station KERFIX, southwest of Kerguelen, Journal of Marine Systems, 17, 571–586, doi:10.1016/S0924-7963(98)00065-7, 1998.

Pilskaln, C. H. and Honjo, S.: The fecal pellet fraction of biogeochemical particle fluxes to the deep sea, Global Biogeochemical Cycles, 1, 31–48, doi:10.1029/GB001i001p00031, 1987.

Planchon, F., Ballas, D., Cavagna, A.-J., Bowie, A. R., Davies, D., Trull, T., Laurenceau-Cornec, E. C., Van Der Merwe, P., and Dehairs, F.: Carbon export in the naturally iron-fertilized Kerguelen area of the Southern Ocean based on the ^{234}Th approach, Biogeosciences, 12, 3831–3848, doi:10.5194/bg-12-3831-2015, 2015.

Pollard, R., Sanders, R., Lucas, M., and Statham, P.: The Crozet Natural Iron Bloom and Export Experiment (CROZEX), Deep Sea Research Part II: Topical Studies in Oceanography, 54, 1905 – 1914, doi:10.1016/j.dsr2.2007.07.023, 2007.

Quéguiner, B.: Iron fertilization and the structure of planktonic communities in high nutrient regions of the Southern Ocean, Deep Sea Research Part II: Topical Studies in Oceanography, 90, 43–54, doi:10.1016/j.dsr2.2012.07.024, 2013.

Riebesell, U., Schloss, I., and Smetacek, V.: Aggregation of algae released from melting sea ice: implications for seeding and sedimentation, Polar biology, 11, 239–248, doi:10.1007/bf00238457, 1991.

Rynearson, T. A., Richardson, K., Lampitt, R. S., Sieracki, M. E., Poulton, A. J., Lyngsgaard, M. M., and Perry, M. J.: Major contribution of diatom resting spores to vertical flux in the sub-polar North Atlantic, Deep Sea Research Part I: Oceanographic Research Papers, 82, 60–71, doi:10.1016/j.dsr.2013.07.013, 2013.

Salter, I., Lampitt, R. S., Sanders, R., Poulton, A., Kemp, A. E. S., Boorman, B., Saw, K., and Pearce, R.: Estimating carbon, silica and diatom export from a naturally fertilised phytoplankton bloom in the Southern Ocean using PELAGRA: A novel drifting sediment trap, Deep Sea Research Part II: Topical Studies in Oceanography, 54, 2233–2259, doi:10.1016/j.dsr2.2007.06.008, 2007.

Salter, I., Kemp, A. E. S., Moore, C. M., Lampitt, R. S., Wolff, G. A., and Holtvoeth, J.: Diatom resting spore ecology drives enhanced carbon export from a naturally iron-fertilized bloom in the Southern Ocean, Global Biogeochemical Cycles, 26, GB1014, doi:10.1029/2010GB003977, 2012.

Savoye, N., Trull, T. W., Jacquet, S. H. M., Navez, J., and Dehairs, F.: ^{234}Th-based export fluxes during a natural iron fertilization experiment in the Southern Ocean (KEOPS), Deep Sea Research Part II: Topical Studies in Oceanography, 55, 841–855, doi:10.1016/j.dsr2.2007.12.036, 2008.

Sigman, D. M. and Boyle, E. A.: Glacial/interglacial variations in atmospheric carbon dioxide, Nature, 407, 859–869, doi:10.1038/35038000, 2000.

Silver, M. W. and Gowing, M. M.: The"Particle" Flux: Origins and biological components, Progress in Oceanography, 26, 75–113, doi:10.1016/0079-6611(91)90007-9, 1991.

Small, L. F., Fowler, S. W., and Ünlü, M. Y.: Sinking rates of natural copepod fecal pellets, Marine Biology, 51, 233–241, doi:10.1007/BF00386803, 1979.

Smetacek, V., Klaas, C., Strass, V. H., Assmy, P., Montresor, M., Cisewski, B., Savoye, N., Webb, A., d'Ovidio, F., Arrieta, J. M., Bathmann, U., Bellerby, R., Berg, G. M., Croot, P., Gonzalez, S., Henjes, J., Herndl, G. J., Hoffmann, L. J., Leach, H., Losch, M., Mills, M. M., Neill, C., Peeken, I., Rottgers, R., Sachs, O., Sauter, E., Schmidt, M. M., Schwarz, J., Terbruggen, A., and Wolf-Gladrow, D.: Deep carbon export from a Southern Ocean iron-fertilized diatom bloom, Nature, 487, 313–319, doi:10.1038/nature11229, 2012.

Suess, E.: Particulate organic carbon flux in the oceans—surface productivity and oxygen utilization, Nature, 288, 260–263, doi:10.1038/288260a0, 1980.

Suzuki, H., Sasaki, H., and Fukuchi, M.: Loss processes of sinking fecal pellets of zooplankton in the mesopelagic layers of the Antarctic Marginal Ice Zone, Journal of Oceanography, 59, 809–818, doi:10.1023/B:JOCE.0000009572.08048.0d, 2003.

Trull, T. W., Bray, S. G., Buesseler, K. O., Lamborg, C. H., Manganini, S., Moy, C., and Valdes, J.: In situ measurement of mesopelagic particle sinking rates and the control of carbon transfer to the ocean interior during the Vertical Flux in the Global Ocean (VERTIGO) voyages in the North Pacific, Deep-Sea Research Part II: Topical Studies in Oceanography, 55, 1684–1695, doi:10.1016/j.dsr2.2008.04.021, 2008.

Trull, T. W., Davies, D. M., Dehairs, F., Cavagna, A.-J., Lasbleiz, M., Laurenceau, E. C., d'Ovidio, F., Planchon, F., Leblanc, K., Quéguiner, B., and Blain, S.: Chemometric perspectives on plankton community responses to natural iron fertilization over and downstream of the Kerguelen Plateau in the Southern Ocean, Biogeosciences Discussions, 11, 13 841–13 903, doi:10.5194/bgd-11-13841-2014, 2014.

Turner, J. T.: Zooplankton fecal pellets, marine snow and sinking phytoplankton blooms, Aquatic Microbial Ecology, 27, 57–102, doi:10.3354/ame027057, 2002.

Urban-Rich, J., Hansell, D. A., and Roman, M. R.: Analysis of copepod fecal pellet carbon using a high temperature combustion method, Marine Ecology Progress Series, 171, 199–208, doi:10.3354/meps171199, 1998.

Volk, T. and Hoffert, M. I.: Ocean carbon pumps: Analysis of relative strengths and efficiencies in ocean-driven atmospheric CO_2 changes, in: The Carbon Cycle and Atmospheric CO_2: Natural Variations Archean to Present, vol. 32, pp. 99–110, AGU, Washington, DC, 1985.

Waite, A. M. and Nodder, S. D.: The effect of in situ iron addition on the sinking rates and export flux of Southern Ocean diatoms, Deep Sea Research Part II: Topical Studies in Oceanography, 48, 2635–2654, doi:10.1016/S0967-0645(01)00012-1, 2001.

Wallace, M. I., Cottier, F. R., Brierley, A. S., and Tarling, G. A.: Modelling the influence of copepod behaviour on faecal pellet export at high latitudes, Polar Biology, 36, 579–592, doi:10.1007/s00300-013-1287-7, 2013.

Wassmann, P.: Relationship between primary and export production in the boreal coastal zone of the North Atlantic, Limnology and oceanography, 35, 464–471, doi:10.4319/lo.1990.35.2.0464, 1990.

Wassmann, P.: Retention versus export food chains: processes controlling sinking loss from marine pelagic systems, Hydrobiologia, 363, 29–57, doi:10.1023/A:1003113403096, 1998.

Wassmann, P., Ypma, J. E., and Tselepides, A.: Vertical flux of faecal pellets and microplankton on the shelf of the oligotrophic Cretan Sea (NE Mediterranean Sea), Progress in Oceanography, 46, 241–258, doi:10.1016/S0079-6611(00)00021-5, 2000.

Wiebe, P., Boyd, S., Davis, B., and Cox, J.: Avoidance of towed nets by the euphausiid *Nematoscelis megalops*, Fishery Bulletin - NOAA, 80, 75–91, 1982.

Wiebe, P. H., Burt, K. H., Boyd, S. H., and Morton, A. W.: A multiple opening/closing net and environment sensing system for sampling zooplankton, Journal of Marine Research, 34, 313–326, 1976.

Yoon, W., Kim, S., and Han, K.: Morphology and sinking velocities of fecal pellets of copepod, molluscan, euphausiid, and salp taxa in the northeastern tropical Atlantic, Marine Biology, 139, 923–928, doi:10.1007/s002270100630, 2001.

Zhou, M., Zhu, Y., d'Ovidio, F., Park, Y. H., Durand, I., Kestenare, E., Sanial, V., Van-Beek, P., Quéguiner, B., Carlotti, F., and Blain, S.: Surface currents and upwelling in Kerguelen Plateau regions, Biogeosciences Discuss., 11, 6845–6876, doi:10.5194/bgd-11-6845-2014, 2014.

Chapter 3

Phytoplankton morphology controls on marine snow sinking velocity

This chapter was published as an article under the same title in Marine Ecology Progress Series, 2015, volume 520, pages 35–66, doi:10.3354/meps11116. It is reproduced here with copyright permission from Inter–Research Science Center.

Emmanuel C. Laurenceau–Cornec[1,2,3], Thomas W. Trull[2,3], Diana M. Davies[2], Christina L. De La Rocha[4], and Stéphane Blain[5]

[1]Institute for Marine and Antarctic Studies, University of Tasmania, Private Bag 129, Hobart, Tasmania 7001, Australia

[2]Antarctic Climate and Ecosystems Cooperative Research Centre, University of Tasmania, Private Bag 80, Hobart, Tasmania 7001, Australia

[3]Commonwealth Scientific and Industrial Research Organisation, Marine and Atmospheric Research, Castray Esplanade, Hobart, Tasmania 7000, Australia

[4]CNRS, UMR 6539, Institut Universitaire Européen de la Mer, Université de Bretagne Occidentale, Technopôle Brest–Iroise, Rue Dumont d'Urville, Plouzané 29280, France

[5]Sorbonne Universités, UPMC Univ. Paris 06, CNRS, UMR 7621, Laboratoire d'Océanographie Microbienne, Observatoire Océanologique, 66650 Banyuls/mer, France

Abstract

During the second KErguelen Ocean and Plateau compared Study (KEOPS2) in October–November 2011, marine snow was formed in roller tanks by physical aggregation of phytoplankton assemblages sampled at 6 stations over and downstream of the Kerguelen Plateau. Sinking velocities, morphology, bulk composition (transparent exopolymer particles, biogenic silica, particulate organic carbon), and phytoplankton contents were measured individually on 66 aggregates to identify controls on sinking velocities. Equivalent spherical diameters (ESD) ranged from 1 to 12 mm, and the particle aspect ratios, Corey shape factors, and fractal dimensions ($D_{F1} = 1.5$, $D_{F2} = 1.8$) were close to those of smaller natural aggregates (0.2 to 1.5 mm) collected in polyacrylamide gel–filled sediment traps ($D_{F1} = 1.2$, $D_{F2} = 1.9$). Sinking velocities ranged between 13 and 260 m d^{-1}, and were correlated with aggregate size only when considering individually the experiments conducted at each station, suggesting that a site–dependent control prevailed over the general influence of size. Variation in dominant diatom morphologies among the sites (classified as small spine–forming or chain without spines) appeared to be a determinant parameter influencing the sinking velocity [SV(m d^{-1}) = 168 − 1.48 × (% small spine–forming cells); ($r^2 = 0.98$)], possibly via a control on species–specific coagulation efficiency affecting particle structure and excess density. Our results emphasize the importance of ecological considerations over that of simple compositional perspectives in the control of particle formation, and in accurate parameterizations of marine snow sinking velocities that are essential to predictions of biological carbon sequestration.

3.1 Introduction

In the ocean, the rain of large biogenic particles is a major pathway for the export of carbon from the surface to the interior (Asper et al., 1992; Fowler and Knauer, 1986; Suess, 1980). This mechanism contributes significantly to the drawdown of atmospheric carbon dioxide, and has become known as the oceanic 'biological carbon pump' (Volk and Hoffert, 1985). Substantial production of particulate organic matter (POM) in the euphotic zone is essential but not sufficient to obtain high carbon export (Buesseler, 1998). The speed at which particles settle is also a critical parameter since it determines the duration of their exposure to extensive physical and biological transformations (Boyd et al., 1999; Karl et al., 1988) responsible for the observed attenuation of the particle flux with depth (Martin et al., 1987; Silver and Gowing, 1991).

In the Southern Ocean, a region known to play a leading role in global climate and carbon systems (Sigman and Boyle, 2000), primary productivity is low due to phytoplankton growth restriction by a combination of iron and light limitation (de Baar et al., 1995; Martin, 1990). These waters are described as 'high nutrient, low chlorophyll' (HNLC) and contain a large amount of unused surface macronutrients capable of fuelling the production of high quantities of organic carbon and potentially its sequestration. Against this background, like oases in deserts, some areas in the Southern Ocean are fertilized by a natural supply of iron and display

remarkable seasonal biomass increases (Sullivan et al., 1993), offering a great opportunity to investigate the controls on carbon export efficiencies in the context of iron fertilization.

This study focuses on the bloom that occurs each year between October and February over and downstream of the Kerguelen Plateau in the Indian sector of the Southern Ocean (Blain et al., 2007). In January–February 2005, the first KErguelen Ocean and Plateau compared Study (KEOPS1) demonstrated that the downward flux of carbon was elevated by a factor of 2 to 3 in comparison to the surrounding HNLC waters (Savoye et al., 2008). Particle size spectra from an in situ camera demonstrated that more and larger particles were present beneath the bloom (to 400 m depth) than in surrounding HNLC waters, although a comparison to size spectra of particles collected in gel–filled sediment traps showed slower sinking velocities (Jouandet et al., 2011), suggesting that sinking velocity was not a simple monotonic function of particle size.

According to theory and empirical studies, size is known to exert a major control on particle sinking velocity (Dietrich, 1982; Gibbs, 1985), but discrepancies in the size–sinking velocity relationship are often reported, and other parameters (e.g. particle composition or structure) can prevail over size in the control of the sinking velocity, as previously noted (Diercks and Asper, 1997; Engel and Schartau, 1999; Iversen and Ploug, 2010). While extensive study of these parameters has verified their importance, it has also turned out to be difficult to define a limited number of parameters suitable to predict carbon export accurately — something that would be of considerable use in computationally expensive models of ocean biogeochemical cycling. Among these parameters, the shape (Alldredge and Silver, 1988; McNown and Malaika, 1950), porosity or compactness (Iversen and Ploug, 2010; Kajihara, 1971), permeability (Matsumoto and Suganuma, 1977), fractal structure (Engel et al., 2009; Johnson et al., 1996), content of high density minerals (Armstrong et al., 2001; Klaas and Archer, 2002; Passow and De La Rocha, 2006) or low density particulate polysaccharides (Azetsu-Scott and Passow, 2004; Engel and Schartau, 1999), phytoplankton species (Padisák et al., 2003; Passow, 1991) and their physiological state (Bienfang et al., 1982; Muggli et al., 1996; Waite et al., 1992) or individual organism size (Boyd and Newton, 1995; Waite et al., 1997a) have been proposed as potential controls of particle sinking velocity. Due to this high complexity and the absence of clear controlling factors provided by empirical research, most biogeochemical models have no other alternative than simple sinking velocity parameterization (e.g. constant or size–dependent). Several modelling studies have focused on the sensitivity to sinking velocity parameterization, testifying to the

awareness that improvements are needed and that more complexity needs to be added to the models (Gehlen et al., 2006; Kriest and Oschlies, 2008, 2013; Losch et al., 2014). Here, we investigate a comprehensive set of morphological and compositional parameters in a single study to identify potential influences on particle sinking velocity and to develop a possible explanation for the inconsistencies often observed between sinking velocity and particle size, offering a potential alternative for biogeochemical model parameterization.

3.1.1 Theory

We refer the reader to the classic textbook on fluid dynamics from Batchelor (1967) for further details on the theory of particle sinking velocity. For a sphere settling in a fluid, the immersed weight (W_i) is the difference between the force of gravity acting downward and the buoyancy force acting upward, and is given by (e.g. Komar and Reimers, 1978):

$$W_\mathrm{i} = \frac{\pi}{6} D^3 (\rho_\mathrm{s} - \rho_\mathrm{f}) g \tag{3.1}$$

where D is the diameter of the sphere, ρ_s and ρ_f are the sphere and fluid densities, respectively, and g (9.81 m s^{-2}) is the acceleration due to gravity. The Reynolds number (Re; Reynolds, 1883) is the parameter that determines a flow field for boundaries of a given form and is given by:

$$\mathrm{Re} = \frac{U_\mathrm{s} D}{\nu} \tag{3.2}$$

where U_s is the sphere sinking velocity and ν is the kinematic viscosity of the fluid. Particles termed 'marine snow' are large aggregates (> 0.5 mm) formed by physical aggregation of phytoplankton and miscellaneous debris: mostly fecal pellets, inorganic particles and zooplankton feeding structures (Alldredge and Gotschalk, 1990; Alldredge and Silver, 1988). Because of their large size and potentially high sinking velocity (Alldredge and Silver, 1988), the settling of marine snow aggregates in the water column occurs at $\mathrm{Re} > 0.5$ (Alldredge and Silver, 1988). For these large particles, it is found empirically (Komar and Reimers, 1978) that the drag force F_D

is proportional to the square of the velocity:

$$F_{\mathrm{D}} = C_{\mathrm{D}} A \frac{\rho_{\mathrm{f}} U_{\mathrm{agg}}^2}{2} \tag{3.3}$$

where U_{agg} is the sinking velocity of the aggregate, C_{D} is the drag coefficient (an empirical proportionality coefficient between F_{D} and U_{agg}^2) and A is the projected area of the aggregate in the direction of motion. At terminal velocity, the drag force is balanced by the immersed weight giving a force balance equation which, after algebraic manipulations, leads to a general expression for the sinking velocity:

$$U_{\mathrm{agg}} = \left[\frac{4}{3} \frac{g(\Delta\rho)D}{C_{\mathrm{D}}\rho_{\mathrm{sw}}}\right]^{1/2} \tag{3.4}$$

where $\Delta\rho$ is the aggregate excess density calculated as the difference between aggregate density and seawater density (ρ_{sw}). In this equation, applicable to all Reynolds numbers, the drag coefficient is a complex function of both aggregate shape and Reynolds number. For simplicity, we refer to Eq. (3.4) as the 'general sinking velocity model' in the rest of the text.

Considering a small perfect sphere settling through a quiescent fluid and assuming that the inertial forces are negligible compared to viscous forces, G. G. Stokes solved in December 1850 the low Reynolds number limit of the Navier–Stokes equations (Stokes, 1851), and obtained a simplified expression of the drag force:

$$F_{\mathrm{D}} = 3\pi\mu D U_{\mathrm{s}} \tag{3.5}$$

where μ is the dynamic viscosity of the fluid. Again, at terminal velocity, the immersed weight equals the drag force yielding the Stokes expression:

$$U_{\mathrm{s}} = \frac{1}{18} \frac{g(\rho_{\mathrm{s}} - \rho_{\mathrm{f}})D^2}{\mu} \tag{3.6}$$

In this expression, the properties of the sphere influencing its settling velocity are only the density and the diameter. Because of the assumptions made by Stokes, Eqs. (3.5) & (3.6) are only valid at small Reynolds number, empirically found to apply to $\mathrm{Re} < 0.5$ (Graf and Acaroglu, 1966; Komar and Reimers, 1978; White, 1974).

By comparing the general model (Eq. 3.4) to its particular case represented by the Stokes'

expression (Eq. 3.6) one can notice that the settling velocity has a weaker dependence on size in the general model since the diameter is raised to the power of 0.5, rather than 2 as in the Stokes' law.

In Fig. 3.1 we plot various empirical and theoretical data of sinking velocity versus size for marine snow, from the present study and others using different methods and approaches. Since these studies were carried out over a range of different water temperatures and salinities, we investigated whether temperature and salinity variations could contribute significantly to sinking velocity variations through their influence on seawater dynamic viscosity (μ) and density (ρ_{sw}). Stokes' law predicts that, at a fixed aggregate porosity and solid content density [e.g. 99% porosity and $\rho_{\mathrm{sol}} = 1170$ kg m^{-3}, corresponding to 30 % transparent exopolymeric particles (TEP), 20 % biogenic silica (BSi), and 50% particulate organic matter (POM) in solid content], a temperature increase from 2 to 20°C or a salinity decrease from 34 to 2 would lead respectively to a 40 and 20% increase in the sinking velocity. It is very likely that the differences between the studies did not exceed these very large range of temperature and salinity variations, and given that Fig. 3.1 is a log–log plot, the effect of temperature and salinity changes on the sinking velocity can reasonably be neglected here.

Overall, the data suggest a relatively weak dependence of sinking velocity on particle size both when considering the whole dataset or each study separately. The general model gives to size a weaker control on sinking velocity and a stronger dependence on drag and excess density influenced by particle structure and composition; our calculations show that the general model provides a better representation of the observations for large particles than the usual Stokes' law (Fig. 3.1). In combination with porosity increasing with size according to a fractal scaling known to apply to marine snow, and using the formula proposed by Logan and Wilkinson (1990; see 'Materials and methods: Measurement of aggregate morphology and structure'), the general model shows poor size–sinking velocity correlation for the large particle size range (Fig. 3.1, line 2). Based on this, it appears that particle structure, morphology and composition could prevail over size in the control of sinking velocity via a control on particle drag and excess density.

Aggregate morphological and structural properties likely to control excess density and drag are numerous, and the combined effects of these 2 parameters make their relative influence on the measured sinking velocity hard to distinguish. The drag experienced by a particle might be the result of several parameters, including shape, permeability, and surface roughness, while

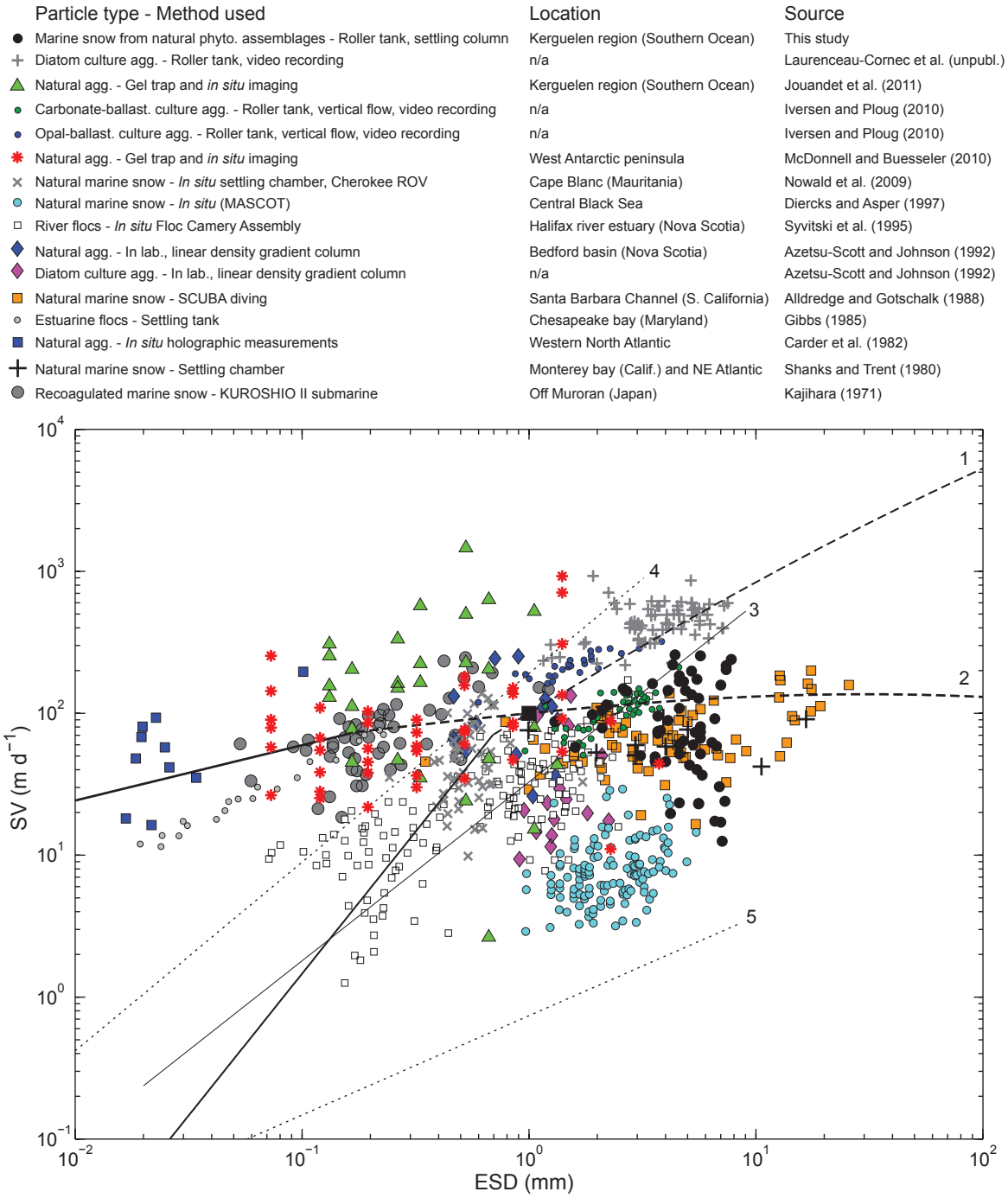

Figure 3.1: Sinking velocity (SV) of large marine aggregates (agg.) versus their equivalent spherical diameter (ESD) for this study and others. Theoretical lines and empirical relationships using different approaches are also represented. 1: Stokes' law (Eq. 3.6) (solid line) and general sinking velocity model (Eq. 3.4) (dashed line) applying to distinct ranges of Reynolds number for solid body particles with constant excess density ($\Delta\rho$ = 0.0014 g cm^{-3}; large black square: specific conditions of the models, fixing the initial drag characteristics of the particle (ESD$_0$ = 1 mm and SV$_0$ = 100 m d^{-1}). 2: Same models with excess density scaled on a typical fractal geometry for marine snow (D_{F3} = 1.39, a = 0.03; Logan and Wilkinson, 1990) (see Fig. 3.3 and 'Results: Sinking velocity' for details). 3: Guidi et al. (2008). 4–5: SV calculated using the coagulation model from Stemmann et al. (2004) with different parameter values (4: excess density $\Delta\rho$ = 0.08, fractal number D_{F3} = 2.33; 5: $\Delta\rho$ = 0.01, D_{F3} = 1.79), Phyto.: phytoplankton; Calif.: California; n/a: not applicable.

excess density depends on aggregate composition and compactness (i.e. porosity). The influence of macroscopic shape, permeability, and surface roughness on the sinking velocity have been investigated in the theoretical, experimental, and engineering fields, on natural and artificial particles, but these parameters have generally been described as poor contributors to the sinking velocity (Achenbach, 1974; Alldredge and Silver, 1988; Baba and Komar, 1981; Li and Logan, 2001; Li and Yuan, 2002; Matsumoto and Suganuma, 1977; Williams, 1966).

The excess density of a marine snow aggregate depends on the density and volume fraction of its solid components (mostly phytoplankton cells in the case of diatom marine snow) and how tightly they are assembled, giving more or less inner space filled by seawater, defined as the porosity (e.g. De La Rocha and Passow, 2007). To our knowledge the species–specific effect of phytoplankton on the alteration of the size–sinking velocity relationship of marine snow aggregates has not been studied to date. We tested here the possible combined effects of varying phytoplankton assemblages on aggregate sinking velocity via ballast effect (Engel et al., 2009) and control on aggregate structure, assuming species–specific aggregate compactness, based on aggregation experiments of phytoplankton cultures (Iversen and Ploug, 2010).

3.1.2 Experimental setup

We focused on marine snow aggregates, a major component of the vertical flux of organic carbon (Fowler and Knauer, 1986). They represented the main numerical fraction of the flux during KEOPS1 (Ebersbach and Trull, 2008) and KEOPS2 (Laurenceau-Cornec et al., 2015b) (Chapter 2), and could represent an efficient way to export carbon over the Kerguelen Plateau if they sink rapidly enough to reach the deep ocean before being consumed or remineralized. Because it is difficult to record in situ the sinking velocity of natural marine snow (Alldredge and Silver, 1988), we took an experimental approach. Marine snow aggregates were formed in rotating cylindrical tanks following the method developed by Shanks and Edmondson (1989). In contrast to the majority of roller tank experiments using phytoplankton cultures, we incubated various natural mixtures of phytoplankton sampled carefully from Niskin bottles to produce aggregates as close as possible to those forming in the water column at different sites. This 'roller tank' technique allows the particles to sink continuously as they would in the water column and thus to aggregate mainly by differential settling (after a short period of shear during the initiation of solid–body rotation) in which fast–sinking particles scavenge suspended and slower–sinking

particles. Thus, the technique minimizes the influences of the 2 other main mechanisms forming marine snow in natural environments: (1) shear, which can also cause disaggregation, and (2) brownian motion, which dominates the collision rate for small (< 1 µm) particles (Burd and Jackson, 2009; McCave, 1984).

Once macroscopic aggregates had formed, they were photographed and their sinking velocities measured. Bulk chemical compositions were determined and the abundances of organisms within the aggregates were examined using light microscopy. To test our hypothesis, all aggregate properties needed to be explored as potential controls of the sinking velocity. Data were thus evaluated in terms of morphological, chemical and biological relative influences on the sinking velocity.

To evaluate the oceanic applicability of the results determined in the roller tank experiments, we compared our aggregates with natural aggregates collected at the same time using polyacrylamide gel–filled sediment traps which allow the sampling of intact particles as they exist in the water column (Ebersbach and Trull, 2008; Jannasch et al., 1980; Laurenceau-Cornec et al., 2015b) (Chapter 2).

3.2 Material and methods

3.2.1 Study site and sampling

This work was conducted during the second KErguelen Ocean and Plateau compared Study (KEOPS2) onboard the RV *Marion Dufresne* from 8 October to 30 November 2011, over and downstream of the Kerguelen Plateau. One of the major purposes was to characterize the downward particle flux by the use of sediment traps and identify the physical and biological controls on the efficiency of carbon export.

In the present work, duplicate sampling was conducted at 6 stations (Fig. 3.2) at surface (20 and 30 m) and deeper layers (65, 80 and 150 m) of high and moderate biomass according to CTD calibrated fluorescence profiles. Stations (Stns) E–3, E–4W (west), E–4E (east), and E–5 formed a time series within a moderate biomass, eddy-like, bathymetrically–trapped recirculation feature in deep waters east of the Kerguelen Islands. Stns F–L and A3–2 were respectively in a region of elevated biomass near the Polar front and at the Kerguelen on-plateau bloom reference station of KEOPS1 (A3). Seawater was sampled using 12 l Niskin bottles mounted on

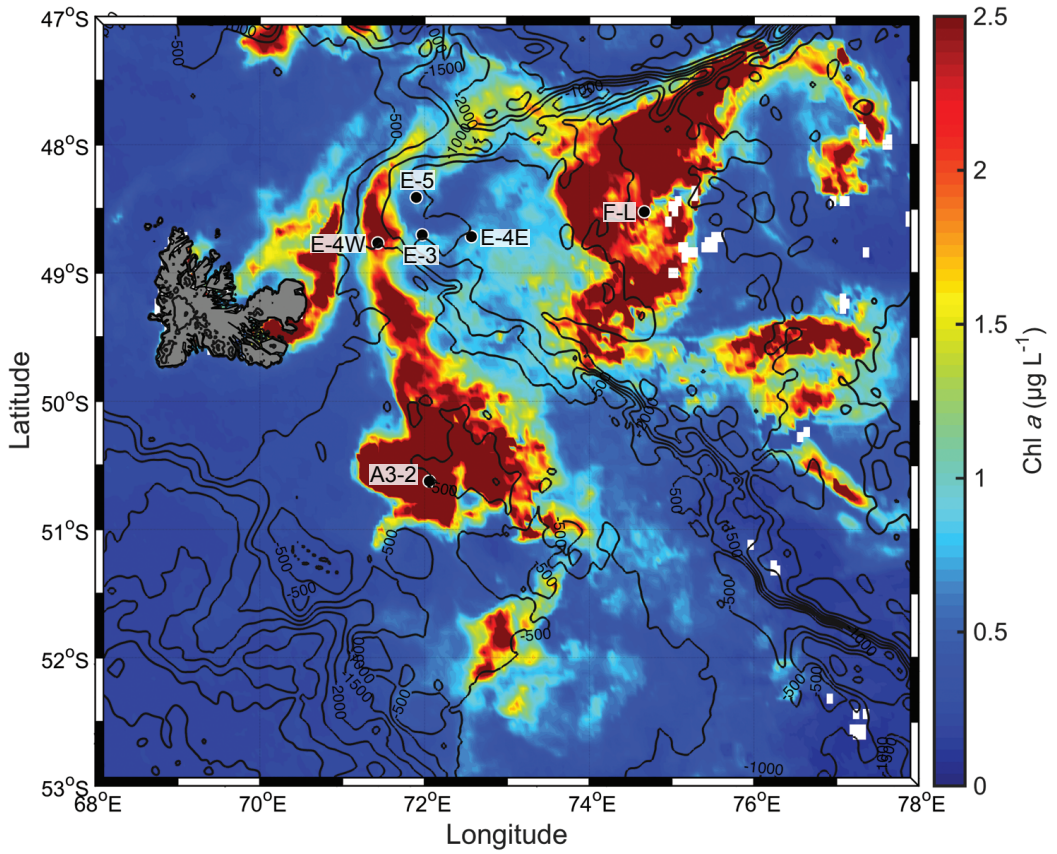

Figure 3.2: Sampling stations over the Kerguelen Plateau on a MODIS satellite image of surface chl *a* concentration on 11 November 2011. Location of each station and sampling date (dd/mm/yyyy): E–3: 71.97°E, 48.704°S (4/11/2011); F–L: 74.668°E, 48.523°S (6/11/2011); E–4W: 71.43°E, 48.766°S (11/11/2011); E–4E: 72.567°E, 48.717°S (13/11/2011); A3–2: 72.055°E, 50.624°S (16/11/2011); E–5: 71.9°E, 48.412°S (19/11/2011)

a CTD rosette frame. At each station the whole content of 2 Niskin bottles was transferred into a clean 30 l carboy to avoid any undersampling of particulate organic matter from the Niskins. Sampling was repeated at 2 different depths at each site (2 carboys per station). The carboys were stored in darkness for 1 d to initiate phytoplankton senescence.

3.2.2 Roller tank experiments

Carboy contents were poured into 10 l transparent cylindrical tanks cleaned previously with 2‰ alkaline detergent (Decon) and washed 3 times with extra sampled seawater. At each station, 4 cylindrical tanks (2 duplicates by depth, except at E–4E where deeper layers were not sampled) were placed on a rolling table at a constant speed of 0.66 rpm and kept in darkness during the entire duration of the incubation. All experiments were conducted at a temperature of ~ 10°C. To obtain sufficient millimeter sized aggregates to perform the chemical measurements

on individual aggregates, incubations lasted from 1 to 4 d. Measurements were conducted on 3 aggregates per tank (12 aggregates per experiment). When possible, aggregate selection was made in order to capture large variations of size, shape (e.g. spherical to elongated), and compactness (e.g. compact to loose). In each experiment, 6 aggregates were used for chemical measurements and 6 preserved in Lugol's solution for post-cruise microscopic observations in the laboratory.

3.2.3 Measurement of aggregate morphology and structure

At the end of the incubation, the tanks were removed from the rolling table and carefully rotated 90° to allow the aggregates to settle to the bottom. The maximum length of the 3 aggregates selected per tank was measured optically. Each aggregate was photographed through the bottom of the tank with a high-resolution Canon Powershot G12 camera (1 pixel $\approx$ 20 µm). The images were thresholded to create binary images and processed using the US National Institutes of Health free software, Image J (Abramoff et al., 2004). The minimum length was taken to be the minimum axis of the ellipse fitted to the shape by the software. The aspect ratio (AR) was calculated from the ratio between smallest and largest axes of the fitted ellipse. The commonly used Corey shape factor (CSF) (Corey, 1949; McNown and Malaika, 1950) representing particle flatness (low values of CSF corresponding to flat particles) was also used as a shape descriptor (assuming that the particles were symmetrical about their polar axis; Alldredge and Gotschalk, 1988). The equivalent spherical diameter (ESD) and volume of aggregates were calculated from the projected area, assuming a sphere.

We characterized the fractal structure of our aggregates by determining their 1-, 2- and 3-dimensional fractal numbers D_{F1}, D_{F2} and D_{F3}, respectively. The number of individual particles (N) composing a fractal aggregate increases non-linearly with its size and can be described by the power relationship (Logan and Wilkinson, 1990):

$$N \sim l^{D_{\mathrm{Fn}}} \tag{3.7}$$

where D_{Fn} is the fractal dimension determined for the object in n dimensions, and l is the maximum length of the aggregate. Since phytoplankton aggregates and their constitutive par-

ticles have finite sizes, they are not strictly self-similar at all scales and their fractal dimensions are approximations to real fractal dimensions obtained only for infinite size objects. The fractal dimension describes intuitively how much the individual particles fill the available space when they aggregate (e.g. Logan and Wilkinson,1990, Kilps et al., 1994, Jackson, 1998, Burd and Jackson, 2009) and is an indicator of particle compactness.

The maxima of D_{F1} =1, $D_{\mathrm{F2}} = 2$ and $D_{\mathrm{F3}} = 3$ are reached for Euclidean objects. For instance, $D_{\mathrm{F3}} = 3$ describes a solid compact sphere having no porosity where all individual particles filled the total volume available when they assembled. Unlike Euclidean objects, aggregates formed in marine systems, such as marine snow, have lower fractal dimension than their maximum values (Logan and Wilkinson, 1990). It implies that the number of particles filling the space during aggregation increases at a lower rate than aggregate maximum length does. It results in the important property that marine snow has a porosity increasing with size (Logan and Wilkinson, 1990), consequently reducing its excess density.

Following Kilps et al. (1994), the 1- and 2-dimensional fractal numbers (D_{F1} and D_{F2}) were calculated from the slopes of log–log relationships of perimeter and area respectively, against the Feret's diameter taken as the largest dimension (e.g. Engel et al., 2009). The 3-dimensional fractal number (D_{F3}) can be calculated from the slope of a log–log relationship between solid content (1 - Porosity) and the largest diameter l, according to the formula proposed by Logan and Wilkinson (1990):

$$(1 - P) = a \times l^{D_{\mathrm{F3}}-3} \tag{3.8}$$

where a is an empirical constant. Due to large uncertainties on solid content estimates, especially for TEP (see 'Chemical measurements' below), D_{F3} values for the experimental aggregates could not be reliably obtained, and only D_{F1} and D_{F2} results, based on image analysis, are presented. To avoid any bias due to small scale heterogeneity between images, no conversion from pixels to size unit was made for D_{F1} and D_{F2} determination.

3.2.4 Sinking velocity measurements

A non–destructive method was required to measure the sinking velocity and still be able to conduct other analyses on single aggregates. A method based on video recording the rotating tanks (Ploug et al., 2010) was not applicable onboard because of the ship motion altering the trajectories of particles. Instead, all the settling rates were measured directly inside the tanks using a 13.5 mm diameter and 23 cm long pipette acting as a static column. Right after the morphological measurements, the pipette was inserted and filled with water sampled at the surface of the tank. An aggregate was then selected at the bottom and gently sucked up into the pipette to the height of the water in the tank. The aggregate then sank freely in the column for several centimeters, and the average sinking velocity was measured over a distance of 7 cm at its apparent terminal velocity. Working directly inside the tanks avoided any transfer of the aggregates likely to alter their structure. Only 1 measurement was done on each aggregate due to their extremely fragile nature and the high probability of breaking, matter loss or structural alteration occurring during repeated manipulations, which would have flawed the study.

The length and diameter of the pipette limited the influence of turbulence induced by ship motion, which otherwise could be responsible for a bias in sinking velocity measurements. Nevertheless, our column dimensions presented possible issues worthy of evaluation. Specifically, the method would be in error if (1) wall effects affected aggregate sinking velocity without a clear correlation with size, thus precluding a reliable correction, or (2) aggregates did not reach their terminal velocity during settling. We determined the wall factor (f; Chhabra, 1995) defined as the ratio between the assumed terminal velocity of a particle in our pipette to that in a 50 cm high and 20 cm wide cylinder considered as an unbounded medium. Following the protocol of Ploug et al. (2010), we made agar spheres of 0.4 to 1 cm, used as model particles and covering most of the size range of our roller tank aggregates. The deviation to the Stokes' law expectations for our pipette and large cylinder was assessed by the use of 1 mm polystyrene beads (Duke Scientific, 4400A, 1004 ± 20 µm, ρ = 1.05 g cm^{-3}) sinking in filtered seawater (temperature T = 21°C; salinity S = 34.57; dynamic viscosity $\mu = 105 \times 10^{-5}$ kg m^{-1}s^{-1}; ρ_{sw} = 1.0243 g cm^{-3}). Over more than 70 measurements, polystyrene beads sank at very similar velocities in the large cylinder and pipette (mean ± SD: 941 ± 37 and 911 ± 51 m d^{-1}, respectively) suggesting that the pipette induced a negligible wall effect and permitted the particles to sink close to their terminal velocity. At this water temperature and salinity, theoretical expectations from Stokes' law

for the minimum and maximum bead sizes possibly encountered in our batch (984 and 1024 µm) led to sinking velocities of 862 and 933 m d^{-1}, respectively, very close to our experimental values. For larger particles, modeled by agar spheres, the pipette induced a wall effect well correlated with size: $f = -0.084 \times \mathrm{ESD(mm)} + 1.1\,(n = 28, r^2 = 0.98, p < 0.005)$. A correction based on this correlation was applied on our aggregate sinking velocities. In addition, as a precaution, all sinking velocity measurements of aggregates > 8 mm ESD (where the largest correction applies) were excluded from the study. The correction augmented the measured values by 50 ± 30% on average. It corresponded to an increase of 30 ± 29 m d^{-1} and represented a limited alteration of the raw data, which extended over 2 orders of magnitude.

3.2.5 Chemical measurements

Each individual aggregate was collected in 10 ml of tank water and directly processed or stored < 1 d at 2°C in 15 ml Falcon tubes. These 10 ml were homogenized and then divided into thirds for particulate organic carbon (POC), BSi and TEP measurements. Since each aggregate was sampled along with 10 ml of tank water, these 3 components were also measured in the tank water, and that amount was subtracted to yield the amount contained only within the aggregate.

BSi was measured following the alkaline extraction and colorimetric analysis procedure of Ragueneau et al. (2005). Subsamples were filtered onto 25 mm polycarbonate 0.4 µm pore filters, dried at 60°C in Eppendorf vials, sealed and stored at room temperature until analysis.

TEP were measured using a spectrophotometric method in accordance with Passow and Alldredge (1995). Subsamples were filtered onto 25 mm polycarbonate 0.4 µm pore filters and stained with 500 µl of a 0.02% aquaeous solution of Alcian blue in 0.06% acetic acid. The filters were stored in Eppendorf vials and immediately frozen at -20°C. Prior to analysis, all samples were soaked onboard for 2 h in 6 ml of 80% H_2SO_4 to redissolve the stain. The absorbance of the solution was measured at 787 nm with a spectrophotometer to quantify the TEP. The calibration curve relating the absorbance to the amount of TEP was established in the laboratory after the voyage with the remaining Alcian blue stock, using a protocol modified from Passow and Alldredge (1995).

TEP determination is semi–quantitative, as the chemical composition varies and is mostly unknown (Passow, 2012). The accuracy of measured TEP content depends on the ability of

the batch of xanthan gum (XG) to behave like TEP during the calibration, and on variations in Alcian blue staining properties between measurements done onboard and calibration done in the laboratory. The use of different batches of XG or Alcian blue leads therefore to a high variability and renders difficult quantitative comparisons between distinct works. Alcian blue is a hydrophilic cationic dye that complexes with anionic carboxyl or halfester–sulfate groups of acidic polysaccharides, and the selectivity of the stain depends on the pH and salt content of the dye solution (Passow and Alldredge, 1995). These properties are of course altered during the staining process, further influencing the possibility of variable or non–specific staining. In addition, the ratio of non–TEP material potentially stainable by Alcian blue to strict TEP may be higher in small or low TEP content samples.

POC content was determined by CHN elemental analysis using a Thermo Finnigan EA1112 Flash Elemental Analyser and acetanilide standards. Each subsample was filtered through a Sartorius T293 13 mm quartz filter (polycarbonate filter holder) with a nominal pore size of 0.8 µm (precombusted at 450°C for 4 h in clean foil to remove carbon contamination). The filters were blown dry using filtered air and then transferred to a clean, gravity circulation oven and dried at 50°C for more than 48 h. On completion of the sample set, the dry filters were loaded into silver 5 × 9 mm capsules (Sercon SC0037), acidified with 40 µl of 2 N HCl, dried for at least 48 h at 60°C, encapsulated and then stored over silica gel. Aggregate content in POM was estimated from POC values assuming a POM:POC mass ratio of 1.87 (Anderson, 1995).

Particulate inorganic carbon (PIC), a potentially important ballast mineral, was not measured because analyses of particles collected by large volume filtration revealed PIC to be very low, at levels that would have been below detection in the individual aggregates.

3.2.6 Microscope observations

Each aggregate reserved for microscopic observation was collected in Eppendorf vials in 1.5 ml of tank water and preserved with 1 drop of Lugol's solution. In the laboratory, the samples were resuspended in 3 ml of artificial seawater and transfered to a microscopy chamber for observation with a Zeiss Axio Observer A1 high–magnification inverted microscope. An average of 60 pictures per sample was taken at several magnifications (×160, 320 and 640) to cover the entire observable field. Pictures were used to identify numbers, sizes and genera (or species when possible) of phytoplankton and other organisms. An average cell diameter (or maximum length

for non–circular species) excluding the length of setae (spines) when present, was calculated by sizing a few to > 10 specimens of the organism, depending on its abundance in the aggregate. In order to investigate the potential influence of various phytoplankton morphological types on the sinking velocity, proportions of chain diatoms without setae (e.g. *Fragilariopsis* spp. and *Eucampia antarctica*) and small setae–forming diatoms (e.g. *Chaetoceros* spp.) were calculated. For simplicity, we refer to chain diatoms without setae as 'type 1' and to small setae–forming diatoms as 'type 2' in the rest of the text.

3.2.7 Multivariate analyses

Multiple regression analyses were conducted to quantify the relative contribution of size, as opposed to the other factors measured, in the prediction of sinking velocity variations. All analyses were performed using the statistical computing language and environment R. Since chemical composition and phytoplankton type contents were analysed on 2 different sets of aggregates, 2 distinct multiple regressions were carried out. The first model, fitted to the chemical composition data (fit 1), regressed sinking velocity against projected area, volume, ESD, Corey shape factor (CSF), aspect ratio (AR), and average mass fractions of BSi, POM and TEP in aggregate solid contents; the second model, fitted to the phytoplankton data (fit 2), regressed sinking velocity against projected area, volume, ESD, CSF, AR, and average type 1 and type 2 phytoplankton cell fractions in aggregates.

Linear regressions were applied, and the relative contribution of the parameters to the correlation was assessed by estimating the variation on the coefficient of determination (r^2) induced by removals of terms from the fit. To limit biases due to collinearity, parameters indicating the same aggregate property (size, shape, chemical or phytoplankton composition) were grouped and removed together. To identify aggregate properties playing the most important controls on the sinking velocity, ANOVAs were performed; the 2 models containing all terms (fits 1 and 2) were compared to the reduced models by a reduced sums of square F–test; with $p < 0.05$ used as indicator of a significant change.

3.3 Results

All morphological properties and compositions of the aggregates are reported in Table 3.1. Comparisons of sinking velocity and several aggregate properties from morphology (AR and CSF) to composition (BSi, TEP, POM and plankton content) were conducted to assess the possible effect of sampling depth on aggregate properties. No significant statistical difference was found between aggregates made from water sampled in surface layers and deeper layers ($1 > p > 0.45$) for a selected sample of the measured properties (sinking velocity, shape, chemical composition, phytoplankton content) and thus no distinction is made between these 2 aggregate groups in the rest of the study.

3.3.1 Sinking velocity

Sinking velocity data, corrected for wall effects, ranged from 13 to 260 m d^{-1} (1 aggregate sank at 569 m d^{-1} but this extreme value was excluded, along with all sinking velocity measurements for aggregates > 8 mm ESD, as explained in 'Materials and methods: Sinking velocity measurements'). In Fig. 3.3, data from each site are compared to expectations from the Stokes' law and general sinking velocity models for porous fractal particles. For these expectations, theoretical excess densities were calculated assuming 3 major solid components in fixed volume fractions (TEP:0.3, BSi:0.2, POM:0.5). These proportions are based on measured values of BSi and POC presenting the best scaling with size (see Fig. 3.6) and using a TEP:POC mass ratio of 0.7 (Alldredge, 1998; Martin et al., 2011). The theoretical porosity was scaled with size according to a fractal relationship (Eq. 3.8).

TEP, BSi, POM and seawater densities were fixed at 800, 2000, 1060 and 1026 Kg m^{-3} respectively, according to documented values (Azetsu-Scott and Passow, 2004; Klaas and Archer, 2002). All calculations assumed a dynamic viscosity of 0.00135 kg m^{-1} s^{-1} chosen according to the conditions existing in the tanks ($T = \sim 10°C$ and S = 34).

Using the drag coefficient calculated at an observed data point from its sinking velocity and size (called here 'specific conditions'), the apparent Reynolds number for this particle was determined by solving numerically the empirical relationship from White (1974), valid for a large range of Re ($0.5 < Re < 2 \times 10^5$):

$$C_{\mathrm{D}} = \frac{24}{\mathrm{Re}} + \frac{6}{1 + \mathrm{Re}^{0.5}} + 0.4 \tag{3.9}$$

The general model curves for other particle sizes were then calculated from this chosen observed value and the linear proportionality between Re and size, i.e. as embedded in the definition of the Reynolds number (Eq. 3.2).

The variation in the relationship between sinking velocity and size was explored for different fractal dimension D_{F3}, empirical constant a (Eq. 3.8), and specific conditions determining distinct initial drag coefficients. Fig. 3.3A shows that the steepest slope is obtained for the solid spheres ($D_{\mathrm{F3}} = 3$) of the Stokes' law model assuming a constant particle excess density. The different general sinking velocity models display decreasing slopes for D_{F3} values from 1.8 to 1.2, leading to a possible decrease of the sinking velocity with increasing size for low fractal numbers. This result suggests that for high fractal dimensions (compact aggregates) the size exerts a stronger control on the sinking velocity than for lower fractal dimensions (loose aggregates) and highlights the possible dominance of structure over size. For distinct specific conditions (distinct initial drag coefficients; 1 and 2 on Fig. 3.3A) the solutions converge when size increases, consistent with a decreasing influence of the drag coefficient in comparison to size.

Fig. 3.3B illustrates the sensitivity of the model curves to the empirical constant a, for 2 distinct fractal dimensions. The large variations of the curve slopes for a varying over several orders of magnitude (0.001 to 100) and particularly for small values of a, suggests that an accurate characterization of aggregate structure requires the fractal dimension to be used in combination with the constant a.

Fig. 3.3C shows tight correlations between sinking velocity and ESD when considering each site separately, suggesting the existence of site–specific parameters which alter the size–sinking velocity relationship. The general sinking velocity models are compared to data from each experiment with specific conditions of sinking velocity and ESD of each model corresponding to an average of all data of the experiment considered, assumed to reflect its drag characteristics. The best model fits to the data, agreeing with realistic values expected for marine snow, were obtained by decreasing D_{F3} from 1.8 in experiments with the highest sinking velocities, to 1.2 in experiments with the lowest sinking velocities. Data slopes were reproduced by the model curves

Table 3.1: Composition and morphological parameters of aggregates (Agg.) made in roller tank experiments conducted at 6 stations (Stn; see Fig. 3.2 for locations and sampling dates). Incub.: days of incubation in each tank; l: length (max/min) of Agg.; ESD: equivalent spherical diameter; SV: sinking velocity; BSi: biogenic silica; POC: particulate organic carbon; TEP: transparent exopolymeric particles; XG: xanthan gum (table continued on next page)

Agg.	Stn	Depth (m)	Tank #	Incub. (d)	l_{max} (mm)	l_{min} (mm)	ESD (mm)	SV (m d^{-1})	BSi (µmol)	POC (µmol)	TEP (µg XG equi–valent)	Mean cell diameter (µm)	% chain diatom without setae	% small setae–forming diatom
1	E–3	30	1	3	12	9	9.2	569	3.6	10.6	488	–	–	–
2	|	|	1	|	3	2	2.7	143	0.1	2.7	210	–	–	–
3	|	|	1	|	4	2	2.6	149	0.1	0.9	199	–	–	–
4	|	|	1	|	3	2	1.9	98	0.2	0.6	232	–	–	–
5	|	|	1	|	5	1	2.2	114	0.1	1.0	199	–	–	–
6	|	|	2	3.3	4	2	3.5	161	–	–	–	52	43	12
7	|	|	2	|	6	3	4.3	220	–	–	–	54	65	5
8	|	|	2	|	3	2	2.1	105	–	–	–	54	69	3
9	|	150	3	3.3	6	4	4.4	258	0.4	1.1	283	–	–	–
10	|	|	3	|	10	3	4.6	168	0.9	4.5	150	–	–	–
11	|	|	4	3.5	20	5	2.2	113	–	–	–	58	65	4
12	|	|	4	|	10	1	4.6	109	–	–	–	69	55	0
13	F–L	20	1	1	7	4	5.2	135	0.6	1.6	272	–	–	–
14	|	|	1	|	6	3	4.1	89	0.4	3.9	272	–	–	–
15	|	|	1	|	10	6	5.6	127	1.9	4.7	439	–	–	–
16	|	|	2	1	10	7	7.0	158	–	–	–	41	30	4
17	|	|	2	|	4	1	1.6	58	–	–	–	48	23	12
18	|	|	2	|	8	4	4.9	145	–	–	–	29	25	13
19	|	65	3	1	7	5	5.7	254	1.4	4.4	286	–	–	–
20	|	|	3	|	5	3	3.7	96	0.2	1.1	209	–	–	–
21	|	|	3	|	3	1	1.3	87	0.1	0.4	242	–	–	–
22	|	|	4	1	12	6	7.4	203	–	–	–	32	13	32
23	|	|	4	|	7	4	4.8	167	–	–	–	35	7	40
24	|	|	4	|	4	2	2.1	79	–	–	–	41	5	36
25	E–4W	30	1	1.2	15	7	8.7	46	0.7	0.3	377	–	–	–
26	|	|	1	|	15	12	10.3	66	1.0	0.8	377	–	–	–
27	|	|	1	|	15	12	12.3	172	1.0	1.7	333	–	–	–
28	|	|	2	1.3	10	7	7.0	17	–	–	–	34	14	56
29	|	|	2	|	10	5	5.6	23	–	–	–	37	11	56
30	|	|	2	|	8	6	5.6	23	–	–	–	36	18	37
31	|	80	3	1.3	8	4	4.6	23	0.5	0.5	109	–	–	–
32	|	|	3	|	10	7	6.9	30	0.4	13.0	298	–	–	–
33	|	|	3	|	10	7	7.1	13	1.0	1.8	287	–	–	–
34	|	|	4	1.4	10	6	6.6	17	–	–	–	25	2	68
35	|	|	4	|	13	8	9.1	60	–	–	–	38	10	44
36	|	|	4	|	10	8	7.3	24	–	–	–	29	15	47
37	E–4E	30	1	1.1	11	6	7.8	240	1.1	2.0	166	–	–	–
38	|	|	1	|	12	6	7.4	217	1.2	2.1	300	–	–	–
39	|	|	1	|	5	3	4.1	145	0.5	2.4	133	–	–	–
40	|	|	2	1.2	6	4	4.6	184	–	–	–	44	26	56
41	|	|	2	|	7	5	5.5	173	–	–	–	58	40	17
42	|	|	2	|	7	5	5.2	198	–	–	–	56	33	30
43	A3–2	30	1	1.2	7	5	5.7	74	0.5	2.1	60	–	–	–
44	|	|	1	|	7	5	4.8	64	0.4	2.6	160	–	–	–
45	|	|	1	|	8	3	4.2	20	0.2	1.2	160	–	–	–
46	|	|	2	1.3	7	5	5.3	60	–	–	–	22	4	77
47	|	|	2	|	6	4	4.0	46	–	–	–	22	8	48
48	|	|	2	|	7	4	4.6	60	–	–	–	17	0	67
49	|	80	3	1.3	7	6	5.4	73	0.6	2.8	156	–	–	–
50	|	|	3	|	7	3	3.6	49	0.6	1.8	289	–	–	–
51	|	|	3	|	7	6	5.7	52	0.3	1.2	78	–	–	–
52	|	|	4	1.4	8	7	6.7	59	–	–	–	14	2	81
53	|	|	4	|	7	5	4.6	52	–	–	–	26	11	53
54	|	|	4	|	7	6	5.8	37	–	–	–	17	2	85
55	E–5	30	1	2.7	8	6	5.7	80	0.7	4.0	335	–	–	–
56	|	|	1	|	7	6	5.7	67	0.6	2.5	290	–	–	–
57	|	|	1	|	5	3	3.6	46	0.2	4.2	68	–	–	–
58	|	|	2	2.7	9	6	6.4	62	–	–	–	58	23	77
59	|	|	2	|	8	6	5.5	40	–	–	–	76	9	48
60	|	|	2	|	8	5	5.1	43	–	–	–	59	25	67
61	|	80	3	2.7	8	6	6.6	91	1.3	2.7	405	–	–	–
62	|	|	3	|	5	3	3.7	72	0.3	3.1	138	–	–	–
63	|	|	3	|	6	4	3.1	50	0.3	2.5	138	–	–	–
64	|	|	4	2.8	5	3	3.8	75	–	–	–	92	40	14
65	|	|	4	|	5	3	3.7	74	–	–	–	89	52	7
66	|	|	4	|	7	3	4.6	60	–	–	–	80	25	25

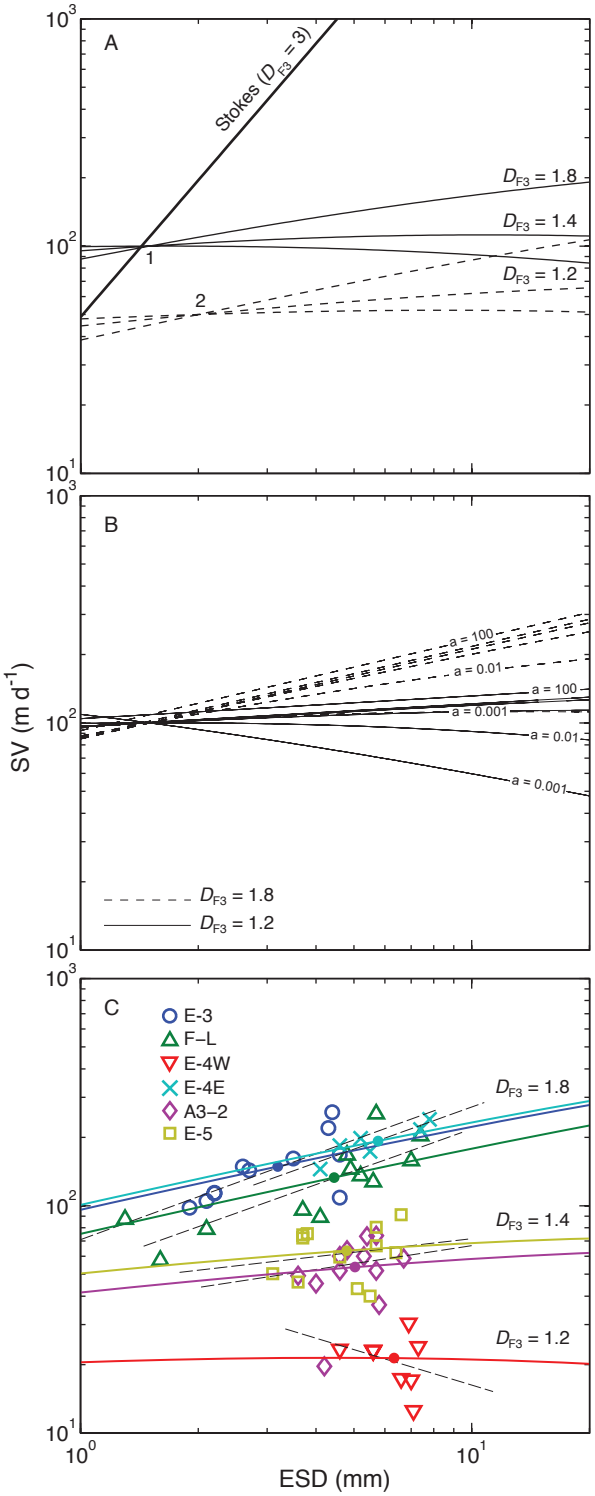

Figure 3.3: Sinking velocities (SV) of aggregates versus their equivalent spherical diameter (ESD) recorded at 6 stations, and theoretical expectations. (A) Stokes' law assuming a solid body with constant excess density (thick line: $\Delta\rho = 0.0014$ g cm^{-3}, $D_{F3} = 3$) and general sinking velocity models (thin and dashed lines) for porous fractal particles with porosity scaled on size for fractal numbers of 1.2, 1.4 and 1.8 and 2 different specific conditions; 1: $ESD_0 = 1.5$ mm, $SV_0 = 100$ m d^{-1}; 2: $ESD_0 = 2$ mm, $SV_0 = 50$ m d^{-1}. (B) Sensitivity of the general sinking velocity model to different values of coefficient a varying over 5 orders of magnitude from 0.001 to 100, for 2 fractal dimensions (dashed lines: $D_{F3} = 1.8$; solid lines: $D_{F3} = 1.2$) and one set of specific conditions: $ESD_0 = 1.5$ mm, $SV_0 = 100$ m d^{-1}. (C) Data for each station (symbols) compared to general sinking velocity models (solid lines) with coefficient a fixed at 0.01 and different D_{F3} values (E–3, F–L, E–4E: $D_{F3} = 1.8$; A3–2, E–5: $D_{F3} = 1.4$; E–4W: $D_{F3} = 1.2$). Filled circles: specific conditions for each model; dashed lines: best fits to data (1 outlier excluded from A3–2 fit). E–3: $y = 71 \times 0.63\,(n = 11, r^2 = 0.49, p < 0.05)$; F–L: $y = 53 \times 0.61\,(n = 13, r^2 = 0.67, p < 0.005)$; E–4W: $y = 53 \times -0.52\,(n = 8, r^2 = 0.1, p = 0.46)$; $E--4E : y = 66 \times 0.62 (n = 6, r^2 = 0.8, p < 0.05)$; A3–2: $y = 36 \times 0.26 (n = 11, r2 = 0.5, p = 0.5)$; E–5: $y = 45 \times 0.2 (n = 12, r^2 = 0.4, p = 0.55)$

with variable accuracy, suggesting that fractal structure may have varied from one experiment to another.

3.3.2 Morphology and fractal numbers D_{F1} and D_{F2}

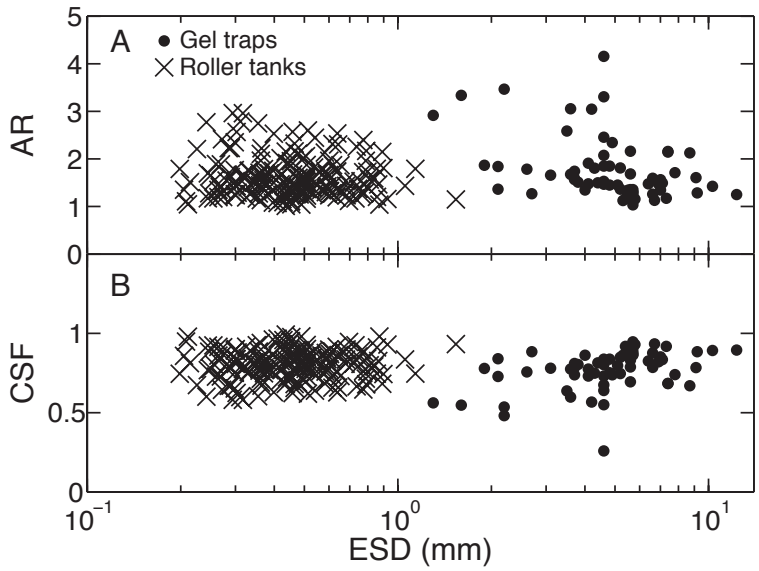

Figure 3.4: Shape descriptors versus equivalent spherical diameter (ESD) for roller tank aggregates (one very long 'comet–shaped' aggregate excluded) and natural aggregates collected in polyacrylamide gel sediment traps deployed during KEOPS2. (A) Aspect ratio (AR) and (B) Corey shape factor (CSF) are in the same range of values for the 2 categories of aggregates

Aggregates formed in roller tanks had similar shapes to aggregates collected in polyacrylamide gel–filled sediment traps at similar times and locations (Fig. 3.4). Maximum lengths ranged from 3 to 20 mm, and projected areas from 1.3 to 118 mm^2, leading to ESD of 1.3 to 12.3 mm (Table 3.1) and volumes of 1.1 to 965 µl. Their aspect ratios extended from 1.03 to 4.15, except one very long 'comet–shaped' aggregate with an extreme value of 13. The Corey shape factors ranged from 0.26 to 0.95. Overall, aggregates produced in roller tank experiments were bigger than natural aggregates (ESD: ∼0.1 to 1.4 mm). This is the result of our choice to maintain incubations over a duration long enough to provide sufficient material for the chemical measurements.

Fractal numbers D_{F1} and D_{F2} of aggregates produced in roller tanks were 1.49 ± 0.16 and 1.82 ± 0.18 respectively (Fig. 3.5) and also close to those of natural aggregates calculated with the same method (D_{F1} = 1.25 ± 0.006 and D_{F2} = 1.86 ± 0.015) suggesting similar fractal structure.

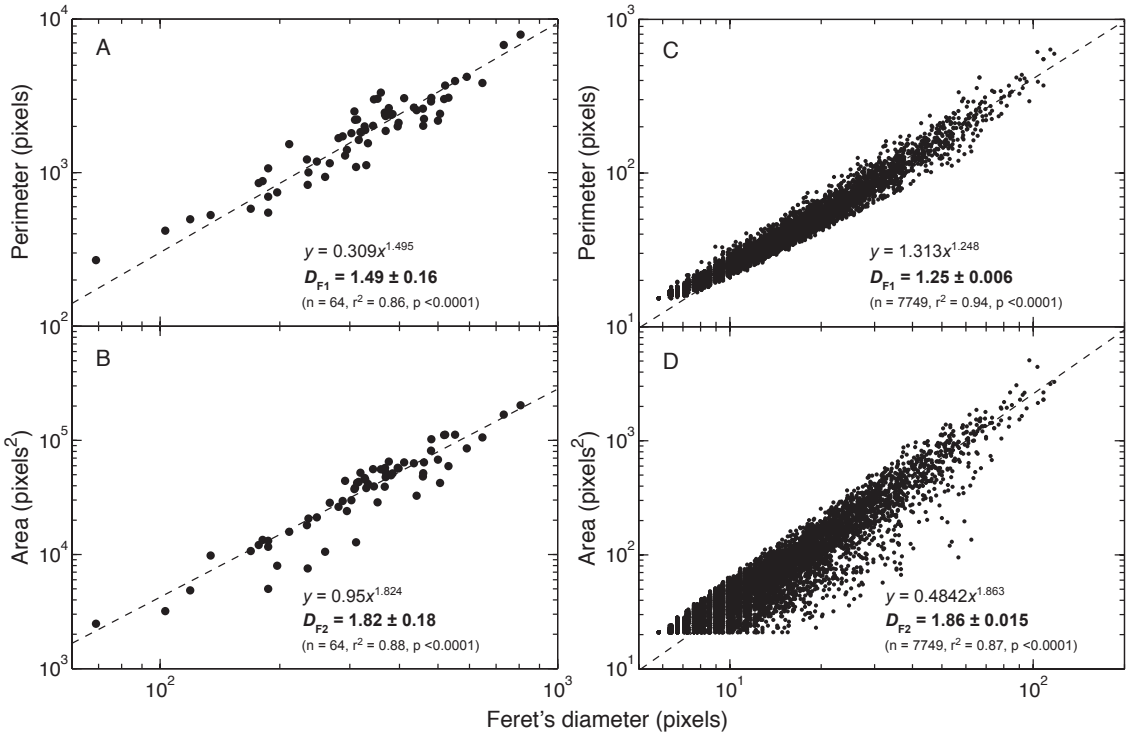

Figure 3.5: Fractal numbers of (A,B) roller tank aggregates (one very long 'comet–shaped' aggregate excluded) and (C,D) natural aggregates collected in polyacrylamide gel sediment traps deployed during KEOPS2 at the same sites. 1– and 2–dimensional fractal numbers (D_{F1} and D_{F2}): calculated from the slope of the relationships between perimeter (A,C) and area (B,D) versus their Feret's diameter. On each panel: best fit lines, fractal numbers (±95% CI) and regression statistics. An area cut–off at 20 pixels^2 was applied on gel trap data (visible in panel D) to exclude from the regression potential 'fake particles' deriving from small gel imperfections

3.3.3 Solid components (BSi, POC, TEP)

The amount of BSi in aggregates increased with size with values ranging from 0.09 to 3.6 µmol (Fig. 3.6). Values of POC and TEP in aggregates ranged from 0.28 to 13 µmol and 60.5 to 488 µg XG equivalent, respectively. POC content in aggregates from the Stn E–4W experiment presented a high variability compared to all other experiments. TEP content did not scale with aggregate volume, possibly suggesting that only one–third of the volume of an aggregate (subsampling in 3.3 ml; see 'Materials and methods: Chemical measurements') represented a too small amount of matter to be detectable by the method used, especially for the smallest aggregates. This study aimed to obtain a complete set of chemical analyses conducted on single aggregates, which unfortunately constrained the analyses to single measurements on amounts well under the usual limits. Replicate measurements and on larger particles would have probably increased the accuracy of TEP measurements, but limited the applicability of our results to natural conditions where smaller particles dominate.

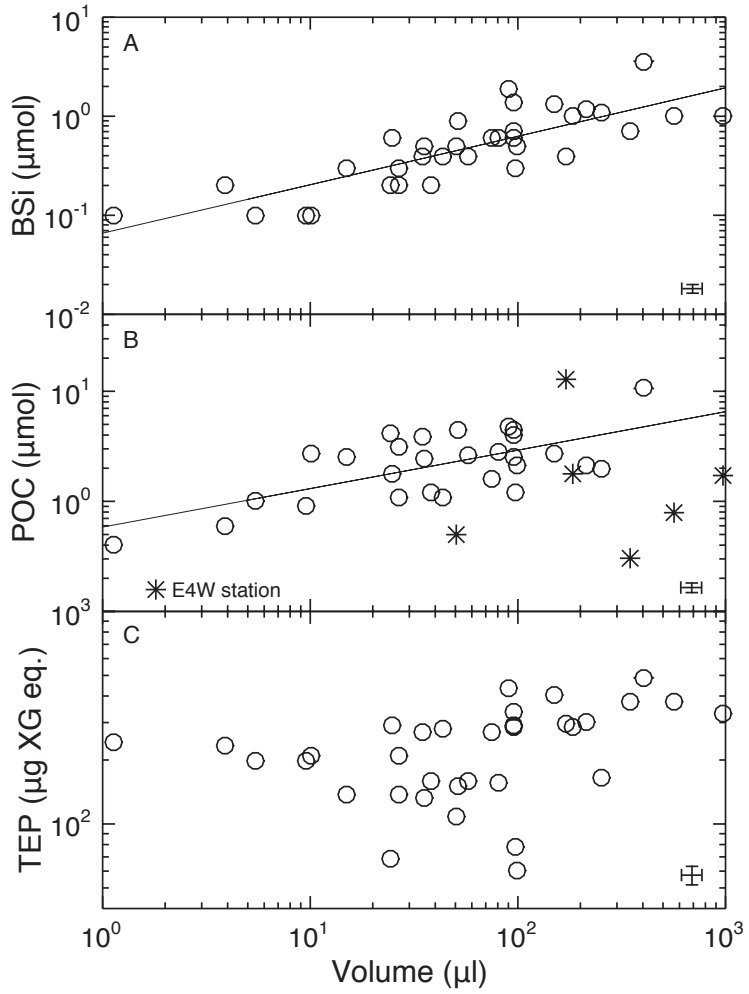

Figure 3.6: Chemical component abundances in aggregates vs. volume. (A) Biogenic silica (BSi); (B) particulate organic carbon (POC); (C) transparent exopolymer particles (TEP; µg xanthan gum equivalent). Best fit lines: BSi, $y = 0.07 \times 0.49; n = 34; r^2 = 0.65; p < 0.0001$; POC, $y = 0.58 \times 0.35; n = 28; r^2 = 0.44; p < 0.0005$. (∗): scattered Stn E–4W values excluded from the fit. (○): all other data. Error bars: 10% uncertainty

3.3.4 High–resolution pictures and phytoplankton content

Aggregates from different sites displayed diverse aspects, colors and apparent compositions as shown in high–resolution pictures (Fig. 3.7). Similar observations were done on natural particles collected in polyacrylamide gel traps at the same sites. Aspects ranged from compact yellow aggregates (e.g. Fig. 3.7A,B & G) to very fluffy, green and fragile aggregates (e.g. Fig. 3.7C,E & H). Microscopic observations revealed distinct phytoplankton species assemblages composing the roller tank aggregates (Fig. 3.7J–L). The proportion and average sizes of phytoplankton cells for the main species or genera identified in the aggregates are reported in Table 3.2. The largest average proportions of the total organisms counted in all aggregates in descending order were *Chaetoceros* subgenus *Hyalochaete* spp. (mean ± SD: 27 ± 24%); *Fragilariopsis* spp. (19

± 20%) including the species *kerguelensis* and *rhombica*; small centrics represented mainly by *Thalassiosira* spp. (13 ± 15%); *Pseudo–nitzschia* spp. (11 ± 7%); and *Eucampia antarctica* (7 ± 8%). The average cell diameter measured over each species ranged from 13.6 ± 1.94 to 91.8 ± 23.3 µm. Phytoplankton classified as type 1 (see 'Materials and methods: Microscopic observations') ranged from 0.24 (Stn A3–2) to 70% (Stn E–3) of total organisms counted in aggregates. Type 2 represented 0 (Stn E–3) to 84.8% (Stn A3–2).

3.3.5 Sinking velocity controls

Results of the multiple regression analyses (Table 3.3) suggest that chemical composition and phytoplankton cell length and type predict the largest part of sinking velocity variations, overcoming the effect of aggregate size or shape. A decrease in the coefficient of determination (r^2) of 0.26 and 0.32 was induced by the removal of chemical composition and phytoplankton type terms, respectively. ANOVA F–tests revealed that models reduced from chemical composition and phytoplankton types were significantly different from the initial models ($p < 0.05$). Conversely, the removal of aggregate size terms from fits 1 and 2 led to decreases in r^2 of 0.17 and 0.12 respectively. The removal of aggregate shape terms from fits 1 and 2 induced decreases of r^2 of 0.09 and 0.03 respectively. None of the models reduced from size or shape terms were significantly different from the complete models.

Two additional multiple regressions were performed to identify which of chemical composition or phytoplankton types presented the best correlation to sinking velocity. This was done by removing aggregate size and shape parameters at the same time from the initial fits (Table 3.3 bottom row), leaving chemical composition and phytoplankton type as unique aggregate properties in fit 1 and fit 2, respectively. A better fit was obtained when sinking velocity was regressed against phytoplankton types than against chemical composition ($n = 30; r^2 = 0.36; p < 0.05$, and $n = 31; r^2 = 0.21; p < 0.5$, respectively).

In addition, data of shape (Corey shape factor and aspect ratio) and solid content (BSi, TEP, POM) were explored separately by site (Fig. 3.8A–E). Results suggest that shape and chemical composition are not site–dependent and exert no clear influence on the sinking velocity. According to our main hypothesis, dominant phytoplankton cell size and morphological types were further investigated as indirect controls of the sinking velocity (Fig. 3.8F–H). The clustering of data from each site suggested that dominant phytoplankton type was a site–dependent factor

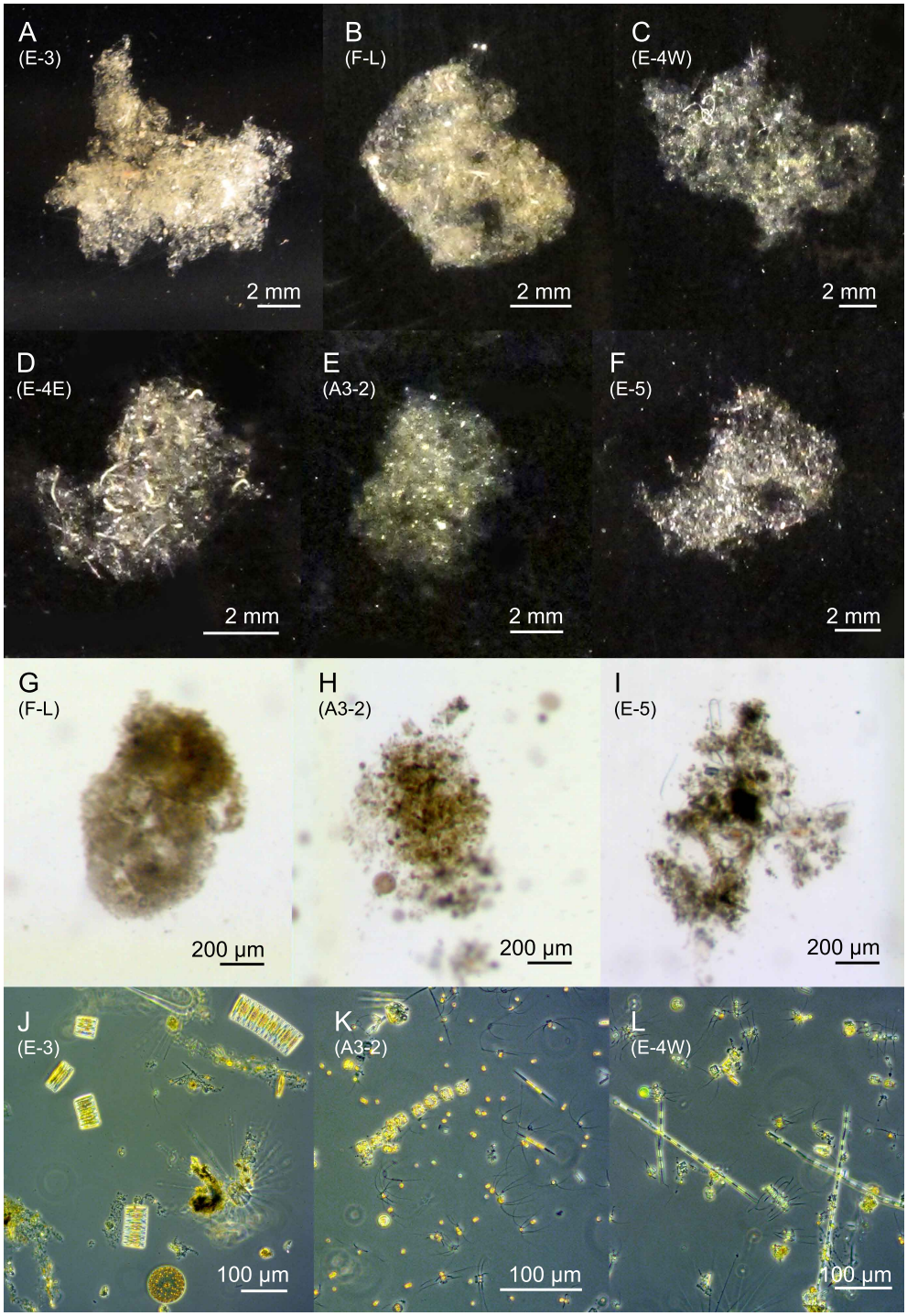

Figure 3.7: Pictures of (A–F) roller tank aggregates formed at each station and (G–I) natural marine snow collected in polyacrylamide gel traps at the same locations (note the similarities in aspect, shape and compactness between natural particles and those formed in roller tanks at the same sites). (J–L) Pictures showing distinct phytoplankton assemblages in roller tank aggregates from Stns E–3 (*Fragilariopsis* spp., *Corethron pennatum* and centric diatoms), A3–2 (*Chaetoceros* subgenus *Hyalochaete* spp., small centric diatoms and *Pseudo–nitzschia* spp.), and E–4W (*Pseudo–nitzschia* spp. and *Chaetoceros* subgenus *Hyalochaete* spp.) respectively

possibly influencing the sinking velocity. The cell length appeared to apply a moderate influence since aggregates where the largest cells were observed had intermediate sinking velocity (Stn E5) and aggregates sinking faster and slower than 100 m d^{-1} contained in average cells having similar length (mean ± SD: 48 ± 12 and 43 ± 25 µm, respectively). However, aggregates sinking faster than 100 m d^{-1} had high proportions of *Eucampia antarctica* and *Fragilariopsis* spp. (type 1; mean ± SD: 39 ± 21%) and low proportions of *Chaetoceros* spp. (type 2; 18 ± 18%). In contrast, aggregates sinking slower than 100 m d^{-1} had low proportions of type 1 (15 ± 13%) and high proportions of type 2 (44 ± 24%).

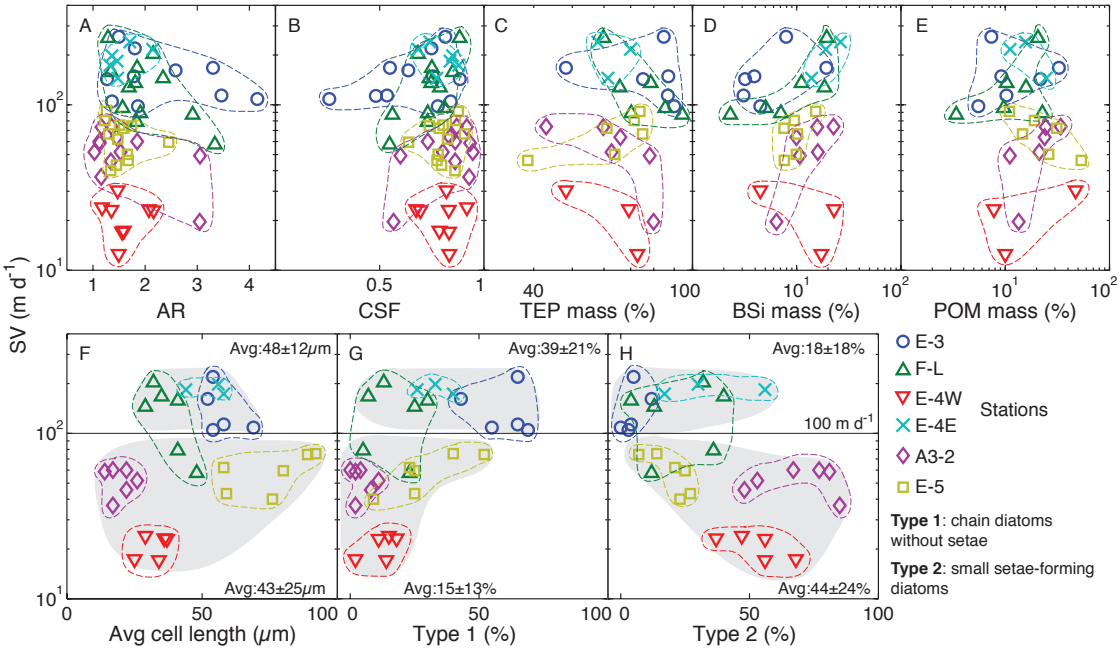

Figure 3.8: Influence of shape, chemical composition and phytoplankton morphology on sinking velocity (SV). (A–E) Aspect ratio (AR), Corey shape factor (CSF), transparent exopolymer particles (TEP), biogenic silica (BSi), and particulate organic matter (POM) mass proportion in solid content, respectively. (F) Average cell length in aggregates; (G,H) proportion in aggregates of chain diatoms without setae (type 1; *Fragilariopsis* spp. and *Eucampia antarctica*) and small setae–forming diatoms (type 2; *Chaetoceros* spp.) respectively. There is no clear influence of shape or chemical composition. Data clustering of morphological properties of phytoplankton at each station suggests a control by phytoplankton cell type. High proportions of type 1 (39 ± 21%) and low proportions of type 2 (18 ± 18%) diatoms are observed in aggregates sinking faster than 100 m d^{-1}. The opposite is found for aggregates sinking slower than 100 m d^{-1} (type 1: 15 ± 13%; type 2: 44 ± 24%)

3.4 Discussion

Our image analyses suggested that the structure of aggregates produced in roller tanks were similar to those of natural aggregates collected in gel traps during KEOPS2. The fractal numbers

Table 3.2: Phytoplankton species or genera proportions (% mean ± SD) in aggregates (agg.) and their cell diameter (ø, mean ± SD) at 6 stations. **In bold**: the 2 major species or genera at each station; the **most and *second most abundant species or genera encountered in aggregates from at least 1 station are also indicated

Phytoplankton species or genera	Stations											
	E–3		F–L		E–4W		E–4E		A3–2		E–5	
	% in agg.	ø (µm)	% in agg.	ø (µm)	% in agg.	ø (µm)	% in agg.	ø (µm)	% in agg.	ø (µm)	% in agg.	ø (µm)
Asteromphalus hookeri	0.8±0.1	79±31	0.1±0.1	123±18	0.0	–	0.1±0.2	78	0.0	–	0.8±0.7	105±22
Chaetoceros atlanticus	1.2±0.2	29±7	0.0	–	0.1±0.2	16	0.1±0.2	24±8	0.1±0.1	17±2	0.1±0.2	19±4
Chaetoceros criophilum	0.0	–	0.8±1.0	21±1	0.0	–	1.6±2.1	–	0.0	–	0.0	–
Chaetoceros decipiens	2.2±0.2	27±6	5.8±6.5	27±3	0.4±0.6	32±3	4.1±0.2	28±8	0.2±0.3	29±2	2.8±2.1	30±8
Chaetoceros dichaeta	0.3±0.1	20±7	0.1±0.1	16±4	1.3±1.0	27±12	2.5±1.7	22±5	0.9±0.5	25±3	5.2±4.9	19±2
Chaetoceros (*Hyalochaete*) spp.**	1.3±0.2	12±5	**16.2 ± 9.3**	13±4	**42.4 ± 21.1**	12±1	**26.4 ± 16.1**	10±1	**67.2 ± 15.5**	10±2	11.3±5.9	12±2
Corethron inermis	1.2±0.2	70±3	0.0	–	0.0	–	0.6±0.8	–	0.1±0.1	95±25	0.8±1.2	108±74
Corethron pennatum	5.8±0.4	191±65	0.7±0.9	179±55	0.4±0.2	304±78	0.8±0.2	213±53	0.2±0.2	105±13	8.8±2.5	212±27
Dactyliosolen antarcticus	1.0±0.1	147±39	0.1±0.2	82±11	0.4±0.4	153±66	1.1±0.7	101±28	0.0	–	1.2±1.0	88±10
*Eucampia antarctica**	2.9±0.3	50±6	10.2± 6.7	55 ± 6	0.8±0.8	50±10	**20.5 ± 4.9**	57±7	0.5±0.5	52±3	6.3±4.0	46±7
Fragilariopsis spp.**	**56.7 ± 4.6**	44±8	7.1±8	32 ±12	9±6.4	38±5	12.5±11.8	39±3	3.9±3.9	37±9	**22.7 ± 13.9**	48±6
Guinardia cylindrus	0.5	88±7	0.0	–	0.0	–	0.3±0.3	–	0.1±0.1	80	2.2±1.6	72±16
Membraneis sp.	0.5±0.1	233±59	0.3±0.3	174±60	0.1±0.1	171±66	0.3±0.2	189±66	0.1±0.1	139±21	0.3±0.4	186±28
Navicula spp.	0.4±0.1	30±4	0.0	–	0.0	–	0.2±0.1	–	0.2±0.2	28±8	0.3±0.4	27±8
Nitzschia sp.	0.8	87±13	0.6±0.6	84±19	0.1±0.1	95±7	0.3±0.3	110±61	0.2±0.2	111±43	0.9±0.8	88±8
Odontella spp.	1.2±0.2	51±6	1.8±1.3	65±5	0.0	–	1.4±1.0	58±1	0.3±0.3	64±12	0.9±0.9	60±13
Proboscia sp.	0.1	–	0.0	–	0.4±0.5	–	0.0	–	0.2±0.2	177±44	0.7±0.9	207±48
Pseudo-nitzschia spp.*	5.3±0.5	106± 30	4.0±2.2	75±21	**12.1 ± 5.6**	95±7	20.1±12.5	97±11	5.9±2.2	94±7	**18.9 ± 7.2**	92±8
Rhizosolenia sp.	0.4	370± 212	0.2±0.4	490±108	0.4±0.5	243±5	0.2±0.2	246±41	0.3±0.6	270	1.7±2.1	363±64
*Thalassionema nitzschioides**	**8.5 ± 1.0**	22±4	8.0±3.3	28±9	5.4±3.2	35±14	1.6±0.3	20±1	4.5±2.5	19±3	7.0±5.3	20±3
Thalassiothrix antarctica	0.0	–	0.3±0.5	778±366	0.0	–	0.6±0.2	825±173	0.0	–	0.8±0.6	756±233
Small centrics**	4.1±0.3	43±11	**42.1 ± 5.1**	28±4	11.6±6.7	34±1	2.9±1.4	25±4	**14.3 ± 9.3**	18±1	3.6±1.6	32±4
Large centrics	2.0±0.1	126±55	0.3±0.2	76±29	0.2±0.2	123	0.1±0.2	96±23	0.3±0.2	82±47	0.4±0.6	88±11
Ceratium sp.	0.1	388	0.0	–	0.0	–	0.0	–	0.0	–	0.2±0.6	161
Silicoflagellates	2.0±0.2	21±2	0.6±0.3	19±2	0.4±0.3	20±3	1.4±0.8	18±1	0.4±0.2	18±1	1.9±1.2	21±3
Tintinnids	0.8±0.1	94±72	0.6±0.6	62±10	0.1±0.1	156±100	0.3±0.3	60±4	0.0	–	0.0	–

Table 3.3: Multiple regression analyses statistics: relative contribution of aggregate properties to sinking velocity (SV) variations. Parameters investigated: aggregate size, shape, chemical composition (BSi, POM and TEP average mass fraction in solid content) and average phytoplankton type in aggregates. New r^2 and p–values (variations in parentheses) after removal of terms from the initial complete fits (1 and 2) are given. Initial and reduced models are compared by performing ANOVA F–tests. Significant modification of the initial model are **in bold** ($p < 0.05$) and show the importance of the terms removed in sinking velocity variations. Type 1 and 2: average proportion (%) of (1) chain diatom cells without setae and (2) small setae–forming diatom cells in aggregates, respectively. ESD: equivalent spherical diameter; CSF: Corey shape factor; AR: aspect ratio; BSi: biogenic silica; POM: particulate organic matter; TEP: transparent exopolymeric particles

Terms removed from the fit	Fit 1			Fit2		
	New r^2	New p–value	F–test p–value	New r^2	New p–value	F–test p–value
Size (projected area, volume, ESD)	0.25 (-0.17)	0.13 (+0.03)	0.17	0.38 (-0.12)	0.03 (-0.01)	0.22
Shape (CSF, AR)	0.33 (-0.09)	0.1	0.25	0.47 (-0.03)	0.02 (-0.02)	0.51
Chemical composition (BSi, POM, TEP)	**0.16 (-0.26)**	**0.54 (+0.44)**	**0.03**	–	–	–
Phytoplankton (cell length, type 1, type 2)	–	–	–	**0.18 (-0.32)**	**0.4 (+0.36)**	**0.01**
Size + shape	0.21 (-0.21)	0.15 (+0.05)	0.27	0.36 (-0.14)	0.01 (-0.03)	0.5

Fit1: SV = f(projected area+volume+ESD+CSF+AR+BSi+POM+TEP); $n = 30; r^2 = 0.42; p = 0.1$
Fit2: SV = f(projected area+volume+ESD+CSF+AR+cell length+type1+type2); $n = 31; r^2 = 0.5; p = 0.04$

D_{F1} and D_{F2} were close to those of natural particles, suggesting that aggregation processes in the roller tanks were somewhat similar to those acting in the water column. This is an encouraging result toward the applicability of this experiment to natural conditions, but needs considerable caution, especially since roller tank experiments have been previously shown to poorly simulate natural aggregation processes and should not be used for quantitative studies (Jackson, 1994). Aggregates formed in the roller tanks were consistently bigger than natural aggregates collected in gel traps. One major feature of roller tank experiments which differs from natural conditions is that fast–sinking particles cannot escape from the tank and tend to form continuously larger particles until complete clearing of the water. Thus, the size of aggregates formed in roller tank experiments depends mainly on the duration of incubation. However, the main objective here was to form marine snow aggregates from a natural mixture of phytoplankton and test if variations in their composition and structure was related to sinking velocity variations. Even if aggregates formed in this experiment were far from natural particles encountered at the same sites (which does not seem to be the case according to our observations) they still can serve as model aggregates to identify factors altering the size–sinking velocity relationship.

While the overall correlation between sinking velocity and particle size is quite weak in our results, several sites exhibited reasonably tight correlations (Fig. 3.3C) and with slopes reasonably close to those expected from general sinking velocity models. This suggests that differences in the initial compositions might be responsible for the overall weak correlation observed when combining all aggregates from distinct sites. A match between size–sinking velocity model curves

and experimental data from each site was obtained by varying the fractal dimension, indicator of particle compactness. In combination, these 2 results suggest that distinct particle sources sampled at different sites formed aggregates having different composition, structure and sinking velocity. Also, the size–sinking velocity relationship appears to be preserved for the most compact aggregates, suggesting that a reduction of the porosity could restore size as a controlling factor. Iversen and Ploug (2010) compared size–sinking velocity relationships for different types of aggregates formed from different primary particles. They also noted a correlation of sinking velocity with size only within homogeneous sources of aggregates, but when compared across different aggregate composition, the sinking velocity appeared size–independent.

Overall, our results suggested a poor contribution from size, shape or chemical composition in aggregate sinking velocity variation among sites. The multiple regression analyses performed (Table 3.3) showed that among all the aggregate properties tested in our experiment, phytoplankton cell type seemed the best property to explain sinking velocity variation. The 2 distinct morphological categories that we selected (type 1: *Eucampia antarctica* and *Fragilariopsis* spp.; and type 2: *Chaetoceros* spp.) could have influenced the sinking velocity either by ballast effect (Iversen and Ploug, 2010; Miklasz and Denny, 2010; Ploug et al., 2008; Waite et al., 1997a), or by influencing aggregate structure through distinct aggregation processes. The absence of correlation between BSi mass fraction in aggregate solid content (Fig. 3.8D) suggests that a ballast effect did not explain a large part of sinking velocity variation; the observed increase in BSi with aggregate volume (Fig. 3.6) as expected for diatom aggregates, suggesting reliable measurements for this component.

Setae are known to promote phytoplankton coagulation by increasing the efficiency of 'mechanical' sticking upon contact (Alldredge and Gotschalk, 1989; Kiorboe et al., 1990). Stickiness (i.e. the probability that 2 particles become attached upon collision) has been demonstrated to be species–specific (Alldredge et al., 1995; Crocker and Passow, 1995; Kiorboe et al., 1990), and Waite et al. (1997b) noted that spine formation, cell surface bound sugars, and TEP controlled phytoplankton cell stickiness and played a role in determining aggregate structure via coagulation processes. High sticking efficiency is not subject only to cell morphology and depends on various other factors including TEP production, which plays a central role in coagulation (Dam and Drapeau, 1995; Jackson, 1995; Kiorboe and Hansen, 1993; Thornton, 2002). Cell concentration and size have also been demonstrated to be critical parameters for coagulation

processes during algal blooms (Jackson, 1990); high algal concentration increases the probability of encounter, and thus a high coagulation efficiency, provided that cell stickiness is sufficiently high and the cells are sufficiently large.

Logan and Wilkinson (1990) used fractal geometry to test if colloidal aggregation mechanisms, well described for inorganic particles, were applicable to marine snow aggregates. They suggested that different types of aggregates form as a function of different particle stickiness and thus collision efficiencies. If the probability of sticking upon collision is high, cells will efficiently stick when they encounter and form highly porous and tenuous structures (diffusion–limited aggregation or DLA). In contrast, if several collisions are required, then more solid and compact aggregates are formed (reaction–limited aggregation or RLA). Meakin (1991) suggested that the processes forming marine aggregates are likely to correspond closely to the diffusion- and reaction–limited cluster–cluster aggregation mechanisms described for colloids. Aggregates formed through these 2 mechanisms may thus have distinct compactness affecting their sinking velocity.

To explore further the hypothesis that species–specific coagulation efficiencies were responsible for different aggregate compactness influencing the sinking velocity, we widened our morphological classification (type 1 and 2) to include the most and second most abundant phytoplankton genera in our samples (Table 3.2). Overall, 6 species dominated aggregate composition: *Chaetoceros* (*Hyalochaete*) spp., *Pseudo–nitzschia* spp., *Fragilariopsis* spp., *E. antarctica*, *Thalassionema nitzschioides* and small centrics. *Chaetoceros* (*Hyalochaete*) spp. was classified as type 2, along with *Pseudo–nitzschia* spp., (even though not producing setae) due to their morphology facilitating attachment upon collision; *Fragilariopsis* spp., *E. antarctica*, *T. nitzschioides* and small centric diatoms were classified as type 1. A strong linear relationship was found between the average proportion of phytoplankton cells of type 2 and the average sinking velocity recorded at each station (Fig. 3.9; Stn E–4E was considered an outlier, rejected at 95% confidence and excluded from the fit). In contrast to other aggregates, Stn E–4E particles contained a relatively large abundance of fecal pellets (Fig. 3.7D). Because fecal pellets are tightly packaged material formed by biological aggregation, this may have increased aggregate density and compactness and thus altered the relation between dominant phytoplankton types and aggregate sinking velocity. Certainly fecal pellets on their own are known to have high densities and sinking velocities (Fowler and Small, 1972; Small et al., 1979; Yoon et al., 2001).

This result emphasizes the complexity of controls on the sinking velocities of marine snow and the importance of ecological considerations, suggesting that controlling factors may vary at very small spatio–temporal scales.

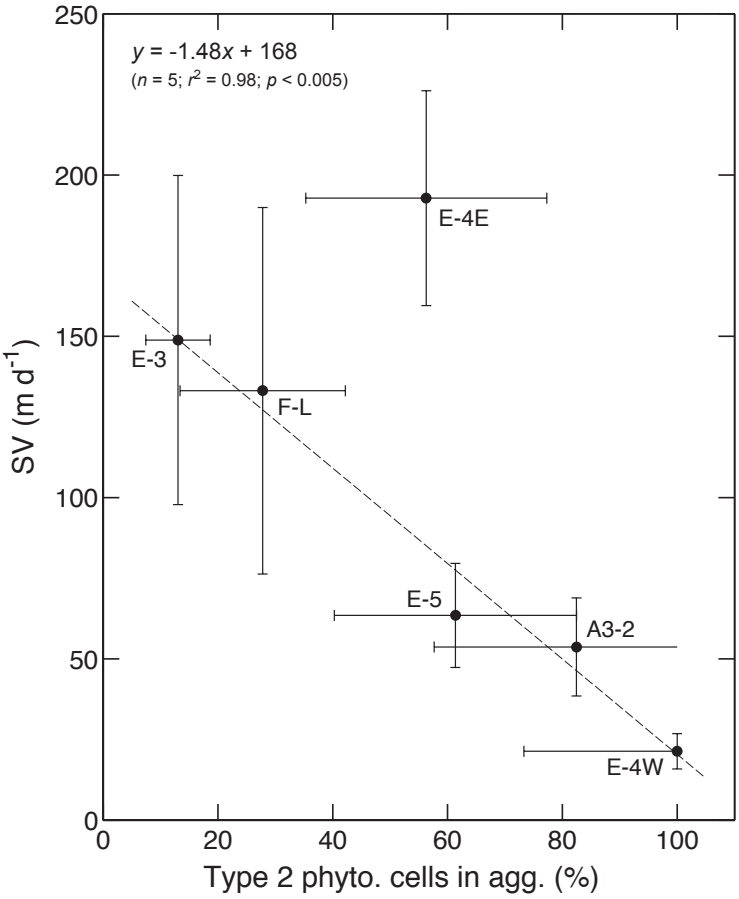

Figure 3.9: Relationship between the average sinking velocity (SV) of aggregates from each station and the average proportion of phytoplankton (phyto.) cells in aggregates that had a morphology facilitating attachment upon collision (type 2; see 'Discussion'). Stn E–4E was excluded from best fit line calculation. Error bars: 1 SD

The variations in the dominance of the 2 phytoplankton types appears to have some relationship to biomass levels at the different stations, and perhaps to the intensity of iron fertilization. For instance, Stns A3–2 and E–4W, where the genus *Chaetoceros* subgenus *Hyalochaete* was dominant, displayed high biomass — characteristic of bloom conditions — and are known to be under the influence of natural iron fertilization (Bowie et al., 2014; Quéroué et al., 2015; van der Merwe et al., 2014). Conversely, Stn E–3 was largely dominated by the ribbon–chain diatom *Fragilariopsis* spp. and was in a central region of moderate biomass with less iron enrichment.

Evaluating the generality of our results will require observations on aggregates across varying levels of total biomass and ecological community structure. When comparing these environ-

ments, it is important to note that phytoplankton community composition and total biomass can have somewhat independent effects on aggregate sinking velocities; i.e. even for setae–forming species, if biomass is sufficient for aggregation to continue until very large particles are formed, then high sinking velocities can still be obtained. This could explain the EIFEX iron fertilization experiment results, during which the setae–forming diatom *C. dichaeta* was abundant, and for which transmissometry profiles were interpreted as representing cm–sized aggregates sinking at rates >500 m d^{-1} (Smetacek et al., 2012). These results are compatible with the perspectives developed here, to the extent that the very large size of the aggregates could have outweighed the expectation of low sinking velocities for aggregates formed from this species. Without any direct observations on either the aggregates or their sinking velocities during EIFEX, it is of course possible that other factors were at play, such as the myriad of influences on sinking velocities as summarized in the introduction, and the diverse nature of deep ocean particles, including living organisms (Silver and Gowing, 1991).

From a cautionary perspective, this study emphasizes that predictions of marine snow sinking velocity should not be based only on size parameterizations, and certainly should not assume that sinking velocities will always increase with size. Further studies may eventually identify those phytoplankton types which are most readily assembled into rapid sinking aggregates, by either physical or biological aggregation, as a path towards greater predictability of carbon export and biological pump efficiencies.

Acknowledgments

This work received support from the Australian Commonwealth Cooperative Research Centres Program to the ACE CRC, and the Australian National Network in Marine Science via UTAS IMAS. We thank the personnel of the RV 'Marion Dufresne', Institut Paul Emile Victor, Institut National des Sciences de l'Univers, and the KEOPS2 voyage leader Bernard Quéguiner and KEOPS2 science team for assistance at sea. Stephen Bray (ACE CRC), Peter Jansen (IMOS), and David Cherry (CSIRO) prepared the free–drifting sediment trap arrays. The MODIS (NASA) satellite ocean–colour image is courtesy of Francesco d'Ovidio (Univ. Paris). The altimeter and colour/temperature products for the Kerguelen area were produced by Ssalto/Duacs and CLS with support from CNES. We thank Simon Wotherspoon (IMAS) for his precious insights into statistical analysis.

References

Abramoff, M. D., Magelhaes, P. J., and Ram, S. J.: Image Processing with ImageJ, Biophotonics International, 11, 36–42, 2004.

Achenbach, E.: Effects of surface roughness and tunnel blockage on the flow past spheres, Journal of fluid mechanics, 65, 113–125, doi:10.1017/S0022112074001285, 1974.

Alldredge, A. L.: The carbon, nitrogen and mass content of marine snow as a function of aggregate size, Deep Sea Research Part I: Oceanographic Research Papers, 45, 529 – 541, doi:10.1016/S0967-0637(97)00048-4, 1998.

Alldredge, A. L. and Gotschalk, C.: In Situ Settling Behavior of Marine Snow, Limnology and Oceanography, 33, 339–351, doi:10.2307/2837008, 1988.

Alldredge, A. L. and Gotschalk, C. C.: Direct observations of the mass flocculation of diatom blooms: characteristics, settling velocities and formation of diatom aggregates, Deep Sea Research Part A. Oceanographic Research Papers, 36, 159–171, doi:10.1016/0198-0149(89)90131-3, 1989.

Alldredge, A. L. and Gotschalk, C. C.: The relative contribution of marine snow of different origins to biological processes in coastal waters, Continental Shelf Research, 10, 41–58, doi:10.1016/0278-4343(90)90034-J, 1990.

Alldredge, A. L. and Silver, M. W.: Characteristics, dynamics and significance of marine snow, Progress in Oceanography, 20, 41–82, doi:10.1016/0079-6611(88)90053-5, 1988.

Alldredge, A. L., Gotschalk, C., Passow, U., and Riebesell, U.: Mass aggregation of diatom blooms: insights from a mesocosm study, Deep-Sea Research Part II: Topical Studies in Oceanography, 42, 9–27, doi:10.1016/0967-0645(95)00002-8, 1995.

Anderson, L. A.: On the hydrogen and oxygen content of marine phytoplankton, Deep Sea Research Part I: Oceanographic Research Papers, 42, 1675–1680, doi:10.1016/0967-0637(95)00072-E, 1995.

Armstrong, R. A., Lee, C., Hedges, J. I., Honjo, S., and Wakeham, S. G.: A new, mechanistic model for organic carbon fluxes in the ocean based on the quantitative association of POC with ballast minerals, Deep-Sea Research Part II: Topical Studies in Oceanography, 49, 219–236, doi:10.1016/S0967-0645(01)00101-1, 2001.

Asper, V. L., Deuser, W. G., Knauer, G. A., and Lohrenz, S. E.: Rapid coupling of sinking particle fluxes between surface and deep ocean waters, Nature, 357, 670–672, doi:10.1038/357670a0, 1992.

Azetsu-Scott, K. and Passow, U.: Ascending marine particles: Significance of transparent exopolymer particles (TEP) in the upper ocean, Limnology and Oceanography, 49, 741–748, doi:10.2307/3597791, 2004.

Baba, J. and Komar, P.: Settling velocities of irregular grains at low Reynolds numbers, Journal of Sedimentary Research, 51, 121–128, 1981.

Batchelor, G.: An introduction to fluid dynamics, Cambridge University Press, The Edinburg Building, Cambridge, United Kingdom, 1967.

Bienfang, P. K., Harrison, P. J., and Quarmby, L. M.: Sinking rate response to depletion of nitrate, phosphate and silicate in four marine diatoms, Marine Biology, 67, 295–302, doi: 10.1007/BF00397670, 1982.

Blain, S., Quéguiner, B., Armand, L., Belviso, S., Bombled, B., Bopp, L., Bowie, A., Brunet, C., Brussaard, C., Carlotti, F., Christaki, U., Corbière, A., Durand, I., Ebersbach, F., Fuda, J. L., Garcia, N., Gerringa, L., Griffiths, B., Guigue, C., Guillerm, C., Jacquet, S., Jeandel, C., Laan, P., Lefèvre, D., Lo Monaco, C., Malits, A., Mosseri, J., Obernosterer, I., Park, Y. H., Picheral, M., Pondaven, P., Remenyi, T., Sandroni, V., Sarthou, G., Savoye, N., Scouarnec, L., Souhaut, M., Thuiller, D., Timmermans, K., Trull, T., Uitz, J., van Beek, P., Veldhuis, M., Vincent, D., Viollier, E., Vong, L., and Wagener, T.: Effect of natural iron fertilization on carbon sequestration in the Southern Ocean, Nature, 446, 1070–1074, doi:10.1038/nature05700, 2007.

Bowie, A. R., van der Merwe, P., Quéroué, F., Trull, T., Fourquez, M., Planchon, F., Sarthou, G., Chever, F., Townsend, A. T., Obernosterer, I., Sallée, J.-B., and Blain, S.: Iron budgets for three distinct biogeochemical sites around the Kerguelen archipelago (Southern Ocean) during the natural fertilisation experiment KEOPS-2, Biogeosciences Discussions, 11, 17 861–17 923, doi:10.5194/bgd-11-17861-2014, 2014.

Boyd, P. and Newton, P.: Evidence of the potential influence of planktonic community structure on the interannual variability of particulate organic carbon flux, Deep Sea Research Part I: Oceanographic Research Papers, 42, 619–639, doi:10.1016/0967-0637(95)00017-Z, 1995.

Boyd, P. W., Sherry, N. D., Berges, J. A., Bishop, J. K. B., Calvert, S. E., Charette, M. A., Giovannoni, S. J., Goldblatt, R., Harrison, P. J., Moran, S. B., Roy, S., Soon, M., Strom, S., Thibault, D., Vergin, K. L., Whitney, F. A., and Wong, C. S.: Transformations of biogenic particulates from the pelagic to the deep ocean realm, Deep Sea Research Part II: Topical Studies in Oceanography, 46, 2761–2792, doi:10.1016/S0967-0645(99)00083-1, 1999.

Buesseler, K. O.: The decoupling of production and particulate export in the surface ocean, Global Biogeochemical Cycles, 12, 297–310, doi:10.1029/97GB03366, 1998.

Burd, A. B. and Jackson, G. A.: Particle Aggregation, Annual Review of Marine Science, 1, 65–90, doi:10.1146/annurev.marine.010908.163904, 2009.

Chhabra, R. P.: Wall effects on free-settling velocity of non-spherical particles in viscous media in cylindrical tubes, Powder Technology, 85, 83–90, doi:10.1016/0032-5910(95)03012-X, 1995.

Corey, A.: Influence of shape on the fall velocity of sand grains, Master's thesis, Colorado A & M College, Fort Collins, Colorado, USA, 1949.

Crocker, K. M. and Passow, U.: Differential aggregation of diatoms, Marine Ecology Progress Series, 117, 249–257, doi:10.3354/meps117249, 1995.

Dam, H. G. and Drapeau, D. T.: Coagulation efficiency, organic-matter glues and the dynamics of particles during a phytoplankton bloom in a mesocosm study, Deep-Sea Research Part II: Topical Studies in Oceanography, 42, 111–123, doi:10.1016/0967-0645(95)00007-D, 1995.

de Baar, H. J. W., de Jong, J. T. M., Bakker, D. C. E., Loscher, B. M., Veth, C., Bathmann, U., and Smetacek, V.: Importance of iron for plankton blooms and carbon dioxide drawdown in the Southern Ocean, Nature, 373, 412–415, doi:10.1038/373412a0, 1995.

De La Rocha, C. L. and Passow, U.: Factors influencing the sinking of POC and the efficiency of the biological carbon pump, Deep Sea Research Part II: Topical Studies in Oceanography, 54, 639–658, doi:10.1016/j.dsr2.2007.01.004, 2007.

Diercks, A.-R. and Asper, V. L.: In situ settling speeds of marine snow aggregates below the mixed layer: Black Sea and Gulf of Mexico, Deep Sea Research Part I: Oceanographic Research Papers, 44, 385–398, doi:10.1016/S0967-0637(96)00104-5, 1997.

Dietrich, W. E.: Settling velocity of natural particles, Water Resources Research, 18, 1615–1626, doi:10.1029/WR018i006p01615, 1982.

Ebersbach, F. and Trull, T. W.: Sinking particle properties from polyacrylamide gels during the KErguelen Ocean and Plateau compared Study (KEOPS): Zooplankton control of carbon export in an area of persistent natural iron inputs in the Southern Ocean, Limnology and Oceanography, 53, 212–224, doi:10.2307/40006162, 2008.

Engel, A. and Schartau, M.: Influence of transparent exopolymer particles (TEP) on sinking velocity of Nitzschia closterium aggregates, Marine Ecology Progress Series, 182, 69–76, doi:10.3354/meps182069, 1999.

Engel, A., Szlosek, J., Abramson, L., Liu, Z., and Lee, C.: Investigating the effect of ballasting by CaCO3 in Emiliania huxleyi: I. Formation, settling velocities and physical properties of aggregates, Deep Sea Research Part II: Topical Studies in Oceanography, 56, 1396–1407, doi:10.1016/j.dsr2.2008.11.027, 2009.

Fowler, S. W. and Knauer, G. A.: Role of large particles in the transport of elements and organic compounds through the oceanic water column, Progress in Oceanography, 16, 147–194, doi:10.1016/0079-6611(86)90032-7, 1986.

Fowler, S. W. and Small, L. F.: Sinking rates of euphausiid fecal pellets, Limnology and Oceanography, 17, 293–296, doi:10.1016/0079-6611(86)90032-7, 1972.

Gehlen, M., Bopp, L., Emprin, N., Aumont, O., Heinze, C., Ragueneau, O., et al.: Reconciling surface ocean productivity, export fluxes and sediment composition in a global biogeochemical ocean model, Biogeosciences, 3, 521–537, doi:10.5194/bg-3-521-2006, 2006.

Gibbs, R. J.: Estuarine flocs: Their size, settling velocity and density, Journal of Geophysical Research: Oceans, 90, 3249–3251, doi:10.1029/JC090iC02p03249, 1985.

Graf, W. and Acaroglu, E.: Settling velocities of natural grains, Hydrological Sciences Journal, 11, 27–43, 1966.

Guidi, L., Jackson, G. A., Stemmann, L., Miquel, J. C., Picheral, M., and Gorsky, G.: Relationship between particle size distribution and flux in the mesopelagic zone, Deep Sea Research Part I: Oceanographic Research Papers, 55, 1364–1374, doi:10.1016/j.dsr.2008.05.014, 2008.

Iversen, M. H. and Ploug, H.: Ballast minerals and the sinking carbon flux in the ocean: carbon-specific respiration rates and sinking velocity of marine snow aggregates, Biogeosciences, 7, 2613–2624, doi:10.5194/bg-7-2613-2010, 2010.

Jackson, G.: Using fractal scaling and two-dimensional particle size spectra to calculate coagulation rates for heterogeneous systems, Journal of colloid and interface science, 202, 20–29, 1998.

Jackson, G. A.: A model of the formation of marine algal flocs by physical coagulation processes, Deep-Sea Research Part I: Oceanographic Research Papers, 37, 1197–1211, doi: 10.1016/0198-0149(90)90038-W, 1990.

Jackson, G. A.: Particle trajectories in a rotating cylinder: implications for aggregation incubations, Deep-Sea Research Part I: Oceanographic Research Papers, 41, 429–437, doi: 10.1016/0967-0637(94)90089-2, 1994.

Jackson, G. A.: TEP and coagulation during a mesocosm experiment, Deep-Sea Research Part II: Topical Studies in Oceanography, 42, 215–222, doi:10.1016/0967-0645(95)00015-I, 1995.

Jannasch, H. W., Zafiriou, O. C., and Farrington, J. W.: A sequencing sediment trap for time-series studies of fragile particles, Limnology and Oceanography, 25, 939–3590, doi:10.4319/lo.1980.25.5.0939, 1980.

Johnson, C. P., Li, X., and Logan, B. E.: Settling velocities of fractal aggregates, Environmental Science & Technology, 30, 1911–1918, doi:10.1021/es950604g, 1996.

Jouandet, M.-P., Trull, T. W., Guidi, L., Picheral, M., Ebersbach, F., Stemmann, L., and Blain, S.: Optical imaging of mesopelagic particles indicates deep carbon flux beneath a natural iron-fertilized bloom in the Southern Ocean, Limnology and Oceanography, 56, 1130–1140, doi:10.4319/lo.2011.56.3.1130, 2011.

Kajihara, M.: Settling velocity and porosity of large suspended particle, Journal of the Oceanographical Society of Japan, 27, 158–162, doi:10.1007/BF02109135, 1971.

Karl, D. M., Knauer, G. A., and Martin, J. H.: Downward flux of particulate organic matter in the ocean: a particle decomposition paradox, Nature, 332, 438–441, doi:10.1038/332438a0, 1988.

Kilps, J. R., Logan, B. E., and Alldredge, A. L.: Fractal dimensions of marine snow determined from image analysis of in situ photographs, Deep Sea Research Part I: Oceanographic Research Papers, 41, 1159–1169, doi:10.1016/0967-0637(94)90038-8, 1994.

Kiorboe, T. and Hansen, J. L. S.: Phytoplankton aggregate formation: observations of patterns and mechanisms of cell sticking and the significance of exopolymeric material, Journal of Plankton Research, 15, 993–1018, doi:10.1093/plankt/15.9.993, 1993.

Kiorboe, T., Andersen, K., and Dam, H.: Coagulation efficiency and aggregate formation in marine phytoplankton, Marine Biology, 107, 235–245, doi:10.1007/BF01319822, 1990.

Klaas, C. and Archer, D. E.: Association of sinking organic matter with various types of mineral ballast in the deep sea: Implications for the rain ratio, Global Biogeochemical Cycles, 16, 1116, doi:10.1029/2001GB001765, 2002.

Komar, P. and Reimers, C.: Grain shape effects on settling rates, The Journal of Geology, pp. 193–209, 1978.

Kriest, I. and Oschlies, A.: On the treatment of particulate organic matter sinking in large-scale models of marine biogeochemical cycles, Biogeosciences, 5, 55–72, doi:10.5194/bg-5-55-2008, 2008.

Kriest, I. and Oschlies, A.: Swept under the carpet: organic matter burial decreases global ocean biogeochemical model sensitivity to remineralization length scale, Biogeosciences, 10, 8401–8422, doi:10.5194/bg-10-8401-2013, 2013.

Laurenceau-Cornec, E. C., Trull, T. W., Davies, D. M., Bray, S. G., Doran, J., Planchon, F., Carlotti, F., Jouandet, M.-P., Cavagna, A.-J., Waite, A. M., and Blain, S.: The relative importance of phytoplankton aggregates and zooplankton fecal pellets to carbon export: insights from free-drifting sediment trap deployments in naturally iron-fertilised waters near the Kerguelen Plateau, Biogeosciences, 12, 1007–1027, doi:10.5194/bg-12-1007-2015, 2015b.

Li, X.-Y. and Logan, B. E.: Permeability of Fractal Aggregates, Water Research, 35, 3373–3380, doi:10.1016/S0043-1354(01)00061-6, 2001.

Li, X.-Y. and Yuan, Y.: Settling velocities and permeabilities of microbial aggregates, Water Research, 36, 3110–3120, doi:10.1016/S0043-1354(01)00541-3, 2002.

Logan, B. E. and Wilkinson, D. B.: Fractal geometry of marine snow and other biological aggregates, Limnology and Oceanography, 35, 130–136, doi:10.2307/2837345, 1990.

Losch, M., Strass, V., Cisewski, B., Klaas, C., and Bellerby, R. G. J.: Ocean state estimation from hydrography and velocity observations during EIFEX with a regional biogeochemical ocean circulation model, Journal of Marine Systems, 129, 437–451, doi:10.1016/j.jmarsys.2013.09.003, 2014.

Martin, J. H.: Glacial-interglacial CO_2 change: The iron hypothesis, Paleoceanography, 5, 1–13, doi:10.1029/PA005i001p00001, 1990.

Martin, J. H., Knauer, G. A., Karl, D. M., and Broenkow, W. W.: VERTEX: carbon cycling in the northeast Pacific, Deep Sea Research Part A. Oceanographic Research Papers, 34, 267–285, doi:10.1016/0198-0149(87)90086-0, 1987.

Martin, P., Lampitt, R. S., Jane Perry, M., Sanders, R., Lee, C., and D'Asaro, E.: Export and mesopelagic particle flux during a North Atlantic spring diatom bloom, Deep Sea Research Part I: Oceanographic Research Papers, 58, 338–349, doi:10.1016/j.dsr.2011.01.006, 2011.

Matsumoto, K. and Suganuma, A.: Settling velocity of a permeable model floc, Chemical Engineering Science, 32, 445–447, doi:10.1016/0009-2509(77)85009-4, 1977.

McCave, I. N.: Size spectra and aggregation of suspended particles in the deep ocean, Deep Sea Research Part A. Oceanographic Research Papers, 31, 329–352, doi:10.1016/0198-0149(84)90088-8, 1984.

McNown, J. S. and Malaika, J.: Effects of particle shape on settling velocity at low Reynolds numbers, Trans. Am. Geophys. Union, 31, 74–82, 1950.

Meakin, P.: Fractal aggregates in geophysics, Reviews of Geophysics, 29, 317–354, doi:10.1029/91RG00688, 1991.

Miklasz, K. and Denny, M.: Diatom sinking speeds: improved predictions and insight from a modified Stokes' law, Limnology and oceanography, 55, 2513–2525, doi:10.4319/lo.2010.55.6.2513, 2010.

Muggli, D. L., Lecourt, M., and Harrison, P. J.: Effects of iron and nitrogen source on the sinking rate, physiology and metal composition of an oceanic diatom from the subarctic Pacific, Marine Ecology Progress Series, 132, 215–227, doi:10.3354/meps132215, 1996.

Padisák, J., Soróczki-Pintér, É., and Rezner, Z.: Sinking properties of some phytoplankton shapes and the relation of form resistance to morphological diversity of plankton—an experimental study, Hydrobiologia, 500, 243–257, doi:10.1023/A:1024613001147, 2003.

Passow, U.: Species-specific sedimentation and sinking velocities of diatoms, Marine Biology, 108, 449–455, doi:10.1007/BF01313655, 1991.

Passow, U.: The abiotic formation of TEP under different ocean acidification scenarios, Marine Chemistry, 128-129, 72–80, doi:10.1016/j.marchem.2011.10.004, 2012.

Passow, U. and Alldredge, A. L.: A dye-binding assay for the spectrophotometric measurement of transparent exopolymer particles (TEP), Limnology and Oceanography, 40, 1326–1335, doi:10.2307/2838691, 1995.

Passow, U. and De La Rocha, C. L.: Accumulation of mineral ballast on organic aggregates, Global Biogeochemical Cycles, 20, GB1013, doi:10.1029/2005gb002579, 2006.

Ploug, H., Iversen, M. H., and Fischer, G.: Ballast, sinking velocity, and apparent diffusivity within marine snow and zooplankton fecal pellets: Implications for substrate turnover by attached bacteria, Limnology and Oceanography, 53, 1878–1886, doi:10.4319/lo.2008.53.5.1878, 2008.

Ploug, H., Terbruggen, A., Kaufmann, A., Wolf-Gladrow, D., and Passow, U.: A novel method to measure particle sinking velocity in vitro, and its comparison to three other in vitro methods, Limnology and Oceanography: Methods, 8, 386–393, doi:10.4319/lom.2010.8.386, 2010.

Quéroué, F., Sarthou, G., Planquette, H. F., Bucciarelli, E., Chever, F., van der Merwe, P., Lannuzel, D., Townsend, A. T., Cheize, M., Blain, S., d'Ovidio, F., and Bowie, A. R.: High variability of dissolved iron concentrations in the vicinity of Kerguelen Island (Southern Ocean), Biogeosciences Discussions, 12, 231–270, doi:10.5194/bgd-12-231-2015, 2015.

Ragueneau, O., Savoye, N., Del Amo, Y., Cotten, J., Tardiveau, B., and Leynaert, A.: A new method for the measurement of biogenic silica in suspended matter of coastal waters: using Si:Al ratios to correct for the mineral interference, Continental Shelf Research, 25, 697–710, doi:10.1016/j.csr.2004.09.017, 2005.

Reynolds, O.: An Experimental Investigation of the Circumstances Which Determine Whether the Motion of Water Shall Be Direct or Sinuous, and of the Law of Resistance in Parallel Channels, Philosophical Transactions of the Royal Society of London, 174, 935–982, 1883.

Savoye, N., Trull, T. W., Jacquet, S. H. M., Navez, J., and Dehairs, F.: ^{234}Th-based export fluxes during a natural iron fertilization experiment in the Southern Ocean (KEOPS), Deep Sea Research Part II: Topical Studies in Oceanography, 55, 841–855, doi:10.1016/j.dsr2.2007.12.036, 2008.

Shanks, A. L. and Edmondson, E. W.: Laboratory-made artificial marine snow: a biological model of the real thing, Marine Biology, 101, 463–470, doi:10.1007/BF00541648, 1989.

Sigman, D. M. and Boyle, E. A.: Glacial/interglacial variations in atmospheric carbon dioxide, Nature, 407, 859–869, doi:10.1038/35038000, 2000.

Silver, M. W. and Gowing, M. M.: The"Particle" Flux: Origins and biological components, Progress in Oceanography, 26, 75–113, doi:10.1016/0079-6611(91)90007-9, 1991.

Small, L. F., Fowler, S. W., and Ünlü, M. Y.: Sinking rates of natural copepod fecal pellets, Marine Biology, 51, 233–241, doi:10.1007/BF00386803, 1979.

Smetacek, V., Klaas, C., Strass, V. H., Assmy, P., Montresor, M., Cisewski, B., Savoye, N., Webb, A., d'Ovidio, F., Arrieta, J. M., Bathmann, U., Bellerby, R., Berg, G. M., Croot, P., Gonzalez, S., Henjes, J., Herndl, G. J., Hoffmann, L. J., Leach, H., Losch, M., Mills, M. M., Neill, C., Peeken, I., Rottgers, R., Sachs, O., Sauter, E., Schmidt, M. M., Schwarz, J., Terbruggen, A., and Wolf-Gladrow, D.: Deep carbon export from a Southern Ocean iron-fertilized diatom bloom, Nature, 487, 313–319, doi:10.1038/nature11229, 2012.

Stemmann, L., Jackson, G., and Gorsky, G.: A vertical model of particle size distributions and fluxes in the midwater column that includes biological and physical processes—Part II: application to a three year survey in the NW Mediterranean Sea, Deep Sea Research Part I: Oceanographic Research Papers, 51, 885–908, doi:10.1016/j.dsr.2004.03.002, 2004.

Stokes, G. G.: On the effect of the internal friction of fluids on the motion of pendulums, Transactions of the Cambridge Philosophical Society, 9, 8–106, 1851.

Suess, E.: Particulate organic carbon flux in the oceans—surface productivity and oxygen utilization, Nature, 288, 260–263, doi:10.1038/288260a0, 1980.

Sullivan, C. W., Arrigo, K. R., McClain, C. R., Comiso, J. C., and Firestone, J.: Distributions of Phytoplankton Blooms in the Southern Ocean, Science, 262, 1832–1837, doi:10.1126/science.262.5141.1832, 1993.

Thornton, D. C. O.: Diatom aggregation in the sea: mechanisms and ecological implications, European Journal of Phycology, 37, 149–161, doi:10.1017/s0967026202003657, 2002.

van der Merwe, P., Bowie, A. R., Quéroué, F., Armand, L., Blain, S., Chever, F., Davies, D., Dehairs, F., Planchon, F., Sarthou, G., Townsend, A. T., and Trull, T.: Sourcing the iron in the naturally-fertilised bloom around the Kerguelen Plateau: particulate trace metal dynamics, Biogeosciences Discussions, 11, 13 389–13 432, doi:10.5194/bgd-11-13389-2014, 2014.

Volk, T. and Hoffert, M. I.: Ocean carbon pumps: Analysis of relative strengths and efficiencies in ocean-driven atmospheric CO_2 changes, in: The Carbon Cycle and Atmospheric CO_2: Natural Variations Archean to Present, vol. 32, pp. 99–110, AGU, Washington, DC, 1985.

Waite, A., Fisher, A., Thompson, P. A., and Harrison, P. J.: Sinking rate versus cell volume relationships illuminate sinking rate control mechanisms in marine diatoms, Marine Ecology Progress Series, 157, 97–108, doi:10.3354/meps157097, 1997a.

Waite, A., Gallager, S., and Dam, H.: New measurements of phytoplankton aggregation in a flocculator using videography and image analysis, Marine Ecology Progress Series, 155, 77–88, doi:10.3354/meps155077, 1997b.

Waite, A. M., Thompson, P. A., and Harrison, P. J.: Does energy control the sinking rates of marine diatoms?, Limnology and Oceanography, 37, 468–477, doi:10.2307/2837978, 1992.

White, F.: Viscous fluid flow, McGraw-Hill, New York, 1974.

Williams, G. P.: Particle roundness and surface texture effects on fall velocity, Journal of Sedimentary Research, 36, 255–259, 1966.

Yoon, W., Kim, S., and Han, K.: Morphology and sinking velocities of fecal pellets of copepod, molluscan, euphausiid, and salp taxa in the northeastern tropical Atlantic, Marine Biology, 139, 923–928, doi:10.1007/s002270100630, 2001.

Chapter 4

Carbon export efficiency modulation by plankton communities in the Southern Ocean: results from a coupled physical–biogeochemical model

A manuscript based on this chapter is in preparation for submission to Global Biogeochemical Cycles.

Emmanuel C. Laurenceau–Cornec[1,2,3], Mathieu Mongin[3], Philip W. Boyd[1], Thomas W. Trull[2,3]

[1]Institute for Marine and Antarctic Studies, University of Tasmania, Private Bag 129, Hobart, Tasmania 7001, Australia

[2]Antarctic Climate and Ecosystems Cooperative Research Centre, University of Tasmania, Private Bag 80, Hobart, Tasmania 7001, Australia

[3]Commonwealth Scientific and Industrial Research Organisation, Marine and Atmospheric Research, Castray Esplanade, Hobart, Tasmania 7000, Australia

4.1 Introduction

The fifth assessment report from the Intergovernmental Panel on Climate Change (IPCC) linked with an unprecedented level of confidence the accelerated increase of atmospheric pCO_2 to anthropogenic activities since the pre–industrial era (IPCC, 2014). The report qualified this increase as *extremely likely* (95–100% likelihood) to be responsible for more than half of the observed increase in global mean surface temperature from 1951 to 2010 (Bindoff et al., 2013). The global ocean moderates this dangerous increase by absorbing about 2.0 ± 1.0 Gt of atmospheric carbon dioxide each year (Takahashi et al., 2009). Estimates suggest that this oceanic carbon pump stores approximately one–third of the total annual anthropogenic emissions (Sabine et al., 2004), with about half of it taken up by the Southern Ocean alone, south of 30°S (Takahashi et al., 2012).

The total oceanic carbon pump includes physically- (termed 'solubility pump') and biologically–mediated processes. The Biological Carbon Pump (BCP) represents the biologically–mediated processes responsible for the downward transfer of organic carbon produced in the well–lit surface ocean to the deep layers via the sinking of organic particles, and its eventual sequestration for geological time scales (Lam et al., 2011; Volk and Hoffert, 1985). Estimations suggest that the BCP could be responsible for approximately two–thirds of the global oceanic carbon pump but large uncertainties remain on the relative contributions of the physical and biological components of the pump (Gruber and Sarmiento, 2002; Passow and Carlson, 2012; Reid et al., 2009). Climate change is expected to alter the efficiency of the BCP (Bopp et al., 2013; Le Quéré et al., 2009; Passow and Carlson, 2012; Turner, 2015) and the largely unknown modes and consequences of this alteration, possibly exacerbating the rate of climate change, are crucial issues that need to be addressed urgently. For these reasons, major research efforts have been placed on understanding its controlling factors, and especially in the Southern Ocean.

The efficiency of the BCP can be expressed as the fraction of the total carbon fixed by photosynthesis in the surface ocean that is exported out of the euphotic zone (E_Z). It has also been defined as the amplitude of the nutrient depletion that the BCP creates in the surface ocean (Sarmiento and Gruber, 2006). Wide variations in carbon export efficiency (over approximately one order of magnitude) occur at large and short spatio–temporal scales (Buesseler, 1998; De La Rocha and Passow, 2007; Henson et al., 2015; Honjo et al., 2008; Neuer et al.,

2002), and no clear consensus has been found to explain such variations. The efficiency of the BCP is expected to be related to surface productivity, but relevant studies conducted in varying ecological conditions (framed by the spatio–temporal context), reported discrepancies between surface production and related carbon export flux, leading to either positive, negative or lack of correlations between surface production and associated export efficiency (Betzer et al., 1984; Buesseler, 1998; Cavan et al., 2015; Dunne et al., 2005; Laws et al., 2000; Maiti et al., 2013; Pace et al., 1987; Suess, 1980; Wassmann, 1990). Many possible explanations have been suggested in these studies and others, including variations in planktonic communities, food web structure, grazing intensity, bacterial activity and potential importance of phytoplankton resting stages as vectors of carbon to depth (Buesseler and Boyd, 2009; Giering et al., 2014; Salter et al., 2012; Wassmann, 1998). The important role of planktonic communities in export processes has been suspected since the 1990's, and extensively studied since then (Boyd and Newton, 1995; Boyd et al., 1999; Guidi et al., 2009; Richardson and Jackson, 2007). However, the exact modes of the leverage that planktonic community structure exerts on export efficiency still remain unclear.

More recently, observed variations of exported particle types have been related to variations of planktonic community structure and trophic relationships. The suspected influence of plankton communities on carbon export efficiency has been explained through the control that trophic structure could exert on the relative fractions of sinking particle and their varying properties leading to differing abilities to export carbon (Ebersbach and Trull, 2008; Ebersbach et al., 2011; Laurenceau-Cornec et al., 2015b; Wiedmann et al., 2014) (Chapter 2). The two main modes of carbon export are: (i) direct, through the physical aggregation of phytoplankton cells and their subsequent sinking in the form of large phytodetrital aggregates, and (ii) through biological aggregation of grazed phytoplankton cells and their sinking in the form of dense zooplankton fecal pellets (Turner, 2015, and references therein). The efficiency of sinking particles to export carbon rely mainly on their sinking velocities (SV) which control the duration of exposure to remineralisation processes (Boyd et al., 1999; Karl et al., 1988; Martin et al., 1987). Parameterisation of sinking velocity used to estimate carbon fluxes in most biogeochemical models, assumes either constant values or scaled on size, excess density and/or depth based on empirical relationships (Baird and Emsley, 1999; Boyd and Stevens, 2002; Gehlen et al., 2006; Kriest and Evans, 1999; Kriest and Oschlies, 2008, 2013; Losch et al., 2014; Pasquer et al., 2005). However,

recent work has shown that size is not always the main controlling factor of the sinking velocity. For instance, phytoplankton morphological types (e.g. with or without spines), through their influence on particle formation and structure may indirectly control large phytodetrital aggregate sinking velocities (Iversen and Ploug, 2010; Laurenceau-Cornec et al., 2015a) (Chapter 3). Based on this, the observed variations between net primary productivity (NPP) and associated carbon export flux could be related to phytoplanktonic community composition via their influence on the nature of the detrital particles produced by the ecosystem. Here we explore the degree of coupling between ecosystem structure and carbon export by focusing on the composition of the detritus produced by plankton communities. More specifically we test the hypothesis that changes in the composition of detritus, closely related to seasonal shifts of surface plankton communities, leads to significant modification of detritus sinking velocities and subsequent alteration of the efficiency, amplitude and timing of carbon export.

To explore the possible influence of different planktonic community structure on the efficiency of carbon export, a complex three–dimensional (3–D) coupled physical–biogeochemical (BGC) model was used. Spatio–temporal variations of planktonic community compositions were obtained by forcing the BGC module with meteorological and physical data from the Southern Ocean Time Series (SOTS) site where an extensive database is available (see Section 'Model Description'). The SOTS site in the Sub–Antarctic Zone (SAZ) has seasonal cycles similar to the region north of the polar front (PF) over the Kerguelen Plateau. Within this physical framework, biogeochemical features characteristic to the Kerguelen Plateau area were used in the initial conditions of the model (e.g. nutrient profiles). The initial model with a constant detritus sinking velocity was modified to incorporate variable sinking velocities. Specifically, detritus sinking velocities were calculated from the relative contributions of small and large phytoplankton and zooplankton fluxes to the detritus pool. The detritus sinking velocity was then calculated at each time step integrating all spatio–temporal changes of plankton communities. This resulted in 4–D variations of the detritus sinking velocity with latitude, longitude, depth and time, which allowed exploration of how small variations of planktonic community structure affect carbon export efficiency.

4.2 Model description

The physical and biogeochemical modules are parts of the Ecosystem Modelling Suite (EMS) developed by the Environmental Modelling group at CSIRO (Commonwealth Scientific and Industrial Research Organisation, Australia), division of Marine and Atmospheric Research (CMAR). A short description of the model is made here in the context of our study, but more details on the different modules of the EMS can be found at:
http://www.emg.cmar.csiro.au/www/en/emg/software/EMS.html.

A 3–D coupled physical–BGC model was needed here to simulate complex variations of plankton communities over space and time controlled by trophic interactions. The BGC module is a widely used generic model of plankton ecosystem dynamics. Most of the parameterisation was done to allow alternative modes of carbon export (direct or through the trophic chain) depending on planktonic community composition. The introduction of a variable sinking velocity based on detritus composition was used as a simple tool to closely link planktonic community variations to carbon export efficiency. The relationship used constrained the detritus dominated by small phytoplankton, large phytoplankton or zooplankton fecal material, to sink at variable velocities accounting for the relative contributions of these different components to the detritus pool.

4.2.1 The physical module: SHOC

The physical module is the Sparse Hydrodynamic Ocean Code (SHOC). It is a finite difference hydrodynamic model resolving water velocity, temperature, salinity, density, passive tracers, mixing coefficients and sea level over three dimensions. The model is driven by inputs of winds, atmospheric pressure gradients, surface heat and water fluxes and has open boundary conditions. Here, SHOC was run for 9 years (2002 to 2011), at the SOTS area southwest of Tasmania, near 140°E, 47°S (Figure 4.1). In this area an extensive physical dataset at high temporal resolution is provided by mooring facilities operated through the Integrated Marine Observing System (IMOS) (Trull et al., 2010). SHOC boundaries were defined by nesting the model in version 3 of the eddy–resolving Bluelink Ocean ReANalysis (BRAN3) model, which resolves three-dimensional time–varying circulation in the Australian sector of the Southern Ocean (Oke et al., 2013). SHOC output are structured in latitude × longitude grids of 20 × 20 cells, and over 30

depths from 1 to 1110 m. It provides horizontal resolution of 0.11° longitude and 0.08° latitude. Vertical resolution decreases exponentially with depth (19 m between the two shallowest cells compared to 135 m between the two deepest cells).

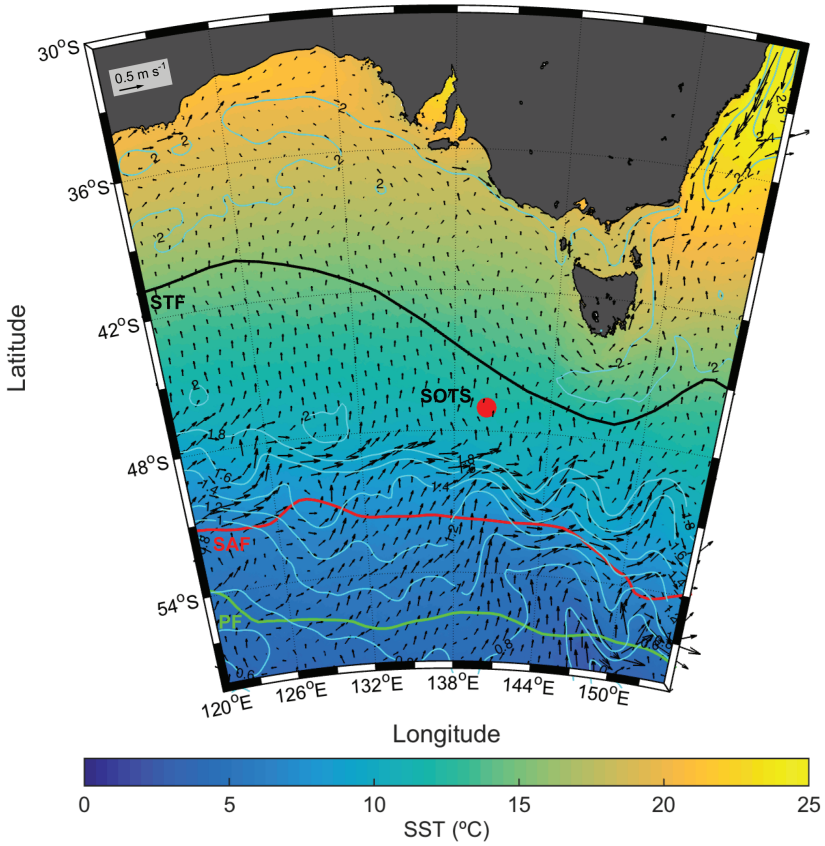

Figure 4.1: Location of the Southern Ocean Time Series (SOTS) region on a map of the summer (Dec. – Mar.) mean Sea Surface Temperature (SST) from the MODIS Aqua satellite (NASA), for the years 2002 to 2011. Surface geostrophic velocities (arrows) derived from sea surface height (m; light blue contours) are represented for the period January 2002 to January 2011 [data from the Integrated Marine Observing System (IMOS)]. Main Southern Ocean fronts based on Orsi et al. (1995), are also indicated. STF: Sub–tropical front (black line); SAF: Sub–Antarctic front (red line); PF: Polar front (green line).

4.2.2 The biogeochemical model

The BGC model is a Nutrient Phytoplankton Zooplankton Detritus (NNPPZZDD) model (Fig. 4.2), in which dissolved and particulate biogeochemical tracers are advected and diffused throughout the model grid in the same manner as temperature and salinity.

Biogeochemical processes are organised into phytoplankton and zooplankton growth and mortality, detritus remineralisation, and fluxes of dissolved tracers. Primary production is determined by the availability of dissolved nutrient and Photosynthetically Available Radiation (PAR). The food web includes primary producers and herbivores with simple trophic interactions

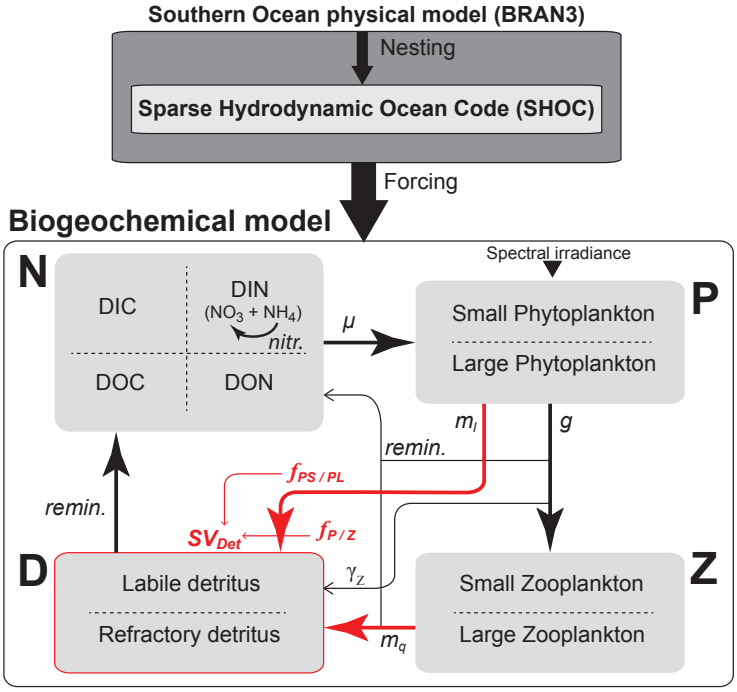

Figure 4.2: Conceptual diagram of the coupled physical–biogeochemical model showing the forcing of the BGC module by the physical module. The nutrient compartment (N) is composed of dissolved inorganic (DI) and organic (DO) matter [C: Carbon; N: Nitrogen as the sum of nitrates (NO_3) and ammonia (NH_4)]. The phytoplankton (P) and zooplankton (Z) compartments are composed of two size classes (small and large). Detritus is partitioned into labile and refractory detritus. Arrows represent the different fluxes between compartments and the processes involved. μ: growth; g: grazing; m_l: phytoplankton natural linear mortality; m_q: zooplankton natural quadratic mortality; γ_Z: fraction of zooplankton growth efficiency lost to the detritus; *nitr.*: nitrification; *remin.*: remineralisation. Fluxes and compartments used in the calculation of the variable detritus sinking velocity (SV_{Det}) are indicated in red: f_{P_S/P_L}: fractions of small and large phytoplankton (P_S and P_L) mortality fluxes to the detritus; $f_{P/Z}$: fractions of total phytoplankton and zooplankton mortality fluxes to the detritus.

based on small and large zooplankton (Z_S and Z_L) grazing respectively on small and large phytoplankton (P_S and P_L). Grazing rates are determined by the encounter rates between predator and prey, and maximum ingestion rates. Half of the fraction of grazed phytoplankton not used for growth (1 - growth efficiency), is lost to labile detritus, while the other half is released as dissolved inorganic carbon (DIC) and ammonia (NH_4). Other fluxes adding to the labile detritus compartment include a proportion of biomass associated with phytoplankton and zooplankton mortality. A fraction of labile detritus is converted to refractory detritus and fractions of labile and refractory detritus break–down to dissolved organic matter (DOM) at different rates (faster for labile and slower for refractory). Dissolved organic matter is finally remineralised at the slowest rate. Parameters and constants used in the biogeochemical processes are reported in Table 4.1. State and derived variables are reported in Table 4.2. Rate equations relevant to this study are detailed in the following sections. NH_4 and NO_3 concentrations, phytoplankton (P)

and zooplankton (Z) biomass, and detritus (Det) are updated at each time step (∂t) by the following processes: phytoplankton growth and mortality ($P_{grow.}$ and $P_{mort.}$), zooplankton growth and mortality ($Z_{grow.}$ and $Z_{mort.}$), detritus remineralisation ($remin.$) and sinking ($sink.$), and nitrification ($nitr.$, not shown here). A brief description of the biogeochemical processes updating each state variables is given for the phytoplankton and zooplankton growth and mortality, putting the emphasis on the fluxes between the NPZD compartments (Fig. 4.2).

$$\frac{\partial[\mathrm{NH_4}]}{\partial t} = -\frac{\partial[\mathrm{NH_4}]}{\partial t}_{P_{grow.}} + \frac{\partial[\mathrm{NH_4}]}{\partial t}_{P_{mort.}} + \frac{\partial[\mathrm{NH_4}]}{\partial t}_{Z_{grow.}} + \frac{\partial[\mathrm{NH_4}]}{\partial t}_{Z_{mort.}} - \frac{\partial[\mathrm{NH_4}]}{\partial t}_{nitr.} \tag{4.1}$$

$$\frac{\partial[\mathrm{NO_3}]}{\partial t} = \frac{\partial N}{\partial t} - \frac{\partial[\mathrm{NH_4}]}{\partial t} \tag{4.2}$$

$$\frac{\partial P}{\partial t} = +\frac{\partial P}{\partial t}_{P_{grow.}} - \frac{\partial P}{\partial t}_{P_{mort.}} - \frac{\partial P}{\partial t}_{Z_{grow.}} \tag{4.3}$$

$$\frac{\partial Z}{\partial t} = +\frac{\partial Z}{\partial t}_{Z_{grow.}} - \frac{\partial Z}{\partial t}_{Z_{mort.}} \tag{4.4}$$

$$\frac{\partial Det}{\partial t} = +\frac{\partial Det}{\partial t}_{P_{mort.}} + \frac{\partial Det}{\partial t}_{Z_{mort.}} + \frac{\partial Det}{\partial t}_{Z_{grow.}} - \frac{\partial Det}{\partial t}_{remin.} - \frac{\partial Det}{\partial t}_{sink.} \tag{4.5}$$

Phytoplankton growth and mortality

In the model, plankton physiological processes depend upon temperature and are scaled on allometric relationships. The phytoplankton growth and mortality model equations are given below. Equations where the phytoplankton structural biomass (P) is used are valid for both small and large phytoplankton.

$$\frac{\partial N}{\partial t} = -\psi D_N N(1 - R_N^*)(P/m_N) \tag{4.6}$$

$$\frac{\partial P}{\partial t}_{P_{grow.}} = \mu_P^{max} R_N^* R_I^* P \tag{4.7}$$

$$\frac{\partial P}{\partial t}_{P_{mort.}} = m_{l_P} P \tag{4.8}$$

$$\frac{\partial Det}{\partial t}_{P_{mort.}} = m_{l_P} P \tag{4.9}$$

Phytoplankton nitrogen uptake (Eq. 4.6) is a function of phytoplankton cell biomass (P) and their normalised nitrogen reserves (R_N^*). The diffusion shape factor (ψ) and nitrogen molecular diffusivity (D_N) determine the rate at which the nitrogen is absorbed (Table 4.2). The rate

of phytoplankton biomass increase (Eq. 4.7) depends upon the phytoplankton stock (P), the maximum growth rate (μ_P^{max}) and normalised reserves of nitrogen (R_N^*) and energy (R_I^*). Phytoplankton linear mortality decreases phytoplankton biomass and increases the detritus pool (Eqs. 4.8 & 4.9) at the mortality rate (m_{l_P}).

Zooplankton growth and mortality

State equations for the zooplankton growth and mortality models are given below. Equations where the zooplankton biomass (Z) is used are valid for both small and large zooplankton.

$$g = \min\Big[\mu_Z^{max} Z/E_Z, \frac{Z}{m_Z}(\phi_{diff} + \phi_{rel} + \phi_{shear})P\Big] \tag{4.10}$$

$$\frac{\partial[\mathrm{NH_4}]}{\partial t}_{Z_{grow.}} = g(1 - E_Z)(1 - \gamma_Z) + gR_N^* \tag{4.11}$$

$$\frac{\partial[\mathrm{NH_4}]}{\partial t}_{Z_{mort.}} = (1 - fm_{q_Z} det)(m_{q_{Z_S}} Z_S^2 + m_{q_{Z_L}} Z_L^2) \tag{4.12}$$

$$\frac{\partial P}{\partial t}_{Z_{grow.}} = g \tag{4.13}$$

$$\frac{\partial Z}{\partial t}_{Z_{grow.}} = E_Z g \tag{4.14}$$

$$\frac{\partial Z_S}{\partial t}_{Z_{mort.}} = m_{q_{Z_S}} Z_S^2 \tag{4.15}$$

$$\frac{\partial Z_L}{\partial t}_{Z_{mort.}} = m_{q_{Z_L}} Z_L^2 \tag{4.16}$$

$$\frac{\partial Det}{\partial t}_{Z_{grow.}} = g(1 - E_Z)\gamma_Z \tag{4.17}$$

$$\frac{\partial Det}{\partial t}_{Z_{mort.}} = fm_{q_Z} det(m_{q_{Z_S}} Z_S^2 + m_{q_{Z_L}} Z_L^2) \tag{4.18}$$

The grazing rate (g; Eq. 4.10) is a function of the encounter rate of the predator and all its prey (ϕ_{diff}, ϕ_{rel}, ϕ_{shear}: encounter rates due to diffusion, relative motion and shear respectively) up until the point at which it saturates the growth of the zooplankton and then remains at a constant level even if the phytoplankton produces increased levels of biomass (Hollings type I grazing; Gentleman 2002). Increase of zooplankton biomass (Eq. 4.14) is function of g and the growth efficiency (E_Z). Zooplankton grazing decreases the phytoplankton biomass (P) at the grazing rate (Eq. 4.13). Half of the fraction of zooplankton growth efficiency lost to the detritus (γ_Z) related to zooplankton grazing can be attributed to 'sloppy feeding' (Corner et al., 1972; Møller, 2005). Sloppy feeding releases dissolved matter directly in the water column at the

grazing rate (Eq. 4.11). The other half of γ_Z is directed into the detritus pool and represents the fecal material (Eq. 4.17). Half of the zooplankton mortality ($fm_{q_Z}det$) is directed toward the detritus compartment (Eq. 4.18) and the other half ($1-fm_{q_Z}det$) is remineralised (Eq. 4.12).

Table 4.1: Parameters and constants used in the biogeochemical processes. P_S, P_L: phytoplankton small and large; Z_S, Z_L: zooplankton small and large. In the calculation of the carbon content of phytoplankton, V is the cell volume. The sinking velocity of total detritus (SV_{Det}) is the constant velocity used in the initial model version. Most of the parameter values (see Table notes for available references) are from the CSIRO parameter library.

Characteristic	Unit	Symbol	Value
Cell radius P_S	µm	r_{P_S}	1
Cell radius P_L	µm	r_{P_L}	4
Cell radius Z_S	µm	r_{Z_S}	5
Cell radius Z_L	µm	r_{Z_L}	320
Reference temperature	°C	T_{ref}	20
Maximum growth rate at T_{ref} P_S	d^{-1}	$\mu_{P_S}^{max}$	1.0
Maximum growth rate at T_{ref} P_L	d^{-1}	$\mu_{P_L}^{max}$	0.65
Maximum growth rate at T_{ref} Z_S	d^{-1}	$\mu_{Z_S}^{max}$	3.0
Maximum growth rate at T_{ref} Z_L	d^{-1}	$\mu_{Z_L}^{max}$	1.5
Growth efficiency Z_S	-	E_{Z_S}	0.341[a]
Growth efficiency Z_L	-	E_{Z_L}	0.308[a]
Natural linear mortality rate P_S	d^{-1}	$m_{l_{P_S}}$	0.17
Natural linear mortality rate P_L	d^{-1}	$m_{l_{P_L}}$	0.11
Natural quadratic mortality rate Z_S	d^{-1} (mg N m^{-3})$^{-1}$	$m_{q_{Z_S}}$	0.02
Natural quadratic mortality rate Z_L	d^{-1} (mg N m^{-3})$^{-1}$	$m_{q_{Z_L}}$	0.001
Sinking velocity P_S	m d^{-1}	SV_{P_S}	0.0
Sinking velocity P_L	m d^{-1}	SV_{P_L}	15[b]
Sinking velocity Z_S	m d^{-1}	SV_{Z_S}	0.0
Sinking velocity Z_L	m d^{-1}	SV_{Z_L}	0.0
Swimming velocity Z_S	m s^{-1}	$swim_{Z_S}$	0.0002
Swimming velocity Z_L	m s^{-1}	$swim_{Z_L}$	0.003
Fraction of Z_S growth efficiency lost to detritus	-	$f\gamma_{Z_S}det$	0.5
Fraction of Z_L growth efficiency lost to detritus	-	$f\gamma_{Z_L}det$	0.5
Fraction of mortality lost to detritus Z	-	$fm_{q_Z}det$	0.5
Breakdown rate of labile detritus	d^{-1}	$remin_{Ldet}$	0.2
Breakdown rate of refractory detritus	d^{-1}	$remin_{Rdet}$	0.018
Breakdown rate of dissolved organic matter	d^{-1}	$remin_{DOM}$	0.00176
Sinking velocity of total zoo–detritus (constant)	m d^{-1}	SV_{Zdet}	320
Sinking velocity of total detritus (constant)	m d^{-1}	SV_{Det}	100
Molecular diffusivity of NO_3	m^2 s^{-1}	D_N	f(T, S)
Carbon content of phytoplankton	mg C $cell^{-1}$	m_C	$12010 \times 9.14 \times 10^3 V$[c]
Nitrogen content of phytoplankton	mg N $cell^{-1}$	m_N	$\frac{14}{12}\frac{16}{106}m_C$

[a] Values from Hansen et al. (1997)

[b] The high sinking velocity of 15 m d^{-1}, at the higher limit of the range reported for marine diatom cells (Passow, 1991; Waite et al., 1997), accounts for the possible direct export of live large phytoplankton either via single cells or aggregated.

[c] Relationship from Straile (1997)

Table 4.2: State and derived variables used in the biogeochemical processes. DIN is given by the sum of nitrate and ammonia concentrations, $[NO_3]+[NH_4]$. Zooplankton body mass: $m_Z = 16000 \times 14.01 \times 10.5 V_Z$ mg N cell^{-1}, where V_Z is the volume of zooplankton (Hansen et al., 1997). The sinking velocity of total detritus (SV_{Det}) is the variable sinking velocity calculated from detritus composition (modified model version). S: small; L: large.

Variable	Unit	Symbol
Dissolved inorganic nitrogen (DIN)	mg N m^{-3}	N
Ammonia	mg N m^{-3}	NH_4
Nitrates	mg N m^{-3}	NO_3
Phytoplankton nitrogen reserves	mg N cell^{-1}	R_N
Phytoplankton structural biomass	mg N m^{-3}	P
Zooplankton biomass	mg N m^{-3}	Z
Maximum P reserves of nitrogen	mg N cell^{-1}	R_N^{max}
P reserves of nitrogen normalised to the max.	-	$R_N^* \equiv R_N / R_N^{max}$
P reserves of energy normalised to the max.	-	$R_I^* \equiv R_I / R_I^{max}$
Phytoplankton cell mass	mg N cell^{-1}	m_P
Zooplankton body mass	mg N cell^{-1}	m_Z
Detritus pool	mg N m^{-3}	Det
Zooplankton grazing rate	mg N m^{-3} s^{-1}	g
Encounter rate coefficient due to molecular diffusion	m^3 s^{-1} cell Z^{-1}	ϕ_{diff}
Encounter rate coefficient due to relative motion	m^3 s^{-1} cell Z^{-1}	ϕ_{rel}
Encounter rate coefficient due to turbulent shear	m^3 s^{-1} cell Z^{-1}	ϕ_{shear}
Phytoplankton diffusion shape factor	m cell^{-1}	ψ
Fluxes of P(S,L) mortalities to detritus	mg N m^{-3} d^{-1}	$\varphi_{P(S,L)det}$
Flux of Z quadratic mortality and fraction of growth efficiency lost to detritus	mg N m^{-3} d^{-1}	φ_{Zdet}
Fraction of small phytodetritus in the total phytodetritus flux	-	f_{PSdet}^{Pdet}
Fraction of phytodetritus in the total detritus flux	-	f_{Pdet}^{Det}
Fraction of zoo–detritus in the total detritus flux	-	f_{Zdet}^{Det}
Sinking velocity of phytodetritus	m d^{-1}	SV_{Pdet}
Sinking velocity of total detritus (variable)	m d^{-1}	SV_{Det}

Detritus composition and sinking velocity

Model equations used to calculate the variable SV of detritus (SV_{Det}) are reported hereafter. The modification of the model baseline version was done by creating new tracers to fluxes of plankton to the detritus compartment ($\varphi_{P(S,L)det}$ and φ_{Zdet}; Eqs. 4.19, 4.20 & 4.24 respectively) i.e. phytoplankton and zooplankton mortalities and half of the fraction of zooplankton growth efficiency lost to the detritus (γ_Z). We used the relationship between the SV of phytoplankton aggregates and their relative content of small phytoplankton found experimentally by Laurenceau-Cornec et al. (2015a) (Chapter 3) to calculate the sinking velocity of all phytodetritus (SV_{Pdet}; Eq. 4.22) based on the fraction of the flux of small phytoplankton to the detritus (f_{PSdet}^{Det}). The SV of total detritus (SV_{Det}; Eq. 4.27) was then calculated by assigning SV_{Pdet} to the fraction of phytodetritus in total detritus (f_{Pdet}^{Det}; Eq. 4.25) and SV_{Zdet}, a constant velocity of 320 m d^{-1}, to the zoo–detritus fraction in total detritus (f_{Zdet}^{Det}; Eq. 4.26) without distinction between small and large zoo–detritus. This value is an average for fecal pellets in the size range

4×10^5 to $10\times10^5 \mu m^3$ produced by copepods fed on the diatom *Thalassiosira weissflogii* (Ploug et al., 2008).

All labile and refractory detritus sank at this variable sinking velocity in the modified model version (called 'var–SV' hereafter) whereas they sank at the constant sinking velocity of 100 m d^{-1} in the non–modified model version ('cst–SV').

$$\varphi_{P_S det} = m_{l_{P_S}} P_S \tag{4.19}$$

$$\varphi_{P_L det} = m_{l_{P_L}} P_L \tag{4.20}$$

$$f^{Pdet}_{P_S det} = \varphi_{P_S det}/(\varphi_{P_S det} + \varphi_{P_L det}) \tag{4.21}$$

$$SV_{Pdet} = 168 - 1.48 \times f^{Pdet}_{P_S det} \times 100/86400 \tag{4.22}$$

$$\varphi_{Pdet} = \varphi_{P_S det} + \varphi_{P_L det} \tag{4.23}$$

$$\varphi_{Zdet} = g(1 - E_Z)\gamma + f^{Det}_{Zdet}(m_{qZ_S} Z_S^2 + m_{qZ_L} Z_L^2) \tag{4.24}$$

$$f^{Det}_{Pdet} = \varphi_{Pdet}/(\varphi_{Pdet} + \varphi_{Zdet}) \tag{4.25}$$

$$f^{Det}_{Zdet} = \varphi_{Zdet}/(\varphi_{Pdet} + \varphi_{Zdet}) \tag{4.26}$$

$$SV_{Det} = f^{Det}_{Zdet} \times 320/86400 + f^{Det}_{Pdet} \times SV_{Pdet} \tag{4.27}$$

4.2.3 Initial conditions, model run and post-run calculations

Two sites (S1 and S2) were selected over the model spatial domain by privileging areas of maximum plankton biomass variability over the duration of the simulations. Figure 4.3 presents the location of S1 and S2 on sea surface temperature (SST) maps, showing the mesoscale structures produced by SHOC. The two versions of the BGC model were run for the first three years of the SHOC outputs (from the 1^{st} of August 2002 to the 1^{st} of August 2005). Recalculation of tracer concentrations at the centre of each grid cell was made every 12 hours. Only the two last years were explored at S2, to exclude from the study a large P_L biomass increase occurring at this station the first year, and presenting unrealistic levels of surface chlorophyll *a* (Chl. *a* = $\sim$ 5 µg Chl *a* L^{-1}). For simplicity, the simulations from the different model versions (with a constant or variable detritus sinking velocity) and at the sites S1 or S2 are designated in the rest of the text by: S1-cst–SV, S1-var–SV, S2-cst–SV, and S2-var–SV respectively.

Initial average concentration of nitrate over the euphotic zone (E_Z) was set at a high value

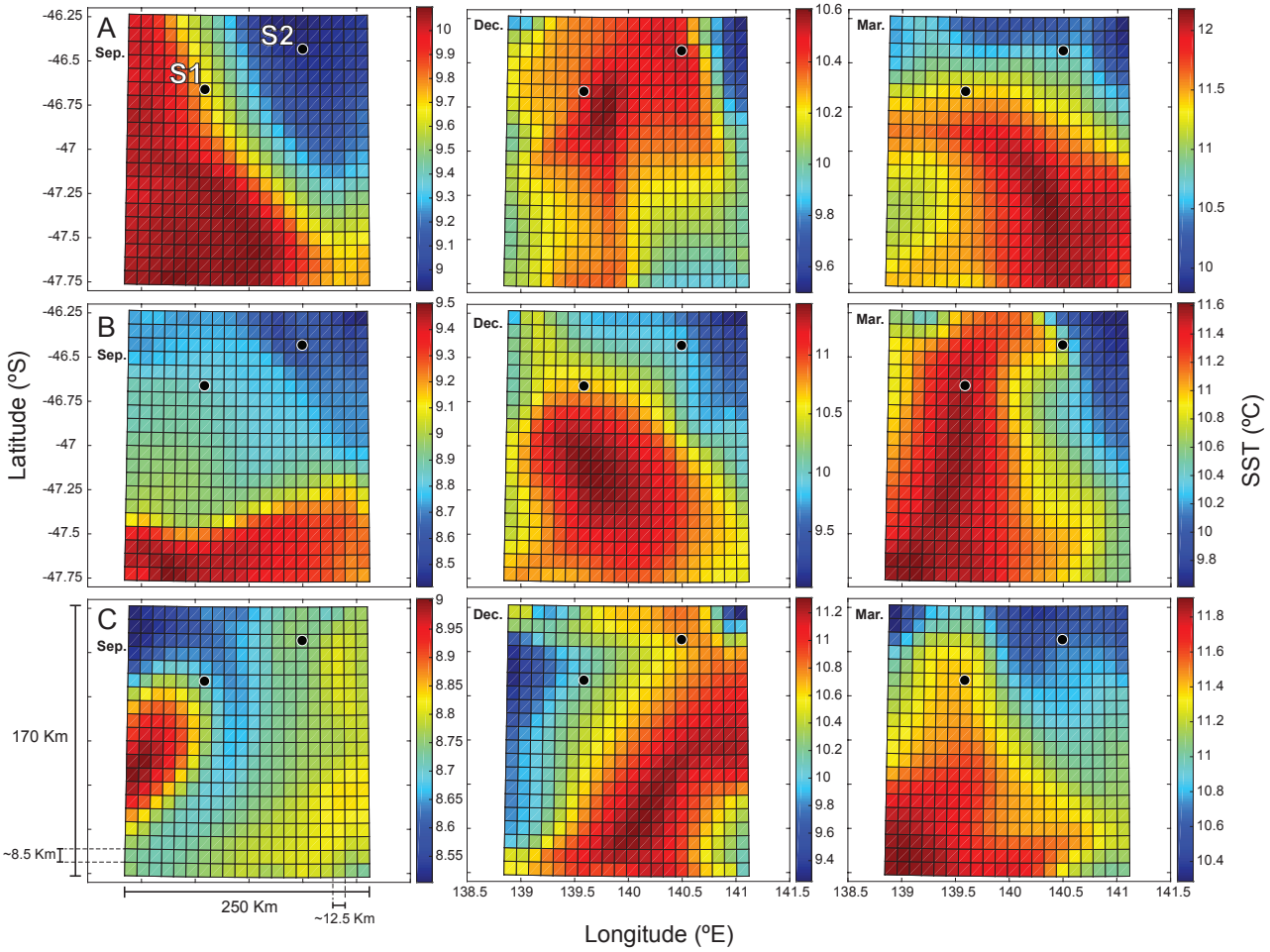

Figure 4.3: Location of the stations on maps of sea surface temperature (SST) from model outputs. Values are monthly averaged (September, December, and March) for the years 2002–03 (A) , 2003–04 (B), and 2004–05 (C). The location of the two stations was selected based on the large range of ecosystem structure variations encountered over the three years. Approximate distances on the model spatial domain (entire and for one cell) are indicated in kilometres. Note the mesoscale structures produced by the physical forcing from SHOC (See section 'Model description').

(434 ± 6 mg m^{-3}) to avoid any limitation of phytoplankton growth by nutrient availability over the three years of simulation. Residual concentrations at the end of the third year were 92 and 90 mg m^{-3} at S1 and S2 respectively (cst–SV), and 88 and 83 mg m^{-3} at S1 and S2 respectively (var–SV).

Initial concentrations of phyto- and zooplankton and their relative fractions were set, based on concentrations measured during the second KErguelen Ocean and Plateau compared Study (KEOPS2). The total Chl. *a* measured from fluorescence CTD profiles during KEOPS2 (Lasbleiz et al., 2014), and used here as initial concentrations, was assumed to be equally partitioned between small and large phytoplankton having each an average E_Z concentration of 0.1µg Chl *a* L^{-1}. Initial levels of zooplankton biomass over the whole water column were based

on abundances observed during the KEOPS2 cruise (Zooscan data from Carlotti et al., 2015, station A3-1 at 250 m: ∼0.88 and 8.9 mg C m^{-3} for small and large zooplankton respectively). Final adjustments based on preliminary model results led to values of 1 and 2 mg C m^{-3} for the small and large zooplankton respectively.

The base of the E_Z was defined as 1% of the PAR. The mixed layer depth (MLD) was calculated using the density difference criterion of 0.02 σ_θ (potential density at MLD = potential density at 10 m depth + 0.02 kg m^{-3}; Park et al., 1998). E_Z and MLD averaged over the entire domain where used in all post-run model calculations. Results are presented in term of plankton biomass, detritus concentration, sinking velocity, carbon flux and export efficiency variations during the three years of simulation at S1 and the two years at S2 for the modified and non–modified model versions. Chl. *a* concentration was used as an indicator of phytoplankton biomass and is expressed in µg Chl *a* L^{-1}. Average (Avg.) zooplankton biomass and detritus concentrations over the euphotic zone were expressed in mg C m^{-3}. Integrations over the euphotic zone (noted $\sum_{E_Z}$ for simplicity) of Chl. *a*, zooplankton biomass, and detritus are also shown and expressed in mg Chl *a* m^{-2}, g C m^{-2} and mg C m^{-2} respectively. Net primary productivity (NPP) was also integrated over the euphotic zone and is expressed in mg C m^{-2} d^{-1}.

The carbon flux was calculated at the base of the euphotic zone (C flux E_Z), at 100 m below the euphotic zone (C flux E_Z+100m), at 100 m depth (C flux 100 m), and at 200 m depth (C flux 200 m). In each grid cell, the flux was computed as the difference in detrital carbon concentration between the cell considered and the cell directly above (thus neglecting horizontal advection) using the formula:

$$Cflux\ (x,y,z,t) = [C_{Det}\ (x,y,z,t) - C_{Det}\ (x,y,z-1,t)] \times SV_{Det}\ (x,y,z-1,t) \qquad (4.28)$$

where x, y, z, t are the cell coordinates in latitude (x), longitude (y), depth (z) and time(t), C_{Det} is the total detritus concentration in the cell (labile + refractory) converted to carbon, and SV_{Det} is the detritus sinking velocity. For simplicity, the carbon concentration is taken at the same time t in the two cells (not at $t-1$ in the upper cell) due to the continuous sinking and advection of tracers adding and removing matter from each cell at each time step. SV_{Det} is constant over time and over the whole model domain for cst–SV and variable at every location and

time for var–SV. Using output data of detritus composition from the cst–SV simulation, a variable sinking velocity was recalculated using equations 4.22 and 4.27 (called hereafter '$SV_{recalc.}$'). $SV_{recalc.}$ was used to re–compute the carbon flux, in order to assess the direct effects of the model modification on sinking velocity values and subsequent carbon flux estimations. This assessment was only possible by this mean because the assignment of a variable sinking velocity to the detritus in var–SV modified their flux inducing additional feedback effects on plankton biomass and thus masking the direct effect of a variable sinking velocity on the carbon flux.

The e–ratio (ratio between carbon export flux and NPP; Downs, 1989) was used as a measure of carbon export efficiency and was calculated as the ratio between the C flux estimated at various depths (see above) and the $\sum_{E_Z}$ NPP.

4.3 Results

4.3.1 Physical context

The seasonal variations of the MLD and E_Z averaged over the model spatial domain are shown on Figure 4.4. Shallowing of the MLD started in October the two first years and in November the third year when the deepest MLD was recorded (595 m), followed by a sharp shallowing. During the first, second and third year, the base of the MLD was shallower or equal to the E_Z during 38, 92 and 87 days respectively, with average E_Z of 62.5±23, 62.3±7 and 53.2±6 m. Seasonal evolution of the PAR is also indicated.

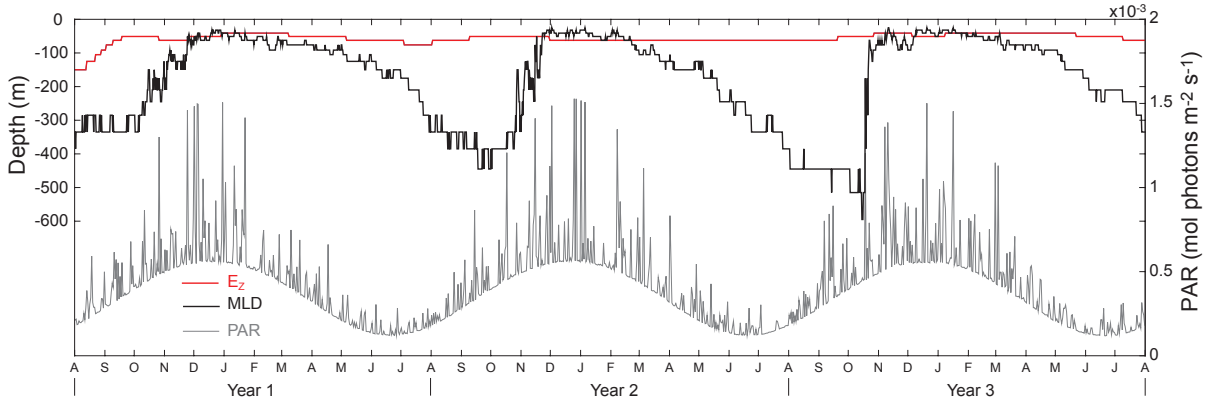

Figure 4.4: Water column physical properties from the physical module SHOC. Red line: depth of the base of the euphotic zone (E_Z) assumed at 1% of the surface photosynthetic available radiation (PAR). Black line: depth of the base of the mixed layer (MLD) calculated using the density difference criterion of $0.02\,\sigma_\theta$ [potential density at MLD = potential density at 10 m + $0.02\,kg\,m^{-3}$ (Park et al., 1998). Grey line: Photosynthetic Available Radiation (PAR).

4.3.2 Variations of phytoplanktonic community structure

Significant increases of phytoplankton biomass (hereafter called 'blooms') were numbered from 1 to 15 (Figs. 4.5 and 4.6) and individually studied for both the cst–SV and var–SV model versions. The main features of each bloom (e.g. initiation date, duration, biomass levels) are reported on Table 4.3. Bloom initiation and end times were determined using the maximum rate of change in increase or decrease of the E_Z integrated Chl. *a* ($\sum_{E_Z}$ Chl. *a*) as a criteria. Figures 4.5 and 4.6 show model outputs from the var–SV and cst–SV simulations respectively, and include MLD and E_Z depths in panels E and K (light and dark grey areas). Because most of the export occurred when the MLD and E_Z were shallower than 100 m, this depth was selected as a reference for carbon export diagnostic and was used for export efficiency evaluation. This choice also allowed to focus on planktonic community variation effects on carbon export efficiency by limiting the influence of remineralisation occurring below this depth.

All blooms were arbitrarily classified into four categories based on similarity of phytoplanktonic community structures. Various metrics from plankton biomass to carbon export efficiency were calculated to explore the links between bloom dynamics and carbon export features. To account for a potential decoupling between surface and deeper observations depending on tracer sinking velocity and lateral advection, annual budgets were calculated (Table 4.4). The four bloom categories distinguished were:

Category A: P_S–dominated with a slowly increasing background of P_L (blooms 1, 5, 8, 11, 13; Figs. 4.5 and 4.6). All these blooms commenced in August (Table 4.3) and lasted for 4.2 ± 1.3 months on average. Their maximum surface Chl. *a* ranged between 0.77 (bloom 11) and 1.25 µg L^{-1} (bloom 5), leading to an average of 0.92 ± 0.2 µg L^{-1}. The $\sum_{E_Z,d}$NPP (summed over the euphotic zone and the bloom duration) ranged between 15 (bloom 11) and 25 g C m^{-2} (bloom 5) with an average of 17.6 ± 4.1 g C m^{-2}.

Category B: P_L–dominated with very low levels of P_S (blooms 2, 9, 12, 14). Blooms from this category started between August (bloom 12) and November (bloom 14) and lasted for 7.5 ± 2.5 months on average. Their maximum surface Chl. *a* ranged between 1.78 (bloom 12) and 2.44 µg L^{-1} (bloom 2) with an average of 2.2 ± 0.3 µg L^{-1}. The $\sum_{E_Z,d}$NPP extended from 44 (blooms 2, 9 and 12) to 57 g C m^{-2} (bloom 14) and averaged 47.2 ± 6.5 g C m^{-2}.

Category C: P_S–dominated with very low levels of P_L (blooms 3, 4 and 10). These blooms started in July (bloom 10) or August (blooms 3 and 4) and lasted for 5.7 ± 1.2 months on

average. Their maximum surface Chl. *a* ranged between 0.81 (bloom 10) and 0.99 µg L^{-1} (bloom 4) with an average of 0.89 ± 0.09 µg L^{-1}. The $\sum_{E_Z,d}$NPP ranged from 20 (bloom 4) to 30 g C m^{-2} (bloom 10) leading to an average of 26 ± 5 g C m^{-2}.

Category D: P_L–dominated with moderate to low biomass levels but maintained over a long time (blooms 6, 7, and 15). These blooms started in September (blooms 7 and 15) or December (bloom 6) and lasted for 9.7 ± 2.3 months on average. Maximum surface Chl. *a* ranged between 0.63 µg Chl *a* L^{-1} (bloom 15) and 1.74 µg Chl *a* L^{-1} (bloom 7) with an overall average of 1.23 ± 0.56 µg Chl *a* L^{-1}. The total production ranged from 19 (bloom 15, sum of small and large phytoplankton) to 66 g C m^{-2} (bloom 7, sum of small and large phytoplankton) with an average of 40 ± 24 g C m^{-2}.

Table 4.3: Main features of the phytoplankton blooms generated by the model. Characteristics are shown only for the dominant phytoplankton in each bloom to remove any influence from increasing or decreasing biomass associated with the next or previous bloom. P_L blooms are indicated in bold.

	Simulation and bloom i.d.s														
	S1–var–SV				S2–var–SV			S1–cst–SV					S2–cst–SV		
Main features	1	2	3	4	5	6	7*	8	9	10	11	12	13	14	15*
Year i.d.	1	**1**	2	3	2	**2**	**3**	1	**1**	2	3	**3**	2	**2**	**3**
Bloom category	A	**B**	C	C	A	**D**	**D**	A	**B**	C	A	**B**	A	**B**	**D**
Dominant phyto. type	P_S	**P_L**	P_S	P_S	P_S	**P_L**	**P_L**	P_S	**P_L**	P_S	P_S	**P_L**	P_S	**P_L**	**P_L**
Initiation time	Aug.	**Nov.**	Sep.	Aug.	Aug.	**Dec.**	**Sep.**	Aug.	**Nov.**	Jul.	Aug.	**Sep.**	Aug.	**Nov.**	**Sep.**
Duration (months)	3	**5.5**	7	5	5	**7**	**11**	3	**6**	5	6	**11**	4	**7.5**	**11**
Max. Chl. *a* (µg Chl *a* L^{-1})	0.86	**2.44**	0.87	0.99	1.25	**1.32**	**1.74**	0.88	**2.39**	0.81	0.77	**1.78**	0.82	**2.23**	**0.63**
$\sum_{E_Z,d}$ NPP (g C m^{-2})	16	**44**	27	20	25	**36**	**66**	16	**44**	30	15	**44**	16	**57**	**19**

* For the blooms 7 and 15 which include an initial P_S bloom, the total net primary productivity integrated over the euphotic zone and bloom duration ($\sum_{E_Z,d}$ NPP) accounts for the small and large phytoplankton.
Max. Chl. *a*: maximum chlorophyll *a* concentration.
P_S: small phytoplankton; P_L: Large phytoplankton.

4.3.3 Annual budgets of planktonic community biomass and associated carbon export fluxes

This section presents results from the var–SV simulation (Fig. 4.5) used to test our initial hypothesis of a link between variability in planktonic community structure and carbon export efficiency via changes in the detritus sinking velocity (within this model formulation, structure, and computing environment). The cst–SV simulation (Fig. 4.6) which served as a reference to assess changes in model behaviour following the introduction of a variable SV of detritus are presented in the 'Discussion' Section.

The model generated a large variety of phytoplankton blooms, in terms of initiation time, biomass level, productivity, and duration (Fig. 4.5 and Table 4.3). Seasonal variations of Chl.

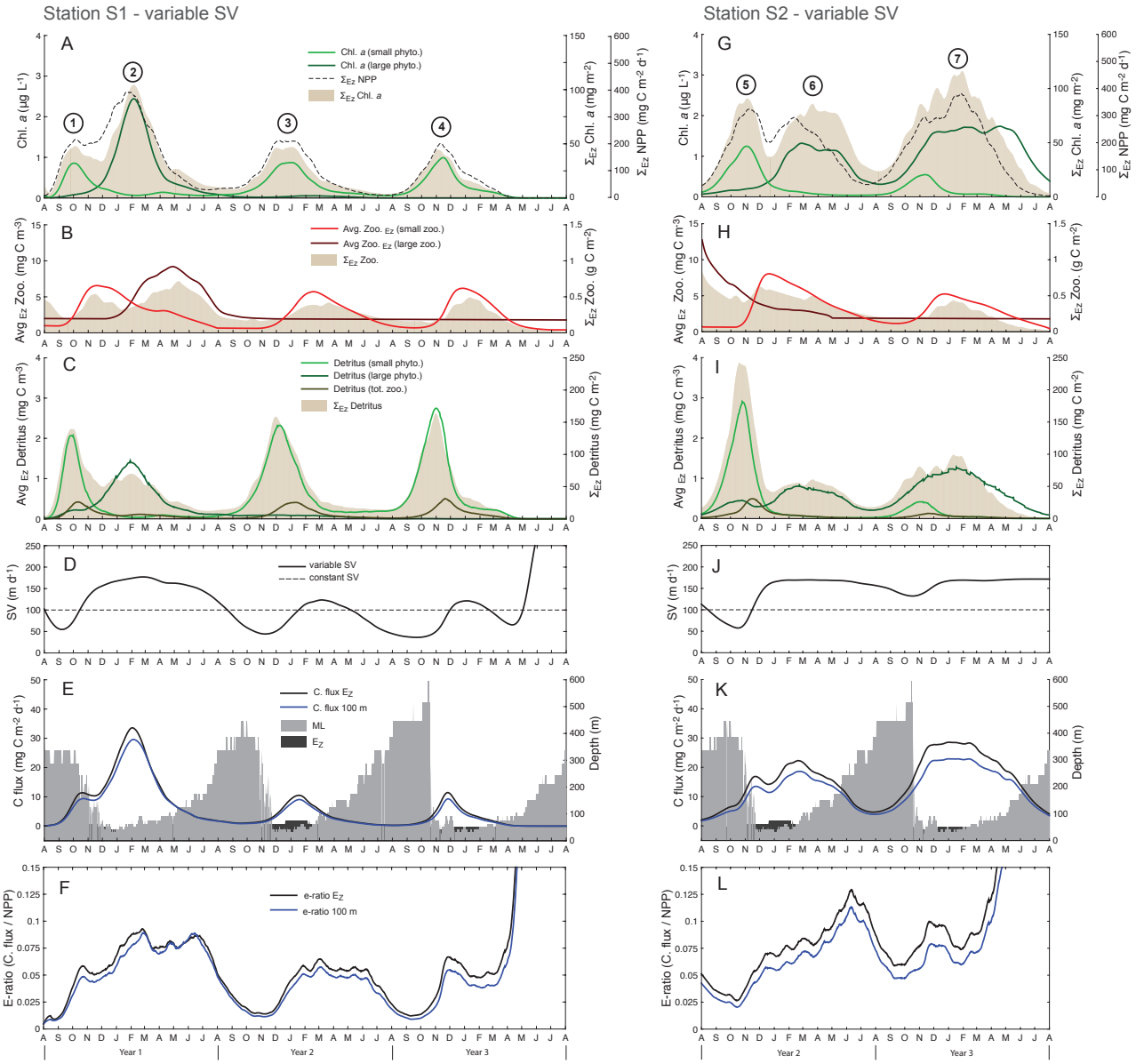

Figure 4.5: Time series of phytoplankton (sequential bloom i.d.s indicated) and zooplankton biomasses, detritus concentration and sinking velocity and associated carbon export flux and e–ratio for the modified version of the model (var–SV) at the two selected sites S1 (Panels A–F) and S2 (Panels G–L). A, G: surface chlorophyll a concentration (Chl. a) for the small and large phytoplankton; shaded area: Chl. a integrated over the euphotic zone (E_Z); dashed line: net primary productivity (NPP) integrated over the E_Z. B, H: small and large zooplankton biomass averaged over the E_Z; shaded area: total zooplankton biomass integrated over the E_Z. C, I: detritus concentration averaged over the E_Z. Shaded area: total detritus concentration integrated over the E_Z. D, J: detritus sinking velocity (SV). E, K: carbon flux (C flux); dark and light grey areas represent the mixed layer (ML) and E_Z respectively. F, L: e–ratio$_{depth}$ = C flux$_{depth}$ / $\sum_{E_Z}$ NPP.

a concentrations of small and large phytoplankton due to natural mortality and zooplankton grazing produced various patterns that were reflected in detritus concentrations and subsequent carbon export. Interestingly, different planktonic community structures were able to induce similar annual budgets of NPP, detritus concentration, carbon export and efficiency. A comparison of the successions from P_S to P_L blooms observed the first year at S1 (called hereafter 'S1–year1') and the second year at S2 (S2–year2) provides a good example (Fig. 4.5). The succession from bloom 1 to bloom 2 (Panel A) was characterised by a moderate P_S bloom (maximum Chl. a = 0.86 µg L^{-1}, Table 4.4) followed by a large P_L bloom (maximum Chl. a = 2.44 µg L^{-1}). An annual budget (Table 4.4) shows a biomass overall dominated by large phytoplankton with $\sum_{E_Z}$ Chl. a of 4.36 and 10.82 g m^{-2} yr^{-1} for the P_S and P_L respectively (ratio $\sum_{E_Z}$ Chl. a P_S:P_L = 0.4). Conversely, the succession from bloom 5 to bloom 6 at S2–year2 (Panel G) displayed similar maxima of Chl. a (1.25 and 1.32 µg L^{-1} for the P_S and P_L respectively). However, the annual biomass was still dominated by the large phytoplankton ($\sum_{E_Z}$ Chl. a P_S:P_L = 0.52) due to a longer P_L bloom duration (bloom 6 lasted ∼1.5 months more than bloom 2, Table 4.3).

Zooplankton biomass variations also presented notable differences (Panels B and H). Z_L dominated at S1–year1 and S2–year2 (ratio $\sum_{E_Z}$ Z_S:Z_L = 0.66 and 0.86 respectively; Table 4.4) but most of the Z_L biomass at S2–year2 ($\sum_{E_Z}$ Z_L = 89.48 g C m^{-2} yr^{-1}) was decreasing continuously during the year, and the high initial levels were related to a very high P_L biomass the previous year (not shown, see section 'Model description' for explanation).

These large differences in phytoplankton and zooplankton biomass were reflected by the composition of the detritus with a dominance of P_L over P_S in the total detritus at S1–year1 (ratio $\sum_{E_Z}$ P_S det:P_L det = 0.78) while P_S dominated at S2–year2 (ratio $\sum_{E_Z}$ P_S det:P_L det = 1.15) and exhibited a high maximum at 2.91 mg C m^{-3}. Despite these differences in planktonic community structures, simulations at S1–year1 and S2–year2 provided very similar estimates of NPP ($\sum_{E_Z}$ NPP = 65 and 68 g C m^{-2} yr^{-1}), carbon flux ($\sum$ C $flux_{100m}$ = 3.9 and 3.78 g C m^{-2} yr^{-1}) and e–ratio (same e–$ratio_{100m}$ = 0.06).

As expected, given the high P_L sinking velocity parameterised in the model (Table 4.1), the carbon export efficiency was always higher when the biomass was dominated by large phytoplankton. The highest e–ratio was observed at S2–year3 and associated with bloom 7 (e–$ratio_{100m}$ = 0.08) dominated by large phytoplankton ($\sum_{E_Z}$ Chl. a P_L = 19.46 µg Chl a L^{-1}

Table 4.4: Annual budgets of various metrics for small and large phytoplankton (P_S and P_L) and zooplankton (Z_S and Z_L) biomass, detritus concentration and sinking velocity and carbon export flux (C flux) and efficiency (e–ratio).

	Metrics	Units	Simulations									
			Station 1 (var–SV)			Station 2 (var–SV)		Station 1 (cst–SV)			Station 2 (cst–SV)	
			Year 1	Year 2	Year 3	Year 2	Year 3	Year 1	Year 2	Year 3	Year 2	Year 3
PHYTOPLANKTON												
	Max. Chl. *a* P_S	µg Chl *a* L^{-1}	0.86	0.87	0.99	1.25	0.55	0.88	0.81	0.77	0.82	0.49
	Max. Chl. *a* P_L	µg Chl *a* L^{-1}	2.44	0.08	0	1.32	1.74	2.39	0.12	1.78	2.23	0.63
	Delay Chl. *a* apexes (P_S to P_L)	Days	125	154	24	116	156	126	80	124	123	15
	$\sum_{E_Z}$ Chl. *a* P_S	g Chl *a* m^{-2} yr^{-1}	4.36	6.23	4.48	7.22	2.56	4.37	6.61	3.77	4.48	2.33
	$\sum_{E_Z}$ Chl. *a* P_L	g Chl *a* m^{-2} yr^{-1}	10.82	0.68	0.01	13.78	19.46	11.2	1.26	12.62	17.28	7.27
	ratio $\sum_{E_Z}$ Chl. *a* (P_S:P_L)	-	0.4	9.16	538.09	0.52	0.13	0.39	5.25	0.3	0.26	0.32
	$\sum_{E_Z}$ NPP	g C m^{-2} yr^{-1}	65	31	20	68	66	65	36	61	79	27
	Fract. $\sum_{E_Z}$ NPP_{P_S}	-	0.3	0.9	1	0.41	0.15	0.3	0.83	0.27	0.23	0.33
	Fract. $\sum_{E_Z}$ NPP_{P_L}	-	0.7	0.1	0	0.59	0.85	0.7	0.17	0.73	0.77	0.67
ZOOPLANKTON												
	Max. $Z_{S\ avg.E_Z}$	mg C m^{-3}	6.56	5.71	6.19	8.05	5.25	6.6	6.8	5.58	7.18	4.91
	Max. $Z_{L\ avg.E_Z}$	mg C m^{-3}	9.2	3.25	1.86	2.95	1.81	8.58	3.25	2.91	8.14	4.17
	Delay apexes Chl. *a* P_S to $Z_{S\ avg.E_Z}$	Days	48	47	41	48	41	46	59	39	58	47
	Delay apexes Chl. *a* P_L to $Z_{L\ avg.E_Z}$	Days	82	n/a	n/a	n/a	n/a	82	n/a	28	91	188
	$\sum_{E_Z}$ Z_S	g C m^{-2} yr^{-1}	63.89	51.03	41.95	76.64	46.33	65.77	81.89	39.27	85.95	43.66
	$\sum_{E_Z}$ Z_L	g C m^{-2} yr^{-1}	96.81	44.31	29.08	89.48	29.22	94.14	46.36	37.5	140.87	45.69
	ratio $\sum_{E_Z}$ Z_S:Z_L	-	0.66	1.15	1.44	0.86	1.59	0.7	1.77	1.05	0.61	0.96
	$\sum_{E_Z}$ Z	g C m^{-2} yr^{-1}	161	95	71	166	76	160	128	77	227	89
	Fract. $\sum_{E_Z}$ Z_S	-	0.4	0.54	0.59	0.46	0.61	0.41	0.64	0.51	0.38	0.49
	Fract. $\sum_{E_Z}$ Z_L	-	0.6	0.46	0.41	0.54	0.39	0.59	0.36	0.49	0.62	0.51
DETRITUS												
	Max. P_S $det_{avg.E_Z}$	mg C m^{-3}	2.07	2.32	2.75	2.91	0.42	1.38	1.12	1.05	1.01	0.62
	Max. P_L $det_{avg.E_Z}$	mg C m^{-3}	1.44	0.11	0.01	0.83	1.28	3.09	0.22	2.41	2.96	1.11
	Max. Z $det_{avg.E_Z}$	mg C m^{-3}	0.42	0.41	0.5	0.49	0.13	0.44	0.4	0.33	0.38	0.2
	$\sum_{E_Z}$ P_S det	g C m^2 yr-1	7.28	13.83	11.64	12.74	2.1	7.1	10.35	5.63	6.32	3.23
	$\sum_{E_Z}$ P_L det	g C m^2 yr-1	9.32	1.51	0.03	11.09	13.94	18.58	2.7	19.4	26.73	14.29
	$\sum_{E_Z}$ Z det	g C m^2 yr-1	2.29	2.43	2.07	2.63	0.83	3.29	3.36	1.76	4.39	1.28
	ratio $\sum_{E_Z}$ P_S det:P_L det	-	0.78	9.13	397.9	1.15	0.15	0.38	3.83	0.29	0.24	0.23
	$\sum_{E_Z}$ Detritus	g C m^{-2} yr^{-1}	19	18	14	26	17	29	16	27	37	19
	Fract. $\sum_{E_Z}$ P_S det	-	0.39	0.78	0.85	0.48	0.12	0.25	0.63	0.21	0.17	0.17
	Fract. $\sum_{E_Z}$ P_L det	-	0.49	0.09	0	0.42	0.83	0.64	0.16	0.72	0.71	0.76
	Fract. $\sum_{E_Z}$ Z det	-	0.12	0.14	0.15	0.1	0.05	0.11	0.2	0.07	0.12	0.07
SINKING VELOCITY*												
	Max. SV $detritus_{E_Z}$	m d^{-1}	177	123	321	170	172	100 [177]	100 [140]	100 [169]	100 [179]	100 [173]
	Min. SV $detritus_{E_Z}$	m d^{-1}	55	44	36	58	132	100 [55]	100 [54]	100 [88]	100 [86]	100 [116]
	Avg. var. 100 m d^{-1} ± SD	m d^{-1}	39±39	-17±27	25±95	38±41	60±13	0 [41±39]	0 [8±25]	0 [41±30]	0 [51±30]	0 [55± 21]
CARBON EXPORT*												
	Max. C $flux_{100m}$	mg C m^{-2} d^{-1}	29.53	8.91	8.74	18.55	22.94	21.14 [37.19] (76)	7.75 [8.43] (9)	15.56 [26.29] (69)	21.46 [38.22] (78)	10.75 [15.85] (47)
	Delay apexes Chl. $a_{surf.}$ to C $flux_{100m}$	Days	2	45	19	-20	-31	2 [6]	15 [35]	-7 [-4]	5 [-2]	19 [27]
	Delay apexes $\sum_{E_Z}$ NPP to C $flux_{100m}$	Days	8	33	15	11	-17	10 [14]	5 [25]	23 [26]	8 [1]	22 [30]
	$\sum$ C $flux_{E_Z}$	g C m^{-2} yr^{-1}	4.31	1.18	0.86	4.53	6.62	3.61 [5.6] (55)	1.68 [1.76] (5)	3.96 [5.92] (49)	4.42 [7.08] (60)	2.89 [4.46] (54)
	$\sum$ C $flux_{100m}$	g C m^{-2} yr^{-1}	3.9	1.01	0.68	3.78	5.38	3.13 [4.88] (56)	1.45 [1.53] (5)	3.2 [4.81] (50)	3.57 [5.75] (61)	2.18 [3.37] (55)
	e–$ratio_{E_Z}$	-	0.07	0.04	0.04	0.07	0.1	0.06 [0.09] (55)	0.05 [0.05] (5)	0.07 [0.1] (49)	0.06 [0.09] (60)	0.11 [0.17] (54)
	e–$ratio_{100m}$	-	0.06	0.03	0.03	0.06	0.08	0.05 [0.07] (56)	0.04 [0.04] (5)	0.05 [0.08] (50)	0.04 [0.07] (61)	0.08 [0.12] (55)

* Values in square brackets (cst–SV) represent post-model run calculations with a re–calculated variable sinking velocity ($SV_{recalc.}$, See 'Model description' Section). Values in parentheses represent the percentage of variation induced by the recalculation.
Chl. *a*: surface chlorophyll *a* concentration.
$\sum_{E_Z}$: integration over the euphotic zone.
Max.: maximum; Fract.: fraction; det: detritus; Avg.: average; SV: sinking velocity. (*).
n/a: Non applicable.

and fract. $\sum_{E_Z}$ NPP$_{P_L}$ = 0.85). Although the $\sum_{E_Z}$ NPP was not the largest observed (maximum of 68 g C m^{-2} yr^{-1} the second year at S2, against 66 the third year, when bloom 7 occurred), the $\sum$ C flux$_{100m}$ was the highest recorded (5.38 g C m^{-2} yr^{-1}) suggesting an efficient sinking of the detritus produced. A comparison of the three years at S1, also illustrates well the importance of the P$_L$ dominance in increasing the efficiency of carbon export. The annual phytoplankton biomass on S1–year1 was dominated by the P$_L$ (cf above) and resulted in an e–ratio$_{100m}$ of 0.06. Conversely, the second and third year at S1 displayed P$_S$–dominated biomasses (relative contribution of P$_S$ to the total NPP: fract. $\sum_{E_Z}$ NPP$_{P_S}$ = 0.9 and 1 respectively) and had both smaller e–ratios$_{100m}$ of 0.03, despite comparable amounts of detritus produced during the three years ($\sum_{E_Z}$ Detritus = 19, 18 and 14 g C m^{-2} yr^{-1} for the first, second and third year respectively). Zoo–detritus were mainly produced by the small zooplankton. This is confirmed by the similar fractions of zoo–detritus during the first and second year (0.12 and 0.14) while the fraction of Z$_L$ dropped from 0.49 to 0.09. The panel C on Figure 4.5 also clearly shows no significant increase in the zoo–detritus following the peak of Z$_L$ visible on panel B.

Daily variability of the e–ratio appeared decoupled from NPP and carbon flux variations. For instance, the first four months at S2 (from August to November) displayed increases in both NPP and carbon flux. The NPP reached a maximum in November of the second year at S2, and the maximum carbon flux at 100 m was recorded 11 days later, showing that it was still increasing after the NPP reached its peak (Table 4.4). However, the daily e–ratio presented a decrease from August to October and then a long increase until June (Panel L) accompanied by small periods of decrease but did not reflect the seasonal variations of the NPP and associated carbon flux. Large increases in the e–ratio at the end of the third year at S1 and S2 (Panels F and L) were also observed and can be related to decreases in the NPP and the carbon flux at the end of the simulation. Another interesting trend on the relationship between NPP, carbon flux and e–ratio is given by bloom 3 occurring at S1–year2 (Panel A). In contrast to most other P$_S$ blooms showing a rapid transition between the ascending and descending phase of the NPP, this bloom exhibited a plateau at its maximum lasting almost two months. The associated plateau of the e–ratio (Panel F) displayed small oscillations that lasted for more than 5 months.

Bloom 7 lasted the longest time (11 months) and generated the highest P_L biomass accumulation ($\sum_{E_Z}$ Chl. *a* P_L = 19.46 g m^{-2} yr^{-1}). Although bloom 7 did not exhibit the highest maximum Chl. *a* nor maximum $\sum$ C $flux_{100m}$ (which belonged to bloom 2), it led to the highest e–ratio of 0.08.

4.4 Discussion

4.4.1 Effects of a detritus–based variable sinking velocity

This section discusses the effect of a variable detritus sinking velocity on the model behaviour. More specifically, we evaluate the need to include this type of relationship in future BGC models to account for the observed complexity of the sinking velocity of large phytodetrital aggregates.

A comparison of the cst–SV and var–SV model versions revealed direct and indirect effects of the variable sinking velocity. 'Direct effects' are defined here as the variations above or below the initial constant sinking velocity (fixed at 100 m d^{-1}) and their direct consequences on carbon export. They were explored by comparing the post–model run recalculations of a variable sinking velocity $SV_{recalc.}$ (see Section 'Model description'; dash lines on panels D–F and J–L of Fig. 4.6) with the cst–SV model version.

Direct effects

Over the whole simulation time (3 years at S1 and 2 years at S2) the recalculated detritus sinking velocity at the base of the E_Z was on average 130±36 m d^{-1} at S1 (maximum and minimum of 177 and 54 m d^{-1}) and 153±26 m d^{-1} at S2 (maximum and minimum of 179 and 86 m d^{-1}). This represents an overall average increase of 39±18 m d^{-1} above the initial 100 m d^{-1} set in the baseline model version. This average increase of less than 40 m d^{-1} had strong consequences on carbon flux estimations. The maximum C $flux_{100m}$ increased on average by 56±29 %. If considering the entire simulation time, the $\sum$ C $flux_{100m}$ increased by 45±23 %. E–ratios increased in the same proportions since the carbon flux was the only parameter in the ratio affected by the recalculations. This significant carbon flux increase is in the same range of variations than those observed between High Nutrient–Low Chlorophyll (HNLC) sites and naturally or artificially iron–fertilised sites in the Southern Ocean (Morris et al., 2007; Planchon

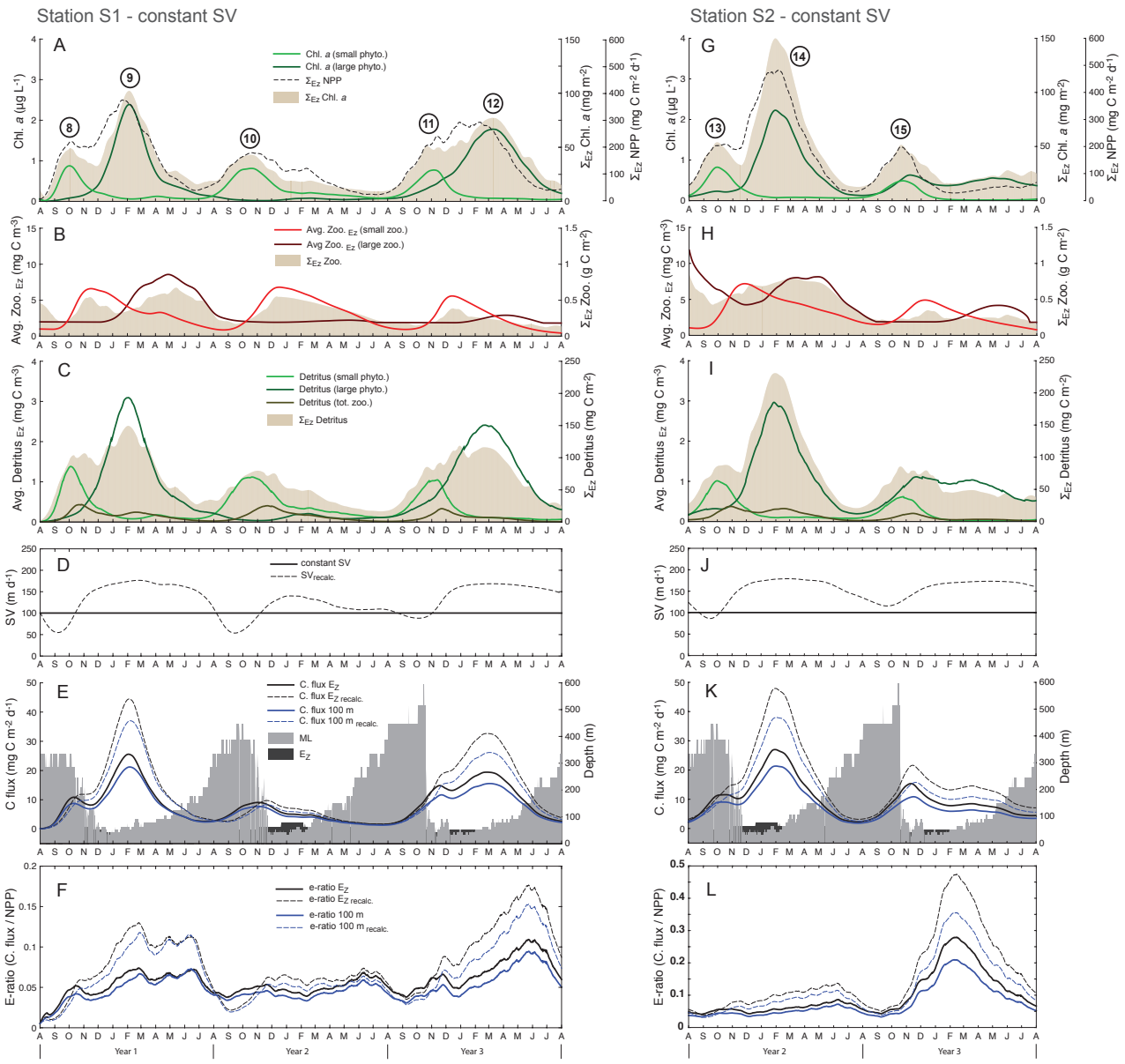

Figure 4.6: Time series of phytoplankton (sequential bloom i.d.s indicated) and zooplankton biomass, detritus concentration and sinking velocity and associated carbon export flux and e–ratio for the non–modified version of the model (cst–SV) at the two selected sites S1 (Panels A–F) and S2 (Panels G–L). A, G: surface chlorophyll *a* concentration (Chl. *a*) for the small and large phytoplankton; shaded area: Chl. *a* integrated over the euphotic zone (E_Z); dashed line: net primary productivity (NPP) integrated over the E_Z. B, H: small and large zooplankton biomass averaged over the E_Z; shaded area: total zooplankton biomass integrated over the E_Z. C, I: detritus concentration averaged over the E_Z. Shaded area: total detritus concentration integrated over the E_Z. D, J: detritus sinking velocity (SV). E, K: carbon flux (C flux); dark and light grey areas represent the mixed layer (ML) and E_Z respectively. F, L: e–ratio$_{depth}$ = C flux$_{depth}$ / $\sum_{E_Z}$ NPP.

et al., 2015; Savoye et al., 2008).

A constant sinking velocity of 100 m d^{-1} probably led to an underestimation of the carbon flux because it could not account for the overall predominance of the P_L–blooms over the P_S–blooms generated by the model. The modified model version reproduced the paradigm of a more efficient export in the case of detritus originated mainly from large phytoplankton (Assmy et al., 2013; Falkowski et al., 1998; Smetacek, 1999). When large phytoplankton dominated the productivity in the cst–SV model version (all years except S1–year2, Table 4.4) the e–ratio$_{100m}$ recalculated with a variable sinking velocity was on average increased by 55±4 %. Conversely, the e–ratio$_{100m}$ recalculated at S1–year2 was increased by only 5% compared to the cst–SV model version. This confirms that most of the misestimation of the carbon flux and efficiency made by the cst–SV model occurred when P_L dominated.

This result suggests that our sinking velocity parameterisation based on detritus composition and not size, reproduced accurately the possible influence of planktonic communities on carbon export. This is an important result, in particular because of the frequently observed discrepancies between the size of large phytodetritus (e.g. large marine aggregates constituting most of the export flux) and their sinking velocity (Alldredge and Gotschalk, 1988; Laurenceau-Cornec et al., 2015a) (Chapter 3), which potentially induce large misestimations of carbon export fluxes calculated from BGC models using a constant sinking velocity.

Additionally to the direct effects, the introduction of a variable sinking velocity changed the model behaviour over time by altering the conditions existing in the water column (e.g. phytoplankton concentration in the E_Z). These 'Indirect (or feedback) effects' are defined here as changes in planktonic community structure caused by the spatio–temporal variations of detritus sinking velocity. These effects are investigated by comparing the results from the cst–SV and var–SV model versions (Figs. 4.5 & 4.6).

Feedback effects

Two differences in model outputs are obvious when comparing Figures 4.5 and 4.6: the large bloom 12 occurring in the cst–SV model version (S1–year3) did not take place in the var–SV version. Conversely, the bloom 7 at S2–year3 occurred in the var–SV but not in the cst–SV

versions. It suggests that variations of the detritus sinking velocity induce variations of the conditions for the following productive season. This is clearly shown by the similarity of the initial successions from bloom 1 to bloom 2 and from bloom 8 to bloom 9 on the first year at S1, for which the modification of the sinking velocity affected only the export component of the model run and not the plankton community itself. By examining the two columns S1–var–SV–year1 and S1–cst–SV–year1 on Table 4.4 from phytoplankton to carbon export, it is noticeable that the earliest significant impact of the variable detritus sinking velocity concerns detritus composition and concentrations (also by comparing Panels C of Figures 4.5 and 4.6). The contribution of the P_L to the detritus decreased from 0.64 (cst–SV) to 0.49 (var–SV) (Table 4.4), while the fraction of P_S in the detritus increased from 0.25 (cst–SV) to 0.39 (var–SV). Interestingly it suggests that the modified model version simulates the retention of the P_S–detritus in the euphotic zone (until rapid export showed by the marked peaks in panel C of Fig. 4.5) and the export of the P_L–detritus. This is consistent with recent observations made during KEOPS2, where the lowest e–ratios were recorded at the sites where small setae–forming species dominated (i.e. *Chaetoceros Hyalochaete* spp., Laurenceau–Cornec et al., 2015b, Chapter 2). However, the var–SV version simulated unexpectedly a higher e–ratio (up to 0.05) associated with bloom 1. This is very likely due to the increase of the detritus sinking velocity due to the production of zoo–detritus following Z_S grazing on P_S.

These slight differences in model results during the first year set different conditions for the next productive season and resulted in large variations of planktonic community structure the following years. A notable alteration of the planktonic community by feedback effect is the disappearance of bloom 12 in the var–SV version. Two possible causes were explored: the limitation of P_L production by nutrient limitation ('bottom–up') and the control of P_L biomass accumulation by the Z_L grazing pressure ('top–down'). On the first day of the third year, the average nitrate concentration in the euphotic zone was very similar in the var–SV and cst–SV model version (179.1±0.0 and 185.8±0.0 mg m^{-3} respectively). It is very unlikely that nutrient limitation was the factor precluding the bloom 12 to occur, knowing that the largest P_L bloom recorded over all simulations (bloom 7; $\sum_{E_Z}$ Chl. a P_L = 19.46 g m^{-2} yr^{-1}) occurred with lower initial average nitrate concentrations in the euphotic zone of 170.4±0.0 mg m^{-3}.

The ideas developed by Riley (1946) and Cushing (1959) giving a large importance to the predator–prey interactions in controlling bloom occurrence, have been recently re–emphasized (Banse, 1992; Behrenfeld, 2010, 2014; Behrenfeld and Boss, 2014; Behrenfeld et al., 2013) in comparison to the classical Sverdrup's Critical Depth Hypothesis (CDH) which focuses on the influence of mixed layer light levels (Sverdrup, 1953). In this 'top–down' control of bloom occurrence subtle imbalances in the predator–prey relations over winter set the conditions for bloom initiation. At the end of the winter preceding the bloom 3 (Fig. 4.5) Z_S displayed a steady biomass level, and P_S initiated a biomass accumulation two months later than in the cst–SV model version (Table 4.3, bloom 3 initiated in September, bloom 10 initiated in July). Differences in export production during the first year (see above) increased the ratios Z_L:P_L of the second year in the var–SV version ($\sum_{E_Z}$ ratio Z_L:P_L = 65.2 in the var–SV and 36.8 g Chl *a* g C^1 in the cst–SV) possibly precluding the occurrence of the bloom.

4.4.2 The relationship between NPP and carbon flux

The difficulty of predicting the efficiency of a given ecosystem structure at exporting carbon, arises in part from the possible decoupling between primary productivity and associated carbon flux. Most of the studies from which either correlations or discrepancies between NPP and carbon flux were noted, compared these two parameters on a monthly to annual basis (Betzer et al., 1984; Brix et al., 2006; Buesseler, 1998; Eppley and Peterson, 1979; Lutz et al., 2007; Maiti et al., 2013; Pace et al., 1987; Suess, 1980; Wassmann, 1990), relying on integrations of daily rates, most often measured in the productive part of the seasonal cycle. This is because of the extreme difficulty of measuring the primary productivity and associated carbon flux at high temporal resolution in the field and especially in the Southern Ocean. In contrast, models can simulate the NPP and 'measure' the related carbon flux (assuming a time lag between them) on a high spatio–temporal resolution to study their close interrelated variations.

Figure 4.7 is a representation of the daily NPP and concurrent carbon flux for the three years at S1 (Panels A and B) and the two years at S2 (Panels C and D). NPP vs C flux relationships for the cst–SV version are also shown for information. The paths followed by the NPP vs C flux relationship (hereafter called 'loops') illustrate how the carbon flux varies in relation to net primary productivity during several complete seasonal cycles. These loops have been poorly documented in the literature using in situ data, and most often have been described in conceptual

or modelling studies (Brix et al., 2006; Henson et al., 2015; Wassmann, 1993, 1998).

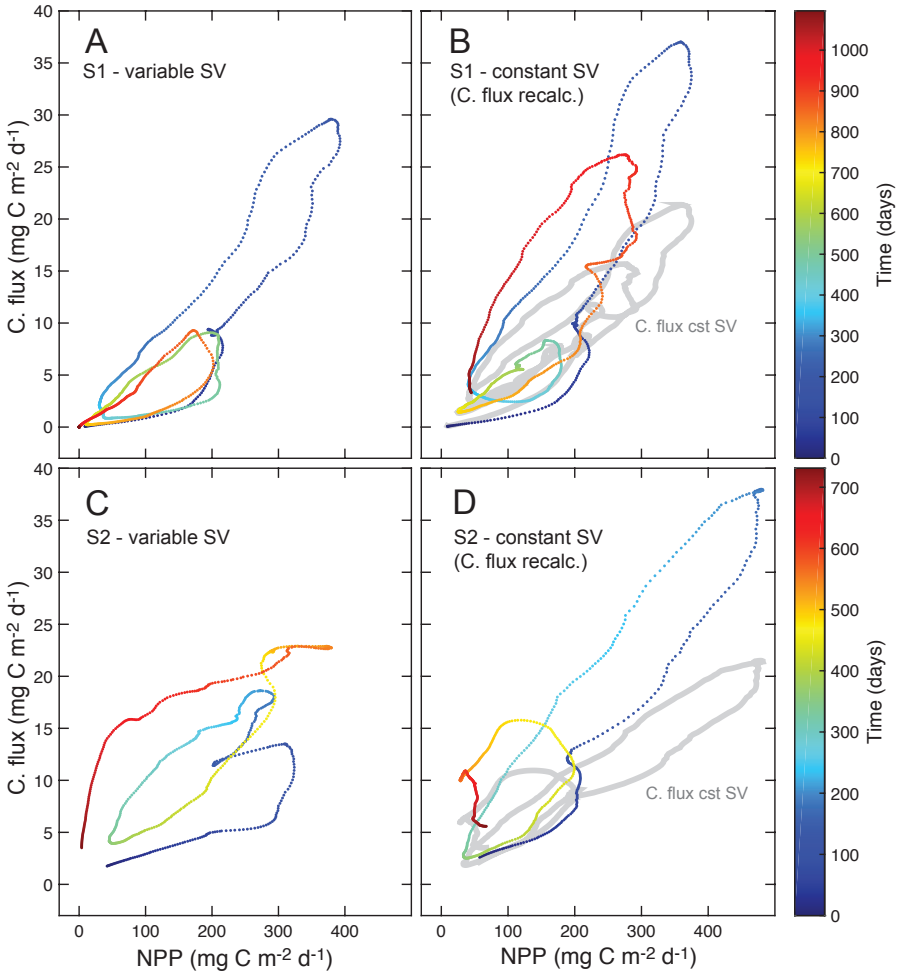

Figure 4.7: Daily relationship between net primary productivity (NPP) integrated over the euphotic zone and carbon flux (C flux) calculated at 100 m for the whole period at site 1 (S1, 3 years) and site 2 (S2, 2 years). A, C: data from the var–SV model version. B, D: data from the cst–SV model version with a carbon flux re–calculated post–model run using a variable sinking velocity ($SV_{recalc.}$); grey lines represent the same relationship from the cst–SV model version without re–calculation.

Each loop is composed of three main phases during which the production and carbon flux increase (phase 1), and then decrease (phase 3) after a transition phase (phase 2). Wassmann (1998) suggested in a conceptual context that the shape and area of the loops are indicators of the type of food web. He contrasted 'retention food webs' which recycle organic matter and nutrient in the euphotic zone (low export efficiency) to 'export food webs' which tend to maximise the losses of most of the new production via downward flux (high export efficiency) (Dugdale and Goering, 1967; Eppley and Peterson, 1979).

An export food web is characterised by a small loop area with a steep slope illustrating that the export flux is well coupled with the primary productivity. At the opposite a wide loop with a gentle slope shows that productivity and export are somewhat decoupled and is characteristic

of a retention food web. Variations aside these general paths present the largest interest since they characterise how the specificity of the ecosystem influence the relationship between NPP and C flux.

Figure 4.7 shows a diversity of pathways delineating different loop sizes, slopes and areas. For instance the blue loop on panel A (S1–var–SV–year1) is narrow, long and symmetric, while the red loop (S1–var–SV–year3) is much smaller and asymmetric. These two loops are associated with two years of the simulation when plankton communities were different. The first year is characterised by the succession P_S to P_L (from bloom 1 to bloom 2), while only a P_S bloom (bloom 4) took place on the last year. Similarly, Panel C shows the two years at S2. The first loop (blue) is related to the bloom 5 and is not closed due to the succession to the bloom 6 causing the productivity to increase again (this small inflexion was also visible on the first loop of the Panel A). This rapid graphical description of a few relationships between NPP and C flux suggests a high potential to aid in explaining the links between different planktonic community structures and carbon export modes.

Figure 4.8 shows the same relationship for each individual bloom with a temporal resolution of 7 days. Each NPP vs C flux relationships are classified according to the bloom category they belong to (see 'Results' Section) to facilitate the link between planktonic community structure and food web type. All blooms from category A show non–closing loops due to the following P_L–bloom precluding a direct return of the NPP and C flux to low levels (see above). However, even if the seasonal relationship is not complete for this bloom category, one feature is evident: the beginning of the cycle is characterised by a gentle slope where the NPP increases much faster than the carbon flux (phase 1; slope $\sim$0.02), then a stronger export flux is responsible for an increase of the slope and thus a widening of the loop (phase 2; slope $\sim$0.5). During the last phase, the NPP decreases more rapidly than the carbon flux following again a gentle slope (phase 3; slope $\sim$0.01). Blooms from the category B present NPP vs C flux relationships with broadly similar steep slopes in the ascending and descending phases ($\sim$0.08) and a short transition phase. It results in a very narrow and elongated loop. In category C, the first phase is very similar to the one observed in category A (slope $\sim$0.01). However, the transition phase presents a very distinctive increase of the carbon flux associated with an almost constant NPP (or even decreasing) resulting in a vertical slope. The decreasing phase presents a straight return

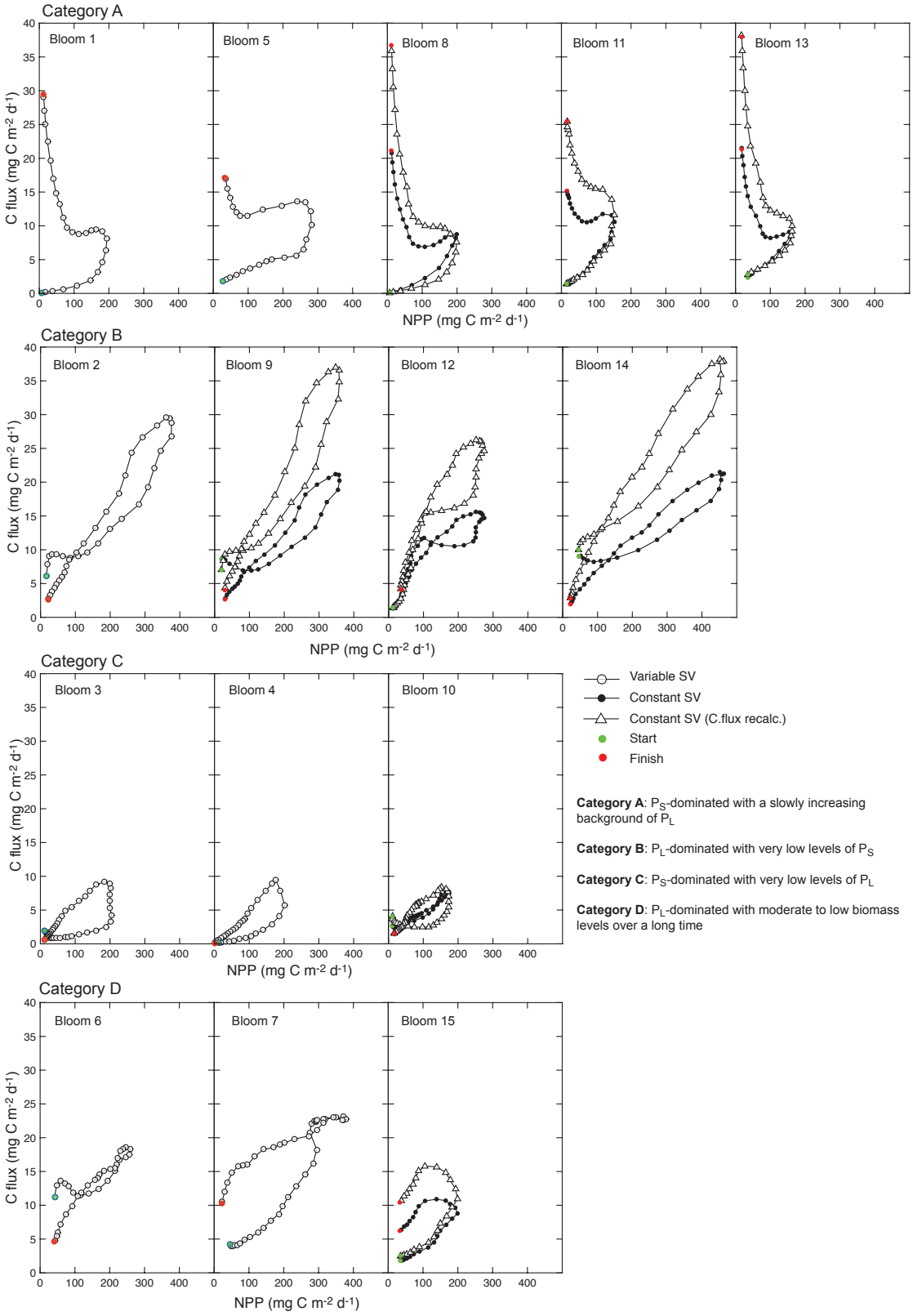

Figure 4.8: Weekly relationship (7 days between two data points) between net primary productivity (NPP) integrated over the euphotic zone and carbon flux (C flux) calculated at 100 m for each bloom simulated by the two versions of the model. Blooms are classified using the categories defined in the 'Results' Section. Start and finish dots (green and red respectively) indicate the initiation and termination times of the bloom considered. White circles: var–SV model version; black circles: cst–SV model version; triangles: same relationship with carbon fluxes re–calculated post–model run using a variable sinking velocity ($SV_{recalc.}$).

to the initial levels of NPP and carbon flux with a moderate slope (∼0.05). The category D presents singular features with a steep increasing phase (∼0.07) which brings the relationship to high fluxes of carbon associated with moderate levels of NPP. The transition phase is long and presents two additional phases: the NPP starts to decrease while the carbon flux still increases, then the carbon flux is almost constant while the NPP increases. Finally a sharp decrease of the carbon flux is combined with a decrease of the NPP.

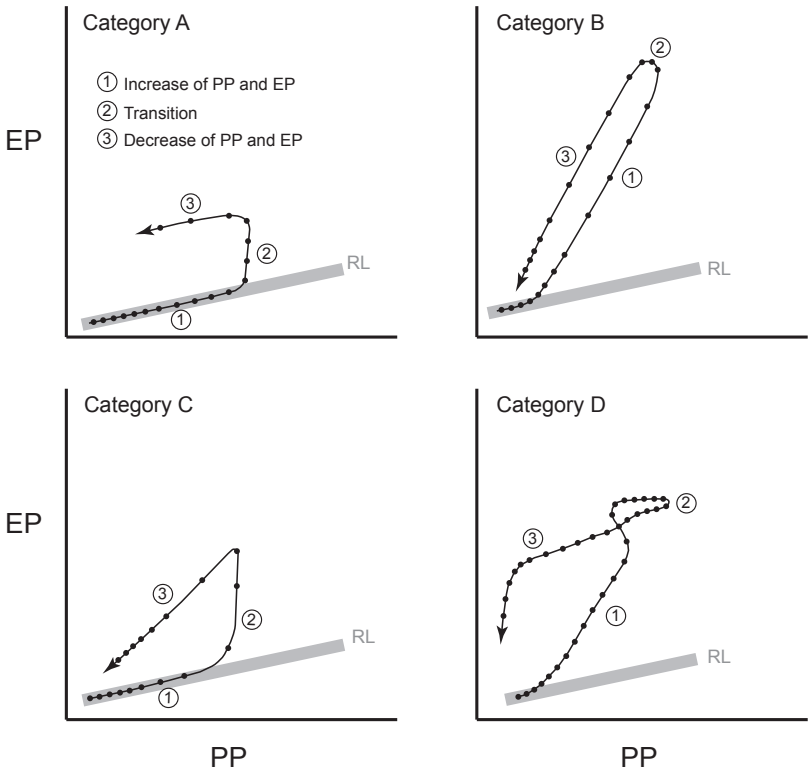

Figure 4.9: Conceptual diagrams showing possible paths of the primary production (PP) vs export production (EP) relationship encountered in the four categories of blooms simulated by the model. Three phases of the relationship (increase, transition, decrease) are indicated in each category. Two successive black dots are similarly spaced in time for each relationship allowing comparisons of the rates of variations during the three phases in each case. RL: retention line.

Figure 4.9 synthesises the four types of loops identified in the form of conceptual diagrams showing the three distinct phases: (1) the increase phase where the NPP and flux of carbon increase, (2) the transition phase representing the shift between increase and decrease and, (3) the decrease phase where the NPP and carbon flux both decrease. The grey line, called 'retention line' (Wassmann, 1998), traces the pathway where the system functions as a retention food web where the production losses are minimised. The processes which moves the relationship out of this line (by changing the slope) are thus responsible for changes in the efficiency of the

system to export organic carbon. Based on this conceptual frame, the next section proposes an explanation of the four main results identified (see 'Results' section):

i. Different planktonic communities can lead to similar carbon export features

ii. In the case of P_S blooms, carbon export depends upon zooplankton grazing and is driven by fecal material (low efficiency). The time lag between phytoplankton production and export (retention time) is increased compared to the direct export of PL blooms (high efficiency).

iii. The highest e–ratio is associated with the largest and longest P_L bloom.

iv. The e–ratio presents complex daily variations not easily related to NPP and carbon flux variations.

4.4.3 Ecosystem controls on the NPP vs carbon flux relationship

Different phytoplankton communities follow different paths of the relationship NPP vs C flux. Despite different pathways, an integration of the productivity and carbon export over the whole year can lead to similar export efficiencies. Combined data showing planktonic community dynamics and related carbon export efficiency in the Southern Ocean are rare. Results from the KEOPS2 study showed similar carbon export efficiencies at different sites where the phytoplankton communities were different. The carbon export efficiencies [e–ratio = particulate organic carbon (POC) flux at 100 m : $\sum_{EZ}$ NPP] measured over and off the Kerguelen Plateau, were respectively 0.01±0.004 and 0.03±0.02 (so similar within the uncertainties; Laurenceau–Cornec et al., 2015b, Chapter 2). The bloom at the on–plateau station was dominated by the small diatom *Chaetoceros Hylaochaete* spp. At the off–plateau station, the phytoplankton assemblage was dominated by a mix of *Thalassionema nitzschioides*, *Chaetoceros Hyalochaete* spp. and small centric diatoms. Annual budgets of carbon export efficiency were based on the integration of the daily productivities and associated carbon flux, and thus depend upon the pathway followed by the relationship NPP vs C flux during the period of integration. The two bloom successions compared here (blooms 1 to 2 and 5 to 6) belong to different categories. However the biomass levels associated with the small and large phytoplankton were different: the fraction

of P_S increased while the P_L decreased (see 'Results' section). One could have expected this modification to lead to a decrease of the efficiency, since the efficient exporters (P_L) were in smaller proportion than the less efficient exporters (P_S). But the panels 'Category A' on Figure 4.8, shows that while the blooms 5 and 1 had somewhat different pathways, bloom 5 reached higher levels of NPP and C flux. Most importantly, this bloom also had a faster decreasing phase combining a higher C flux with a lower NPP, so in a domain of high export efficiency. The same comparison between blooms 2 and 6 shows that both had straight narrow loops with similar slopes, suggesting that the efficiency was similar for these two blooms despite their different biomass levels.

Conversely, model results also showed that different types of phytoplankton led to contrasted efficiencies, reproducing the paradigm that large phytoplankton (e.g. the large heavily–silicified diatoms in the Southern Ocean) are the most efficient exporters of carbon (Assmy et al., 2013; Boyd, 2013; Smetacek et al., 2012). Like many others, our model suggested that large phytoplankton export their POC preferentially by direct fast sinking and escape zooplankton grazing (Boyd and Newton, 1999; Laws et al., 2000; Michaels and Silver, 1988). A comparison of the shapes of the NPP vs C flux for the category A and B (Fig. 4.9) clearly confirms the view that P_L–dominated blooms worked as export food webs with an early 'take off' out of the retention line (i.e. the point where the NPP vs C flux relationship leaves the retention line) and a straight and narrow loop presenting a steep slope showing a tight coupling between production and export. On the contrary, the P_S–blooms worked as retention food webs with a long period along the retention line and a late take off. An essential question remains: what process is responsible for the late take off in the case of the small phytoplankton, or in other term, what mechanism retains the small phytoplankton in the euphotic zone?

Variations in particle residence time in the mixed layer (or retention time) have been attributed to gas evolution within aggregates affecting particle buoyancy (Karl and Tilbrook, 1994; Riebesell, 1992), and levels of intracellular carbohydrates content related to algal physiological stress (Fisher and Harrison, 1996). Zooplankton grazing has also been suggested to either increase organic matter retention in the surface layer or promote its export via fast–sinking fecal pellets (Wassmann, 1998; Wexels Riser et al., 2007). Recent studies tend to confirm this dual

view and zooplankton have been shown to work in close coupling with bacteria in the recycling loop (Giering et al., 2014), or to increase the export production in significant proportions (Berline et al., 2011). This versatile role of zooplankton grazing is probably in a large part responsible for most of the deviations observed from the retention line and should be regarded as a key factor in the control of the seasonal NPP vs C flux relationship. Large zooplankton (e.g. krill) tend to produce large loose fecal pellets prone to rapid degradation and thus are likely to be poor exporters of carbon (Suzuki et al., 2003). Conversely, smaller zooplankton (e.g. copepods) produce tight fecal pellets protected by a complete peritrophic membrane (Gauld, 1957; Martens, 1978; Yoon et al., 2001) more likely to carry efficiently the carbon to depth (assuming limited coprophagy, coprorhexy and coprochaly).

Results from the model confirm that when the biomass is dominated by small phytoplankton, zooplankton grazing is the main process driving the export. For instance, grazing on the bloom 3 induced the production of zoo–detritus which started around mid–November. This time coincides with the rapid increase of detritus sinking velocity and carbon flux. When the biomass was dominated by large phytoplankton, the grazing produced comparatively much less detritus than for the small zooplankton grazing (Fig. 4.6 and 4.5). In this case zooplankton grazing may reduce the efficiency of carbon export by inducing respiration losses without benefit of a fecal pellet–mediated export. Without contradicting it, this view differs slightly from the conceptual scheme produced by Wassmann (1993, 1998) on the effect of zooplankton grazing pressure on the NPP vs C flux loop. In those studies the zooplankton grazing flattens the loop forcing it to stay close to the retention line. Results presented here, however, suggests that zooplankton grazing on small phytoplankton, widens the loop by promoting the initiation of an export event.

The highest efficiency recorded over all model simulations corresponded to the last year at S2 (bloom 7). Interestingly, the relationship NPP vs C flux for this bloom does not describe a straight narrow and steep loop as one would expect in the case of the highest export efficiency. It suggests that the slope and the shape of the loop may not be the only descriptors of the export efficiency. The singularity of this bloom compared to others is the additional loop visible during the transition phase at the extremity of the main path (Fig. 4.8), and corresponding to a long time (∼3 months) during which the productivity increased at a very slow rate while the

carbon flux was still at a high value. Every day spent in this high efficiency domain of the NPP vs C flux diagram participated to the increase of the integrated e–ratio. It suggests the crucial importance of rates of increase or decrease of the NPP compared to its associated carbon flux in the control of export efficiency. It also explains why the variations of the e–ratio appears decoupled from the primary productivity (see 'Results' section).

Figure 4.10 shows the variations of the e–ratio for different variation rates (slopes) of NPP and carbon flux from the model output and for a large range of theoretical situations. Examples are provided for blooms 2, 3 and 7 (the initial levels of carbon flux and NPP were chosen arbitrarily at 50 and 300 mg C m^{-2} d^{-1} respectively to allow large theoretical decreases). Two slopes are indicated for each bloom and represent different phases of the seasonal cycle (increasing, transitional or decreasing). The figure indicates for instance that in the increasing phase of bloom 7 (green line) the e–ratio was steady in spite of NPP and C flux both increasing but at different rates. Also, in the decreasing phase of bloom 7 (cyan line), the NPP and the C flux were decreasing but the e–ratio was increasing due to the large difference of slope between the NPP and C flux decrease. These differences of rate variations originated from decoupling between NPP and carbon flux. It highlights an aspect essential to the understanding of the discrepancies reported in the literature between NPP and e–ratio. As reiterated recently by (Henson et al., 2015), the decoupling between primary production and export can result in large variations of the e–ratio and extrapolations of the global carbon export from few instantaneous measurements can result in large errors. Figure 4.11 shows several situations where the time and frequency of the measurements of NPP and concurrent carbon flux can lead to situations for which the e–ratio can be wrongly interpreted. Sparse observations made at different moments of the seasonal cycle will lead to either positive, negative or lack of correlation between the NPP and C flux, and consequently the e–ratio. The figure also shows that the risk of errors could be larger in the case of P_S blooms because of the largest temporal decoupling between NPP and carbon flux originated from the long initial path along the retention line. Issues arising from sparse observations of the NPP and C flux have been known for decades but costs and technical difficulties of field measurements still preclude a better temporal resolution. It appears that a single measurement of the NPP and concurrent C flux should be accompanied by a metric of their decoupling, indicative of the position of the measurement in the NPP vs C flux relationship.

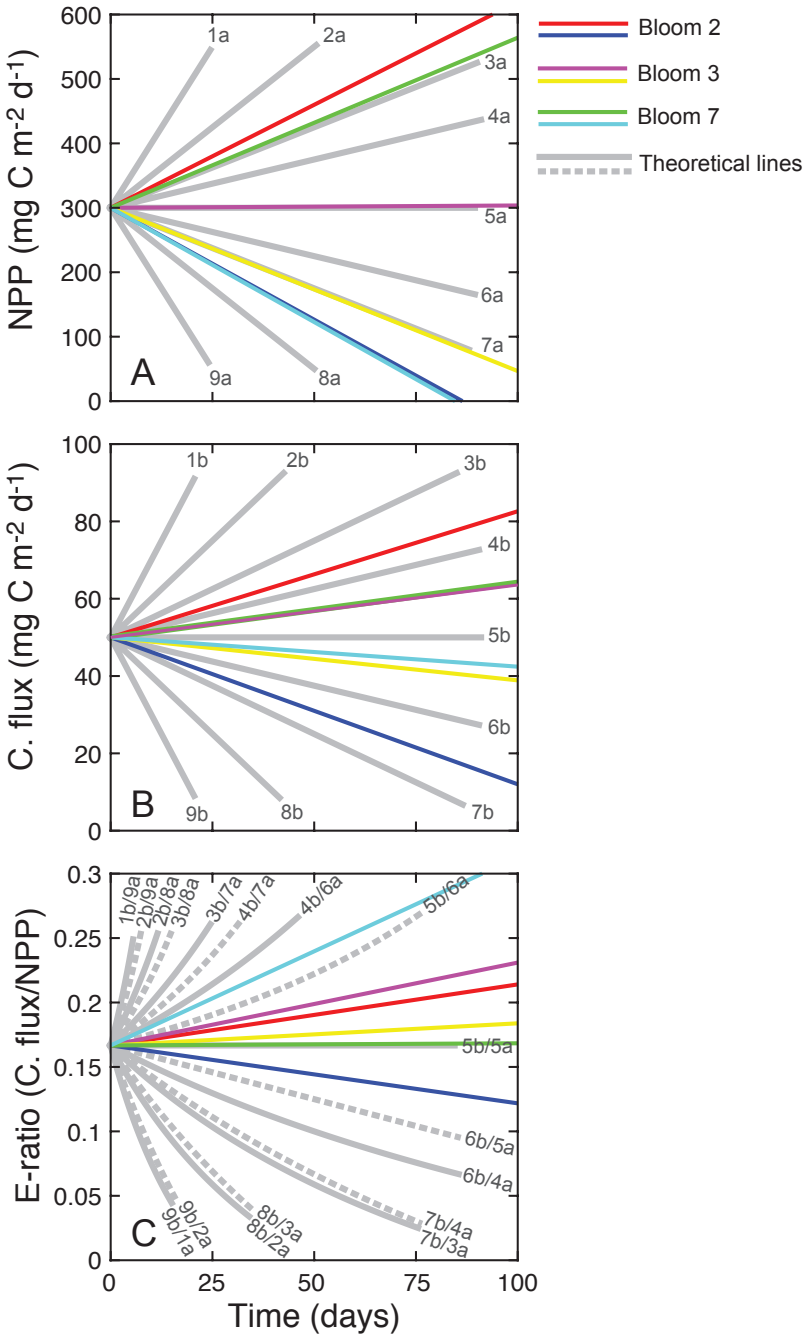

Figure 4.10: Relative rates of variations of net primary productivity (NPP, Panel A), carbon flux (C flux, Panel B) and export efficiency (e–ratio, Panel C) calculated as the ratio between NPP and C flux. Colour lines indicate rates of variations for different phases of the blooms 2, 3 and 7 (var–SV model version). Each line show the relative variations of the slope of the e–ratio for different combinations of NPP and C flux slopes. Example: the green line on Panel C is the ratio of the green lines in Panel B (C flux) and Panel A (NPP). Similarly theoretical lines in grey show the effect on the e–ratio of a large range of slope differences between NPP and C flux. Example: line 6b/5a on Panel C is the ratio between line 6b on Panel B and line 5a on Panel A. The figure illustrates the possible positive, negative or absent correlation between NPP and e–ratio depending on subtle slopes differences between NPP and C flux.

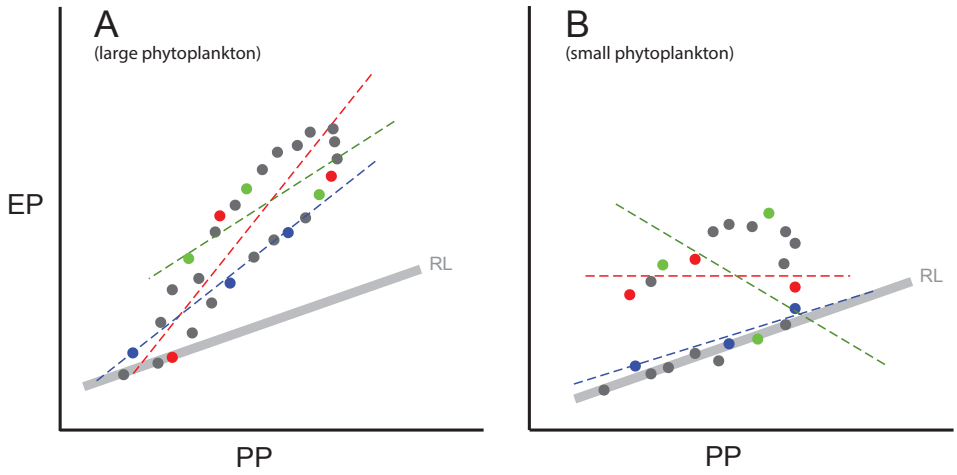

Figure 4.11: Conceptual diagram showing the importance of observation timing and frequency along the seasonal primary production (PP) vs export production (EP) relationship for large (A) and small (B) phytoplankton. RL: retention line. The figure suggests that different sets of observation (blue, green and red) of the same bloom and associated carbon export can lead to different interpretations of the correlation between PP and EP. The figure also suggests that the higher coupling between PP and EP in the case of large phytoplankton blooms could minimise the risk of misinterpretations compared to small phytoplankton blooms.

Figure 4.12 shows all the daily relationships NPP vs C.flux for all simulations (var–SV, cst–SV and recalculations). In the Panel A, the colour of each point correspond to its e–ratio based on its position in the NPP vs carbon flux domain. This is the traditional use of the e–ratio to estimate the efficiency based on a fixed value of NPP and carbon flux. The efficiencies attributed to the different phases of the seasonal cycle depend then on the location of each data point and not on the stage of the seasonal cycle at which the observation was made. Therefore, phases during which the efficiency relative to the seasonal cycle is maximal [e.g. (a) on the Panel A, fig. 4.12], can have an absolute low efficiency while phases of low relative efficiency [e.g. (b) on the Panel A, fig. 4.12], will be associated to absolute high efficiencies. The dynamic aspect of the period of low and high efficiencies depending on the decoupling between NPP and C flux is thus missed. On panel B the colour of each data point represents an e–ratio accounting for the slope of the relationship NPP vs C flux calculated for a determined time lag Δt before and after the observation (called hereafter 'e–ratio$_{sl.\Delta t}$', eq. 4.29).

$$e\text{-}ratio_{sl.\Delta t}(t) = \frac{Cflux_{\,t+\Delta t/2} - Cflux_{\,t-\Delta/2}}{npp_{\,t+\Delta t/2} - npp_{\,t-\Delta t/2}} \tag{4.29}$$

In this representation the efficiency depends on the time period within the seasonal cycle when it is estimated. In the phases when the path leaves the retention line (increase of the slope), the e–ratio$_{sl.\Delta t}$ displays higher values reflecting a phase where the carbon is exported more efficiently. At the opposite the e–ratio$_{sl.\Delta t}$ will take negative values in the decreasing phase of the cycle, when both the NPP and the carbon flux decrease.

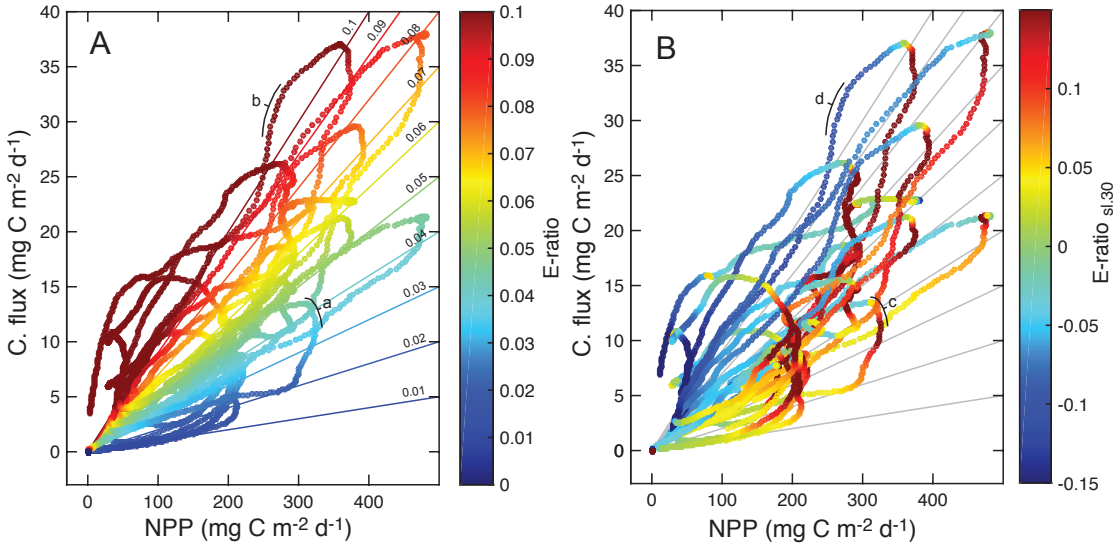

Figure 4.12: Relationship between net primary productivity (NPP) integrated over the euphotic zone and carbon flux (C flux) calculated at 100 m with a 12 hours–time interval for all model simulations. A: colours indicate values of the e–ratio calculated as the ratio between C flux and NPP. B: colours indicate values of the e–ratio$_{sl.30}$ representing at each data point the slope of the relationship calculated from 30 days before and after the time considered. The figure illustrates that the e–ratio (Panel A) is not affected by the phase of the relationship but by its position in the diagram NPP vs C flux. Example: (a) indicates a phase when the NPP decreases and C flux increases (high efficiency) but displays low e–ratios; conversely (b) indicates a strong decrease of the C flux associated with a small decrease of the NPP (low efficiency) but displays high e–ratios. On panel B, the e–ratio$_{sl.30}$ accounting for the slope of the relationship is high when the C flux increases faster than NPP (c), and low when it decreases faster than NPP (d).

This dynamic measure of the efficiency accounts for the decoupling between NPP and C flux at the time of the observation. Although it cannot be used to calculate an absolute integrated efficiency, it gives an instantaneous efficiency of the system considered in relation to its position along bloom evolution. The choice of the time lag Δt is important since it determines the duration over which the rates of variation of NPP and C flux will be calculated. A too long time lag including several phases of the bloom cycle (e.g. end of increase, transition and start of decrease) will lead to errors on the estimation of the rates of NPP and C flux changes. On the contrary, a too short time lag might not represent accurately the temporal decoupling between NPP and C flux. Concepts discussed here suggest that the dominant type of phytoplankton encountered in a bloom (P_S or P_L) is an important factor to consider when deciding

the frequency of measurements of NPP and C flux. An intensification of combined observations of the NPP vs C flux relationship and associated phytoplankton bloom types will probably help establish general patterns in the Southern Ocean. These could then be used to infer more global predictions of carbon export efficiency from a limited number of measurements, assuming an accurate understanding of the dynamic of the system at the time of these sparse observations.

4.5 Conclusion

Our study confirmed several aspects central to the relationship between carbon export efficiency and ecosystem structure. Here are some considerations that may improve our understanding of the BCP efficiency.

i. A variable SV of detritus calculated from the relative contributions of different plankton sources could improve the accuracy of carbon flux estimations made by BGC models. Our study confirmed that a constant sinking velocity underestimates or overestimates the carbon flux, depending on the type of phytoplankton bloom considered. Additional regional datasets of phytoplankton species content in phytodetritus and associated sinking velocity are needed to establish empirical relationships valid across different ecosystem structures. Without considering these regional relationships, global estimation of carbon export efficiency could still suffer large uncertainties.

ii. When exploring the dynamic of a bloom dominated by small phytoplankton, the time lag between two successive observations should be as shortest as possible to avoid any misinterpretation (Fig. 4.11). It is less crucial in the case of large phytoplankton–dominated blooms for which there is a close temporal coupling between production and export.

iii. The decoupling between production and export occurring in retention food webs appears responsible for the large discrepancies observed in the correlation between NPP and e–ratio. Rather than using absolute estimation of the e–ratio, an understanding of ecosystem controls on the efficiency of carbon export would possibly benefit from including metrics of the dynamic of the system at the time of the observation.

Acknowledgments

We thank the Environmental Modelling group at CSIRO, who developed the coupled physical–biogeochemical model. In particular, we thank Dr. Mark Baird, leader of the Coastal Environmental Modelling team at CSIRO, for his help in model parameterisation and invaluable advices. Thanks to Dr. Marion Fourquez (IMAS, ACE CRC) for her inspiring ideas on the graphical representation used in Figure 4.12.

References

Alldredge, A. L. and Gotschalk, C.: In Situ Settling Behavior of Marine Snow, Limnology and Oceanography, 33, 339–351, doi:10.2307/2837008, 1988.

Assmy, P., Smetacek, V., Montresor, M., Klaas, C., Henjes, J., Strass, V. H., Arrieta, J. M., Bathmann, U., Berg, G. M., Breitbarth, E., Cisewski, B., Friedrichs, L., Fuchs, N., Herndl, G. J., Jansen, S., Krägefsky, S., Latasa, M., Peeken, I., Röttgers, R., Scharek, R., Schüller, S. E., Steigenberger, S., Webb, A., and Wolf-Gladrow, D.: Thick-shelled, grazer-protected diatoms decouple ocean carbon and silicon cycles in the iron-limited Antarctic Circumpolar Current, Proceedings of the National Academy of Sciences, 110, 20 633–20 638, doi:10.1073/pnas.1309345110, 2013.

Baird, M. and Emsley, S.: Towards a mechanistic model of plankton population dynamics, Journal of Plankton Research, 21, 85–126, doi:10.1093/plankt/21.1.85, 1999.

Banse, K.: Grazing, Temporal Changes of Phytoplankton Concentrations, and the Microbial Loop in the Open Sea, in: Primary Productivity and Biogeochemical Cycles in the Sea, edited by Falkowski, P. G., Woodhead, A. D., and Vivirito, K., vol. 43 of *Environmental Science Research*, pp. 409–440, Springer US, 1992.

Behrenfeld, M. J.: Abandoning Sverdrup's Critical Depth Hypothesis on phytoplankton blooms, Ecology, 91, 977–989, doi:10.1890/09-1207.1, 2010.

Behrenfeld, M. J.: Climate-mediated dance of the plankton, Nature Clim. Change, 4, 880–887, doi:10.1038/nclimate2349, 2014.

Behrenfeld, M. J. and Boss, E. S.: Resurrecting the Ecological Underpinnings of Ocean Plankton Blooms, Annual Review of Marine Science, 6, 167–194, doi:10.1146/annurev-marine-052913-021325, 2014.

Behrenfeld, M. J., Doney, S. C., Lima, I., Boss, E. S., and Siegel, D. A.: Annual cycles of ecological disturbance and recovery underlying the subarctic Atlantic spring plankton bloom, Global Biogeochemical Cycles, 27, 526–540, doi:10.1002/gbc.20050, 2013.

Berline, L., Stemmann, L., Vichi, M., Lombard, F., and Gorsky, G.: Impact of appendicularians on detritus and export fluxes: a model approach at DyFAMed site, Journal of Plankton Research, 33, 855–872, doi:10.1093/plankt/fbq163, 2011.

Betzer, P. R., Showers, W. J., Laws, E. A., Winn, C. D., DiTullio, G. R., and Kroopnick, P. M.: Primary productivity and particle fluxes on a transect of the equator at 153°W in the Pacific Ocean, Deep Sea Research Part A. Oceanographic Research Papers, 31, 1–11, doi:10.1016/0198-0149(84)90068-2, 1984.

Bindoff, N., Stott, P., AchutaRao, K., Allen, M., Gillett, N., Gutzler, D., Hansingo, K., Hegerl, G., Hu, Y., Jain, S., Mokhov, I., Overland, J., Perlwitz, J., Sebbari, R., and Zhang, X.: Detection and Attribution of Climate Change: from Global to Regional. from Global to

Regional., in: Climate Change 2013: The Physical Science Basis. Contribution of Working Group I to the Fifth Assessment Report of the Intergovernmental Panel on Climate Change, edited by Stocker, T., Qin, D., Plattner, G.-K.and Tignor, M., Allen, S., Boschung, J., Nauels, A., Xia, Y., Bex, V., and Midgle, P., Cambridge University Press, United Kingdom and New York, NY, USA, 2013.

Bopp, L., Resplandy, L., Orr, J. C., Doney, S. C., Dunne, J. P., Gehlen, M., Halloran, P., Heinze, C., Ilyina, T., Séférian, R., Tjiputra, J., and Vichi, M.: Multiple stressors of ocean ecosystems in the 21st century: projections with CMIP5 models, Biogeosciences, 10, 6225–6245, doi:10.5194/bg-10-6225-2013, 2013.

Boyd, P. and Newton, P.: Evidence of the potential influence of planktonic community structure on the interannual variability of particulate organic carbon flux, Deep Sea Research Part I: Oceanographic Research Papers, 42, 619–639, doi:10.1016/0967-0637(95)00017-Z, 1995.

Boyd, P. and Newton, P.: Does planktonic community structure determine downward particulate organic carbon flux in different oceanic provinces?, Deep Sea Research Part I: Oceanographic Research Papers, 46, 63 – 91, doi:10.1016/S0967-0637(98)00066-1, 1999.

Boyd, P. W.: Diatom traits regulate Southern Ocean silica leakage, Proceedings of the National Academy of Sciences, 110, 20 358–20 359, doi:10.1073/pnas.1320327110, 2013.

Boyd, P. W. and Stevens, C. L.: Modelling particle transformations and the downward organic carbon flux in the NE Atlantic Ocean, Progress in Oceanography, 52, 1–29, doi:10.1016/S0079-6611(02)00020-4, 2002.

Boyd, P. W., Sherry, N. D., Berges, J. A., Bishop, J. K. B., Calvert, S. E., Charette, M. A., Giovannoni, S. J., Goldblatt, R., Harrison, P. J., Moran, S. B., Roy, S., Soon, M., Strom, S., Thibault, D., Vergin, K. L., Whitney, F. A., and Wong, C. S.: Transformations of biogenic particulates from the pelagic to the deep ocean realm, Deep Sea Research Part II: Topical Studies in Oceanography, 46, 2761–2792, doi:10.1016/S0967-0645(99)00083-1, 1999.

Brix, H., Gruber, N., Karl, D. M., and Bates, N. R.: On the relationships between primary, net community, and export production in subtropical gyres, Deep Sea Research Part II: Topical Studies in Oceanography, 53, 698 – 717, doi:10.1016/j.dsr2.2006.01.024, 2006.

Buesseler, K. O.: The decoupling of production and particulate export in the surface ocean, Global Biogeochemical Cycles, 12, 297–310, doi:10.1029/97GB03366, 1998.

Buesseler, K. O. and Boyd, P. W.: Shedding light on processes that control particle export and flux attenuation in the twilight zone of the open ocean, Limnology and Oceanography, 54, 1210–1232, doi:10.4319/lo.2009.54.4.1210, 2009.

Carlotti, F., Jouandet, M.-P., Nowaczyk, A., Harmelin-Vivien, M., Lefèvre, D., Guillou, G., Zhu, Y., and Zhou, M.: Mesozooplankton structure and functioning during the onset of the Kerguelen phytoplankton bloom during the Keops2 survey, Biogeosciences Discussions, 12, 2381–2427, doi:10.5194/bgd-12-2381-2015, 2015.

Cavan, E. L., Le Moigne, F. A. C., Poulton, A. J., Tarling, G. A., Ward, P., Daniels, C. J., Fragoso, G. M., and Sanders, R. J.: Attenuation of particulate organic carbon flux in the Scotia Sea, Southern Ocean, is controlled by zooplankton fecal pellets, Geophysical Research Letters, 42, 821–830, doi:10.1002/2014GL062744, 2015.

Corner, E. D. S., Head, R. N., and Kilvington, C. C.: On the nutrition and metabolism of zooplankton. VIII. the grazing of *Biddulphia* cells by *Calanus helgolandicus*, Journal of the Marine Biological Association of the United Kingdom, 52, 847–861, doi:10.1017/S0025315400040595, 1972.

Cushing, D. H.: The seasonal variation in oceanic production as a problem in population dynamics, Journal du Conseil, 24, 455–464, doi:10.1093/icesjms/24.3.455, 1959.

De La Rocha, C. L. and Passow, U.: Factors influencing the sinking of POC and the efficiency of the biological carbon pump, Deep Sea Research Part II: Topical Studies in Oceanography, 54, 639–658, doi:10.1016/j.dsr2.2007.01.004, 2007.

Downs, J.: Export of production in oceanic systems: information from phaeopigment carbon and nitrogen analyses, Ph.D. thesis, Univ. of Wash., Seattle, 1989.

Dugdale, R. C. and Goering, J. J.: Uptake of New and Regenerated Forms of Nitrogen in Primary Productivity, Limnology and Oceanography, 12, 196–206, doi:10.2307/2833031, 1967.

Dunne, J. P., Armstrong, R. A., Gnanadesikan, A., and Sarmiento, J. L.: Empirical and mechanistic models for the particle export ratio, Global Biogeochemical Cycles, 19, GB4026, doi:10.1029/2004GB002390, 2005.

Ebersbach, F. and Trull, T. W.: Sinking particle properties from polyacrylamide gels during the KErguelen Ocean and Plateau compared Study (KEOPS): Zooplankton control of carbon export in an area of persistent natural iron inputs in the Southern Ocean, Limnology and Oceanography, 53, 212–224, doi:10.2307/40006162, 2008.

Ebersbach, F., Trull, T. W., Davies, D. M., and Bray, S. G.: Controls on mesopelagic particle fluxes in the Sub-Antarctic and Polar Frontal Zones in the Southern Ocean south of Australia in summer—Perspectives from free-drifting sediment traps, Deep Sea Research Part II: Topical Studies in Oceanography, 58, 2260 – 2276, doi:10.1016/j.dsr2.2011.05.025, 2011.

Eppley, R. W. and Peterson, B. J.: Particulate organic matter flux and planktonic new production in the deep ocean, Nature, 282, 677–680, doi:10.1038/282677a0, 1979.

Falkowski, P. G., Barber, R. T., and Smetacek, V.: Biogeochemical Controls and Feedbacks on Ocean Primary Production, Science, 281, 200–206, doi:10.1126/science.281.5374.200, 1998.

Fisher, A. E. and Harrison, P. J.: Does carbohydrate content affect the sinking rates of marine diatoms?, Journal of Phycology, 32, 360–365, doi:10.1111/j.0022-3646.1996.00360.x, 1996.

Gauld, D. T.: A Peritrophic Membrane in Calanoid Copepods, Nature, 179, 325–326, doi:10.1038/179325a0, 1957.

Gehlen, M., Bopp, L., Emprin, N., Aumont, O., Heinze, C., Ragueneau, O., et al.: Reconciling surface ocean productivity, export fluxes and sediment composition in a global biogeochemical ocean model, Biogeosciences, 3, 521–537, doi:10.5194/bg-3-521-2006, 2006.

Gentleman, W.: A chronology of plankton dynamics in silico: how computer models have been used to study marine ecosystems, Hydrobiologia, 480, 69–85, doi:10.1023/A:1021289119442, 2002.

Giering, S. L. C., Sanders, R., Lampitt, R. S., Anderson, T. R., Tamburini, C., Boutrif, M., Zubkov, M. V., Marsay, C. M., Henson, S. A., Saw, K., Cook, K., and Mayor, D. J.: Reconciliation of the carbon budget in the ocean's twilight zone, Nature, 507, 480–483, doi:10.1038/nature13123, 2014.

Gruber, N. and Sarmiento, J. L.: Large-scale biogeochemical-physical interactions in elemental cycles, in: The sea, edited by Robinson, A. R., McCarthy, J. J., and Rothschild, B. J., vol. 12, chap. 9, pp. 337–399, John Wiley & Sons, 2002.

Guidi, L., Stemmann, L., Jackson, G. A., Ibanez, F., Claustre, H., Legendre, L., Picheral, M., and Gorsky, G.: Effects of phytoplankton community on production, size and export of large aggregates: A world-ocean analysis, Limnology and Oceanography, 54, 1951–1963, doi:10.4319/lo.2009.54.6.1951, 2009.

Hansen, P. J., Bjørnsen, P. K., and Hansen, B. W.: Zooplankton grazing and growth: Scaling within the 2-2,000 μm body size range, Limnology and Oceanography, 42, 687–704, doi:10.4319/lo.1997.42.4.0687, 1997.

Henson, S. A., Yool, A., and Sanders, R.: Variability in efficiency of particulate organic carbon export: A model study, Global Biogeochemical Cycles, 29, 33–45, doi:10.1002/2014GB004965, 2015.

Honjo, S., Manganini, S. J., Krishfield, R. A., and Francois, R.: Particulate organic carbon fluxes to the ocean interior and factors controlling the biological pump: A synthesis of global sediment trap programs since 1983, Progress in Oceanography, 76, 217–285, doi:10.1016/j.pocean.2007.11.003, 2008.

IPCC: Climate Change 2014: Synthesis Report. Contribution of Working Groups I, II and III to the Fifth Assessment Report of the Intergovernmental Panel on Climate Change [Core Writing Team, R.K. Pachauri and L.A. Meyer (eds.)], IPCC, Geneva, Switzerland, 151 pp.

Iversen, M. H. and Ploug, H.: Ballast minerals and the sinking carbon flux in the ocean: carbon-specific respiration rates and sinking velocity of marine snow aggregates, Biogeosciences, 7, 2613–2624, doi:10.5194/bg-7-2613-2010, 2010.

Karl, D. M. and Tilbrook, B. D.: Production and transport of methane in oceanic particulate organic matter, Nature, 368, 732–734, doi:10.1038/368732a0, 1994.

Karl, D. M., Knauer, G. A., and Martin, J. H.: Downward flux of particulate organic matter in the ocean: a particle decomposition paradox, Nature, 332, 438–441, doi:10.1038/332438a0, 1988.

Kriest, I. and Evans, G. T.: Representing phytoplankton aggregates in biogeochemical models, Deep Sea Research Part I: Oceanographic Research Papers, 46, 1841–1859, doi:10.1016/S0967-0637(99)00032-1, 1999.

Kriest, I. and Oschlies, A.: On the treatment of particulate organic matter sinking in large-scale models of marine biogeochemical cycles, Biogeosciences, 5, 55–72, doi:10.5194/bg-5-55-2008, 2008.

Kriest, I. and Oschlies, A.: Swept under the carpet: organic matter burial decreases global ocean biogeochemical model sensitivity to remineralization length scale, Biogeosciences, 10, 8401–8422, doi:10.5194/bg-10-8401-2013, 2013.

Lam, P. J., Doney, S. C., and Bishop, J. K. B.: The dynamic ocean biological pump: Insights from a global compilation of particulate organic carbon, $CaCO_3$, and opal concentration profiles from the mesopelagic, Global Biogeochemical Cycles, 25, GB3009, doi:10.1029/2010GB003868, 2011.

Lasbleiz, M., Leblanc, K., Blain, S., Ras, J., Cornet-Barthaux, V., Hélias Nunige, S., and Quéguiner, B.: Pigments, elemental composition (C, N, P, and Si), and stoichiometry of particulate matter in the naturally iron fertilized region of Kerguelen in the Southern Ocean, Biogeosciences, 11, 5931–5955, doi:10.5194/bg-11-5931-2014, 2014.

Laurenceau-Cornec, E. C., Trull, T. W., Davies, D. M., De La Rocha, C. L., and Blain, S.: Phytoplankton morphology controls on marine snow sinking velocity, Marine Ecology Progress Series, 520, 35–56, doi:10.3354/meps11116, 2015a.

Laurenceau-Cornec, E. C., Trull, T. W., Davies, D. M., Bray, S. G., Doran, J., Planchon, F., Carlotti, F., Jouandet, M.-P., Cavagna, A.-J., Waite, A. M., and Blain, S.: The relative importance of phytoplankton aggregates and zooplankton fecal pellets to carbon export: insights from free-drifting sediment trap deployments in naturally iron-fertilised waters near the Kerguelen Plateau, Biogeosciences, 12, 1007–1027, doi:10.5194/bg-12-1007-2015, 2015b.

Laws, E. A., Falkowski, P. G., Smith, W. O., Ducklow, H., and McCarthy, J. J.: Temperature effects on export production in the open ocean, Global Biogeochemical Cycles, 14, 1231–1246, doi:10.1029/1999GB001229, 2000.

Le Quéré, C., Raupach, M. R., Canadell, J. G., and Marland et al., G.: Trends in the sources and sinks of carbon dioxide, Nature Geoscience, 2, 831–836, doi:10.1038/ngeo689, 2009.

Losch, M., Strass, V., Cisewski, B., Klaas, C., and Bellerby, R. G. J.: Ocean state estimation from hydrography and velocity observations during EIFEX with a regional biogeochemical ocean circulation model, Journal of Marine Systems, 129, 437–451, doi:10.1016/j.jmarsys.2013.09.003, 2014.

Lutz, M. J., Caldeira, K., Dunbar, R. B., and Behrenfeld, M. J.: Seasonal rhythms of net primary production and particulate organic carbon flux to depth describe the efficiency of biological pump in the global ocean, Journal of Geophysical Research: Oceans, 112, C10 011, doi:10.1029/2006JC003706, 2007.

Maiti, K., Charette, M. A., Buesseler, K. O., and Kahru, M.: An inverse relationship between production and export efficiency in the Southern Ocean, Geophysical Research Letters, 40, 1557–1561, doi:10.1002/grl.50219, 2013.

Martens, P.: Faecal pellets, in: Fiches d'identification du zooplancton, edited by Fraser, J., vol. 162, p. 4, Conseil International pour l'Exploration de la Mer, 1978.

Martin, J. H., Knauer, G. A., Karl, D. M., and Broenkow, W. W.: VERTEX: carbon cycling in the northeast Pacific, Deep Sea Research Part A. Oceanographic Research Papers, 34, 267–285, doi:10.1016/0198-0149(87)90086-0, 1987.

Michaels, A. F. and Silver, M. W.: Primary production, sinking fluxes and the microbial food web, Deep Sea Research Part A. Oceanographic Research Papers, 35, 473–490, doi:10.1016/0198-0149(88)90126-4, 1988.

Møller, E. F.: Sloppy feeding in marine copepods: prey-size-dependent production of dissolved organic carbon, Journal of Plankton Research, 27, 27–35, doi:10.1093/plankt/fbh147, 2005.

Morris, P. J., Sanders, R., Turnewitsch, R., and Thomalla, S.: ^{234}Th-derived particulate organic carbon export from an island-induced phytoplankton bloom in the Southern Ocean, Deep Sea Research Part II: Topical Studies in Oceanography, 54, 2208–2232, doi:10.1016/j.dsr2.2007.06.002, 2007.

Neuer, S., Davenport, R., Freudenthal, T., Wefer, G., Llinás, O., Rueda, M.-J., Steinberg, D. K., and Karl, D. M.: Differences in the biological carbon pump at three subtropical ocean sites, Geophysical Research Letters, 29, 32–1–32–4, doi:10.1029/2002GL015393, 2002.

Oke, P. R., Sakov, P., Cahill, M. L., Dunn, J. R., Fiedler, R., Griffin, D. A., Mansbridge, J. V., Ridgway, K. R., and Schiller, A.: Towards a dynamically balanced eddy-resolving ocean reanalysis: BRAN3, Ocean Modelling, 67, 52 – 70, doi:10.1016/j.ocemod.2013.03.008, 2013.

Pace, M. L., Knauer, G. A., Karl, D. M., and Martin, J. H.: Primary production, new production and vertical flux in the eastern Pacific Ocean, Nature, 325, 803–804, doi:10.1038/325803a0, 1987.

Park, Y. H., Charriaud, E., Pino, D. R., and Jeandel, C.: Seasonal and interannual variability of the mixed layer properties and steric height at station KERFIX, southwest of Kerguelen, Journal of Marine Systems, 17, 571–586, doi:10.1016/S0924-7963(98)00065-7, 1998.

Pasquer, B., Laruelle, G., Becquevort, S., Schoemann, V., Goosse, H., and Lancelot, C.: Linking ocean biogeochemical cycles and ecosystem structure and function: results of the complex SWAMCO-4 model, Journal of Sea Research, 53, 93–108, doi:10.1016/j.seares.2004.07.001, 2005.

Passow, U.: Species-specific sedimentation and sinking velocities of diatoms, Marine Biology, 108, 449–455, doi:10.1007/BF01313655, 1991.

Passow, U. and Carlson, C.: The biological pump in a high CO_2 world, Marine Ecology Progress Series, 470, 249–271, doi:10.3354/meps09985, 2012.

Planchon, F., Ballas, D., Cavagna, A.-J., Bowie, A. R., Davies, D., Trull, T., Laurenceau-Cornec, E. C., Van Der Merwe, P., and Dehairs, F.: Carbon export in the naturally iron-fertilized Kerguelen area of the Southern Ocean based on the ^{234}Th approach, Biogeosciences, 12, 3831–3848, doi:10.5194/bg-12-3831-2015, 2015.

Ploug, H., Iversen, M. H., Koski, M., and Buitenhuis, E. T.: Production, oxygen respiration rates, and sinking velocity of copepod fecal pellets: Direct measurements of ballasting by opal and calcite, Limnology and Oceanography, 53, 469–476, doi:10.4319/lo.2008.53.2.0469, 2008.

Reid, P. C., Fischer, A. C., Lewis-Brown, E., Meredith, M. P., Sparrow, M., Andersson, A. J., Antia, A., Bates, N. R., Bathmann, U., Beaugrand, G., Brix, H., Dye, S., Edwards, M., Furevik, T., Gangstø, R., Hátún, H., Hopcroft, R. R., Kendall, M., Kasten, S., Keeling, R., Quéré, C. L., Mackenzie, F. T., Malin, G., Mauritzen, C., Ólafsson, J., Paull, C., Rignot, E., Shimada, K., Vogt, M., Wallace, C., Wang, Z., and Washington, R.: Impacts of the Oceans on Climate Change, in: Advances in Marine Biology, edited by Sims, D. W., vol. 56 of *Advances in Marine Biology*, chap. 1, pp. 1–150, Academic Press, 2009.

Richardson, T. L. and Jackson, G. A.: Small Phytoplankton and Carbon Export from the Surface Ocean, Science, 315, 838–840, doi:10.1126/science.1133471, 2007.

Riebesell, U.: The formation of large marine snow and its sustained residence in surface waters, Limnology and oceanography, 37, 63–76, doi:10.4319/lo.1992.37.1.0063, 1992.

Riley, G. A.: Factors controlling phytoplankton populations on Georges Bank, Journal of Marine Research, 6, 54–73, 1946.

Sabine, C., Feely, R., Gruber, N., Key, R., Lee, K., Bullister, J., Wanninkhof, R., Wong, C., Wallace, D., Tilbrook, B., et al.: The oceanic sink for anthropogenic CO_2, Science, 305, 367–371, doi:10.1126/science.1097403, 2004.

Salter, I., Kemp, A. E. S., Moore, C. M., Lampitt, R. S., Wolff, G. A., and Holtvoeth, J.: Diatom resting spore ecology drives enhanced carbon export from a naturally iron-fertilized bloom in the Southern Ocean, Global Biogeochemical Cycles, 26, GB1014, doi:10.1029/2010GB003977, 2012.

Sarmiento, J. L. and Gruber, N.: Ocean biogeochemical dynamics, Princeton University Press, 2006.

Savoye, N., Trull, T. W., Jacquet, S. H. M., Navez, J., and Dehairs, F.: ^{234}Th-based export fluxes during a natural iron fertilization experiment in the Southern Ocean (KEOPS), Deep Sea Research Part II: Topical Studies in Oceanography, 55, 841–855, doi:10.1016/j.dsr2.2007.12.036, 2008.

Smetacek, V.: Diatoms and the Ocean Carbon Cycle, Protist, 150, 25–32, doi:10.1016/S1434-4610(99)70006-4, 1999.

Smetacek, V., Klaas, C., Strass, V. H., Assmy, P., Montresor, M., Cisewski, B., Savoye, N., Webb, A., d'Ovidio, F., Arrieta, J. M., Bathmann, U., Bellerby, R., Berg, G. M., Croot, P., Gonzalez, S., Henjes, J., Herndl, G. J., Hoffmann, L. J., Leach, H., Losch, M., Mills, M. M., Neill, C., Peeken, I., Rottgers, R., Sachs, O., Sauter, E., Schmidt, M. M., Schwarz, J., Terbruggen, A., and Wolf-Gladrow, D.: Deep carbon export from a Southern Ocean iron-fertilized diatom bloom, Nature, 487, 313–319, doi:10.1038/nature11229, 2012.

Straile, D.: Gross growth efficiencies of protozoan and metazoan zooplankton and their dependence on food concentration, predator-prey weight ratio, and taxonomic group, Limnology and Oceanography, 42, 1375–1385, doi:10.4319/lo.1997.42.6.1375, 1997.

Suess, E.: Particulate organic carbon flux in the oceans—surface productivity and oxygen utilization, Nature, 288, 260–263, doi:10.1038/288260a0, 1980.

Suzuki, H., Sasaki, H., and Fukuchi, M.: Loss processes of sinking fecal pellets of zooplankton in the mesopelagic layers of the Antarctic Marginal Ice Zone, Journal of Oceanography, 59, 809–818, doi:10.1023/B:JOCE.0000009572.08048.0d, 2003.

Sverdrup, H. U.: On conditions for the vernal blooming of phytoplankton, Journal du Conseil, 18, 287–295, 1953.

Takahashi, T., Sutherland, S. C., Wanninkhof, R., Sweeney, C., Feely, R. A., Chipman, D. W., Hales, B., Friederich, G., Chavez, F., and Sabine, C.: Climatological mean and decadal change in surface ocean pCO2, and net sea-air CO2 flux over the global oceans, Deep Sea Research Part II: Topical Studies in Oceanography, 56, 554–577, doi:10.1016/j.dsr2.2008.12.009, 2009.

Takahashi, T., Sweeney, C., Hales, B., Chipman, D. W., Newberger, T., Goddard, J. G., Iannuzzi, R. A., and Sutherland, S. C.: The changing carbon cycle in the Southern Ocean, Oceanography, 25, 26–37, doi:10.5670/oceanog.2012.71, 2012.

Trull, T., Schulz, E., Bray, S., Pender, L., McLaughlan, D., Tilbrook, B., Rosenberg, M., and Lynch, T.: The Australian Integrated Marine Observing System Southern Ocean Time Series facility, in: OCEANS 2010 IEEE - Sydney, pp. 1–7, 2010.

Turner, J. T.: Zooplankton fecal pellets, marine snow, phytodetritus and the ocean's biological pump, Progress in Oceanography, 130, 205 – 248, doi:10.1016/j.pocean.2014.08.005, 2015.

Volk, T. and Hoffert, M. I.: Ocean carbon pumps: Analysis of relative strengths and efficiencies in ocean-driven atmospheric CO_2 changes, in: The Carbon Cycle and Atmospheric CO_2: Natural Variations Archean to Present, vol. 32, pp. 99–110, AGU, Washington, DC, 1985.

Waite, A., Fisher, A., Thompson, P. A., and Harrison, P. J.: Sinking rate versus cell volume relationships illuminate sinking rate control mechanisms in marine diatoms, Marine Ecology Progress Series, 157, 97–108, doi:10.3354/meps157097, 1997.

Wassmann, P.: Relationship between primary and export production in the boreal coastal zone of the North Atlantic, Limnology and oceanography, 35, 464–471, doi:10.4319/lo.1990.35.2.0464, 1990.

Wassmann, P.: Regulation of vertical export of particulate organic matter from the euphotic zone by planktonic heterotrophs in eutrophicated aquatic environments, Marine Pollution Bulletin, 26, 636 – 643, doi:10.1016/0025-326X(93)90503-C, 1993.

Wassmann, P.: Retention versus export food chains: processes controlling sinking loss from marine pelagic systems, Hydrobiologia, 363, 29–57, doi:10.1023/A:1003113403096, 1998.

Wexels Riser, C., Reigstad, M., Wassmann, P., Arashkevich, E., and Falk-Petersen, S.: Export or retention? Copepod abundance, faecal pellet production and vertical flux in the marginal ice zone through snap shots from the northern Barents Sea, Polar Biology, 30, 719–730, doi: 10.1007/s00300-006-0229-z, 2007.

Wiedmann, I., Reigstad, M., Sundfjord, A., and Basedow, S.: Potential drivers of sinking particle's size spectra and vertical flux of particulate organic carbon (POC): Turbulence, phytoplankton, and zooplankton, Journal of Geophysical Research: Oceans, 119, 6900–6917, doi:10.1002/2013JC009754, 2014.

Yoon, W., Kim, S., and Han, K.: Morphology and sinking velocities of fecal pellets of copepod, molluscan, euphausiid, and salp taxa in the northeastern tropical Atlantic, Marine Biology, 139, 923–928, doi:10.1007/s002270100630, 2001.

Chapter 5

Conclusions and future directions

5.1 Controls on carbon export efficiency identified

This study identified three main controls of ecosystem structure on carbon export efficiency over the Kerguelen Plateau. These controls are summarised on Figure 5.1. Below is a brief description of each of these main findings.

i. The highest carbon export efficiency recorded over the Kerguelen Plateau during KEOPS2 was associated with direct export via phytodetritus. This carbon export mode occurred when grazing was limited either due to grazing-resistant species or to low phytoplankton biomass levels insufficient to induce an increase of zooplankton biomass. It was demonstrated by comparing the particle flux collected in polyacrylamide gel sediment traps and their associated carbon flux measured using standard PPS3/3 traps. Model simulations confirmed that the most efficient export occurred in absence of grazing and when net primary productivity presented a close coupling with carbon flux. This efficient carbon export was mediated via fast-sinking detritus originated from large-sized phytoplankton.

ii. Roller tank experiments suggested that the dominant morphology of phytoplankton cells in a bloom can influence marine snow sinking velocity via a control on aggregation processes and aggregate structure. In this case, structure and associated excess density seems to overcome the influence of size on the sinking velocity. This could explain the frequent discrepancies between size and sinking velocity observed for large marine aggregates. In particular, it seems that large biomass accumulation of small setae-forming phytoplankton species (i.e. *Chaetoceros Hyalochaete* spp.) presenting high coagulation efficiencies leads preferentially to the formation of large but loose slow-sinking aggregates responsible for a high biomass retention in the surface layer.

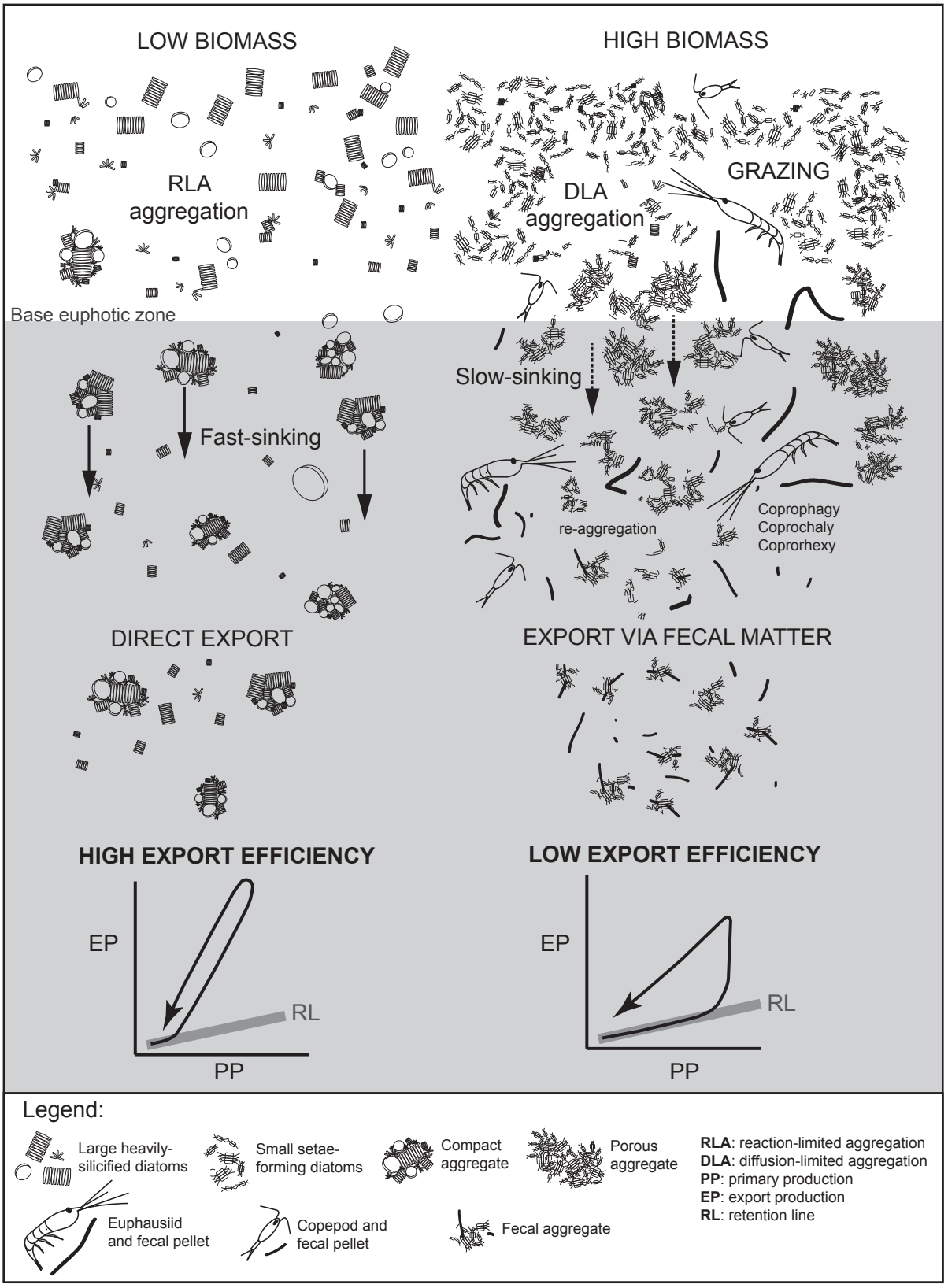

Figure 5.1: Scheme of the different processes of the BCP identified in this study.

iii. Model simulations confirmed that initial retention in the euphotic zone occurs in the case of blooms dominated by small phytoplankton species producing slow–sinking phytodetritus. However, when zooplankton biomass reaches sufficient levels, active grazing triggers the export by producing fast–sinking zoo–detritus but with large losses. Sediment trap collections suggested that this export mode is less efficient than direct export, mainly because the flux of fecal pellets seems to undergo a rapid attenuation at depth. On the contrary to direct carbon export, this initial retention of the biomass produced in the euphotic zone induces a decoupling between primary productivity and associated carbon flux. Particularly in small phytoplankton-dominated blooms, an inadequate timing and frequency of observations could be responsible for the discrepancies observed between net primary productivity and associated carbon flux or e–ratio. Results suggest that isolated measures of carbon export efficiency, when used to evaluate the influences of ecological processes, should account for the differences between rates of production and export.

5.2 From local observations to global scale models

The main objective of the intense research effort on understanding the BCP is ultimately to predict its future in relation to climate change. Based on the findings of this thesis, this section discusses the current research directions and poses future questions to be addressed.

The aspects of the BCP explored here suggest that its understanding at a global scale requires a regional approach since global models cannot account for the local diversity and complexity of planktonic community structure (Kostadinov et al., 2010). Phytoplankton functional types (PFTs) are large groups of phytoplankton species sharing similar biogeochemical functions and physiological traits. The main PFTs relevant to ocean ecology and biogeochemistry are diatoms, dinoflagellates, coccolithophores, silicoflagellates and diazotrophs. Recent advances in remote sensing include algorithms able to identify spatial repartition of several PFTs from satellite detection (Alvain et al., 2005, 2008; Raitsos et al., 2008). For the first time in 30 years of explorations of the BCP, this progress gives the perspective of an estimation of biogeochemical fluxes at a global scale based on combined remote detections of ecological and physical parameters (Siegel et al., 2014). However, results presented here pose the question whether these groups are constrained enough to account for controls exerted at genera or species levels? In particular,

the PFT of diatoms is based on their functional ability to produce silicified skeletons therefore qualified as 'silicifiers'. But the classical paradigm of diatoms as efficient carbon exporters in the Southern Ocean (Smetacek, 1999; Smetacek et al., 2012), might need to be nuanced since diatom species appear differently efficient to export carbon and not only because of their variable level of silicification (Armstrong et al., 2001; Klaas and Archer, 2002). Recent studies related diatom traits to their role in decoupling carbon and silica cycle (Assmy et al., 2013; Boyd, 2013; Quéguiner, 2013), supporting the view that an increased complexity is needed to understand how phytoplankton might affect global biogeochemical cycles. The present work suggested how morphological differences of diatoms, although belonging to the same PFT, can lead to very contrasted export efficiencies that may be significant to global scale estimations. Especially, processes that appear of limited significance at local scale might be of major importance if the phytoplankton they affect present high productivities in the ocean (Richardson and Jackson, 2007). Also, it appears important to assess the uncertainties in the estimations of BCP efficiency possibly induced by this over-simplification and compare it with other major sources of uncertainties. In other terms, how does the uncertainty derived from an assumption that all diatom blooms have the same efficiency at exporting carbon, compares to the other uncertainties in the estimation of the global BCP?

Uncertainties on recent estimations of the total ocean carbon pump were expressed within a range of $\pm$ 1 standard deviation representing a likelihood of 68% that the true value is within the range displayed (average uptake rate of CO_2 by the global ocean was estimated at 2.6$\pm$0.5 Gt C yr^{-1} for the period 2004–2013; Le Queré, 2014). The relative contributions of the biological (BCP) and physical components of the total ocean carbon pump, called respectively the 'soft tissue and solubility pumps' (Volk and Hoffert, 1985), are also poorly constrained (Gruber and Sarmiento, 2002; Reid et al., 2009). Moreover, important other components of the BCP (i.e. bacterial activity) occur in the mesopelagic zone where most ecological processes remain to be discovered (Giering et al., 2014). Based on this, it appears difficult to weight the relative uncertainties underlying every estimation used in a global calculation of the ocean carbon pump. The use of the global repartition of PFTs in global biogeochemical models to infer estimations of carbon export opens exciting perspectives. But no reduction of the uncertainties will be achieved if these models are not constrained by regional to local relationships between planktonic communities and their related export efficiencies.

This thesis showed the importance of considering small scale variations of plankton communities when evaluating the efficiency of a given ecosystem structure to export the carbon produced in the surface layer. Seasonal phytoplankton successions are based on subtle biomass imbalances between primary producers and their predators controlled by their growth and mortality rates. Under the pressure of these very competitive interactions, some organisms develop survival strategies. Diatoms present resting stages in their life cycle that allow them to persist over variable durations (days to decades) without undergoing cell division (McQuoid and Hobson, 1996). Most of the resting stages are morphologically and physiologically different from vegetative cells: they exhibit thicker valves and a condensed cytoplasm with a high content of storage material leading to high volume to carbon content ratio (Hargraves and French, 1983). Recent studies noted the importance of these resting stages in a Southern Ocean bloom in enhancing the carbon export via a fast-sinking to the deep ocean (Rembauville et al., 2014; Salter et al., 2012). It reinforces the idea that ecological processes relevant to our understanding of the biological carbon pump may lie at species levels or even lower.

This thesis highlighted at several occasions the versatile but essential role of zooplankton grazing in carbon export. In blooms dominated by small phytoplankton species unable to export their biomass by an efficient direct export, zooplankton grazing could represent an alternative way to form fast-sinking aggregates (i.e. fecal pellets) where physical aggregation can only form loose slow-sinking flocs. Also, zooplankton grazing is viewed as a process which promotes the retention and recycling of the carbon produced in the surface layer, and thus precludes an efficient export. The conditions under which zooplankton can be considered as promoters or reducers of the carbon flux are yet to be clarified. The contrasted sensitivities of the fecal pellets produced by different groups of mesozooplankton to degradation (e.g. euphausiids vs copepods) holds probably most of the answers. This study suggested a large attenuation of the flux of cylindrical fecal pellets at depth, possibly related to a rapid degradation due to alterations by zooplankton migrating with the flux, combined with bacterial degradation. Fecal pellet resistance to degradation along with zooplankton migration and feeding behaviour on the sinking flux are other subtle ecological considerations that may require parameterisations in future biogeochemical models for their potential relevance in carbon export.

Overall, the most important question to address regarding the BCP is how its processes will be altered due to climate change. Global warming related to anthropogenic activity affects the ocean in various ways, including temperature increase and subsequent increased stratification (Barnett et al., 2005; Lyman et al., 2010), and increased dissolved CO_2 responsible for ocean acidification (Feely et al., 2004). In his review Turner (2015) gave an extensive list of the potential effects of this 'changing ocean' on the functioning of the BCP. Depending on the components of the BCP affected and the modalities of the changes, studies predict either increases or decreases of the carbon export flux. Alterations through changes of plankton communities are the most relevant to this thesis. Decrease in nutrient supply due to increased stratification may induce shifts from diatoms to coccolithophorids (Cermeño et al., 2008), genera recognized to have opposite effects on the BCP in the Southern Ocean (Salter et al., 2014), or from large diatoms to small microflagellates and cyanobacteria (Falkowski and Oliver, 2007), thus tending to channel carbon through a long food chain rather than exporting it directly. Clearly, the way that the BCP will respond to ocean changes is highly uncertain. However, results presented in this thesis suggest that intensification of the research effort should be directed toward investigations of small scale ecological processes, to provide invaluable insights to constrain the global scale models and improve their predictions.

References

Alvain, S., Moulin, C., Dandonneau, Y., and Bréon, F.: Remote sensing of phytoplankton groups in case 1 waters from global SeaWiFS imagery, Deep Sea Research Part I: Oceanographic Research Papers, 52, 1989 – 2004, doi:10.1016/j.dsr.2005.06.015, 2005.

Alvain, S., Moulin, C., Dandonneau, Y., and Loisel, H.: Seasonal distribution and succession of dominant phytoplankton groups in the global ocean: A satellite view, Global Biogeochemical Cycles, 22, GB3001, doi:10.1029/2007GB003154, 2008.

Armstrong, R. A., Lee, C., Hedges, J. I., Honjo, S., and Wakeham, S. G.: A new, mechanistic model for organic carbon fluxes in the ocean based on the quantitative association of POC with ballast minerals, Deep-Sea Research Part II: Topical Studies in Oceanography, 49, 219–236, doi:10.1016/S0967-0645(01)00101-1, 2001.

Assmy, P., Smetacek, V., Montresor, M., Klaas, C., Henjes, J., Strass, V. H., Arrieta, J. M., Bathmann, U., Berg, G. M., Breitbarth, E., Cisewski, B., Friedrichs, L., Fuchs, N., Herndl, G. J., Jansen, S., Krägefsky, S., Latasa, M., Peeken, I., Röttgers, R., Scharek, R., Schüller, S. E., Steigenberger, S., Webb, A., and Wolf-Gladrow, D.: Thick-shelled, grazer-protected diatoms decouple ocean carbon and silicon cycles in the iron-limited Antarctic Circumpolar Current, Proceedings of the National Academy of Sciences, 110, 20 633–20 638, doi:10.1073/pnas.1309345110, 2013.

Barnett, T. P., Pierce, D. W., AchutaRao, K. M., Gleckler, P. J., Santer, B. D., Gregory, J. M., and Washington, W. M.: Penetration of Human-Induced Warming into the World's Oceans, Science, 309, 284–287, doi:10.1126/science.1112418, 2005.

Boyd, P. W.: Diatom traits regulate Southern Ocean silica leakage, Proceedings of the National Academy of Sciences, 110, 20 358–20 359, doi:10.1073/pnas.1320327110, 2013.

Cermeño, P., Dutkiewicz, S., Harris, R. P., Follows, M., Schofield, O., and Falkowski, P. G.: The role of nutricline depth in regulating the ocean carbon cycle, Proceedings of the National Academy of Sciences, 105, 20 344–20 349, doi:10.1073/pnas.0811302106, 2008.

Falkowski, P. G. and Oliver, M. J.: Mix and match: how climate selects phytoplankton, Nat Rev Micro, 5, 813–819, doi:10.1038/nrmicro1751, 2007.

Feely, R. A., Sabine, C. L., Lee, K., Berelson, W., Kleypas, J., Fabry, V. J., and Millero, F. J.: Impact of Anthropogenic CO_2 on the $CaCO_3$ System in the Oceans, Science, 305, 362–366, doi:10.1126/science.1097329, 2004.

Giering, S. L. C., Sanders, R., Lampitt, R. S., Anderson, T. R., Tamburini, C., Boutrif, M., Zubkov, M. V., Marsay, C. M., Henson, S. A., Saw, K., Cook, K., and Mayor, D. J.: Reconciliation of the carbon budget in the ocean's twilight zone, Nature, 507, 480–483, doi:10.1038/nature13123, 2014.

Gruber, N. and Sarmiento, J. L.: Large-scale biogeochemical-physical interactions in elemental cycles, in: The sea, edited by Robinson, A. R., McCarthy, J. J., and Rothschild, B. J., vol. 12, chap. 9, pp. 337–399, John Wiley & Sons, 2002.

Hargraves, P. E. and French, F. W.: Diatom resting spores: Significance and strategies, in: Survival Strategies of the Algae, edited by Fryxell, G., pp. 49–68, Cambridge University Press, New York, 1983.

Klaas, C. and Archer, D. E.: Association of sinking organic matter with various types of mineral ballast in the deep sea: Implications for the rain ratio, Global Biogeochemical Cycles, 16, 1116, doi:10.1029/2001GB001765, 2002.

Kostadinov, T. S., Siegel, D. A., and Maritorena, S.: Global variability of phytoplankton functional types from space: assessment via the particle size distribution, Biogeosciences, 7, 3239–3257, doi:10.5194/bg-7-3239-2010, 2010.

Le Quéré, C., Moriarty, R., Andrew, R. M., Peters, G. P., Ciais, P., Friedlingstein, P., Jones, S. D., Sitch, S., Tans, P., Arneth, A., Boden, T. A., Bopp, L., Bozec, Y., Canadell, J. G., Chevallier, F., Cosca, C. E., Harris, I., Hoppema, M., Houghton, R. A., House, J. I., Jain, A., Johannessen, T., Kato, E., Keeling, R. F., Kitidis, V., Klein Goldewijk, K., Koven, C., Landa, C. S., Landschützer, P., Lenton, A., Lima, I. D., Marland, G., Mathis, J. T., Metzl, N., Nojiri, Y., Olsen, A., Ono, T., Peters, W., Pfeil, B., Poulter, B., Raupach, M. R., Regnier, P., Rödenbeck, C., Saito, S., Salisbury, J. E., Schuster, U., Schwinger, J., Séférian, R., Segschneider, J., Steinhoff, T., Stocker, B. D., Sutton, A. J., Takahashi, T., Tilbrook, B., van der Werf, G. R., Viovy, N., Wang, Y.-P., Wanninkhof, R., Wiltshire, A., and Zeng, N.: Global carbon budget 2014, Earth System Science Data Discussions, 7, 521–610, doi:10.5194/essdd-7-521-2014, 2014.

Lyman, J. M., Good, S. A., Gouretski, V. V., Ishii, M., Johnson, G. C., Palmer, M. D., Smith, D. M., and Willis, J. K.: Robust warming of the global upper ocean, Nature, 465, 334–337, doi:10.1038/nature09043, 2010.

McQuoid, M. R. and Hobson, L. A.: Diatom resting stages, Journal of Phycology, 32, 889–902, doi:10.1111/j.0022-3646.1996.00889.x, 1996.

Quéguiner, B.: Iron fertilization and the structure of planktonic communities in high nutrient regions of the Southern Ocean, Deep Sea Research Part II: Topical Studies in Oceanography, 90, 43–54, doi:10.1016/j.dsr2.2012.07.024, 2013.

Raitsos, D. E., Lavender, S. J., Maravelias, C. D., Haralabous, J., Richardson, A. J., and Reid, P. C.: Identifying four phytoplankton functional types from space: An ecological approach, Limnology and Oceanography, 53, 605–613, doi:10.4319/lo.2008.53.2.0605, 2008.

Reid, P. C., Fischer, A. C., Lewis-Brown, E., Meredith, M. P., Sparrow, M., Andersson, A. J., Antia, A., Bates, N. R., Bathmann, U., Beaugrand, G., Brix, H., Dye, S., Edwards, M., Furevik, T., Gangstø, R., Hátún, H., Hopcroft, R. R., Kendall, M., Kasten, S., Keeling, R., Quéré, C. L., Mackenzie, F. T., Malin, G., Mauritzen, C., Ólafsson, J., Paull, C., Rignot, E., Shimada, K., Vogt, M., Wallace, C., Wang, Z., and Washington, R.: Impacts of the Oceans on Climate Change, in: Advances in Marine Biology, edited by Sims, D. W., vol. 56 of *Advances in Marine Biology*, chap. 1, pp. 1–150, Academic Press, 2009.

Rembauville, M., Blain, S., Armand, L., Quéguiner, B., and Salter, I.: Export fluxes in a naturally fertilized area of the Southern Ocean, the Kerguelen Plateau: ecological vectors of carbon and biogenic silica to depth (Part 2), Biogeosciences Discussions, 11, 17 089–17 150, doi:10.5194/bgd-11-17089-2014, 2014.

Richardson, T. L. and Jackson, G. A.: Small Phytoplankton and Carbon Export from the Surface Ocean, Science, 315, 838–840, doi:10.1126/science.1133471, 2007.

Salter, I., Kemp, A. E. S., Moore, C. M., Lampitt, R. S., Wolff, G. A., and Holtvoeth, J.: Diatom resting spore ecology drives enhanced carbon export from a naturally iron-fertilized bloom in the Southern Ocean, Global Biogeochemical Cycles, 26, GB1014, doi:10.1029/2010GB003977, 2012.

Salter, I., Schiebel, R., Ziveri, P., Movellan, A., Lampitt, R., and Wolff, G. A.: Carbonate counter pump stimulated by natural iron fertilization in the Polar Frontal Zone, Nature Geoscience, 7, 885–889, doi:10.1038/ngeo2285, 2014.

Siegel, D. A., Buesseler, K. O., Doney, S. C., Sailley, S. F., Behrenfeld, M. J., and Boyd, P. W.: Global assessment of ocean carbon export by combining satellite observations and food-web models, Global Biogeochemical Cycles, 28, 2013GB004 743, doi:10.1002/2013GB004743, 2014.

Smetacek, V.: Diatoms and the Ocean Carbon Cycle, Protist, 150, 25–32, doi:10.1016/S1434-4610(99)70006-4, 1999.

Smetacek, V., Klaas, C., Strass, V. H., Assmy, P., Montresor, M., Cisewski, B., Savoye, N., Webb, A., d'Ovidio, F., Arrieta, J. M., Bathmann, U., Bellerby, R., Berg, G. M., Croot, P., Gonzalez, S., Henjes, J., Herndl, G. J., Hoffmann, L. J., Leach, H., Losch, M., Mills, M. M., Neill, C., Peeken, I., Rottgers, R., Sachs, O., Sauter, E., Schmidt, M. M., Schwarz, J., Terbruggen, A., and Wolf-Gladrow, D.: Deep carbon export from a Southern Ocean iron-fertilized diatom bloom, Nature, 487, 313–319, doi:10.1038/nature11229, 2012.

Turner, J. T.: Zooplankton fecal pellets, marine snow, phytodetritus and the ocean's biological pump, Progress in Oceanography, 130, 205 – 248, doi:10.1016/j.pocean.2014.08.005, 2015.

Volk, T. and Hoffert, M. I.: Ocean carbon pumps: Analysis of relative strengths and efficiencies in ocean-driven atmospheric CO_2 changes, in: The Carbon Cycle and Atmospheric CO_2: Natural Variations Archean to Present, vol. 32, pp. 99–110, AGU, Washington, DC, 1985.

Appendix A

Carbon export in the naturally iron-fertilized Kerguelen area of the Southern Ocean based on the ^{234}Th approach

F. Planchon[1], D. Ballas[2], A.-J. Cavagna[2], A.R. Bowie[3,4], D.M. Davies[4], T.W. Trull[3,4,5], E.C. Laurenceau-Cornec[3,4,5], P. van der Merwe[4], F. Dehairs[2]

[1]Laboratoire des Sciences de l'Environnement Marin (LEMAR), Université de Brest, CNRS, IRD, UMR6539, IUEM, Technopôle Brest Iroise, Place Nicolas Copernic, 29280 Plouzané, France

[2]Vrije Universiteit Brussel, Analytical, Environmental and Geo-Chemistry and Earth System Sciences, Brussels, Belgium

[3]Institute for Marine and Antarctic Studies, University of Tasmania, Hobart, 7001, Australia

[4]Antarctic Climate and Ecosystems Cooperative Research Centre, Hobart, 7001, Australia

[5]CSIRO Marine and Atmospheric Research, Hobart, 7001, Australia

Biogeosciences, 12, 3831–3848, 2015
www.biogeosciences.net/12/3831/2015/
doi:10.5194/bg-12-3831-2015

Biogeosciences Open Access

Carbon export in the naturally iron-fertilized Kerguelen area of the Southern Ocean based on the ^{234}Th approach

F. Planchon[1], D. Ballas[2], A.-J. Cavagna[2], A. R. Bowie[3,4], D. Davies[4], T. Trull[3,4,5], E. C. Laurenceau-Cornec[3,4,5], P. Van Der Merwe[4], and F. Dehairs[2]

[1]Laboratoire des Sciences de l'Environnement Marin (LEMAR), Université de Bretagne Occidentale, CNRS, IRD, UMR 6539, IUEM; Technopôle Brest Iroise, Place Nicolas Copernic, 29280 Plouzané, France
[2]Vrije Universiteit Brussel, Analytical, Environmental and Geo-Chemistry and Earth System Sciences, Brussels, Belgium
[3]Institute for Marine and Antarctic Studies, University of Tasmania, Hobart, 7001, Australia
[4]Antarctic Climate and Ecosystems Cooperative Research Centre, Hobart, 7001, Australia
[5]CSIRO Marine and Atmospheric Research, Hobart, 7001, Australia

Correspondence to: F. Planchon (frederic.planchon@univ-brest.fr)

Received: 3 October 2014 – Published in Biogeosciences Discuss.: 25 November 2014
Revised: 30 March 2015 – Accepted: 16 April 2015 – Published: 23 June 2015

Abstract. This study examined upper-ocean particulate organic carbon (POC) export using the ^{234}Th approach as part of the second KErguelen Ocean and Plateau compared Study expedition (KEOPS2). Our aim was to characterize the spatial and the temporal variability of POC export during austral spring (October–November 2011) in the Fe-fertilized area of the Kerguelen Plateau region. POC export fluxes were estimated at high productivity sites over and downstream of the plateau and compared to a high-nutrient low-chlorophyll (HNLC) area upstream of the plateau in order to assess the impact of iron-induced productivity on the vertical export of carbon.

Deficits in ^{234}Th activities were observed at all stations in surface waters, indicating early scavenging by particles in austral spring. ^{234}Th export was lowest at the reference station R-2 and highest in the recirculation region (E stations) where a pseudo-Lagrangian survey was conducted. In comparison ^{234}Th export over the central plateau and north of the polar front (PF) was relatively limited throughout the survey. However, the ^{234}Th results support that Fe fertilization increased particle export in all iron-fertilized waters. The impact was greatest in the recirculation feature (3–4 fold at 200 m depth, relative to the reference station), but more moderate over the central Kerguelen Plateau and in the northern plume of the Kerguelen bloom (∼ 2-fold at 200 m depth).

The C : Th ratio of large (> 53 µm) potentially sinking particles collected via sequential filtration using in situ pumping (ISP) systems was used to convert the ^{234}Th flux into a POC export flux. The C : Th ratios of sinking particles were highly variable (3.1 ± 0.1 to 10.5 ± 0.2 µmol dpm^{-1}) with no clear site-related trend, despite the variety of ecosystem responses in the fertilized regions. C : Th ratios showed a decreasing trend between 100 and 200 m depth suggesting preferential carbon loss relative to ^{234}Th possibly due to heterotrophic degradation and/or grazing activity. C : Th ratios of sinking particles sampled with drifting sediment traps in most cases showed very good agreement with ratios for particles collected via ISP deployments (> 53 µm particles).

Carbon export production varied between 3.5 ± 0.9 and 11.8 ± 1.3 mmol m^{-2} d^{-1} from the upper 100 m and between 1.8 ± 0.9 and 8.2 ± 0.9 mmol m^{-2} d^{-1} from the upper 200 m. The highest export production was found inside the PF meander with a range of 5.3 ± 1.0 to 11.8 ± 1.1 mmol m^{-2} d^{-1} over the 19-day survey period. The impact of Fe fertilization is highest inside the PF meander with 2.9–4.5-fold higher carbon flux at 200 m depth in comparison to the HNLC control station. The impact of Fe fertilization was significantly less over the central plateau (stations A3 and E-4W) and in the northern branch of the bloom (station F-L) with 1.6–2.0-fold higher carbon flux compared to the reference station R. Export efficiencies (ratio of export to primary production and ratio of export to new production) were particularly variable with relatively high values in the recirculation feature (6 to 27 %, respectively) and low values (1 to 5 %, respectively)

over the central plateau (station A3) and north of the PF (station F-L), indicating spring biomass accumulation. Comparison with KEOPS1 results indicated that carbon export production is much lower during the onset of the bloom in austral spring than during the peak and declining phases in late summer.

1 Introduction

Nutrient limitation is an essential control of upper-ocean productivity (Moore et al., 2013) and affects the associated uptake of carbon and its transfer to the deep ocean as sinking particulate organic matter. Attention has focused on iron (Fe) as a limiting nutrient since the *iron hypothesis* of Martin (1990), who suggested that increased iron supply to the Southern Ocean (SO) during the last glacial maximum could have contributed to the drawdown of atmospheric CO_2 by stimulating the oceanic biological pump. For the present-day ocean, iron limitation is now validated for several high-nutrient low-chlorophyll (HNLC) regions, including the SO (Boyd et al., 2000, 2007; Coale et al., 2004; Martin et al., 1990, 1991; Sedwick et al., 1999; Smetacek et al., 2012). However, it is still under debate whether the positive growth response of phytoplankton due to iron addition results in enhanced export of biogenic particles and contributes to the long-term sequestration of carbon. This remains central to understanding the role of iron on the oceanic carbon cycle and ultimately on the past and future climate of the Earth.

Mesoscale iron addition experiments have revealed no clear trend in carbon export. Export fluxes estimated during Southern Ocean Iron RElease Experiment (SOIREE; polar waters south of Australia), the SOLAS air-sea gas exchange experiment (SAGE; subpolar waters south of New Zealand), European Iron Enrichment Experiment in the Southern Ocean (EisenEx; Atlantic polar waters) and Indo-German iron fertilization experiment (LOHAFEX; South Atlantic waters) report no major differences between the Fe-fertilized patch and the adjacent control site (Buesseler et al., 2005, 2004; Martin et al., 2013; Nodder et al., 2001). By contrast, the experiments SOFEX-South (polar waters south of New Zealand) and EIFEX (Atlantic polar waters south of Africa) showed increased vertical flux of particulate organic carbon (POC) due to iron addition (Buesseler et al., 2005; Jacquet et al., 2008; Smetacek et al., 2012). Enhanced export appears associated with experiments carried out (1) in high silicic acid waters south of the Antarctic polar front (PF) allowing fast-sinking, large diatoms to develop under low grazing pressure and (2) over a survey period sufficiently long to cover the time lag between the bloom development and the export event. However, the key results obtained with purposeful iron addition still differ and are difficult to scale up to regional and seasonal scales (Boyd et al., 2007).

Alternatives to short-term artificial experiments are the large and persistent phytoplankton blooms that develop annually in the vicinity of sub-Antarctic islands (Blain et al., 2007; Borrione and Schlitzer, 2013; Morris and Charette, 2013; Pollard et al., 2009) and close to the Antarctic continent (Alderkamp et al., 2012; Zhou et al., 2013) due to natural iron supply. These particular settings represent large-scale natural laboratories, where the role of Fe on ecosystems ecology, productivity, structure, and associated export can be monitored over an entire seasonal cycle. Two previous important field studies were carried out in natural Fe-fertilized areas: the CROZet natural iron bloom and EXport experiment (CROZEX, 2004–2005) (Pollard et al., 2009), and the KErguelen Ocean and Plateau compared study (KEOPS, 2005) (Blain et al., 2007). CROZEX studied the Crozet Islands region located in the sub-Antarctic waters of the Indian Ocean where a bloom occurs north of the islands in October/November followed by a secondary bloom in January. CROZEX results confirmed that the bloom is fueled with iron from Crozet Island (Planquette et al., 2007) and that phytoplankton uptake rates are much larger in the bloom area than in the HNLC control area (Lucas et al., 2007; Seeyave et al., 2007). For carbon export, the primary bloom results in a $\sim$ 3-fold higher flux at the Fe-fertilized site than at the control site, and for the secondary bloom, no substantial differences are reported (Morris et al., 2007). Sinking particles collected by a neutrally buoyant sediment trap (PELAGRA) were dominated by diatom cells of various species and size indicating a pronounced contribution of primary producers to the export (Salter et al., 2007).

The second study (KEOPS) focused on the high productivity area of the Kerguelen Islands in the Indian sector of the SO. The Kerguelen bloom has two main features, a northern branch that extends northeast of the islands north of the PF (also called the plume), and a larger bloom covering $\sim 45\,000\,km^2$ south of the PF and largely constrained to the shallow bathymetry of the Kerguelen Plateau (< 1000m) (Mongin et al., 2008). In austral summer 2004–2005, the bloom started in early November, peaked in December and January, and then rapidly declined in February (Blain et al., 2007). Fe fertilization over the plateau was demonstrated during KEOPS and attributed to vertical exchanges between the surface and the deep iron-rich reservoir existing above the plateau (Blain et al., 2008). The waters in the bloom showed higher biomass, greater silicate depletion, and important CO_2 drawdown compared to the control site (Blain et al., 2007; Jouandet et al., 2008; Mosseri et al., 2008). Carbon export in the Fe-fertilized area in comparison to HNLC waters was 2-fold higher as estimated using the ^{234}Th proxy (Savoye et al., 2008), and 3-fold higher based on a seasonal dissolved inorganic carbon (DIC) budget (Jouandet et al., 2008). Direct observations of sinking particles using polyacrylamide gel traps indicates a dominant fraction of fecal pellets and fecal aggregates and suggests a strong influence of particle repackaging by grazers during the late stage of the Kergue-

len bloom (Ebersbach and Trull, 2008). The unprecedented results obtained from CROZEX and KEOPS clearly highlight the crucial role of Fe in natural ecosystems and demonstrate the stimulation of the biological carbon pump in the SO resulting in an enhanced CO_2 sink and carbon export at depth.

The KEOPS2 project was designed to improve the spatial and temporal coverage of the Kerguelen region. KEOPS2 was carried out in austral spring to document the early stages of the bloom and to complement results of KEOPS1 obtained in summer during the peak and decline of the bloom. The principal aims were to better constrain the mechanism of Fe supply to surface waters and to determine the response of ecosystems to Fe fertilization including the impact on vertical export of carbon. The sampling strategy covered two distinct areas: the principal bloom already investigated during KEOPS1 and located over the central plateau, and the plume downstream to the east of the islands and north of the PF.

In this study, we report upper-ocean POC export production estimated using the ^{234}Th-based approach (Cochran and Masqué, 2003). POC fluxes at 100, 150, and 200 m depth were inferred from total ^{234}Th export fluxes estimated from ^{234}Th deficit in surface waters by applying the modeling approach of Savoye et al. (2006) for the ^{234}Th activity balance. ^{234}Th export fluxes were then converted into POC fluxes using POC / ^{234}Th ratio of large (> 53 µm) potentially sinking particles at the depth of export. Upper-ocean ^{234}Th and carbon export obtained in HNLC and Fe-enriched waters were used to assess the impact of natural fertilization on the vertical transfer of carbon. ^{234}Th-derived fluxes were compared to free-drifting sediment and polyacrylamide gel trap data (Laurenceau-Cornec et al., 2015a). Using primary production estimates (Cavagna et al., 2014) we examine spatial and temporal variations in export efficiency during the survey. Finally, using KEOPS1 results, early and late bloom conditions are compared.

2 Material and method

2.1 Study area and sampling strategy

The KEOPS2 cruise took place between October and November 2011 on board the R/V *Marion Dufresne*. The studied region encompasses the Kerguelen Plateau located between Kerguelen and Heard islands, and the deeper offshore basin to the east of the islands (Fig. 1). Details of the large-scale circulation in this area can be found elsewhere (Park et al., 2008b). Briefly, the Kerguelen Plateau represents a major barrier to the eastward flow of the Antarctic Circumpolar Current (ACC). The ACC is divided into two branches with the most intense flow passing to the north of the islands and associated with the subantarctic front (SAF). The second branch is associated with the PF and passes south of the islands. When crossing the plateau, the southern branch turns back north and forms a large meander isolating a mesoscale recirculation structure south of the PF (Fig. 1).

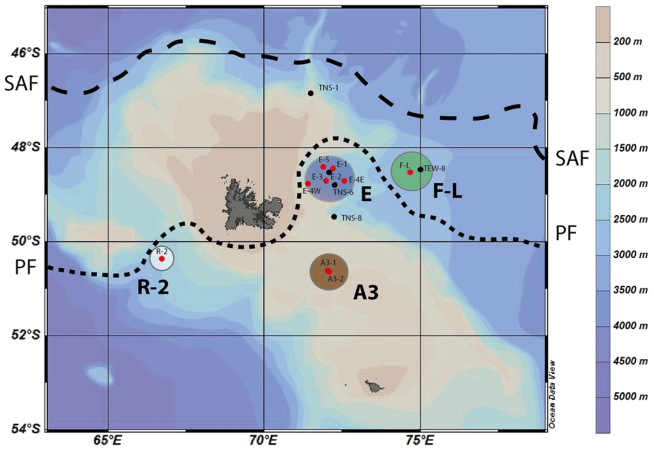

Figure 1. Stations map of ^{234}Th measurements during the KEOPS2 expedition. Also, shown are the positions of the subantarctic front (SAF) and the PF adapted from Park et al. (2008b). Colored circles refer to the following clusters of stations showing similar characteristics: Control station R-2, north of the PF station F-L, plateau station A3, and PF meander E stations (see text for details).

The sampling strategy aimed at characterizing the spatial and the temporal variability of high productivity sites located on and off the plateau. The survey included two transects from south to north (TNS-1 to TNS-10) and from west to east (TEW-1 to TEW-8) for physics and stock parameters, and nine process stations (R-2, A3-1, A3-2, E-1, E-3, E-4W, E-4E, E-5, and F-L) where more intensive sampling including large-volume in situ filtration and sediment trap deployments were carried out. For this study, 14 stations were investigated including 5 transects stations (TNS-8, TNS-6, TNS-1, E-2, and TEW-8) sampled for total ^{234}Th activity and 9 process stations where total ^{234}Th, particulate ^{234}Th, and POC profiles obtained simultaneously allowed to estimate POC export production. Sediment traps deployed and successfully recovered at four process stations were also determined for ^{234}Th activity. Process stations were carried out in four distinct areas showing different characteristics (see Fig. 1):

- The reference station (R-2) was chosen in HNLC waters upstream of the islands in a non-Fe-fertilized area.

- The shallow central plateau was sampled at station A3, which corresponds to the plateau bloom reference station of KEOPS1. Station A3 was sampled twice (A3-1 and A3-2) over a period of 27.7 days (20 October–16 November).

- The northern branch of the bloom, which develops north of the PF in the polar front zone (PFZ), was sampled at station F-L (6 November).

– The recirculation feature in the PF meander (station E) received detailed attention with four successive visits (E-1, E-3, E-4E, and E-5) as part of a pseudo-Lagrangian time series over 19.6 days. In the same area, a highly productive station (E4W) located on the western edge of the recirculation feature and close to the jet of the PF was sampled but excluded from the pseudo-Lagrangian study.

2.2 Total ^{234}Th activities

Total ^{234}Th activities were obtained from 4 L seawater samples collected from 12 L Niskin bottles. For transect stations, 13 depths were sampled between the surface and 20–90 m above the seafloor. For plateau station A3, samples were collected at 11 depths between the surface and 30–80 m above the seafloor. For deep stations (R, E-1, E-3, E-4E, E-4W, E-5, F-L), 14 depths were sampled between the surface and 900 m, and two deep water samples (1000–2000 m) were systematically collected for calibration purposes (except at E-4W).

Seawater samples were processed for total ^{234}Th activity measurement following the double-spike procedure developed by Pike et al. (2005) and modified as per Planchon et al. (2013). Briefly, samples were acidified with nitric acid (pH 2), spiked with ^{230}Th yield tracer, and left for 12 hours equilibration before co-precipitation with MnO_2 (pH 8.5). Co-precipitated samples were filtered on high-purity quartz microfiber filters (QMA, Sartorius; nominal pore size = 1 µm; ∅ 25 mm), dried overnight and mounted on nylon filter holders covered with Mylar and Al foil for beta counting. Samples were counted twice on board using a low level beta counter (Risø, Denmark) and measurement was stopped when counting uncertainty was below 2 % (RSD – relative standard deviation). Residual beta activity was measured for each sample after a delay of six ^{234}Th half-lives (∼ 6 months) and was subtracted from the gross counts obtained on-board.

After background counting, all samples were processed for ^{234}Th recovery using ^{229}Th as a second yield tracer and with a simplified procedure described elsewhere (Planchon et al., 2013). Briefly, MnO_2 co-precipitates were dissolved in 10 ml of an 8M HNO_3/10 % H_2O_2 solution, heated overnight, and filtered using Acrodisc 0.2 µm syringe filters. Determination of ^{230}Th / ^{229}Th ratios was carried out on high purity water diluted samples (10 to 20 times) by HR-ICP-MS (Element2, Thermo Scientific). The overall precision of ^{230}Th / ^{229}Th ratio measurements was 1.8 % (RSD) using triplicate samples and multiple standards analyzed over several analytical sessions. Average ^{234}Th recovery was 88 ± 11 % ($n = 200$). Uncertainties of total ^{234}Th activity were estimated using error propagation law and represent 0.07 dpm L^{-1} on average. Standard deviation of the mean ^{234}Th / ^{238}U ratio obtained for deep waters (> 1000 m) was 0.03 dpm L^{-1} ($n = 19$). ^{238}U activity (dpm L^{-1}) was calculated using the relationship $^{238}\mathrm{U}\ (\pm 0.047) = (0.0786 \pm 0.0045) \times S\ -\ (0.315 \pm 0.158)$ (Owens et al., 2011).

2.3 ^{234}Th flux

^{234}Th export fluxes were calculated using a 1-D box model, which accounts for total ^{234}Th mass balance. Detailed equations can be found elsewhere (Savoye et al., 2006). ^{234}Th export flux was estimated at 100, 150, and 200 m depth in order to account for (1) variations in the vertical distribution of ^{234}Th deficits and (2) total depth-integrated losses of ^{234}Th via export. This allows for comparison between stations at the same depth horizon, as well as with KEOPS1 study where a similar approach was used (Savoye et al., 2008). At all stations, ^{234}Th flux was estimated under steady state (SS) assumption, i.e., considering constant total ^{234}Th activity over time and neglecting advective and diffusive flux of ^{234}Th. For re-visited stations (A3 and E stations), ^{234}Th flux was also estimated under non-steady state (NSS) assumption. At A3, the NSS model was applied for the second visit with a time delay of 27.7 days. At E stations, NSS ^{234}Th export flux was estimated when the time delay was greater than 1 week as recommended by Savoye et al. (2006). Consequently, the NSS calculation was carried out only at E-4E (14.6 days) and E-5 (19.6 days). The revisited stations E-2 and E-4W were not considered part of the pseudo-Lagrangian study at the E study site and were excluded from the NSS calculation.

In order to check the assumption that physical transport did not impact the ^{234}Th budget, the vertical diffusive flux (Vz) was estimated using the vertical gradient of ^{234}Th activity and a range of vertical diffusivity coefficients (Kz values) between 10^{-4} and 10^{-5} m^2 s^{-1} calculated from the Shih model (Park et al., 2014b). This range of Kz values for KEOPS2 is much lower than for KEOPS1 (4×10^{-4} m^2 s^{-1}) obtained using the Osborn model (Park et al., 2008a). Vz was calculated using total ^{234}Th activities instead of the dissolved ^{234}Th (total ^{234}Th–particulate ^{234}Th) because of a poor vertical resolution of particulate ^{234}Th data in the first 200 m. For all stations, the diffuse flux (Vz) estimated at 100, 150, and 200 m depth was always below 50 dpm m^2 d^{-1} and represents a negligible contribution to the particle-associated export flux.

Lateral transport may also impact the ^{234}Th budget (Savoye et al., 2006) especially for stations located downstream of the Kerguelen Islands. From our data, this contribution cannot be quantified precisely, and is only qualitatively considered. Given the mean residence of surface water parcels over the plateau at station A3 (2–3 months) (Park et al., 2008b) or inside the recirculation feature (0.5–1 month) compared to the mean residence of ^{234}Th (∼ 1 month), lateral contribution is likely to be minimal in these areas. Circulation at the northern station F-L is more dynamic and under the influence of northern Kerguelen shelf waters enriched in dissolved iron (dFe) (Quéroué et al., 2015). Shelf waters are probably depleted in ^{234}Th relative to ^{238}U due to the ear-

lier development of the bloom in this area, as well as due to sediment resuspension and deposition (Savoye et al., 2008). However, water parcel trajectory calculations (d'Ovidio et al., 2015) suggest that shelf waters are transported in times of less than 0.5–1 month to station F-L. This relatively short transit time still remains long enough for ^{234}Th-poor waters to re-equilibrate with ^{238}U due to ^{234}Th in-growth, thus limiting a potential lateral component to the ^{234}Th export flux.

2.4 Particulate ^{234}Th and POC

Suspended particulate matter was collected at nine process stations for particulate ^{234}Th and POC via large-volume (150–1000 L) in situ filtration systems (Challenger Oceanics and McLane WTS6-1-142LV pumps) equipped with 142 mm diameter filter holders. Two size classes of particles (> 53 and 1–53 µm) were collected via sequential filtration across a 53 µm mesh nylon screen (SEFAR-PETEX®) and a 1 µm pore size quartz fiber filter (QMA, Sartorius). To limit C and N blanks, the filters were pre-conditioned prior to sampling. For large particles (> 53 µm), the PETEX screens were soaked in HCl 5%, rinsed with Milli-Q water, dried at ambient temperature in a laminar flow hood, and stored in clean plastic bags. QMA filters were pre-combusted and acid cleaned following Bowie et al. (2010).

After collection, filters were subsampled under clean room conditions with acid cleaned ceramic scissors for PETEX screen and a 25 mm Plexiglas punch for QMA. For large particles, one-fourth of the 142 mm nylon screen was dedicated to ^{234}Th and POC. Particles were re-suspended in filtered seawater in a laminar flow clean hood and collected on 25 mm diameter silver (Ag) filters (1.0 µm porosity). For small particles, two 25 mm diameter punches were subsampled from the 142 mm QMA filters. Ag and QMA filters were dried overnight and mounted on nylon filter holders covered with Mylar and Al foil for beta counting. As for total ^{234}Th activity, particulate samples were counted twice on board until the RSD was below 2 %. The procedure was similar for sediment traps samples. Sediment traps samples were re-suspended in filtered seawater, collected on Ag filters, dried, and mounted on nylon filter holder. Residual beta activity was measured in the home-based laboratory after six ^{234}Th half-lives (∼ 6 months) and was subtracted from the on-board measured values.

Following beta counting, particulate samples (QMA and Ag filters) were processed for POC measurement by an elemental analyzer – isotope ratio mass spectrometer (EA-IRMS). Samples were dismounted from filters holders and fumed under HCl vapor for 4 h inside a glass desiccator to remove the carbonate phase. After overnight drying at 50 °C, samples were packed in silver cups and analyzed with a Carlo Erba NA 1500 elemental analyzer configured for C analysis and coupled on-line via a Con-Flo III interface to a Thermo Finnigan Delta V isotope ratio mass spectrometer. Acetanilide standards were used for calibration. C blanks were 1.46 µmol for Ag filters and 0.52 µmol for 25 mm QMA punch. Results obtained for two size-segregated POC fractions (> 53 and 1–53 µm) are reported in Appendix 2 along with particulate ^{234}Th activity measured in the same samples.

3 Results

3.1 ^{234}Th activity profiles

The complete data set of total ^{234}Th ($^{234}Th_{tot}$), ^{238}U activities (dpm L^{-1}), and associated $^{234}Th / ^{238}U$ ratios can be found in Table S1 in the Supplement. At all stations, the deficit of $^{234}Th_{tot}$ relative to ^{238}U was observed in surface waters ($^{234}Th / ^{238}U = 0.78$–$0.95$). $^{234}Th_{tot}$ activities increased progressively with depth and were back to equilibrium with ^{238}U at variable depths according to station: above 100 m at R, TNS-1, and F-L, between 100 and 150 m at A3-1, TEW-8, E-4E, and E-4W, and between 150 and 200 m at TNS-6, TNS-8, E-1, E-2, E-3, E-5, and A3-2. Such a pattern is typically encountered in the open ocean (Le Moigne et al., 2013) including the SO (Buesseler et al., 2001; Cochran et al., 2000; Morris et al., 2007; Planchon et al., 2013; Rutgers van der Loeff et al., 2011; Savoye et al., 2008) and indicate scavenging of ^{234}Th with sinking particles. In Fig. S1 in the Supplement, the early season trend in $^{234}Th / ^{238}U$ ratios is presented along the south-to-north transect from the central plateau (first visit to A3, A3-1), on the downward slope of the plateau (TNS-8), across the E stations (TNS-6) to the warmer less-saline PFZ waters north of the PF (TNS-1). Surface $^{234}Th / ^{238}U$ ratios varied from 0.92 (A3-1) to 0.85 (TNS-8) and indicates that export of particles had already occurred early for this time of the season (mid-October). Deficit was higher inside the PF meander ($^{234}Th / ^{238}U$ ratios of 0.85 to 0.88 at TNS-8 and TNS-6, respectively) and north of the PF ($^{234}Th / ^{238}U = 0.88$ at TNS-1) compared to the shallow central plateau ($^{234}Th / ^{238}U = 0.92$ at A3-1). Over the plateau, bottom water (∼ 50–80 m above seafloor) exhibited the lowest $^{234}Th / ^{238}U$ ratios (0.75). This pattern has already been documented (Savoye et al., 2008) and supports ^{234}Th removal due to sediment re-suspension.

At process stations, $^{234}Th_{tot}$ profiles were obtained in combination with particulate ^{234}Th ($^{234}Th_p$) for two size fractions (1–53 µm, > 53 µm). Results obtained in the different areas are shown in Fig. 2 for $^{234}Th_{tot}$, $^{234}Th_p$ (sum of the two size fractions, see Table S2), and dissolved ^{234}Th (total−particulate, $^{234}Th_d$) along with ^{238}U activity (dpm L^{-1}) deduced from salinity using the equation of Owens et al. (2011). The average $^{234}Th_{tot}$ within the first 100 m exhibited a relatively small variability over the KEOPS2 area with 2.21 ± 0.10 ($n = 4$, $^{234}Th / ^{238}U = 0.95 \pm 0.04$) at R-2, 2.18 ± 0.05 ($n = 5$, $^{234}Th / ^{238}U = 0.93 \pm 0.02$) at A3-1, 2.07 ± 0.20 ($n = 4$, $^{234}Th / ^{238}U = 0.89 \pm 0.08$) at F-L, and 1.98 ± 0.03 dpm L^{-1} ($n = 4$, $^{234}Th / ^{238}U = 0.84 \pm 0.01$) at E-1. In contrast, surface $^{234}Th_p$ activity, which reflects par-

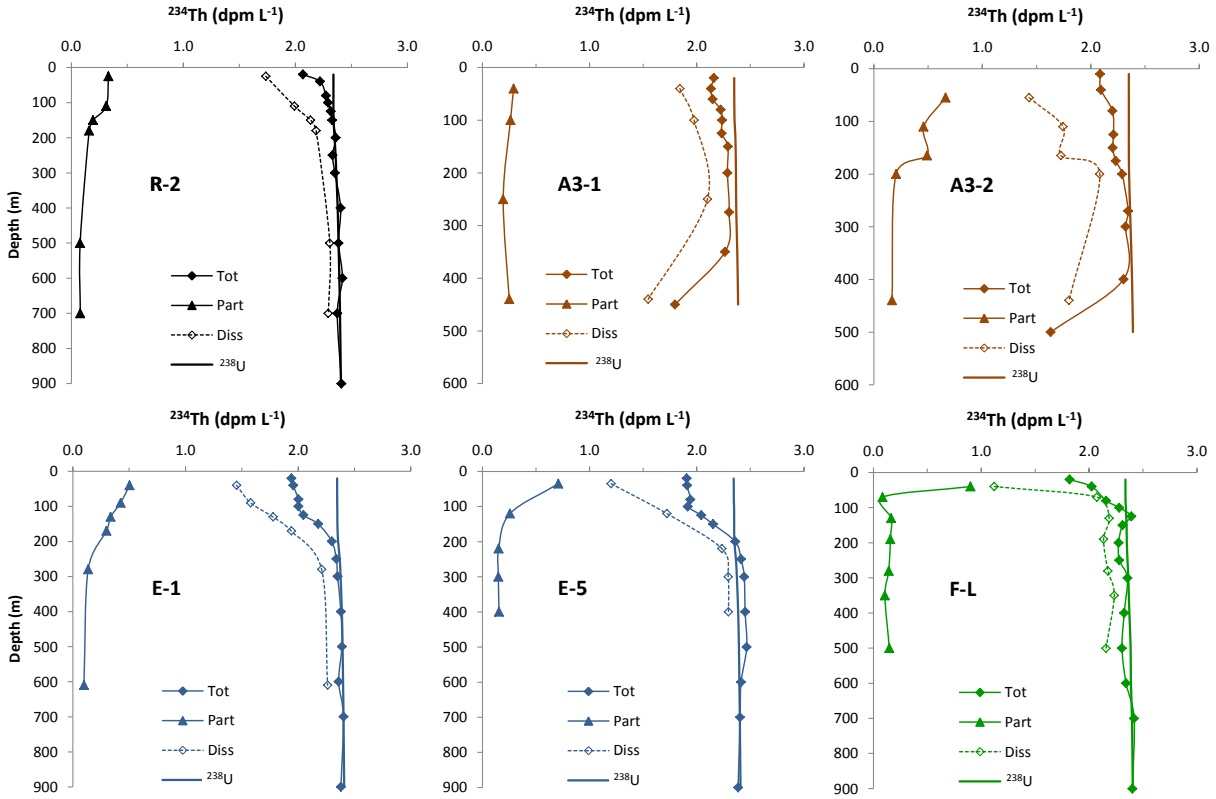

Figure 2. Depth profiles of total ^{234}Th (^{234}Th$_{tot}$), particulate ^{234}Th$_p$ (sum of the two size fractions), and dissolved ^{234}Th (total−particulate, ^{234}Th$_d$) activity (dpm L^{-1}) along with ^{238}U activity (dpm L^{-1}, solid lines) deduced from salinity at HNLC reference station R, central plateau station A3 (A3-1, first visit 20 October; A3-2, second visit 16 November), PF meander station E (E-1, first visit 30 October; E-5, fourth visit 8 November), and north of PF station F-L.

ticle concentration (Rutgers van der Loeff et al., 1997), was subject to larger variations. ^{234}Th$_p$ activity was low at R-2 (0.33 dpm L^{-1}) and at A3-1 (0.29 dpm L^{-1}), intermediate at E-1 (0.50 dpm L^{-1}), and highest at F-L (0.90 dpm L^{-1}). Over the course of the survey, averaged ^{234}Th$_{tot}$ activity within the first 100 m remained remarkably stable over the plateau, with 2.13 ± 0.06 ($n = 3$, ^{234}Th / ^{238}U $= 0.90 \pm 0.03$) at A3-2 (27.7 days later), and in the PF meander, with 1.91 ± 0.07 ($n = 4$, ^{234}Th / ^{238}U $= 0.82 \pm 0.03$) at E-3 (4.5 days later) and 1.92 ± 0.02 dpm L^{-1} (n = 4, ^{234}Th / ^{238}U $= 0.82 \pm 0.01$) at E-5 (19.6 days later). For the particulate phase, the situation was different. At A3, ^{234}Th$_p$ increased from 0.29 to 0.66 dpm L^{-1} between the two visits. At site E, ^{234}Th$_p$ varied from 0.50 to 0.70 dpm L^{-1} between the first (E-1) and the last (E-5) visit, suggesting an increase in particle concentrations in surface waters at both A3 and E stations.

3.2 ^{234}Th flux

Total ^{234}Th activity profiles were used for estimating export fluxes based on SS and NSS assumptions. Cumulated export fluxes of total ^{234}Th are presented in Fig. 3 and Table S3. Using the SS calculation, ^{234}Th export from the first 100 m ranged from 412 ± 134 at R-2 to 1326 ± 110 dpm m^{-2} d^{-1} at E-3. ^{234}Th export increased below 100 m depth except at station R-2 and north of the PF (stations F-L, TEW-8, and TNS-1) where ^{234}Th was back to equilibrium with ^{238}U above 100 m. At 200 m depth, ^{234}Th export reached 993 ± 200 at A3-2, 1372 ± 255 at TNS-8, and between 1296 ± 193 and 1995 ± 176 dpm m^{-2} d^{-1} at E stations. At A3, the NSS ^{234}Th export was 736 ± 186 at 100 m and 1202 ± 247 dpm m^{-2} d^{-1} at 200 m and compares well with SS export. At E stations, NSS export from the first 100 m were 911 ± 242 at E-4E and 1383 ± 177 dpm m^{-2} d^{-1} at E-5 and also compares well with SS export. Between 100 and 200 m, NSS ^{234}Th export increased at E-5 (2034 ± 299 dpm m^{-2} d^{-1}) and decreased at E-4E (520 ± 402 dpm m^{-2} d^{-1}). In addition to water column data, export of ^{234}Th was determined from sediment traps deployed at 200 m depth (see Fig. 3 and Table 1). Details of trap deployments carried out at E-1, E-3, E-5, and A3-2 can be found elsewhere (Laurenceau-Cornec et al., 2015a). Export of ^{234}Th measured in trap samples ranged from 506 ± 21 at A3-2 to 1129 ± 177 dpm m^{-2} d^{-1} at E-3 and represented ~ 50 % of the SS and NSS export determined from ^{234}Th$_{tot}$ activity profiles.

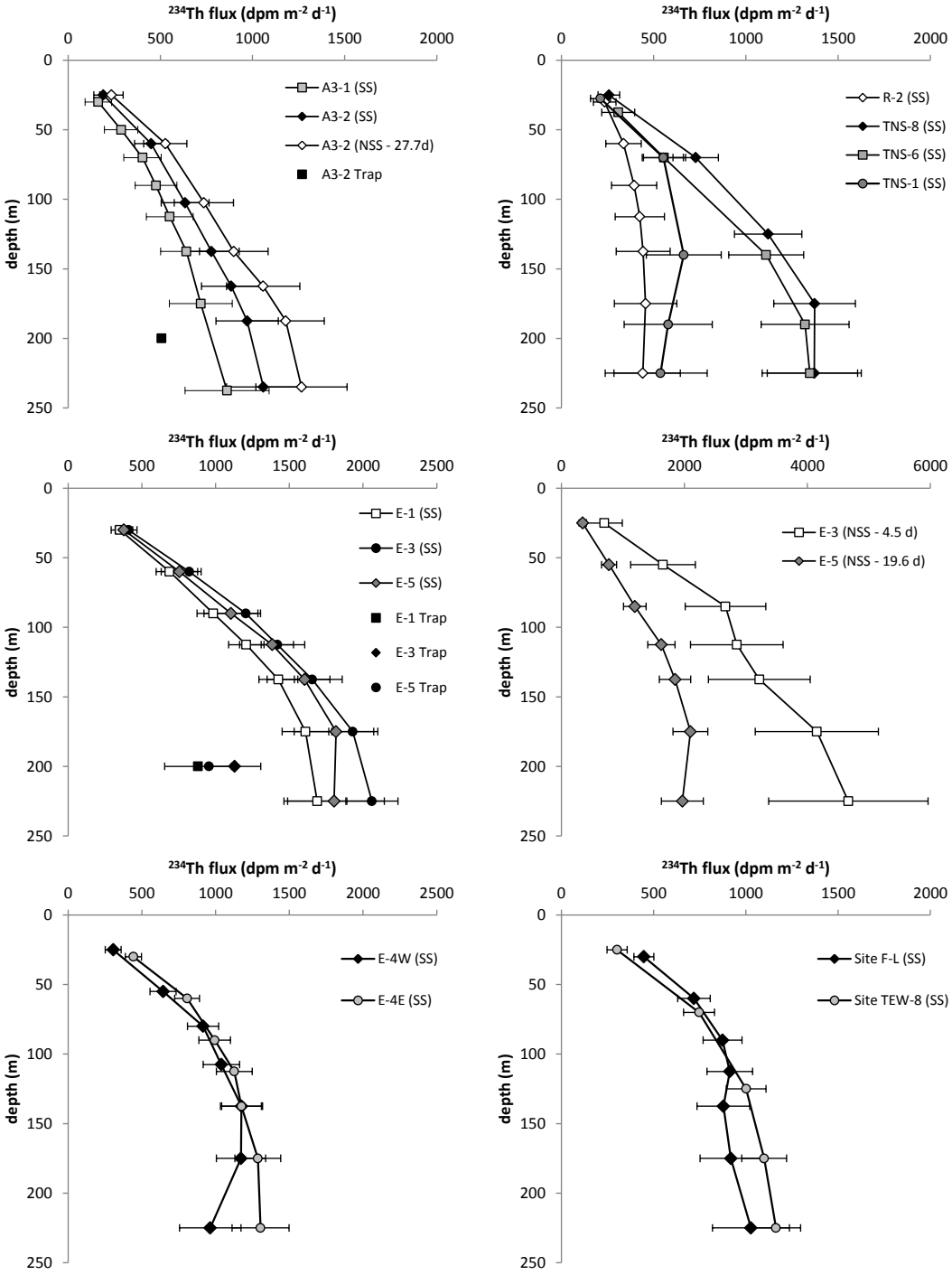

Figure 3. Depth profiles of cumulated total ^{234}Th export fluxes from the surface to 250 m depth using steady state (SS) and non-steady state (NSS) models and comparison with ^{234}Th export fluxes estimated from sediment traps at 200 m.

3.3 C : Th ratio of particles

At process stations, particulate ^{234}Th activities and POC were obtained in two size fractions of particles (1–53 µm, > 53 µm). Profiles of POC : ^{234}Th ratios (C : Th) are shown in Fig. 4. C : Th ratios were highly variable, ranging from 1.8 to 21.5 in 1–53 µm particles and from 1.0 to 12.5 in > 53 µm particles. For both size classes, C : Th ratios were high in surface waters (0–150 m) with a range of 6.3–9.6 at R, 6.9–13.1 at A3, and 5.7–11.4 µmol dpm^{-1} at E stations with no clear site-related trend. For open-ocean stations, C : Th ratios decreased rapidly with depth for the two size classes of particles

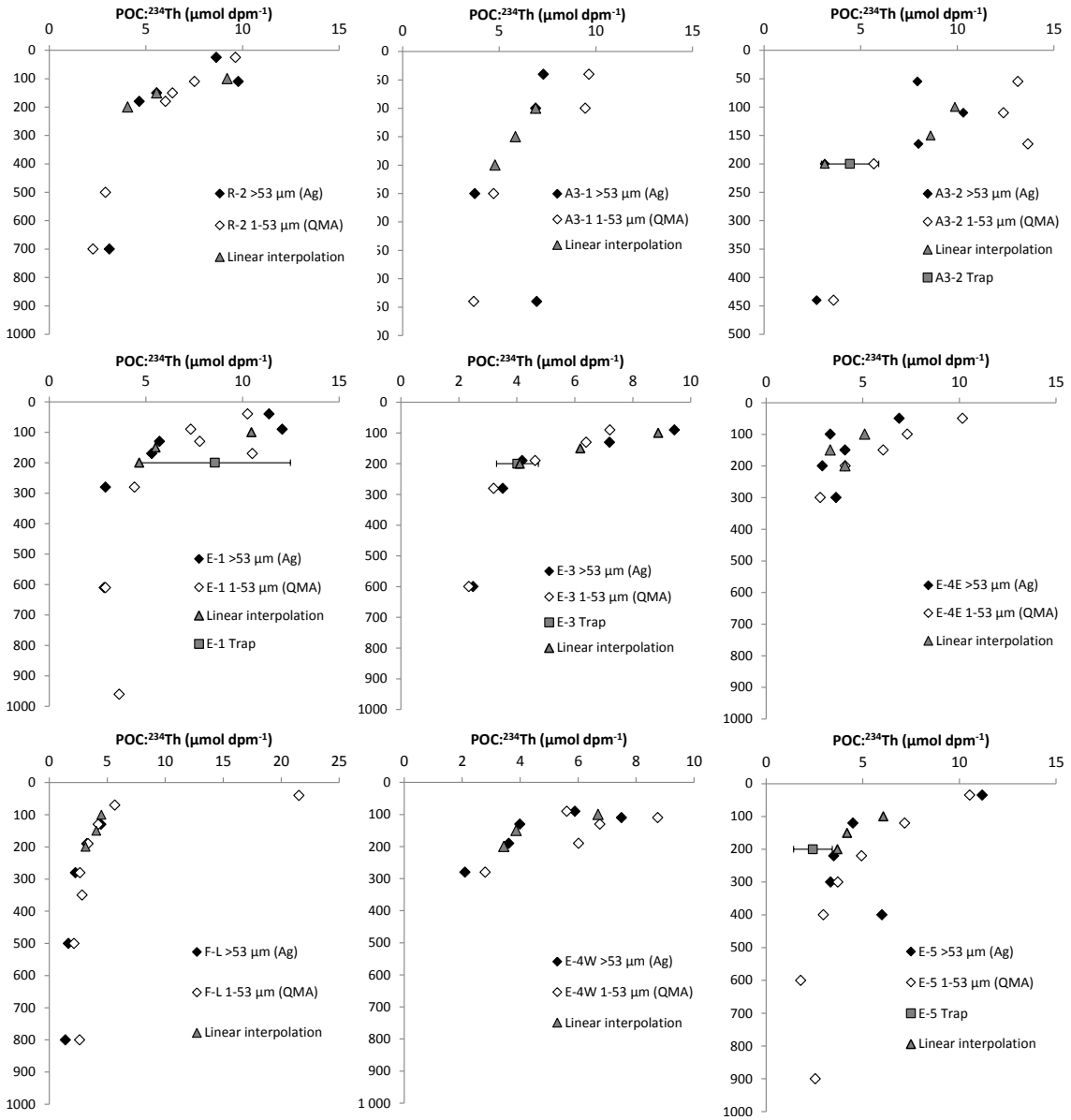

Figure 4. POC : ^{234}Th (C : Th) ratio in size-fractionated (1–53 and > 53 µm) suspended particulate matter collected by ISP and comparison with sinking particles collected via sediment traps at 200 m depth. Also, shown is a linear interpolation of C : Th ratios at 100, 150, and 200 m depth for carbon flux estimates. Linear interpolation was obtained using a straight line fit between the upper and the lower data point relative to the target depth (i.e., 100, 150, and 200 m depth).

and reached relatively constant values in the mesopelagic zone with 2.8–4.8 at R-2, 2.6–4.5 at E stations, and 1.6–2.7 µmol dpm^{-1} at F-L. According to particle size, C : Th ratios showed different trends. At R-2, E-1, E-3, E-4W, and E-5, C : Th ratios were comparable in small and large particles. At plateau stations A3-1 and A3-2, and to a lesser extent at E-4E, C : Th ratios increased with decreasing size of particles.

3.4 C : Th ratio of sinking particles

To estimate the POC export flux using the ^{234}Th-based approach, the C : Th ratio of sinking particles needs to be determined at the depth of export (Buesseler et al., 1992). Assuming the larger particle size class to be representative of the sinking material (Buesseler et al., 2006), we used the C : Th ratios of > 53 µm particles to convert ^{234}Th fluxes into POC fluxes. C : Th ratios were estimated at fixed depths of 100, 150, and 200 m, and results are listed in Table 1 and plotted in Fig. 4. For A3-1, A3-2, E-1, E-3, E-4W, and E-5, C : Th

Table 1. ^{234}Th and POC export fluxes and C : Th ratios of sinking particles estimated at 100, 150, and 200 m depth, and carbon export efficiency (ThE and export production / new production (EP / NP) ratios) during KEOPS2 (bold text indicates that non-steady state calculations were used). ThE ratio defined as the ratio of POC export to net primary production (NPP) and EP / NP ratio defined as the ratio of POC export to new production (NP).

Station	Date	Depth (m)	^{234}Th flux (dpm m^{-2} d^{-1})	C : Th (µmol dpm^{-1})	POC flux (mmol m^{-2} d^{-1})	ThE (%)	EP / NP (%)
R-2	25 Oct	100	412 ± 134	9.2 ± 0.5	3.8 ± 1.2	34	73
R-2	25 Oct	150	448 ± 146	5.6 ± 0.4	2.5 ± 0.8	22	48
R-2	25 Oct	200	449 ± 203	4.1 ± 0.5	1.8 ± 0.9	16	35
A3-1	20 Oct	100	509 ± 127	6.9 ± 0.7	3.5 ± 0.9		
A3-1	20 Oct	150	666 ± 140	5.8 ± 0.7	3.9 ± 0.9		
A3-1	20 Oct	200	776 ± 171	4.8 ± 0.5	3.7 ± 0.9		
A3-2	16 Nov	100	463 ± 151	9.9 ± 0.1	4.6 ± 1.5	3	3
A3-2	16 Nov	150	829 ± 169	8.6 ± 0.1	7.1 ± 1.5	5	5
A3-2	16 Nov	200	993 ± 200	3.1 ± 0.1	3.1 ± 0.6	2	2
A3-2 trap	15–17 Nov	200	506 ± 21	4.5 ± 1.5	2.2 ± 0.7		
A3-2	**20 Oct–16 Nov**	**100**	**736 ± 186**	**9.9 ± 0.1**	**7.3 ± 1.8**	**5**	**5**
A3-2	**20 Oct–16 Nov**	**150**	**975 ± 209**	**8.6 ± 0.1**	**8.4 ± 1.8**	**5**	**5**
A3-2	**20 Oct–16 Nov**	**200**	**1202 ± 247**	**3.1 ± 0.1**	**3.8 ± 0.8**	**2**	**2**
F-L	6 Nov	100	902 ± 117	4.5 ± 0.4	4.1 ± 0.6	1	2
F-L	6 Nov	150	891 ± 164	4.1 ± 0.4	3.6 ± 0.8	1	1
F-L	6 Nov	200	973 ± 207	3.1 ± 0.5	3.0 ± 0.8	1	1
E-1	30 Oct	100	1111 ± 120	10.5 ± 0.2	11.6 ± 1.3	27	34
E-1	30 Oct	150	1504 ± 158	5.5 ± 0.2	8.3 ± 0.9	19	24
E-1	30 Oct	200	1665 ± 201	4.7 ± 0.2	7.7 ± 1.0	18	23
E-1 trap	29 Oct–3 Nov	200	881 ± 226	8.6 ± 3.9	7.0 ± 2.3		
E-3	3 Nov	100	1326 ± 110	8.9 ± 0.3	11.8 ± 1.1	21	32
E-3	3 Nov	150	1742 ± 142	6.2 ± 0.2	10.8 ± 0.9	19	29
E-3	3 Nov	200	1995 ± 176	4.1 ± 0.2	8.2 ± 0.8	14	22
E-3 trap	5–9 Nov	200	1129 ± 177	4.0 ± 0.7	4.9 ± 1.5		
E-4E	13 Nov	100	1051 ± 121	5.1 ± 0.3	5.4 ± 0.7	7	9
E-4E	13 Nov	150	1210 ± 155	3.3 ± 0.1	4.0 ± 0.5	5	7
E-4E	13 Nov	200	1296 ± 193	4.1 ± 0.4	5.3 ± 1.0	7	9
E-4E	**30 Oct–13 Nov**	**100**	**911 ± 242**	**5.1 ± 0.3**	**4.6 ± 1.3**	**6**	**8**
E-4E	**30 Oct–13 Nov**	**150**	**726 ± 315**	**3.3 ± 0.1**	**2.4 ± 1.0**	**3**	**4**
E-4E	**30 Oct–13 Nov**	**200**	**525 ± 402**	**4.1 ± 0.4**	**2.1 ± 1.7**	**3**	**4**
E-5	18 Nov	100	1262 ± 116	6.1 ± 0.1	7.7 ± 0.7	10	14
E-5	18 Nov	150	1671 ± 153	4.2 ± 0.2	7.0 ± 0.7	9	12
E-5	18 Nov	200	1810 ± 190	3.7 ± 0.2	6.7 ± 0.8	9	12
E-5 trap	18–19 Nov	200	955 ± 546	2.4 ± 0.1	2.0 ± 1.0		
E-5	**30 Oct–18 Nov**	**100**	**1383 ± 177**	**6.1 ± 0.2**	**8.4 ± 1.1**	**11**	**15**
E-5	**30 Oct–18 Nov**	**150**	**1928 ± 235**	**4.2 ± 0.2**	**8.1 ± 1.0**	**10**	**14**
E-5	**30 Oct–18 Nov**	**200**	**2034 ± 299**	**3.7 ± 0.2**	**7.5 ± 1.2**	**10**	**13**
E-4W	11 Nov	100	1003 ± 124	6.7 ± 0.2	6.7 ± 0.9	3	3
E-4W	11 Nov	150	1174 ± 168	3.9 ± 0.1	4.5 ± 0.7	2	2
E-4W	11 Nov	200	1068 ± 208	3.4 ± 0.2	3.7 ± 0.7	2	2

ratios of sinking particles were estimated from linear interpolation of measured C : Th ratios. At R-2, the C : Th ratio at 100 m represents the average ratio measured between 25 and 110 m. At F-L, the 100 m C : Th ratio was taken to be equal to the value at 130 m. For E-4E, C : Th of large particles were measured directly at the depths of 100, 150, and 200 m and were not interpolated. As illustrated in Fig. 4 and in Table 1, C : Th ratios of sinking particles at 200 m estimated using ISP samples showed good agreement with sedi-

ment trap data within uncertainty (3–6 and 18–46 % RSD for ISP and trap C : Th ratios, respectively) .

3.5 POC export flux

POC export fluxes were estimated at 100 m (EP100), 150 m (EP150), and 200 m (EP200) by multiplying the corresponding ^{234}Th export flux with the C : Th ratio of sinking particles at the depth of export. Results are listed in Table 1. EP100 estimated with the SS model were lowest at A3-1 (3.5 ± 0.9 mmol m^{-2} d^{-1}) and at R-2 (3.8 ± 1.2 mmol m^{-2} d^{-1}) and highest at E-1 with 11.8 ± 1.3 mmol m^{-2} d^{-1}. The EP100 at F-L was 4.1 ± 0.6 mmol m^{-2} d^{-1} and was similar to the value for the control station R-2 and the plateau station A3. In the PF meander, EP100 remained stable between the two first visits (E-3) with 11.8 ± 1.1, but decreased at the third visit (E-4E) to 5.4 ± 0.7 at E4-E, and increased to 7.7 ± 0.7 mmol m^{-2} d^{-1} at the last visit (E-5). Station E-4W, not included in the time series, had an EP100 of 6.7 ± 0.9 mmol m^{-2} d^{-1}, very similar to E-4E on the eastern edge of the PF meander. At 200 m, export fluxes ranged between 1.8 ± 0.9 (R-2) and 8.2 ± 0.8 mmol m^{-2} d^{-1} (E-3). At the re-visited stations, carbon export was also estimated using the NSS model approach. NSS EP100 varied from 4.6 ± 1.3 (E-4E) to 8.4 ± 1.1 mmol m^{-2} d^{-1} (E-5). Within the uncertainty, NSS EP100 were similar (E-5 and E-4E) or higher (A3) in comparison to SS EP100. EP200 determined with the ^{234}Th proxy could be directly compared to fluxes estimated with sediment traps deployed at the same depth (Table 1). Trap fluxes in comparison to EP200 were in very good agreement within uncertainties at E-1 (7.0 ± 2.3 and 7.7 ± 1.0 mmol m^{-2} d^{-1} for trap and ^{234}Th-based fluxes, respectively) and A3-2 (2.2 ± 0.7 and 3.1 ± 0.6 mmol m^{-2} d^{-1} for trap and ^{234}Th-based fluxes, respectively), and 1.7-fold and 3.3-fold lower at E-3 and E-5, respectively.

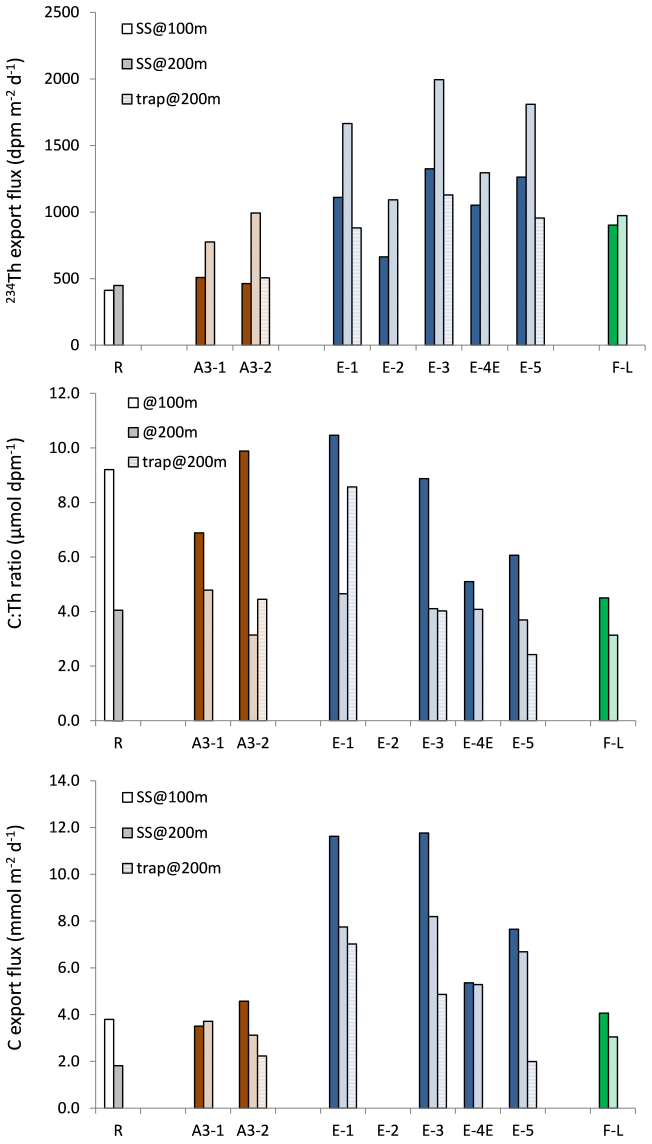

Figure 5. Summary results of ^{234}Th export fluxes (dpm m^{-2} d^{-1}), sinking particles C : Th ratios (µmol dpm^{-1}), and POC export fluxes (mmol m^{-2} d^{-1}) obtained at 100 and 200 m depth and comparison with sediment trap data obtained at 200 m depth during KEOPS2 survey.

4 Discussion

The principal aim of this study was to estimate how natural Fe fertilization affects carbon export at high productivity sites over and off-plateau during the early stages of the bloom. In the following sections, results obtained with the ^{234}Th-based approach and summarized in Fig. 5 are discussed according to the four distinct zones investigated during the survey (control station R-2, north of the PF station F-L, plateau station A3, and PF meander E stations). For each zone, we briefly review the mode and timing of iron supply, described in more details elsewhere (Trull et al., 2015), deduced from dissolved and particulate iron inventories (Quéroué et al., 2015; van der Merwe et al., 2015) and from iron budgets in the surface mixed-layer (Bowie et al., 2015). We examine POC export efficiencies using two different metrics (Table 1): (1) ThE ratio defined as the ratio of POC export to net primary production (NPP) (Buesseler, 1998) and (2) EP / NP ratio estimated as the ratio between POC export to new production (NP) (Joubert et al., 2011; Planchon et al., 2013). NPP and NP are estimated from short-term (24 h) deck board ^{13}C-HCO_3^-, ^{15}N-NO_3^-, ^{15}N-NH_4^+ incubation experiments (Cavagna et al., 2014). NP, the fraction of C uptake supported by NO_3^- assimilation, is estimated from the NPP and the f-ratio (Cavagna et al., 2014). NP is considered to provide an estimate of potentially "exportable production" based on a number of assumptions (Sambrotto

and Mace, 2000) and despite several limitations (Henson et al., 2011).

4.1 Reference site R-2

At reference station R-2, the observed EP100 of 3.8 ± 1.2 mmol m^{-2} d^{-1} is very small and reflects mainly a small and shallow export of ^{234}Th (412 ± 134 dpm m^{-2} d^{-1} at 100 m). Low EP100 is consistent with the HNLC conditions at station R-2, where high concentrations of nitrate (25 µM), silicic acid (12–13 µM) (Blain et al., 2015), and very low biomass (Lasbleiz et al., 2014) are observed in surface waters. Dissolved iron (< 0.1 nmol L^{-1}) and particulate iron (pFe) levels (0.3 nmol L^{-1}) are also very low in surface waters (Quéroué et al., 2015; van der Merwe et al., 2015). Fluxes of dFe to the surface mixed layer are estimated to be very limited (94 nmol m^{-2} d^{-1}) and essentially driven by vertical supplies (Bowie et al., 2015). Biomass at station R-2 appears to be dominated by small, slow-growing phytoplankton (Trull et al., 2015), which offer a limited potential for export. This feature is reflected in the partitioning of POC and ^{234}Th$_p$, with ~ 90 % being associated with the small (1–53 µm) size fraction between 25 and 110 m depth. C : Th ratios of particles show no variation with particle size (Fig. 5) and suggest that large sinking particles may be a result of aggregation processes (Buesseler et al., 2006). This is supported by gel trap observations, revealing that phytodetrital aggregates are an important fraction of sinking material between 110 and 430 m depth (Laurenceau-Cornec et al., 2015a).

The flux obtained at the KEOPS2 reference station is similar to results obtained during the first leg of CROZEX (November–December 2004) at control sites M2 and M6, with carbon export of 4.9 ± 2.7 and 5.8 ± 3.9 mmol m^{-2} d^{-1}, respectively (Morris et al., 2007). Our value for C export is however much lower than the flux obtained in summer at the KEOPS1 control site C11 (12.2 ± 3.3 mmol m^{-2} d^{-1}; January–February 2005; Savoye et al., 2008) or during the second Leg of CROZEX (December 2004–January 2005) with 18.8 ± 3.4 at M2 and 14.4 ± 3.0 mmol m^{-2} d^{-1} at M6 (Morris et al., 2007).

For the reference station R-2, ThE and EP / NP ratios were high with 34 and 73 %, respectively, and indicate a relatively efficient carbon pump despite the limited magnitude of carbon export and uptake (NPP = 11.2 mmol m^{-2} d^{-1}). The ThE ratio falls in the range of most literature data for the SO, which is generally elevated (> 10 %) in HNLC waters (Buesseler et al., 2003; Savoye et al., 2008). During KEOPS1, a ThE ratio as high as 58 % was observed at the reference station C11 (Savoye et al., 2008). The reasons for this high efficiency could be numerous, and a detailed discussion can be found elsewhere (Laurenceau-Cornec et al., 2015a). Briefly, efficient scavenging of POC at the low productivity site (R-2) may be mediated by fast-sinking aggregates composed of heavily silicified diatoms. Although BSi levels are low (Lasbleiz et al., 2014), this scenario is supported by the diatom community found at the reference station R-2, which was dominated by the heavily silicified *Fragilariopsis* spp. and *Thalassionema nitzschioides* (Laurenceau-Cornec et al., 2015b and references therein). In addition, the limited zooplankton biomass at R-2 (Carlotti et al., 2015) and the rarity of fecal pellets in exported material (Laurenceau-Cornec et al., 2015a) suggest that attenuation/transformation of the POC flux through grazing is rather limited, and thus could also partly explain the high export efficiency at the reference station R-2.

With depth, carbon export decreased rapidly at station R-2, and more than 50 % of EP100 was lost between 100 and 200 m depth. Consequently, export efficiency decreased at 200 m depth to 16 and 34 % based on the ThE and NP ratios, respectively. A similar trend was deduced from gel traps (Laurenceau-Cornec et al., 2015a). In our case, a sharp decrease of export with depth seems to be essentially driven by the C : Th ratio of sinking particles, which decreases from 9.2 to 4.1 µmol dpm^{-1} between 100 and 200 m (Fig. 4). Such a decrease may support a preferential loss of C relative to ^{234}Th due to a partial degradation of sinking particles (Buesseler et al., 2006). This feature could involve heterotrophic bacterial activity, since high content of bacteria cells (2.9×10^5 cell mL^{-1}) are found between 100–150 m (Christaki et al., 2014).

4.2 North of PF site (F-L)

The northern PF station (F-L) exhibits moderate dFe enrichment in surface waters (~ 0.26 nmol L^{-1}) (Quéroué et al., 2015). Enrichment is much higher for pFe (1–2.5 nmol L^{-1}) presumably reflecting biological iron uptake and conversion into biogenic particulate fraction (van der Merwe et al., 2015). The iron budget is not available for station F-L so it is difficult to determine the mode of iron fertilization. However, dFe is likely to be supplied by both vertical exchanges with the Fe-rich reservoir from below and by lateral advection of iron-rich coastal waters from the northern Kerguelen shelf along the northern side of the PF jet (d'Ovidio et al., 2015; Park et al., 2014a; Trull et al., 2015). Analysis of drifter trajectories and altimetry-based geostrophic currents (d'Ovidio et al., 2015) indicate that advection of water parcels from the Kerguelen shelf is relatively short to station F-L (0.5 to 1 month). However, iron-rich waters rapidly disperse in this area and limit the persistence of iron fertilization (Trull et al., 2015).

EP100 at station F-L is low (4.1 ± 0.6 mmol m^{-2} d^{-1}) and is only 1.1-fold higher than at the control station R-2. This suggests no impact of Fe fertilization on upper-ocean carbon export in early bloom conditions. However, ^{234}Th export at F-L is 2.2 times higher in comparison to the reference station at the same depth, and indicates a more efficient scavenging of particles in the PFZ. This is supported further by the similar 100 m ^{234}Th flux observed in the same area

at TEW-8 (886 ± 162 dpm m^{-2} d^{-1}, see Table S3). It should be mentioned that EP100 at F-L may be underestimated because the C : Th ratio used to convert the ^{234}Th flux into C flux was taken at 130 m depth and may be lower than at 100 m depth. As an example, C : Th ratio of 1–53 µm particle at station F-L is 6.0 at 70 m and strongly decreases to 4.5 µmol dpm^{-1} at 130 m. However, considering deeper export, EP200 at F-L (3.0 ± 0.8 mmol m^{-2} d^{-1}) appears 1.6-fold higher than EP200 at the reference station R-2 suggesting an early impact of Fe fertilization on C export at this depth. In this area, EP200 estimated using the ^{234}Th proxy shows excellent agreement with fluxes deduced from gel traps (Laurenceau-Cornec et al., 2015a).

The observed trend in EP drastically contrasts with the very high productivity at F-L. A massive bloom rapidly developed in early November in this area as revealed by satellite images (F. D'Ovidio, personal communication, 2014) and station F-L was visited only a few days after the start of the bloom. Phytoplankton biomass was high with total Chl *a* up to 5.0 µg L^{-1}, total BSi up to 3.9 and POC up to 28.2 µmol L^{-1} (Lasbleiz et al., 2014), with the diatom-dominated phytoplankton community in the fast-growing phase as revealed by Si (Closset et al., 2014) and C (Cavagna et al., 2014) uptake rates. The phytoplankton community was composed of a broad spectrum of size and taxa (Trull et al., 2015). Considering the three size fractions dominated by phytoplankton (5–20, 20–50, 50–210 µm), 48 and 52 % of POC was found above and below 50 µm, respectively, with small species presumably originating from Fe-rich waters of the northern Kerguelen shelf, and large species being characteristic of low biomass waters south of the PF offshore of the islands (Trull et al., 2015). It is interesting to note that the high biomass content is reflected in the partitioning of ^{234}Th showing very high ^{234}Th$_p$ activity (0.9 dpm L^{-1} at 40 m, see Fig. 2). Furthermore, ^{234}Th$_p$ appears to be evenly distributed between small and large particles similarly to phytoplankton community structure. Between 40 and 70 m depth, 40 % of ^{234}Th$_p$ is found with the small (1–53 µm) particles and 60 % with the large (> 53 µm) particles. This size spectrum of particles clearly offers higher potential for C export at F-L compared to the HNLC reference station.

However, comparison with NPP and NP reveals that export efficiency is very low at F-L with ThE and EP / NP ratios of 1 and 2 %, respectively. The two indicators clearly support an inefficient transfer of C to depth and indicate a pronounced decoupling between export and production. Observed decoupling may partly result from methodological mismatches in the measurements since time and space scales integrated by NPP and NP (24 h incubation) differs from the ^{234}Th approach ($\sim$ 1 month). However, very low ThE and EP / NP ratios may also indicate that biomass is in an accumulation phase at station F-L and a major export event is likely to be delayed until later in the season. Such an accumulation scenario is supported by the small, fast-growing, and less-silicified phytoplankton species observed at F-L (Trull et al., 2015) which are presumably less efficient at exporting carbon to depth. Furthermore, high mesozooplankton biomass (4.5 gC m^{-2}) (Carlotti et al., 2015) as well as the dominance of cylindrical fecal pellets in gel traps (Laurenceau-Cornec et al., 2015a) supports an intense grazing activity at F-L, which may contribute to the reduction of the POC flux and to the low export efficiency.

Comparison with literature data shows that EP100 at F-L (4.1 ± 0.6 mmol m^{-2} d^{-1}) remains substantially lower than POC export reported during CROZEX experiment both during leg 1 (range 4.9–17 mmol m^{-2} d^{-1}) and leg 2 (13–30.0 mmol m^{-2} d^{-1}), even though similar Fe-rich waters of the PFZ were sampled (Morris et al., 2007).

Attenuation of export production with depth is relatively weak at F-L, as only 25 % of EP100 is lost between 100 and 200 m depth. This decrease is due to the decreasing C : Th ratio of sinking particles from 4.5 to 3.1 µmol dpm^{-1} between 130 and 200 m. As already mentioned for the reference site, this trend may involve heterotrophic degradation of sinking particles. However, bacterial production at F-L is most intense in the first 60 m and decreases rapidly with depth to reach values similar to the reference station below 100 m depth (Christaki et al., 2014). At F-L, large particles seems to be more resistant to heterotrophic degradation and this may be linked to the higher abundance of fast-sinking cylindrical fecal pellets (Laurenceau-Cornec et al., 2015a).

4.3 Plateau site A3

Station A3 was located in iron- and silicic acid-rich waters over the central plateau and was visited twice, early (20 October) and late (16 November) in the survey. Surface mixed layer dFe levels were high at A3-1 (0.28–0.32 nmol3 L^{-1}) and decreasing at A3-2 (0.14–0.18 nmol L^{-1}) probably due to biological uptake (Quéroué et al., 2015). Surface pFe exhibits a similar trend as dFe, with higher concentrations at A3-1 compared to A3-2, but with a more important biogenic fraction at A3-2 (van der Merwe et al., 2015). Vertical dFe fluxes are by far the dominant sources of iron over the Plateau, and fuel the surface waters during episodic deepening of the upper mixed-layer (Bowie et al., 2015). Consequently, fertilization over the plateau is considered to be relatively recent, occurring during the maximum winter mixing period in August–September (Trull et al., 2015) and persisting over 2–3 months based on the estimated residence times of water parcels over the plateau (Park et al., 2008b).

EP100 over the plateau was very limited, with 3.5 ± 0.9 and 4.6 ± 1.5 mmol m^{-2} d^{-1} at A3-1 and A3-2, respectively, based on the SS model. Based on the NSS model, EP100 at A3-2 appears slightly higher with 7.3 ± 1.8 mmol m^{-2} d^{-1}. EP100 at A3 shows no difference or a maximum of 1.9-fold higher flux in comparison to the HNLC reference station R-2 suggesting limited impact of Fe fertilization. Interestingly, the ^{234}Th deficit follows the density structure and extends to the bottom of the mixed layer at 150–200 m.

This is much deeper than at stations R-2 or F-L, and consequently ^{234}Th export increases to 776 ± 171 at A3-1 and to 993 ± 200 dpm m^{-2} d^{-1} at A3-2 between 100 and 200 m depth. At A3-2, POC flux was the highest at 150 m depth with EP150 of 7.1 ± 1.5 and of 8.4 ± 1.8 mmol m^{-2} d^{-1} based on SS and NSS model respectively, and is 2.8–3.4-fold higher in comparison to EP150 at the HNLC station. At 200 m, increasing ^{234}Th export is canceled out by the simultaneous decrease of C : Th ratios resulting in low carbon export similar to A3-1. Comparison of PPS3/3 and gel sediment traps can be conducted at A3-2. First, we observe excellent agreement between ISP and PPS3/3 trap C : Th ratios (Fig. 5), indicating that the choice of large (> 53 µm) particles collected via ISP as representative of sinking particles was appropriate. Second, EP200 estimated in this study (3.1 ± 0.6 and 3.8 ± 0.8 mmol m^{-2} d^{-1} with SS and NSS model, respectively) compare well with PPS3/3 trap flux (2.2 ± 0.7 mmol m^{-2} d^{-1}) and are smaller than gel trap-derived fluxes (5.5 mmol m^{-2} d^{-1}) (Laurenceau-Cornec et al., 2015a). The low flux collected with PPS3/3 traps may indicate under-trapping, but given that the trap was deployed only for 1 day, this site is particularly susceptible to temporal mismatch resulting from short–term variations in particle fluxes. However, it is worth mentioning that the good agreement found between the different and totally independent approaches is encouraging and tends to confirm that export production over the central plateau was rather low throughout the survey.

Low export at A3 contrasts with the rapid biomass increase that occurred a few days before the second visit as revealed by satellite images (F. D'Ovidio, personal communication, 2014). The phytoplankton bloom at A3 showed different characteristics compared to station F-L, suggesting variable biological responses to Fe fertilization. The bloom over the central plateau was dominated by fast-growing, large, and heavily silicified diatoms (Trull et al., 2015) showing very high Si uptake rates (Closset et al., 2014). The change in biomass levels at A3 is well reproduced by ^{234}Th$_p$ activity which increases from 0.25 to 0.55 dpm L^{-1} between the first and the second visit. These changes are observed also in the size partitioning of ^{234}Th$_p$. While at A3-1, 95 % of ^{234}Th$_p$ is found to be associated with small (1–53 µm) particles, at A3-2 ∼ 70 % is found to be associated with large (> 53 µm) particles between 55 and 165 m depth. This clearly suggests a very high potential for export at A3-2, although the massive export event had not yet commenced. Delayed export is suggested further by the very low ThE and EP / NP ratios at 100 m depth of 3 and 5 %, respectively, at A3-2, which indicates that biomass was accumulating in the mixed layer.

Over the central plateau, EP200 during the early stages of the bloom (range of 3.1 ± 0.6–3.8 ± 0.8 mmol m^{-2} d^{-1}) are 4.4 to 12 times smaller than during the KEOPS1 late summer condition at the same depth horizon (13.9 ± 5.9–37.7 ± 13.3 mmol m^{-2} d^{-1}) (Savoye et al., 2008). This difference is essentially due to much higher ^{234}Th fluxes reported during KEOPS1 (range 2249 ± 772–8016 ± 949 dpm m^{-2} d^{-1}), indicating that particle scavenging is much more intense in January–February during the peak and decline of the bloom. Interestingly, the C : Th ratio of sinking particles exhibits a similar range over the entire growth season, 3.1–9.9 during KEOPS1 and 4.7–7.7 µmol dpm^{-1} during KEOPS-2, between 100 and 200 m depth. This is relatively surprising because sinking particles are very different between the early and late bloom period over the plateau. During KEOPS2, sinking particles were dominantly composed of phytodetrital aggregates (Laurenceau-Cornec et al., 2015a), and rapid aggregation of diatom cells was also evidenced from underwater vision profiler observations and modeling (Jouandet et al., 2014). During KEOPS1, the export process was different and the majority of the particle flux (composed of fecal pellets and fecal aggregates) was processed through the heterotrophic food web (Ebersbach and Trull, 2008).

4.4 PF meander site E

Export in the recirculation feature south of the PF (E stations) was the highest for the whole survey (Fig. 5). The four visits carried out as a pseudo-Lagrangian survey (E-1, E-3, E-4E, and E-5) revealed the short-term temporal variability of carbon export over 19.6 days. Surface waters in this area show low-to-moderate enrichment in dFe levels relative to the reference station R-2 but with a high variability (range of 0.06–0.38 nmol L^{-1}) (Quéroué et al., 2015). Mode and timing of iron fertilization appears to be complex in the PF meander and differs from over the plateau. The iron budgets suggest that lateral supplies of dFe are the dominant sources of iron for the recirculation feature (4–5-fold greater than the vertical flux) (Bowie et al., 2015). Based on water parcel trajectories, the recirculation region could be fueled with Fe-rich waters from the northern Kerguelen shelf, similarly to the north of PF region (station F-L) but delayed. Also, waters derived from northeast are diluted with waters derived from the south (d'Ovidio et al., 2015; Park et al., 2014a). Thus, fertilization of the recirculation region is likely to be less recent and less intense than at station F-L, but is probably more persistent (Trull et al., 2015).

EP100 was particularly elevated at the first (11.6 ± 1.3 mmol m^{-2} d^{-1}, E-1) and second visit (11.8 ± 1.1 mmol m^{-2} d^{-1}, E-3), decreased at the third visit (5.4 ± 0.7 mmol m^{-2} d^{-1}, E-4E), and then increased again during the fourth visit (7.7 ± 1.3 mmol m^{-2} d^{-1}, E-5). A comparison with the reference station indicates 1.4–3-fold enhanced export (at 100 m) within the recirculation feature suggesting an early impact of Fe fertilization. High EP100 appears primarily influenced by an elevated 100 m ^{234}Th export, ranging between 1051 ± 121 and 1326 ± 110 dpm m^{-2} d^{-1}. Note that high ^{234}Th export was also observed in the same area earlier in the survey (21–22 October) at transect stations TNS-6 and TNS-8 (see

Table S3). These results support an early export event in the PF meander that had occurred before the start of the bloom and was associated with moderate biomass levels. The integrated total Chl *a* stocks at 200 m were relatively stable with 141 at E-1, 112 at E-2, 96 at E-3, 108 at E-4E, and 126 mg m^{-2} at E-5 (Closset et al., 2014). Furthermore, the relatively constant ^{234}Th flux over the 19-day period may indicate that particle scavenging is at steady state, i.e., constant export (Savoye et al., 2006). This is supported also by the excellent agreement found between SS and NSS estimates of 100 m ^{234}Th fluxes at E-4E and E-5 (Table 1). However, local variation in ^{234}Th distribution seems to exist in the PF meander as seen with the smaller ^{234}Th flux recorded at station E-2 which was part of the west-to-east transect (TEW, Table S3 and Fig. 5). The smaller deficit at this station may have been caused by lateral advection of ^{234}Th-rich (lower deficit) waters originating from the jet of the PF passing to the north. The second controlling factor of EP100 was the sinking particles C : Th ratio, showing elevated values at E-1 (10.5 ± 0.2 µmol dpm^{-1}) and E-3 (8.9 ± 0.3 µmol dpm^{-1}), decreasing progressively at E-4E (5.1 ± 0.3 µmol dpm^{-1}), and increasing again at E-5 (6.1 ± 0.2 µmol dpm^{-1}). As already mentioned, such a decrease may indicate preferential loss of carbon relative to ^{234}Th (Buesseler et al., 2006). This may involve food web interactions including bacterial production in the mixed layer increasing from 30 (E-1) to 54.7 nmol C L^{-1} d^{-1} (E-5) (Christaki et al., 2014) and grazing activity by zooplankton (Carlotti et al., 2015).

EP200 was also elevated in the recirculation feature (range of 5.3 ± 1.0 to 8.2 ± 0.8 mmol m^{-2} d^{-1}) but shows less temporal variability. High EP200 results from a very deep ^{234}Th deficit extending down to 200 m depth, except at E-4E where the export depth (depth at which ^{234}Th is to back equilibrium with ^{238}U) is shallower ($\sim$ 150 m). Consequently, important increases in ^{234}Th export (up to a factor of 2 at E-5) were observed between 100 and 200 m depth. This feature is not in line with the relatively shallow mixed layer depth estimated in the PF meander (range of 38 to 74 m depth) and seems to follow the depth of the winter mixed layer. Note that macronutrients (nitrate and silicic acid) and dissolved trace elements profiles (Quéroué et al., 2015) display similar patterns to the ^{234}Th deficit. Such a vertical distribution suggests important vertical mixing in the area and tends to confirm that ^{234}Th export has occurred earlier in the survey. The ^{234}Th export at 200 m displays little variability over the 19.6 days of sampling and this feature is also observed in sediment traps deployed at E-1, E-3, and E-5, even though the traps have collected $\sim$ 50% of the flux deduced from the ^{234}Th deficit. The C : Th ratio in sinking particles decreases sharply between 100 and 200 m depth at E-1 and E-3 and to a lesser extent at E-4E and E-5 (Fig. 5). Ratios estimated from ISP show very good agreement with trap C : Th ratios at E-3 and E-5 but not at E-1. The trap C : Th ratio at E-1 was highly variable (8.6 ± 3.9 µmol dpm^{-1}) and appears closer to C : Th ratios of small (1–53 µm) particles, suggesting a potential contribution of these particles to the overall export. A decreasing C : Th ratio results in lower EP200 compared with EP100. However, a comparison with the HNLC reference station reveals between 2.9- and 4.5-fold higher carbon fluxes in the PF meander at 200 m depth. This suggests a strong impact of Fe fertilization in this area which is subjected to low-to-moderate dFe inputs. The impact of Fe fertilization on carbon export at this location is higher compared to the KEOPS1 study over the plateau ($\sim$ 2-fold higher POC flux) (Savoye et al., 2008).

High export in the PF meander remains relatively unexpected considering the temporal variation of surface phytoplankton community structure. Initially dominated by small particles including small centric and pennate diatoms, the larger phytoplankton fraction increased progressively and became dominant by the end of the time series (E-5) (Trull et al., 2015). This variability is also observed in ^{234}Th$_p$ and POC partitioning between the surface and 150 m depth. At E1, E-3, and E-4E, small particles represent the dominant fraction of ^{234}Th$_p$ and POC, 60–80 %, while at E-5 small particles fraction decreases to 50 %. This suggests an increasing potential for export, whereas EP tends to decrease with time. The same feature is observed for C (Cavagna et al., 2014) and Si uptake rates (Closset et al., 2014) showing low productivity at the beginning increasing progressively during the course of the survey. These inverse temporal variations between export and production are supported further by the ThE and EP / NP ratios at 100 m depth, where high values were observed initially (27 and 34 %, respectively) at E-1 decreasing progressively until E-5 (10 and 14 %, respectively). The reason for this decoupling may be numerous and highlights the complexity of export processes that cannot be easily resolved based only on primary and new production variability. One hypothesis involves food web interactions through grazing pressure, since fecal material is one of the main carriers of the POC export in the upper 200 m at the E stations (Laurenceau-Cornec et al., 2015a).

The early bloom export in the PF meander can be compared to the late summer situation reported for station A11 during KEOPS1 located in similar deep waters east of the Kerguelen Islands (Savoye et al., 2008). POC flux at A11 in late summer (range of 19.4–26.3 mmol m^{-2} d^{-1}) is substantially higher than EP100 (range of 5.4–11.6 mmol m^{-2} d^{-1}) and EP200 (5.3–7.7 mmol m^{-2} d^{-1}) at E stations confirming that an important fraction of the seasonal export was not sampled during KEOPS2. At A11, the C : Th ratio was 11.0 ± 1.2 and 6.3 µmol dpm^{-1} at 100 and 200 m depth, respectively, and appears very close to the C : Th ratios measured at E-1 and E-3, and higher than the ratios measured at E-4E and E-5.

5 Conclusions

In the present study, we investigated upper-ocean carbon export production in the naturally Fe-fertilized area adjacent to the Kerguelen Islands as part of the KEOPS2 expedition. Spatial and temporal variations in water column total ^{234}Th activity combined with the C : Th ratios of large potentially sinking particles were used to infer carbon export between 100 and 200 m depth. Export production in the Fe-fertilized area reveals large spatial variability during the early stages of bloom development with low export found at high productivity sites located over the central plateau (A3 site) and north of the PF in deep water downstream of the islands (F-L site). The highest export was observed south of the permanent meander of the PF (E stations), where a detailed time series was obtained as part of a pseudo-Lagrangian study. The comparison with the HNLC reference station located south of the PF and upstream of the islands indicates that Fe fertilization increased carbon export in all iron-fertilized waters during the early stage of the Kerguelen bloom but at variable degrees. The increase is particularly significant inside the PF meander, but more moderate over the central Kerguelen Plateau and in the northern plume of the Kerguelen bloom. Export efficiencies were particularly low at high productivity sites over and off the plateau (A3 and F-L sites) and clearly indicate that biomass was in accumulation phase rather than in export phase. The varied response of ecosystems to natural iron inputs results in varied phytoplankton community size structures, which in turn impacts the potential for carbon export. Accordingly, station A3 over the central plateau showing high biomass dominated by large diatoms may offer higher potential for carbon export compared to F-L and E sites. Comparison with late summer POC export obtained during KEOPS1 reveals a much smaller carbon export during the early stages of the bloom in spring than in late summer.

The Supplement related to this article is available online at doi:10.5194/bg-12-3831-2015-supplement.

Acknowledgements. We are grateful to KEOPS2 chief scientists Stéphane Blain and Bernard Quéguiner, and to the captain and crew of R/V *Marion Dufresne* for their assistance and help during the cruise. This research was supported by the French National Research Agency (grant no. ANR-10-BLAN-0614), the LEFE-CYBER program of Institut des Sciences de l'Univers (INSU), Institut Paul Emile Victor. Financial support was obtained from Belgian Science Policy (BELSPO, grant SD/CA/05A), Flanders Research Foundation (FWO, grant G071512N), Vrije Universiteit Brussel (Strategic Research Plan), the Antarctic Climate and Ecosystem Cooperative Research Centre (ACE-CRC, Hobart, Australia). We are very grateful to Michael Korntheuer for state-of-the-art beta counter maintenance, and Jacques Navez and Laurence Monin for helpful laboratory assistance. We would like to thank Lionel Scouarnec, Anne Royer, and Fabien Perault from the Technical Division of INSU in Brest for their assistance during the cruise.

Edited by: S. Blain

References

Alderkamp, A.-C., Mills, M. M., van Dijken, G. L., Laan, P., Thuróczy, C.-E., Gerringa, L. J. A., de Baar, H. J. W., Payne, C. D., Visser, R. J. W., Buma, A. G. J., and Arrigo, K. R.: Iron from melting glaciers fuels phytoplankton blooms in the Amundsen Sea (Southern Ocean): Phytoplankton characteristics and productivity, Deep-Sea Res. Pt. II, 71–76, 32–48, 2012.

Blain, S., Queguiner, B., Armand, L., Belviso, S., Bombled, B., Bopp, L., Bowie, A., Brunet, C., Brussaard, C., Carlotti, F., Christaki, U., Corbiere, A., Durand, I., Ebersbach, F., Fuda, J.-L., Garcia, N., Gerringa, L., Griffiths, B., Guigue, C., Guillerm, C., Jacquet, S., Jeandel, C., Laan, P., Lefevre, D., Lo Monaco, C., Malits, A., Mosseri, J., Obernosterer, I., Park, Y.-H., Picheral, M., Pondaven, P., Remenyi, T., Sandroni, V., Sarthou, G., Savoye, N., Scouarnec, L., Souhaut, M., Thuiller, D., Timmermans, K., Trull, T., Uitz, J., van Beek, P., Veldhuis, M., Vincent, D., Viollier, E., Vong, L., and Wagener, T.: Effect of natural iron fertilization on carbon sequestration in the Southern Ocean, Nature, 446, 1070–1074, 2007.

Blain, S., Sarthou, G., and Laan, P.: Distribution of dissolved iron during the natural iron-fertilization experiment KEOPS (Kerguelen Plateau, Southern Ocean), Deep-Sea Res. Pt. II, 55, 594–605, 2008.

Blain, S., Capparos, J., Guéneuguès, A., Obernosterer, I., and Oriol, L.: Distributions and stoichiometry of dissolved nitrogen and phosphorus in the iron-fertilized region near Kerguelen (Southern Ocean), Biogeosciences, 12, 623–635, doi:10.5194/bg-12-623-2015, 2015.

Borrione, I. and Schlitzer, R.: Distribution and recurrence of phytoplankton blooms around South Georgia, Southern Ocean, Biogeosciences, 10, 217–231, doi:10.5194/bg-10-217-2013, 2013.

Bowie, A. R., Townsend, A. T., Lannuzel, D., Remenyi, T. A., and van der Merwe, P.: Modern sampling and analytical methods for the determination of trace elements in marine particulate material using magnetic sector inductively coupled plasma–mass spectrometry, Anal. Chim. Ac., 676, 15–27, 2010.

Bowie, A. R., van der Merwe, P., Quéroué, F., Trull, T., Fourquez, M., Planchon, F., Sarthou, G., Chever, F., Townsend, A. T., Obernosterer, I., Sallée, J. B., and Blain, S.: Iron budgets for three distinct biogeochemical sites around the Kerguelen archipelago (Southern Ocean) during the natural fertilisation experiment KEOPS-2, Biogeosciences, in review, 2015.

Boyd, P. W., Watson, A. J., Law, C. S., Abraham, E. R., Trull, T., Murdoch, R., Bakker, D. C. E., Bowie, A. R., Buesseler, K. O., Chang, H., Charette, M., Croot, P., Downing, K., Frew, R., Gall, M., Hadfield, M., Hall, J., Harvey, M., Jameson, G., LaRoche, J., Liddicoat, M., Ling, R., Maldonado, M. T., McKay, R. M., Nodder, S., Pickmere, S., Pridmore, R., Rintoul, S., Safi, K., Sutton, P., Strzepek, R., Tanneberger, K., Turner, S., Waite, A., and Zeldis, J.: A mesoscale phytoplankton bloom in the polar South-

ern Ocean stimulated by iron fertilization, Nature, 407, 695–702, 2000.

Boyd, P. W., Jickells, T., Law, C. S., Blain, S., Boyle, E. A., Buesseler, K. O., Coale, K. H., Cullen, J. J., de Baar, H. J. W., Follows, M., Harvey, M., Lancelot, C., Levasseur, M., Owens, N. P. J., Pollard, R., Rivkin, R. B., Sarmiento, J., Schoemann, V., Smetacek, V., Takeda, S., Tsuda, A., Turner, S., and Watson, A. J.: Mesoscale iron enrichment experiments 1993–2005: Synthesis and future directions, Science, 315, 612–617, 2007.

Buesseler, K., Andrews, J., Pike, S., and Charette, M.: The Effects of Iron Fertilization on Carbon Sequestration in the Southern Ocean, Science, 304, 414–417, 2004.

Buesseler, K., Andrews, J., Pike, S. M., Charette, M. A., Goldson, L. E., Brzezinski, M. A., and Lance, V. P.: Particle export during the Southern Ocean Iron Experiment (SOFeX), Limnol. Oceanogr., 50, 311–327, 2005.

Buesseler, K. O.: The decoupling of production and particulate export in the surface ocean, Global Biogeochem. Cy., 12, 297–310, 1998.

Buesseler, K. O., Bacon, M. P., Kirk Cochran, J., and Livingston, H. D.: Carbon and nitrogen export during the JGOFS North Atlantic Bloom experiment estimated from $^{234}Th:^{238}U$ disequilibria, Deep-Sea Res. Pt. A, 39, 1115–1137, 1992.

Buesseler, K. O., Ball, L., Andrews, J., Cochran, J. K., Hirschberg, D. J., Bacon, M. P., Fleer, A., and Brzezinski, M.: Upper ocean export of particulate organic carbon and biogenic silica in the Southern Ocean along 170° W, Deep-Sea Res. Pt. II, 48, 4275–4297, 2001.

Buesseler, K. O., Barber, R. T., Dickson, M.-L., Hiscock, M. R., Moore, J. K., and Sambrotto, R.: The effect of marginal ice-edge dynamics on production and export in the Southern Ocean along 170° W, Deep-Sea Res. Pt. II, 50, 579–603, 2003.

Buesseler, K. O., Benitez-Nelson, C. R., Moran, S. B., Burd, A., Charette, M., Cochran, J. K., Coppola, L., Fisher, N. S., Fowler, S. W., Gardner, W. D., Guo, L. D., Gustafsson, Ã., Lamborg, C., Masque, P., Miquel, J. C., Passow, U., Santschi, P. H., Savoye, N., Stewart, G., and Trull, T.: An assessment of particulate organic carbon to thorium-234 ratios in the ocean and their impact on the application of ^{234}Th as a POC flux proxy, Mar. Chem., 100, 213–233, 2006.

Carlotti, F., Jouandet, M.-P., Nowaczyk, A., Harmelin-Vivien, M., Lefèvre, D., Guillou, G., Zhu, Y., and Zhou, M.: Mesozooplankton structure and functioning during the onset of the Kerguelen phytoplankton bloom during the Keops2 survey, Biogeosciences Discuss., 12, 2381–2427, doi:10.5194/bgd-12-2381-2015, 2015.

Cavagna, A. J., Fripiat, F., Elskens, M., Dehairs, F., Mangion, P., Chirurgien, L., Closset, I., Lasbleiz, M., Flores–Leiva, L., Cardinal, D., Leblanc, K., Fernandez, C., Lefèvre, D., Oriol, L., Blain, S., and Quéguiner, B.: Biological productivity regime and associated N cycling in the vicinity of Kerguelen Island area, Southern Ocean, Biogeosciences Discuss., 11, 18073–18104, doi:10.5194/bgd-11-18073-2014, 2014.

Christaki, U., Lefèvre, D., Georges, C., Colombet, J., Catala, P., Courties, C., Sime-Ngando, T., Blain, S., and Obernosterer, I.: Microbial food web dynamics during spring phytoplankton blooms in the naturally iron-fertilized Kerguelen area (Southern Ocean), Biogeosciences, 11, 6739–6753, doi:10.5194/bg-11-6739-2014, 2014.

Closset, I., Lasbleiz, M., Leblanc, K., Quéguiner, B., Cavagna, A.-J., Elskens, M., Navez, J., and Cardinal, D.: Seasonal evolution of net and regenerated silica production around a natural Fe-fertilized area in the Southern Ocean estimated with Si isotopic approaches, Biogeosciences, 11, 5827–5846, doi:10.5194/bg-11-5827-2014, 2014.

Coale, K. H., Johnson, K. S., Chavez, F. P., Buesseler, K. O., Barber, R. T., Brzezinski, M. A., Cochlan, W. P., Millero, F. J., Falkowski, P. G., Bauer, J. E., Wanninkhof, R. H., Kudela, R. M., Altabet, M. A., Hales, B. E., Takahashi, T., Landry, M. R., Bidigare, R. R., Wang, X., Chase, Z., Strutton, P. G., Friederich, G. E., Gorbunov, M. Y., Lance, V. P., Hilting, A. K., Hiscock, M. R., Demarest, M., Hiscock, W. T., Sullivan, K. F., Tanner, S. J., Gordon, R. M., Hunter, C. N., Elrod, V. A., Fitzwater, S. E., Jones, J. L., Tozzi, S., Koblizek, M., Roberts, A. E., Herndon, J., Brewster, J., Ladizinsky, N., Smith, G., Cooper, D., Timothy, D., Brown, S.L., Selph, K. E., Sheridan, C. C., Twining, B. S., and Johnson, Z. I.: Southern Ocean Iron Enrichment Experiment: Carbon Cycling in High- and Low-Si Waters, Science, 304, 408–414, 2004.

Cochran, J. K. and Masqué, P.: Short-lived U / Th series radionuclides in the ocean: tracers for scavenging rates, export fluxes and particle dynamics, Uranium-Series Geochem., 52, 461–492, 2003.

Cochran, J. K., Buesseler, K. O., Bacon, M. P., Wang, H. W., Hirschberg, D. J., Ball, L., Andrews, J., Crossin, G., and Fleer, A.: Short-lived thorium isotopes (^{234}Th, ^{228}Th) as indicators of POC export and particle cycling in the Ross Sea, Southern Ocean, Deep-Sea Res. Pt. II, 47, 3451–3490, 2000.

d'Ovidio, F., Della Penna, A., Trull, T. W., Nencioli, F., Pujol, I., Rio, M. H., Park, Y.-H., Cotté, C., Zhou, M., and Blain, S.: The biogeochemical structuring role of horizontal stirring: Lagrangian perspectives on iron delivery downstream of the Kerguelen plateau, Biogeosciences Discuss., 12, 779–814, doi:10.5194/bgd-12-779-2015, 2015.

Ebersbach, F. and Trull, T. W.: Sinking particle properties from polyacrylamide gels during the KErguelen Ocean and Plateau compared Study (KEOPS): Zooplankton control of carbon export in an area of persistent natural iron inputs in the Southern Ocean, Limnol. Oceanogr. 53, 212–224, 2008.

Henson, S. A., Sanders, R., Madsen, E., Morris, P. J., Le Moigne, F., and Quartly, G. D.: A reduced estimate of the strength of the ocean's biological carbon pump, Geophys. Res. Lett., 38, L04606, doi:10.1029/2011GL046735, 2011.

Jacquet, S. H. M., Savoye, N., Dehairs, F., Strass, V. H., and Cardinal, D.: Mesopelagic carbon remineralization during the European Iron Fertilization Experiment, Global Biogeochem. Cy., 22, GB1023, doi:10.1016/j.dsr2.2007.12.038, 2008.

Jouandet, M. P., Blain, S., Metzl, N., Brunet, C., Trull, T. W., and Obernosterer, I.: A seasonal carbon budget for a naturally iron-fertilized bloom over the Kerguelen Plateau in the Southern Ocean, Deep-Sea Res. Pt. II, 55, 856–867, 2008.

Jouandet, M.-P., Jackson, G. A., Carlotti, F., Picheral, M., Stemmann, L., and Blain, S.: Rapid formation of large aggregates during the spring bloom of Kerguelen Island: observations and model comparisons, Biogeosciences, 11, 4393–4406, doi:10.5194/bg-11-4393-2014, 2014.

Joubert, W. R., Thomalla, S. J., Waldron, H. N., Lucas, M. I., Boye, M., Le Moigne, F. A. C., Planchon, F., and Speich, S.: Nitro-

gen uptake by phytoplankton in the Atlantic sector of the Southern Ocean during late austral summer, Biogeosciences, 8, 2947–2959, doi:10.5194/bg-8-2947-2011, 2011.

Lasbleiz, M., Leblanc, K., Blain, S., Ras, J., Cornet-Barthaux, V., Hélias Nunige, S., and Quéguiner, B.: Pigments, elemental composition (C, N, P, and Si), and stoichiometry of particulate matter in the naturally iron fertilized region of Kerguelen in the Southern Ocean, Biogeosciences, 11, 5931–5955, doi:10.5194/bg-11-5931-2014, 2014.

Laurenceau-Cornec, E. C., Trull, T. W., Davies, D. M., Bray, S. G., Doran, J., Planchon, F., Carlotti, F., Jouandet, M.-P., Cavagna, A.-J., Waite, A. M., and Blain, S.: The relative importance of phytoplankton aggregates and zooplankton fecal pellets to carbon export: insights from free-drifting sediment trap deployments in naturally iron-fertilised waters near the Kerguelen Plateau, Biogeosciences, 12, 1007–1027, doi:10.5194/bg-12-1007-2015, 2015a.

Laurenceau-Cornec, E. C., Trull, T. W., Davies, D. M., De La Rocha, C. L., and Blain, S.: Phytoplankton morphology controls on marine snow sinking velocity, Mar. Ecol. Prog. Ser., 520, 35–56, 2015b.

Le Moigne, F. A. C., Henson, S. A., Sanders, R. J., and Madsen, E.: Global database of surface ocean particulate organic carbon export fluxes diagnosed from the ^{234}Th technique, Earth Syst. Sci. Data, 5, 295–304, doi:10.5194/essd-5-295-2013, 2013.

Lucas, M., Seeyave, S., Sanders, R., Mark Moore, C., Williamson, R., and Stinchcombe, M.: Nitrogen uptake responses to a naturally Fe-fertilised phytoplankton bloom during the 2004/2005 CROZEX study, Deep-Sea Res. Pt. II, 54, 2138–2173, 2007.

Martin, J. H.: Glacial-interglacial CO_2 change: The Iron Hypothesis, Paleoceanography, 5, 1–13, 1990.

Martin, J. H., Fitzwater, S. E., and Gordon, R. M.: Iron deficiency limits phytoplankton growth in Antarctic waters, Global Biogeochem. Cy., 4, 5–12, 1990.

Martin, J. H., Gordon, R. M., and Fitzwater, S. E.: The case for iron, Limnol. Oceanogr., 36, 1793–1802, 1991.

Martin, P., van der Loeff, M. R., Cassar, N., Vandromme, P., d'Ovidio, F., Stemmann, L., Rengarajan, R., Soares, M., González, H. E., Ebersbach, F., Lampitt, R. S., Sanders, R., Barnett, B. A., Smetacek, V., and Naqvi, S. W. A.: Iron fertilization enhanced net community production but not downward particle flux during the Southern Ocean iron fertilization experiment LOHAFEX, Global Biogeochem. Cy., 27, 871–881, 2013.

Mongin, M., Molina, E., and Trull, T. W.: Seasonality and scale of the Kerguelen plateau phytoplankton bloom: A remote sensing and modeling analysis of the influence of natural iron fertilization in the Southern Ocean, Deep-Sea Res. Pt. II, 55, 880–892, 2008.

Moore, C. M., Mills, M. M., Arrigo, K. R., Berman-Frank, I., Bopp, L., Boyd, P. W., Galbraith, E. D., Geider, R. J., Guieu, C., Jaccard, S. L., Jickells, T. D., La Roche, J., Lenton, T. M., Mahowald, N. M., Maranon, E., Marinov, I., Moore, J. K., Nakatsuka, T., Oschlies, A., Saito, M. A., Thingstad, T. F., Tsuda, A., and Ulloa, O.: Processes and patterns of oceanic nutrient limitation, Nature Geosci., 6, 701–710, 2013.

Morris, P. J. and Charette, M. A.: A synthesis of upper ocean carbon and dissolved iron budgets for Southern Ocean natural iron fertilisation studies, Deep-Sea Res. Pt. II, 90, 147–157, 2013.

Morris, P. J., Sanders, R., Turnewitsch, R., and Thomalla, S.: 234Th-derived particulate organic carbon export from an island-induced phytoplankton bloom in the Southern Ocean, Deep-Sea Res. Pt. II, 54, 2208–2232, 2007.

Mosseri, J., Quéguiner, B., Armand, L., and Cornet-Barthaux, V.: Impact of iron on silicon utilization by diatoms in the Southern Ocean: A case study of Si / N cycle decoupling in a naturally iron-enriched area, Deep-Sea Res. Pt. II, 55, 801–819, 2008.

Nodder, S. D., Charette, M. A., Waite, A. M., Trull, T. W., Boyd, P. W., Zeldis, J., and Buesseler, K. O.: Particle transformations and export flux during an in situ iron-stimulated algal bloom in the Southern Ocean, Geophys. Res. Lett., 28, 2409–2412, 2001.

Owens, S. A., Buesseler, K. O., and Sims, K. W. W.: Re-evaluating the ^{238}U-salinity relationship in seawater: Implications for the ^{238}U–^{234}Th disequilibrium method, Mar. Chem., 127, 31–39, 2011.

Park, Y.-H., Fuda, J.-L., Durand, I., and Naveira Garabato, A. C.: Internal tides and vertical mixing over the Kerguelen Plateau, Deep-Sea Res. Pt. II, 55, 582–593, 2008a.

Park, Y.-H., Roquet, F., Durand, I., and Fuda, J.-L.: Large-scale circulation over and around the Northern Kerguelen Plateau, Deep-Sea Res. Pt. II, 55, 566–581, 2008b.

Park, Y.-H., Durand, I., Kestenare, E., Rougier, G., Zhou, M., d'Ovidio, F., Cotté, C., and Lee, J.-H.: Polar Front around the Kerguelen Islands: An up-to-date determination and associated circulation of surface/subsurface waters, J. Geophys. Res.-Oceans, 119, 6575–6592, 2014a.

Park, Y.-H., Lee, J.-H., Durand, I., and Hong, C.-S.: Validation of Thorpe-scale-derived vertical diffusivities against microstructure measurements in the Kerguelen region, Biogeosciences, 11, 6927–6937, doi:10.5194/bg-11-6927-2014, 2014b.

Pike, S. M., Buesseler, K. O., Andrews, J., and Savoye, N.: Quantification of 234Th recovery in small volume sea water samples by inductively coupled plasma-mass spectrometry, J. Radioanal. Nucl. Chem., 263, 355–360, 2005.

Planchon, F., Cavagna, A.-J., Cardinal, D., André, L., and Dehairs, F.: Late summer particulate organic carbon export and twilight zone remineralisation in the Atlantic sector of the Southern Ocean, Biogeosciences, 10, 803–820, doi:10.5194/bg-10-803-2013, 2013.

Planquette, H., Statham, P. J., Fones, G. R., Charette, M. A., Moore, C. M., Salter, I., Nédélec, F. H., Taylor, S. L., French, M., Baker, A. R., Mahowald, N., and Jickells, T. D.: Dissolved iron in the vicinity of the Crozet Islands, Southern Ocean, Deep-Sea Res. Pt. II, 54, 1999–2019, 2007.

Pollard, R. T., Salter, I., Sanders, R. J., Lucas, M. I., Moore, C. M., Mills, R. A., Statham, P. J., Allen, J. T., Baker, A. R., Bakker, D. C. E., Charette, M. A., Fielding, S., Fones, G. R., French, M., Hickman, A. E., Holland, R. J., Hughes, J. A., Jickells, T. D., Lampitt, R. S., Morris, P. J., Nedelec, F. H., Nielsdottir, M., Planquette, H., Popova, E. E., Poulton, A. J., Read, J. F., Seeyave, S., Smith, T., Stinchcombe, M., Taylor, S., Thomalla, S., Venables, H. J., Williamson, R., and Zubkov, M. V.: Southern Ocean deep-water carbon export enhanced by natural iron fertilization, Nature, 457, 577–580, 2009.

Quéroué, F., Sarthou, G., Planquette, H. F., Bucciarelli, E., Chever, F., van der Merwe, P., Lannuzel, D., Townsend, A. T., Cheize, M., Blain, S., d'Ovidio, F., and Bowie, A. R.: High variability of dissolved iron concentrations in the vicinity of Kerguelen Is-

land (Southern Ocean), Biogeosciences Discuss., 12, 231–270, doi:10.5194/bgd-12-231-2015, 2015.

Rutgers van der Loeff, M. M., Friedrich, J., and Bathmann, U. V.: Carbon export during the Spring Bloom at the Antarctic Polar Front, determined with the natural tracer ^{234}Th, Deep-Sea Res. Pt. II, 44, 457–478, 1997.

Rutgers van der Loeff, M., Cai, P. H., Stimac, I., Bracher, A., Middag, R., Klunder, M. B., and van Heuven, S. M. A. C.: ^{234}Th in surface waters: distribution of particle export flux across the Antarctic Circumpolar Current and in the Weddell Sea during the GEOTRACES expedition ZERO and DRAKE, Deep-Sea Res. Pt. II, 58, 2749–2766, 2011.

Salter, I., Lampitt, R. S., Sanders, R., Poulton, A., Kemp, A. E. S., Boorman, B., Saw, K., and Pearce, R.: Estimating carbon, silica and diatom export from a naturally fertilised phytoplankton bloom in the Southern Ocean using PELAGRA: A novel drifting sediment trap, Deep-Sea Res. Pt. II, 54, 2233–2259, 2007.

Sambrotto, R. N. and Mace, B. J.: Coupling of biological and physical regimes across the Antarctic Polar Front as reflected by nitrogen production and recycling, Deep-Sea Res. Pt. II, 47, 3339–3367, 2000.

Savoye, N., Benitez-Nelson, C., Burd, A. B., Cochran, J. K., Charette, M., Buesseler, K. O., Jackson, G. A., Roy-Barman, M., Schmidt, S., and Elskens, M.: ^{234}Th sorption and export models in the water column: A review, Mar, Chem., 100, 234–249, 2006.

Savoye, N., Trull, T. W., Jacquet, S. H. M., Navez, J., and Dehairs, F.: 234Th-based export fluxes during a natural iron fertilization experiment in the Southern Ocean (KEOPS), Deep-Sea Res. Pt. II, 55, 841–855, 2008.

Sedwick, P. N., DiTullio, G. R., Hutchins, D. A., Boyd, P. W., Griffiths, F. B., Crossley, A. C., Trull, T. W., and Quéguiner, B.: Limitation of algal growth by iron deficiency in the Australian Subantarctic Region, Geophys. Res. Lett., 26, 2865–2868, 1999.

Seeyave, S., Lucas, M.I., Moore, C. M., and Poulton, A. J.: Phytoplankton productivity and community structure in the vicinity of the Crozet Plateau during austral summer 2004/2005, Deep-Sea Res. Pt. II, 54, 2020–2044, 2007.

Smetacek, V., Klaas, C., Strass, V. H., Assmy, P., Montresor, M., Cisewski, B., Savoye, N., Webb, A., d'Ovidio, F., Arrieta, J. M., Bathmann, U., Bellerby, R., Berg, G. M., Croot, P., Gonzalez, S., Henjes, J., Herndl, G. J., Hoffmann, L. J., Leach, H., Losch, M., Mills, M. M., Neill, C., Peeken, I., Rottgers, R., Sachs, O., Sauter, E., Schmidt, M. M., Schwarz, J., Terbruggen, A., and Wolf-Gladrow, D.: Deep carbon export from a Southern Ocean iron-fertilized diatom bloom, Nature, 487, 313–319, 2012.

Trull, T. W., Davies, D. M., Dehairs, F., Cavagna, A.-J., Lasbleiz, M., Laurenceau-Cornec, E. C., d'Ovidio, F., Planchon, F., Leblanc, K., Quéguiner, B., and Blain, S.: Chemometric perspectives on plankton community responses to natural iron fertilisation over and downstream of the Kerguelen Plateau in the Southern Ocean, Biogeosciences, 12, 1029–1056, doi:10.5194/bg-12-1029-2015, 2015.

van der Merwe, P., Bowie, A. R., Quéroué, F., Armand, L., Blain, S., Chever, F., Davies, D., Dehairs, F., Planchon, F., Sarthou, G., Townsend, A. T., and Trull, T. W.: Sourcing the iron in the naturally fertilised bloom around the Kerguelen Plateau: particulate trace metal dynamics, Biogeosciences, 12, 739–755, doi:10.5194/bg-12-739-2015, 2015.

Zhou, M., Zhu, Y., Measures, C.I., Hatta, M., Charette, M.A., Gille, S.T., Frants, M., Jiang, M., and Greg Mitchell, B.: Winter mesoscale circulation on the shelf slope region of the southern Drake Passage, Deep-Sea Res. Pt. II, 90, 4–14, 2013.